ISSN 2663-9092 (Online)

Ukrainian Neurosurgical Journal

Том 32, №2, 2026

Науково-практичний журнал (спеціалізоване видання для лікарів)
Заснований у квітні 1995 року. Виходить 4 рази на рік.
Свідоцтво про державну реєстрацію КВ №23771-13611ПР від 14 лютого 2019 р.

Журнал входить до Переліку наукових фахових видань України, в яких можуть бути опубліковані результати дисертаційних робіт на здобуття наукових ступенів доктора наук, кандидата наук та ступеня доктора філософії (Наказ МОН України від 10.12.2024 № 1721)
Ідентифікатор у Реєстрі суб'єктів у сфері медіа: R40-07048.
Журнал включено до наукометричної бази Scopus.

Всі рукописи, що надходять до редакції, обов'язково рецензуються

Засновники
Інститут нейрохірургії ім. акад. А.П. Ромоданова НАМН України
Українська Асоціація Нейрохірургів
Національна академія медичних наук України

Видавець
Інститут нейрохірургії ім. акад. А.П. Ромоданова НАМН України

Адреса видавця та редакції
вул.Платона Майбороди, 32, Київ, 04050, Україна
Тел. +380 44 483-91-98
Факс +380 44 489-35-61
E-mail: unj.office@gmail.com
http://theunj.org

Підписано до публікації
з оригінал-макета 27.03.2026

Оригінал-макет журналу затверджений і рекомендований до друку та поширення через Інтернет на спільному засіданні Редакційної колегії Ukrainian Neurosurgical Journal та вченої ради Інституту нейрохірургії ім. акад. А.П. Ромоданова НАМН України (протокол №3 від 27.03.2026)

Перша сторінка обкладинки

Рисунок до статті Irakli B. Goginava, Giorgi Murvelashvili, Mikheil A. Shavgulidze, Mariia V. Riezunenko, Giorgi L. Giorgidze "Bifid median nerve: case report" , стор. 126-128

Зміст

Review article

Ukrainian Neurosurgical Journal. 2026;32(2):3-11
doi: 10.25305/unj.350308

Neuroinflammation: molecular mechanisms, triggers, and biomarkers for clinical stratification

Mykhailo V. Khyzhnyak [1], Iryna H. Vasilyeva [2], Yuriy G. Gafiychuk [3]

[1] Department of Minimally and Laser Spinal Neurosurgery, Romodanov Neurosurgery Institute, Kyiv, Ukraine
[2] Department of Neurobiochemistry, Romodanov Neurosurgery Institute, Kyiv, Ukraine
[3] Neurosurgery Department, Military Medical Clinical Center of the Southern Region, Odesa, Ukraine

Received: 20 January 2026
Accepted: 27 February 2026

Address for correspondence:
Iryna G. Vasilyeva, Department of Neurobiochemistry, Romodanov Neurosurgery Institute, 32 Platona Maiborody st., Kyiv, 04050, Ukraine, e-mail: vigvasileva@gmail.com

Neuroinflammation is increasingly regarded as a key factor in the progression of neurological disorders. At the same time, in clinical practice it is often interpreted in an overly simplified manner and reduced to nonspecific activation of inflammatory responses.

Objective: to integrate contemporary molecular and cellular evidence in order to conceptualize neuroinflammation as a context-dependent and stage-determined biological program, and to delineate mechanistic determinants relevant to biomarker interpretation and therapeutic stratification.

Materials and methods: A narrative analysis of contemporary experimental, translational, and clinical studies focusing on innate protective mechanisms of the central nervous system was performed. The review emphasizes PRR-mediated recognition of pathogen-associated and damage-associated molecular patterns, intracellular inflammatory signaling pathways (NF-κB, MAPK, JAK/STAT, inflammasome complexes), mechanisms of inflammatory termination and resolution, and the regulatory role of the blood–brain barrier (BBB). Particular attention was given to data on glial cell biology, neurovascular unit signaling, biomarker profiles in cerebrospinal fluid and blood, and disease-specific neuroinflammatory phenotypes.

Results: The synthesized data indicate that neuroinflammation is not a uniform pathological state but represents a dynamic, multicomponent program shaped by the balance between initiation, amplification, resolution, and chronic persistence of inflammatory responses. Two closely interrelated components can be distinguished. The first is a resident innate neuroinflammatory program, predominantly mediated by microglia, astrocytes, and endothelial cells through PRR-dependent protective signaling mechanisms. The second is an adaptive immune component characterized by infiltration of peripheral immune cells and the development of antigen-specific responses. Disruption of resolution mechanisms, insufficient clearance of damage-associated signals, and sustained PRR activation promote the development of chronic neuroinflammation and neurodegenerative changes. The functional state of the BBB emerges as a critical modifier of neuroinflammatory dynamics, directly affecting biomarker interpretation, therapeutic access and clinical response.

Conclusions: Neuroinflammation should be conceptualized as a potentially modifiable biological program rather than a fixed pathological entity. Effective diagnostic and therapeutic strategies require context- and stage-specific stratification that takes into account the dominant inflammatory component, disease phase, etiological triggers, and the functional state of the BBB. Approaches aimed at limiting inflammatory amplification, restoring resolution mechanisms, and stabilizing barrier function are likely to offer greater translational potential than nonspecific anti-inflammatory suppression.

Keywords: *neuroinflammation; pattern recognition receptors; innate protective mechanisms; microglia; blood–brain barrier; inflammasome; resolution of inflammation; biomarkers; translational neuroscience*

Introduction

Inflammation is an evolutionarily conserved, regulated protective–adaptive tissue response to injury or threat to homeostasis, aimed at limiting damage, eliminating injured structures, and initiating repair. Under conditions of effective resolution, the inflammatory process culminates in functional tissue recovery, whereas dysregulation leads to its persistence and transition into a chronic pathological state [1, 2].

Inflammation of the central nervous system (neuroinflammation) has several clinically significant features determined by the structural isolation of the central nervous system (CNS), the presence of the blood–brain barrier (BBB), and the relatively limited involvement of adaptive immune cells. In contrast to peripheral tissues, inflammatory responses within the CNS parenchyma are predominantly mediated by glial cells—microglia, astrocytes, and oligodendrocytes—

whereas neutrophil–monocyte mechanisms become dominant mainly under conditions of substantial disruption of barrier integrity [3, 4]. Microglia integrate immune, trophic, and synaptic regulatory functions, which accounts for the close relationship between inflammatory activation and neuronal dysfunction [4].

From a clinical perspective, neuroinflammation is associated with a high functional "cost": even moderate or prolonged activation of inflammatory mechanisms may be linked to impaired synaptic transmission, excitotoxicity, reduced neuroplasticity, and progression of neurodegenerative changes. These processes underlie cognitive, motor, and neuropsychiatric disturbances across a broad spectrum of acute and chronic CNS disorders.

At the molecular level, neuroinflammation engages universal inflammatory response programs, including activation of pattern recognition receptors (PRRs), such as Toll-like receptors (TLRs) and NOD-like receptors (NLRs), signaling pathways involving NF-κB, MAPK, and JAK/STAT, as well as production of key pro-inflammatory mediators, including IL-1β (interleukin-1β), TNF-α (tumour necrosis factor-α), IL-6, and HMGB1 (High Mobility Group Box 1) [5]. Of clinical relevance, these signaling cascades and regulatory circuits determine the balance between inflammatory resolution with tissue recovery and chronic persistence, the latter being associated with progressive neurodegeneration and poorer prognosis [2].

Thus, neuroinflammation should be regarded as a context-dependent manifestation of a universal inflammatory program under CNS conditions, characterized by specific cellular mechanisms, substantial influence on disease course, and potential relevance as a target for diagnostic and therapeutic interventions.

Given the clinical heterogeneity of neuroinflammation and its decisive role in determining the course and prognosis of CNS disorders, understanding the molecular and cellular mechanisms underlying inflammatory activation is of major importance. Analysis of the signaling cascades, cellular interactions, and regulatory circuits governing the initiation, maintenance, and resolution of neuroinflammation is a necessary prerequisite for the identification of diagnostic biomarkers and the development of targeted therapeutic strategies [6].

The aim of this review was to examine the key mechanisms of neuroinflammation with emphasis on their clinical and translational significance.

Mechanisms of neuroinflammation

Initiation of neuroinflammation: PAMP/DAMP → PRR

Neuroinflammation is initiated in response to a broad spectrum of injurious stimuli, including infectious agents, ischemia/reperfusion, oxidative stress, mechanical trauma, and accumulation of pathological protein aggregates during neurodegeneration [7, 8]. Under these conditions, disruption of tissue homeostasis is accompanied by the release of two major classes of inflammatory inducers: pathogen-associated molecular patterns (PAMPs) during infection and damage-associated molecular patterns (DAMPs) during sterile injury [7]. These signals are detected by PRRs.

Of clinical importance, PRR activation may occur before the appearance of overt structural abnormalities on neuroimaging, making these early molecular triggers promising targets for biomarker-based risk stratification and early therapeutic intervention [8,9].

Pattern recognition receptors in the CNS (PRR-mediated sensing)

A central event in the initiation of neuroinflammation is the activation of PRRs, which provide early sensing of both infectious agents and sterile tissue injury within the central nervous system (CNS). The principal classes of PRRs include: (1) TLRs, transmembrane receptors that recognize PAMPs and DAMPs in the extracellular space and within endosomes; (2) NLRs, cytoplasmic sensors whose activation leads to inflammasome assembly and subsequent release of pro-inflammatory cytokines; (3) RIG-I-like receptors (RLRs), intracellular sensors responsible for recognition of viral RNA; and (4) scavenger receptors (SRs), involved in the clearance of modified lipoproteins, amyloid peptides, and cellular debris [10–13].

Within brain tissue, microglia are the principal cellular carriers of PRRs. Astrocytes and oligodendrocytes also express a broad spectrum of PRRs and participate not only in the initiation of inflammatory responses but also in barrier regulation and reparative processes [3, 4]. Data obtained in recent years indicate the expression of specific PRRs on neurons, enabling them to respond to danger signals, modulate intracellular stress responses, and influence cell survival and synaptic function [8].

From a functional perspective, PRR-mediated sensing in the CNS serves as a mechanism of continuous surveillance of cerebral homeostasis. Activation of TLRs and RLRs predominantly mediates the initiation and amplification of inflammatory signaling, whereas NLR-dependent inflammasome pathways convert these signals into an effector response. In a clinical and translational context, PRR signaling is regarded as one of the earliest and potentially modifiable levels of the neuroinflammatory response, thereby creating opportunities for selective therapeutic strategies aimed at modifying disease course rather than merely suppressing inflammatory symptoms.

Chronic or dysregulated PRR activation is associated with the establishment of persistent inflammatory circuits and plays an important role in the pathogenesis of multiple sclerosis and other chronic neuroinflammatory and neurodegenerative conditions [6, 7]. In this context, PRRs and their downstream signaling cascades are considered key pathogenetic mechanisms, as well as promising therapeutic targets and biomarkers of neuroinflammatory activity [6, 7].

Molecular transduction of inflammatory signals in the nervous system

The inflammatory response in the nervous system is formed through coordinated activation of families of innate (sensory) immune receptors, including TLRs, NLRs, RLRs, and SRs. These sensors exhibit cell-specific expression patterns: the highest levels are characteristic of microglia, whereas astrocytes, oligodendrocytes, and neurons demonstrate a more limited and context-dependent profile, reflecting their involvement in homeostatic and stress-associated responses.

Toll-like receptors

TLRs are localized on the plasma membrane and within endosomes, where they mediate the primary recognition of PAMPs and DAMPs. Their activation is accompanied by recruitment of the adaptor proteins MyD88 or TRIF, which, through the TAK1 signaling

node, activate the IKK/NF-κB and MAPK/AP-1 signaling axes. As a result, transcription of pro-inflammatory mediators (IL-1β, IL-6, TNF-α), inflammatory enzymes (cyclooxygenase-2 (COX-2), inducible nitric oxide synthase (iNOS)), chemokines, and adhesion molecules is induced. Importantly, TLR signaling provides the "priming" phase of the inflammatory response by promoting synthesis of inactive precursor forms of IL-1β and IL-18, as well as upregulation of inflammasome components. A distinct role is played by the TRIF-dependent axis (predominantly associated with TLR3 and TLR4), which leads to induction of type I interferons and secondary activation of JAK/STAT signaling. The combination of primary NF-κB/MAPK activation and secondary JAK/STAT amplification forms stable autocrine and paracrine feedback loops that determine response duration and the potential for chronic neuroinflammation [14–16].

NOD-like receptors

NLRs are cytoplasmic sensors that respond to intracellular PAMPs and DAMPs and play a key role at the post-transcriptional stage of the inflammatory response. Activation of inflammasome complexes, particularly NLRP3, leads to recruitment and activation of caspase-1, which mediates proteolytic maturation of pro-IL-1β and pro-IL-18 into their biologically active forms. Thus, NLRs integrate danger signals with the mechanisms of secretion of key cytokines and determine the intensity of the effector phase of inflammation [17, 18].

RIG-I-like receptors

RLRs are intracellular sensors of viral RNA that function in the cytosol and mediate the antiviral component of innate immunity. Following binding to viral RNA, these receptors interact with the adaptor MAVS (mitochondrial antiviral signaling protein), localized on the outer mitochondrial membrane, thereby initiating activation of the transcription factors IRF3/IRF7 and NF-κB. This leads to synthesis of type I interferons and pro-inflammatory cytokines. Functionally, RLR signaling converges with TLR pathways at the level of NF-κB and may modulate inflammasome responses through mitochondrial mechanisms, thereby linking antiviral defense with the broader inflammatory program [19].

Scavenger receptors (SRs)

SRs mediate the clearance of modified lipids, amyloid peptides, and cellular debris, thereby playing a crucial role in maintaining tissue homeostasis. In the nervous system, they are most prominently expressed in microglia, where they execute phagocytic functions, whereas in other CNS cell types they are primarily involved in regulating metabolism and the local microenvironment. Functionally, SRs act as co-receptors, enhancing the efficiency of TLR and RLR activation through ligand delivery, and they also activate the NLR inflammasome via the induction of lysosomal and mitochondrial stress [20].

Signal integration

Thus, TLRs and RLRs are responsible for the initiation and transcriptional priming of the inflammatory response; NLRs mediate the maturation and secretion of key cytokines; whereas SRs modulate the intensity and spatial organization of these processes. The coordinated interplay among these receptor systems forms a multilayered signaling network that determines the nature of neuroinflammation—ranging from an acute protective response to chronic degenerative changes [2, 4, 6, 7].

Clearance of PAMPs and DAMPs as a critical stage in the resolution of neuroinflammation

Although PRR activation and the production of proinflammatory mediators define the initiation and amplification of the neuroinflammatory response, its resolution critically depends on the efficient cellular clearance of PAMPs and DAMPs. In the CNS, this process is primarily carried out by microglia through phagocytosis, efferocytosis, and receptor-mediated clearance, including mechanisms involving SRs, complement-dependent pathways, and lysosomal degradation [21]. Astrocytes also contribute by facilitating metabolic detoxification, spatial containment of damaged areas, and maintenance of barrier integrity, whereas neurons predominantly serve as passive targets rather than active effectors of clearance [22]. With effective elimination of molecular danger patterns, PRR signaling gradually subsides, promoting a shift of glial cells toward homeostatic and reparative programs. Conversely, impaired clearance of PAMPs/DAMPs leads to their persistence within tissues, sustains chronic PRR activation, and establishes self-perpetuating inflammatory circuits that drive the transition of neuroinflammation into a chronic maladaptive state [23].

Table 1 summarizes the principal PRR platforms involved in neuroinflammation, the relationships between their dominant signaling pathways and functional consequences, and the molecular biomarkers of activation, resolution, and chronicization. The presented scheme illustrates the organization of innate neuroinflammatory signaling (from transcriptional priming to the effector cytokine response) and demonstrates how dysregulated PRR activation contributes to the establishment of persistent inflammatory circuits and neurodegenerative progression.

Termination of inflammation and mechanisms of neuroinflammatory response chronicity

The inflammatory response is neither a linear nor a self-sustaining process. Under physiological conditions, it is accompanied by the activation of termination and resolution mechanisms aimed at restoring tissue homeostasis. Crucially, the same signaling platforms that initiate inflammation (TLRs, RLRs, and NLRs) may, under specific conditions, trigger negative regulatory circuits that limit the duration and intensity of the response.

Mechanisms of inflammatory termination and resolution

Termination of inflammation involves the coordinated attenuation of PRR signaling, switching of transcriptional programs, and activation of specialized anti-inflammatory pathways. Key events include the induction of negative regulators of TLR signaling (A20, SOCS, IRAK-M), which suppress NF-κB and MAPK activation [24]; increased production of anti-inflammatory cytokines (primarily IL-10 and TGF-β), which shift the phenotype of microglia and astrocytes toward reparative programs [25, 26]; activation of specialized pro-resolving mediators (resolvins, protectins, and maresins), which reduce chemotaxis and support debris clearance [27]; inhibition of inflammasome activity and reduced secretion of IL-1β and IL-18 [28]; and efficient phagocytosis of apoptotic cells and damage-associated products (efferocytosis), which itself generates anti-inflammatory signals [29].

Within the nervous system, these processes are accompanied by the transition of microglia from a

Table 1. Integration of prr signaling with resolution, chronicity, and biomarker profiles of neuroinflammation

PRR / Platform	Key signaling pathway	Functional outcome	Activation markers	Resolution markers	Chronicity markers
TLR (TLR2/4/3/7/9)	MyD88 / TRIF → NF-κB, MAPK, IRF	Transcriptional initiation of inflammation (Signal 1)	TNF-α, IL-6, pro-IL-1β, CXCL8, IFN-β	IL-10, TGF-β, SOCS1/3	PersistentTNF-α, IL-6, STAT3- signature
RLR (RIG-I, MDA5)	MAVS → IRF3/7, NF-κB	Antiviral state + priming	IFN-α/β, ISG (MX1, OAS1)	↓IFN-I, normalization of ISGs	Chronic IFN signature, ISG persistence
NLR (NLRP3)	Inflammasome → caspase-1	Maturation of IL-1β/IL-18 (Signal 2)	IL-1β, IL-18, ASC-specks	Caspase-1 inhibition, ↓IL-1β	Recurrent activation of IL-1β/IL-18
Scavenger receptors (CD36, SR-A1)	Phagocytosis → lysosomal / mitochondrial stress	Clearance or maintenance of the DAMP loop	oxLDL, β- amyloid, HMGB1	Efferocytosis, ↓DAMPs	Cellular debris, oxLDL, sCD36
Microglia	PRR- integration	Cellular hub of neuroinflammation	sTREM2, YKL-40	Normalization of sTREM2	Chronically ↑YKL-40
Astrocytes	TLR/NF-κB, JAK/STAT	Modulation of the microenvironment	GFAP (CSF), CCL2	↓GFAP, IL-10	Sustained ↑GFAP, CCL2
Impaired clearance	Persistence of PAMPs/DAMPs → PRR reactivation	Maintenance of self-amplifying inflammatory circuits	HMGB1, mtDNA, oxLDL	Absent or reduced	IL-6, IL-1β, YKL-40, GFAP, sCD36

Note: Signal 1 refers to transcriptional priming; Signal 2 denotes inflammasome activation. ASC specks are aggregates of ASC (apoptosis-associated speck-like protein containing a CARD), indicating inflammasome assembly.

pro-inflammatory to a homeostatic or reparative state, normalization of astrocytic reactivity, and stabilization of neuron–glia interactions [30].

Features and molecular determinants of chronicity. Inflammatory chronicity develops when resolution mechanisms are insufficient or impaired. The principal processes indicating transition to the chronic phase include persistent PRR activation in response to endogenous DAMPs (mitochondrial DNA, oxidized lipids, aggregated proteins) [31]; sustained NF-κB and JAK/STAT activation, maintaining autocrine and paracrine inflammatory loops [14]; stable or recurrent activation of the NLRP3 inflammasome with chronic production of IL-1β and IL-18 [32]; impaired SR-mediated clearance of cellular and myelin debris, which sustains low-grade inflammation [30]; and phenotypic fixation of microglia and astrocytes in a reactive state accompanied by loss of homeostatic functions [33, 34].

Triggers of the neuroinflammatory process: etiological and infectious context

Despite the universality of PRR-dependent signaling mechanisms, the clinical interpretation of neuroinflammation is impossible without consideration of the etiological triggers that initiate or sustain inflammatory processes within the central nervous system. Such triggers include both infectious agents and sterile injurious factors capable of activating common PRR-mediated inflammatory programs (***Table 2***).

Of particular clinical importance are persistent or latent neurotropic infections, especially herpesviruses, which may remain within nervous tissue for prolonged periods and undergo periodic reactivation without overt manifestations of acute infection. Under such conditions, chronic or intermittent activation of RLR-dependent and TLR-dependent pathways occurs, sustaining low-grade neuroinflammation even in the absence of clinically manifest infectious disease [35].

In this context, the neuroinflammatory response may be characterized by a persistent interferon signature, inflammasome activation, and progressive BBB dysfunction, thereby shaping a phenotype of chronic neuroinflammation. Detection of viral DNA/RNA or specific antibodies in cerebrospinal fluid (CSF) and blood enables differentiation between infection-mediated neuroinflammatory processes and sterile inflammation, which is of fundamental importance for the selection of an appropriate therapeutic strategy [35].

Interpretation of PRR-mediated inflammatory signatures without etiological verification of infectious triggers may result in the misclassification of neuroinflammatory conditions and, consequently, in suboptimal therapeutic decisions [35]. Therefore, etiological verification of the pathogen or its immunological markers should be considered a contextual modifier in the interpretation of PRR activation, biomarker profiles, and treatment response.

An important, yet often underestimated, component in the initiation and maintenance of the neuroinflammatory process is inflammatory activation of the CNS vascular endothelium. Endothelial cells express PRRs and are capable of directly responding to systemic and local danger signals, including PAMPs and DAMPs. Their activation is accompanied by the induction of NF-κB-dependent and MAPK-dependent programs, expression of adhesion molecules (ICAM-1, VCAM-1), and secretion of cytokines and chemokines [36, 37].

Endothelial inflammation leads to BBB dysfunction, disruption of tight junctions, and increased permeability. Even in the absence of overt structural barrier damage, the endothelium may translate systemic inflammation into a central immune response by activating microglia and modulating neuronal function through paracrine mechanisms [36, 37].

The blood–brain barrier as a modifier of the neuroinflammatory process

The blood–brain barrier is not merely a physical boundary between the systemic circulation and the CNS, but also an active modifier of the neuroinflammatory process (***Table 3***), determining the intensity, spatial organization, and dynamics of the inflammatory response within the CNS. Its functional state changes in response to PRR-dependent signaling, as well as to the effects of cytokines, interferons, and products of tissue injury [38].

During the acute phase of inflammation or CNS injury, the BBB is frequently characterized by increased permeability, creating a therapeutic "window" while simultaneously contributing to secondary injury. In subacute and chronic conditions, the BBB may appear structurally restored while remaining functionally dysregulated, with impaired transport and persistent endothelial activation. This reduces the effectiveness of systemic therapy and increases the risk of inflammatory chronicization [39, 40].

Context-dependent manifestation of neuroinflammation across different nosologies. Although the fundamental mechanisms of neuroinflammation are universal, their manifestation differs substantially depending on the specific nosology (***Table 4***). In neurotrauma and ischemia, acute DAMP-mediated responses predominate, whereas neurodegenerative diseases are characterized by prolonged low-symptom glial activation [41]. In CNS tumors, neuroinflammation is integrated with an immunosuppressive microenvironment [42], while in chronic pain and neuropsychiatric disorders it is associated with disrupted neuron–glia communication [43, 44].

Table 2. Contextual relationship between etiological triggers and neuroinflammatory profiles

Context	What is determined?	Purpose
Suspected virus-induced inflammation	Viral DNA/RNA in the CSF	Confirmation of active or persistent infection
Latent or previous infection	IgG, CSF/serum antibody index	Identification of a potential trigger of chronicization
IFN signature without a clearly defined etiology	Antibodies + ISGs	Differentiation of sterile inflammation from infection-associated inflammation
Impaired BBB integrity	Antibodies + Q-albumin	Accurate interpretation of antibody penetration

Table 3. Therapeutic strategies in the context of the functional state of the blood–brain barrier and expected biomarkers

Therapeutic approach	Functional state of the BBB	Expected therapeutic effect	Expected biomarkers (CSF/Blood)
Corticosteroids	Acutely disrupted, "open"	Reduction of edema and suppression of cytokine release	↓IL-6, ↓TNF-α, ↓MMP-9, ↓ Q-albumin
Anti-IL-1β/anti-TNF therapy	Partially disrupted	Reduction of inflammasome and NF-κB activation	↓IL-1β, ↓IL-18, ↓CRP
JAK/STAT inhibitors	Dysfunctional, with chronic activation	Limitation of autocrine/paracrine inflammatory loops	↓STAT3-сигнатура, ↓IL-6
Antiviral therapy/IFN modulation	Acute inflammation with RLR activation	Reduction of viral load and normalization of IFN	↓IFN-α/β, ↓ISG (MX1, OAS1)
Nanoparticles, exosomes	Relatively intact	Improved drug delivery to the CNS	Targeted therapeutic markers, stable Q-albumin
Intranasal delivery	Intact	BBB bypass with localized therapeutic action	Local changes in biomarkers without systemic activation

Table 4. Nosology-specific patterns of blood–brain barrier dysfunction and mechanisms of neuroinflammation

Nosology	Typical BBB State	Dominant Mechanisms of Inflammation	Therapeutic Implications	Clinically Relevant Biomarkers (CSF/Blood)
Acute traumatic brain injury	Severely disrupted, transiently "open"	TLR/NLR activation, inflammasome activation, matrix metalloproteinases	Utilization of the therapeutic window; control of secondary injury	↑Q-albumin, ↑IL-1β, ↑TNF-α, ↑MMP-9, ↑GFAP
Ischemic stroke	Phase-dependent disruption (acute → partially restored)	TLR4, NLRP3, oxidative stress	Phase-oriented therapy; limitation of reperfusion injury	↑IL-6, ↑IL-1β, ↑S100B, ↑CRP
Neuroinfections (viral)	Disrupted	RLR → IFN-I, TLR3/7	Antiviral therapy adjusted for BBB permeability	↑IFN-α/β, ↑ISG (MX1), ↑CXCL10
Multiple sclerosis	Chronically dysfunctional	TLR/NLR signaling, adaptive immunity	Immunomodulation combined with control of barrier function	↑OCB, ↑CXCL13, ↑GFAP
Alzheimer's disease	Functionally impaired (low-grade leakage)	SR (CD36), NLRP3, DAMPs	Targeting resolution pathways and clearance mechanisms	↑Aβ, ↑p-tau, ↑YKL-40, ↑sTREM2
Parkinsonism	Partially disrupted	Microglial activation, NLRP3	Modulation of neuroinflammation	↑IL-6, ↑α-synuclein, ↑GFAP
Chronic posttraumatic encephalopathy	Dysregulated, incompletely restored	Persistent NF-κB activation, DAMPs	Combined therapy (anti-inflammatory + pro-resolution)	↑IL-6, ↑GFAP, ↑NfL
Neuro-Oncology (perifocal inflammation)	Locally disrupted	TLR/SR signaling, cytokine microenvironment	Local drug delivery and edema control	↑VEGF, ↑IL-8, ↑GFAP

Discussion

This review summarizes current concepts of neuroinflammation as a multilevel biological process arising from the interaction between sensing mechanisms, intracellular signal transduction, regulation of barrier structures, and the tissue-specific vulnerability of the CNS. Neuroinflammation is not a homogeneous pathological condition. Rather, it should be regarded as a dynamic, phase-specific program whose clinical consequences are determined by the balance among initiation, amplification, resolution, and BBB-mediated modulation [1–3].

Conceptually, it is important to distinguish at least two interconnected, yet non-identical, levels of immune activity within the CNS. The first level is the innate neuroinflammatory program, implemented predominantly by resident cells (microglia, astrocytes, and endothelial cells of the neurovascular unit) and initiated through PRR signaling in response to infectious and sterile danger signals. The second level is the adaptive immune component, characterized by the involvement of peripheral T cells and B cells, the development of clonally specific responses, and tissue-mediated injury, which may coexist with the neuroinflammatory program or predominate in certain nosologies and phases of the process [1,4]. Such stratified differentiation is required not to "divide" a single process, but to ensure accurate interpretation

of biomarkers, prognosis, and therapeutic strategy selection.

The principal conclusion is that activation of the innate neuroinflammatory program is not inherently pathological. PRR-dependent signaling provides a surveillance mechanism enabling rapid detection of infectious and sterile threats. Short-term activation of Toll-like and NOD-like receptors supports anti-infectious defense, clearance of damaged structures, and tissue adaptation. Pathological consequences arise predominantly not from activation itself, but from impaired termination and resolution, resulting in prolonged signaling, fixation of the reactive glial phenotype, and progressive tissue dysfunction [2,4]. At the same time, under conditions of a substantial contribution from the adaptive immune component (with clonal specificity and cellular infiltration), mechanisms of injury and therapeutic targets may shift from regulation of resident glia and PRR-associated pathways toward control of cellular migration, antigen-mediated responses, and effector functions of T cells and B cells [1].

The analyzed data emphasize the importance of distinguishing between the initiation phase and the persistence (chronicization) phase of neuroinflammation. At early stages, PRR-mediated activation reflects an adaptive response to acute injury, whereas prolonged activation maintained by autocrine and paracrine cytokine loops drives the transition toward a chronic, maladaptive process. This has direct translational implications: nonspecific suppression of early stages of the innate program may weaken protective mechanisms, whereas interventions aimed at controlling amplification, persistence, and/or enhancing resolution possess greater disease-modifying potential [2,4]. If the adaptive immune component predominates in a clinical context, the critical factors become the recruitment and retention phases of effector cells within the CNS, as well as the barrier mechanisms determining the intensity of infiltration. In such circumstances, the same "cytokine" signature may have different implications depending on whether it results from resident glial activation or accompanies a clonally mediated immune response [1, 3].

The BBB plays a distinct integrative role in shaping the neuroinflammatory process. It should be regarded not merely as an obstacle to drug penetration, but also as an active regulator of neuroinflammatory dynamics and therapeutic responsiveness. Inflammation-induced alterations in endothelial tight junctions, transporter expression, and neurovascular interactions transform the CNS microenvironment, influencing both immune communication and the availability of pharmacological agents. Accordingly, variability in the functional state of the BBB may explain differences in clinical responses to identical interventions depending on disease stage or individual patient characteristics [3,5–7]. Within the proposed stratification framework, the BBB has a dual role: it modulates the intensity of the innate neuroinflammatory program through endothelial activation and neurovascular signaling, while simultaneously determining the magnitude of the adaptive immune component by controlling the migration and penetration of peripheral immune cells into the CNS [3, 6].

This approach challenges the simplified use of inflammatory biomarkers. Elevated cytokine levels in blood or CSF do not invariably reflect active neuroinflammation and cannot automatically be interpreted as therapeutic targets. Interpretation should be integrative, taking into account disease phase, etiological context, and BBB status. It should also include assessment of which component predominates — the resident (innate) neuroinflammatory program or the infiltrative (adaptive immune) component. Without such differentiation, the risk of erroneous clinical decisions and overestimation of "inflammatory activity" as the sole basis for therapy substantially increases [1, 7, 8].

The situation is further complicated by the interaction between infectious and sterile triggers. Infectious insults may leave a prolonged immunological "imprint," lowering the activation threshold of the innate neuroinflammatory program during subsequent noninfectious injury. Conversely, sterile processes may mimic infectious responses through shared PRR-mediated pathways. This highlights the limitations of a purely etiological approach and substantiates the need for mechanistically grounded stratification in diagnosis and treatment [2, 3].

From a therapeutic perspective, the findings of this review support a paradigm shift from generalized anti-inflammatory suppression toward context-dependent and resolution-oriented strategies. Targeting key signaling nodes, stabilizing barrier functions, and stimulating active resolution mechanisms may provide superior outcomes compared with nonspecific cytokine blockade. At the same time, the timing of intervention is critically important: therapies effective during early stages may lose efficacy or even exert adverse effects once persistence of the neuroinflammatory program has been established or when the infiltrative adaptive immune component predominates, under which therapeutic priorities and biomarker targets may differ [1, 2, 4, 7].

Overall, neuroinflammation should be considered a modifiable biological program rather than a fixed pathological entity. Its clinical significance arises from the interaction of molecular signals, cellular responses, and barrier mechanisms that evolve over time. Recognition of this dynamic nature and of the stratification between the resident (innate) neuroinflammatory program and the infiltrative (adaptive immune) component constitutes a necessary prerequisite for translating fundamental knowledge into effective clinical strategies [1, 3].

Conclusions

Neuroinflammation is a complex, dynamic, and context-dependent biological process that extends beyond the simplified concept of local or systemic overproduction of pro-inflammatory mediators. The data summarized in this review indicate that the clinical significance of neuroinflammation is determined not by immune activation itself, but by the balance among initiation, amplification, resolution, and barrier regulation of the inflammatory response within the CNS.

A fundamental aspect is the distinction between two interconnected components of the neuroinflammatory process. The first is the innate neuroinflammatory program, implemented predominantly by resident CNS cells (microglia, astrocytes, and endothelial cells of the neurovascular unit) and initiated through PRR-dependent

sensing of infectious and sterile danger signals. Its short-term activation constitutes an essential component of immune surveillance, adaptation to injury, and tissue repair. The second is the adaptive immune component, characterized by the involvement of peripheral T cells and B cells, clonally specific responses, and tissue-mediated effects that may coexist with the innate program or predominate in certain nosologies and phases of the process.

The pathological consequences of neuroinflammation arise primarily from impaired mechanisms of termination and resolution of the innate program and/or from its sustained integration with the adaptive immune component. Persistent signaling, fixation of the reactive glial phenotype, formation of self-sustaining cytokine loops, and barrier dysfunction transform an initially protective response into a chronic pathological process underlying neurodegeneration, cognitive impairment, and reduced functional recovery.

The blood–brain barrier is a key modifier of both components of neuroinflammation. On the one hand, it regulates the intensity and spatial organization of the innate neuroinflammatory program through endothelial activation and neurovascular communication; on the other hand, it determines the magnitude and nature of the adaptive immune component by controlling the penetration and retention of peripheral immune cells within the CNS. The functional state of the BBB directly influences both biomarker interpretation and the variability of clinical responses to therapy.

The presented findings highlight the limitations of universal anti-inflammatory strategies. Effective treatment requires a context-dependent and stage-specific approach that takes into account: (1) the predominance of the innate neuroinflammatory program or the adaptive immune component, (2) the phase of the process (initiation or persistence), (3) the functional state of the BBB, and (4) the biomarker profile in blood and CSF. Under such conditions, priority should be given to strategies aimed not only at suppressing inflammation, but also at controlling amplification, stabilizing barrier functions, and stimulating active resolution mechanisms.

Overall, neuroinflammation should be regarded as a modifiable and potentially manageable biological program rather than a fixed pathological entity. A clear distinction between the resident (innate) neuroinflammatory program and the infiltrative (adaptive immune) component provides the methodological basis for accurate biomarker interpretation, personalization of therapeutic interventions, and effective translation of fundamental mechanisms into clinically meaningful solutions.

Disclosure

Acknowledgments

Certain fragments of the text were generated or edited with the assistance of ChatGPT (OpenAI, San Francisco, USA). All statements were verified by the authors.

Conflict of Interest

The authors declare no conflict of interest.

Funding

This research received no external funding.

References

1. Gong T, Liu L, Jiang W, Zhou R. DAMP-sensing receptors in sterile inflammation and inflammatory diseases. Nat Rev Immunol. 2020;20(2):95–112. doi: 10.1038/s41577-019-0215-7
2. Nathan C. Nonresolving inflammation redux. Immunity. 2022;55(4):592–605. doi: 10.1016/j.immuni.2022.03.016
3. Escartin C, Galea E, Lakatos A, O'Callaghan JP, Petzold GC, Serrano-Pozo A, Steinhäuser C, Volterra A, Carmignoto G, Agarwal A, Allen NJ, Araque A, Barbeito L, Barzilai A, Bergles DE, Bonvento G, Butt AM, Chen WT, Cohen-Salmon M, Cunningham C, Deneen B, De Strooper B, Díaz-Castro B, Farina C, Freeman M, Gallo V, Goldman JE, Goldman SA, Götz M, Gutiérrez A, Haydon PG, Heiland DH, Hol EM, Holt MG, Iino M, Kastanenka KV, Kettenmann H, Khakh BS, Koizumi S, Lee CJ, Liddelow SA, MacVicar BA, Magistretti P, Messing A, Mishra A, Molofsky AV, Murai KK, Norris CM, Okada S, Oliet SHR, Oliveira JF, Panatier A, Parpura V, Pekna M, Pekny M, Pellerin L, Perea G, Pérez-Nievas BG, Pfrieger FW, Poskanzer KE, Quintana FJ, Ransohoff RM, Riquelme-Perez M, Robel S, Rose CR, Rothstein JD, Rouach N, Rowitch DH, Semyanov A, Sirko S, Sontheimer H, Swanson RA, Vitorica J, Wanner IB, Wood LB, Wu J, Zheng B, Zimmer ER, Zorec R, Sofroniew MV, Verkhratsky A. Reactive astrocyte nomenclature, definitions, and future directions. Nat Neurosci. 2021 Mar;24(3):312-325. doi: 10.1038/s41593-020-00783-4
4. Prinz M, Masuda T, Wheeler MA, Quintana FJ. Microglia and Central Nervous System-Associated Macrophages-From Origin to Disease Modulation. Annu Rev Immunol. 2021 Apr 26;39:251-277. doi: 10.1146/annurev-immunol-093019-110159
5. Kawai T, Akira S. Regulation of innate immune signalling pathways by the tripartite motif (TRIM) family proteins. EMBO Mol Med. 2011 Sep;3(9):513-27. doi: 10.1002/emmm.201100160
6. Hampel H, Caraci F, Cuello AC, Caruso G, Nisticò R, Corbo M, Baldacci F, Toschi N, Garaci F, Chiesa PA, Verdooner SR, Akman-Anderson L, Hernández F, Ávila J, Emanuele E, Valenzuela PL, Lucía A, Watling M, Imbimbo BP, Vergallo A, Lista S. A Path Toward Precision Medicine for Neuroinflammatory Mechanisms in Alzheimer's Disease. Front Immunol. 2020 Mar 31;11:456. doi: 10.3389/fimmu.2020.00456
7. Zhang W, Xiao D, Mao Q, Xia H. Role of neuroinflammation in neurodegeneration development. Signal Transduct Target Ther. 2023 Jul 12;8(1):267. doi: 10.1038/s41392-023-01486-5
8. Paolicelli RC, Sierra A, Stevens B, Tremblay ME, Aguzzi A, Ajami B, Amit I, Audinat E, Bechmann I, Bennett M, Bennett F, Bessis A, Biber K, Bilbo S, Blurton-Jones M, Boddeke E, Brites D, Brône B, Brown GC, Butovsky O, Carson MJ, Castellano B, Colonna M, Cowley SA, Cunningham C, Davalos D, De Jager PL, de Strooper B, Denes A, Eggen BJL, Eyo U, Galea E, Garel S, Ginhoux F, Glass CK, Gokce O, Gomez-Nicola D, González B, Gordon S, Graeber MB, Greenhalgh AD, Gressens P, Greter M, Gutmann DH, Haass C, Heneka MT, Heppner FL, Hong S, Hume DA, Jung S, Kettenmann H, Kipnis J, Koyama R, Lemke G, Lynch M, Majewska A, Malcangio M, Malm T, Mancuso R, Masuda T, Matteoli M, McColl BW, Miron VE, Molofsky AV, Monje M, Mracsko E, Nadjar A, Neher JJ, Neniskyte U, Neumann H, Noda M, Peng B, Peri F, Perry VH, Popovich PG, Pridans C, Priller J, Prinz M, Ragozzino D, Ransohoff RM, Salter MW, Schaefer A, Schafer DP, Schwartz M, Simons M, Smith CJ, Streit WJ, Tay TL, Tsai LH, Verkhratsky A, von Bernhardi R, Wake H, Wittamer V, Wolf SA, Wu LJ, Wyss-Coray T. Microglia states and nomenclature: A field at its crossroads. Neuron. 2022 Nov 2;110(21):3458-3483. doi: 10.1016/j.neuron.2022.10.020
9. Deczkowska A, Weiner A, Amit I. The Physiology, Pathology, and Potential Therapeutic Applications of the TREM2 Signaling Pathway. Cell. 2020 Jun 11;181(6):1207-1217. doi: 10.1016/j.cell.2020.05.003
10. Pascual M, Calvo-Rodriguez M, Núñez L, Villalobos C, Ureña J, Guerri C. Toll-like receptors in neuroinflammation, neurodegeneration, and alcohol-induced brain damage.

IUBMB Life. 2021 Jul;73(7):900-915. doi: 10.1002/iub.2510
11. Kodi T, Sankhe R, Gopinathan A, Nandakumar K, Kishore A. New Insights on NLRP3 Inflammasome: Mechanisms of Activation, Inhibition, and Epigenetic Regulation. J Neuroimmune Pharmacol. 2024 Feb 29;19(1):7. doi: 10.1007/s11481-024-10101-5
12. Stok JE, Vega Quiroz ME, van der Veen AG. Self RNA Sensing by RIG-I-like Receptors in Viral Infection and Sterile Inflammation. J Immunol. 2020 Aug 15;205(4):883-891. doi: 10.4049/jimmunol.2000488
13. Garcia-Bonilla L, Sciortino R, Shahanoor Z, Racchumi G, Janakiraman M, Montaner J, Zhou P, Anrather J, Iadecola C. Role of microglial and endothelial CD36 in post-ischemic inflammasome activation and interleukin-1β-induced endothelial activation. Brain Behav Immun. 2021 Jul;95:489-501. doi: 10.1016/j.bbi.2021.04.010
14. Ageeva T, Rizvanov A, Mukhamedshina Y. NF-κB and JAK/STAT Signaling Pathways as Crucial Regulators of Neuroinflammation and Astrocyte Modulation in Spinal Cord Injury. Cells. 2024 Mar 26;13(7):581. doi: 10.3390/cells13070581
15. Andronie-Cioara FL, Ardelean AI, Nistor-Cseppento CD, Jurcau A, Jurcau MC, Pascalau N, Marcu F. Molecular Mechanisms of Neuroinflammation in Aging and Alzheimer's Disease Progression. Int J Mol Sci. 2023 Jan 18;24(3):1869. doi: 10.3390/ijms24031869
16. Müller L, Di Benedetto S, Müller V. The dual nature of neuroinflammation in networked brain. Front Immunol. 2025 Aug 20;16:1659947. doi: 10.3389/fimmu.2025.1659947
17. He KL, Yu X, Xia L, Xie YD, Qi EB, Wan L, Hua XM, Jing CH. A new perspective on the regulation of neuroinflammation in intracerebral hemorrhage: mechanisms of NLRP3 inflammasome activation and therapeutic strategies. Front Immunol. 2025 Feb 27;16:1526786. doi: 10.3389/fimmu.2025.1526786
18. Darabniya A. The neuroinflammatory triumvirate: NF-κB, NLRP3, and mTOR in spinal cord injury. Inflammopharmacology. 2025 Oct;33(10):5769-5775. doi: 10.1007/s10787-025-01952-2
19. Dorrity TJ, Shin H, Gertie JA, Chung H. The Sixth Sense: Self-nucleic acid sensing in the brain. Adv Immunol. 2024;161:53-83. doi: 10.1016/bs.ai.2024.03.001
20. Ding S, Choi SH, Miller YI. Amyloid β-Induced Inflammarafts in Alzheimer's Disease. Int J Mol Sci. 2025 May 10;26(10):4592. doi: 10.3390/ijms26104592
21. Hassan H, Rawlinson C, Lan YL, Jenkins S, Chen R. Microglia-Mediated Phagocytosis in Alzheimer's Disease: Mechanisms, Heterogeneity, and Therapeutic Insights. Biomolecules. 2025 Nov 20;15(11):1629. doi: 10.3390/biom15111629
22. He L, Zhang R, Yang M, Lu M. The role of astrocyte in neuroinflammation in traumatic brain injury. Biochim Biophys Acta Mol Basis Dis. 2024 Mar;1870(3):166992. doi: 10.1016/j.bbadis.2023.166992
23. Roh JS, Sohn DH. Damage-Associated Molecular Patterns in Inflammatory Diseases. Immune Netw. 2018 Aug 13;18(4):e27. doi: 10.4110/in.2018.18.e27
24. Wang AG, Son M, Kenna E, Thom N, Tay S. NF-κB memory coordinates transcriptional responses to dynamic inflammatory stimuli. Cell Rep. 2022 Aug 16;40(7):111159. doi: 10.1016/j.celrep.2022.111159
25. Cavalcanti RR, Almeida FM, Martinez AMB, Freria CM. Neuroinflammation: targeting microglia for neuroprotection and repair after spinal cord injury. Front Immunol. 2025 Oct 6;16:1670650. doi: 10.3389/fimmu.2025.1670650
26. Lößlein L, Linnerbauer M, Zuber F, Tsaktanis T, Vandrey O, Peter A, Panier F, Zissler J, Riekher V, Bäuerle T, Hanspach J, Laun FB, Nagel L, Mészáros L, Zunke F, Winkler J, Naumann UJ, Schwingen N, Neumaier E, Liesz A, Quintana F, Rothhammer V. TGFα controls checkpoints in CNS resident and infiltrating immune cells to promote resolution of inflammation. Nat Commun. 2025 Jun 19;16(1):5344. doi: 10.1038/s41467-025-60363-7
27. Serhan CN, Chiang N. Resolvins and cysteinyl-containing pro-resolving mediators activate resolution of infectious inflammation and tissue regeneration. Prostaglandins Other Lipid Mediat. 2023 Jun;166:106718. doi: 10.1016/j.prostaglandins.2023.106718
28. Xu W, Huang Y, Zhou R. NLRP3 inflammasome in neuroinflammation and central nervous system diseases. Cell Mol Immunol. 2025 Apr;22(4):341-355. doi: 10.1038/s41423-025-01275-w
29. Andoh M, Koyama R. Comparative Review of Microglia and Monocytes in CNS Phagocytosis. Cells. 2021 Sep 27;10(10):2555. doi: 10.3390/cells10102555
30. Ahremenko E, Andreev A, Apushkin D, Korkotian E. Glial Cells in the Early Stages of Neurodegeneration: Pathogenesis and Therapeutic Targets. Int J Mol Sci. 2025 Dec 12;26(24):11995. doi: 10.3390/ijms262411995
31. Lin H, Xiong W, Fu L, Yi J, Yang J. Damage-associated molecular patterns (DAMPs) in diseases: implications for therapy. Mol Biomed. 2025 Aug 29;6(1):60. doi: 10.1186/s43556-025-00305-3
32. Chiarini A, Gui L, Viviani C, Armato U, Dal Prà I. NLRP3 Inflammasome's Activation in Acute and Chronic Brain Diseases-An Update on Pathogenetic Mechanisms and Therapeutic Perspectives with Respect to Other Inflammasomes. Biomedicines. 2023 Mar 23;11(4):999. doi: 10.3390/biomedicines11040999
33. Taban Q, Mumtaz PT, Masoodi KZ, Haq E, Ahmad SM. Scavenger receptors in host defense: from functional aspects to mode of action. Cell Commun Signal. 2022 Jan 3;20(1):2. doi: 10.1186/s12964-021-00812-0
34. Walz W. Reactive microglia and astrocyte phenotype transitions: a framework. In: The Gliocentric Brain. Cham: Springer; 2023. doi: 10.1007/978-3-031-48105-5_4
35. Graninger M, Puchhammer-Stöckl E, Vietzen H. Herpesvirus-host interactions in neurological diseases: the immunogenetic role of HLA-E. J Virol. 2025 Dec 23;99(12):e0086925. doi: 10.1128/jvi.00869-25
36. Acioglu C, Elkabes S. Innate immune sensors and regulators at the blood brain barrier: focus on toll-like receptors and inflammasomes as mediators of neuro-immune crosstalk and inflammation. J Neuroinflammation. 2025 Feb 15;22(1):39. doi: 10.1186/s12974-025-03360-3
37. Gullotta GS, Costantino G, Sortino MA, Spampinato SF. Microglia and the Blood-Brain Barrier: An External Player in Acute and Chronic Neuroinflammatory Conditions. Int J Mol Sci. 2023 May 23;24(11):9144. doi: 10.3390/ijms24119144
38. Gryka-Marton M, Grabowska AD, Szukiewicz D. Breaking the Barrier: The Role of Proinflammatory Cytokines in BBB Dysfunction. Int J Mol Sci. 2025 Apr 9;26(8):3532. doi: 10.3390/ijms26083532
39. Wu D, Chen Q, Chen X, Han F, Chen Z, Wang Y. The blood-brain barrier: structure, regulation, and drug delivery. Signal Transduct Target Ther. 2023 May 25;8(1):217. doi: 10.1038/s41392-023-01481-w
40. Archie SR, Al Shoyaib A, Cucullo L. Blood-Brain Barrier Dysfunction in CNS Disorders and Putative Therapeutic Targets: An Overview. Pharmaceutics. 2021 Oct 26;13(11):1779. doi: 10.3390/pharmaceutics13111779
41. French SR, Meyer BP, Arias JC, Levendovzsky SR, Weinkauf CC. Biomarkers of blood-brain barrier and neurovascular unit integrity in human cognitive impairment and dementia. Alzheimers Dement. 2025 Mar;21(3):e70104. doi: 10.1002/alz.70104
42. Stanzione R, Forte M, Cotugno M, Bianchi F, Marchitti S, Rubattu S. Role of DAMPs and leukocyte infiltration in ischemic stroke: insights from animal models and translation to the human disease. Cell Mol Neurobiol. 2022;42(3):545-56. doi: 10.1007/s10571-020-00966-4
43. Bao Y, Chen Z, Su Y, Guo T, Du H, Jia X. From neuroinflammation to gliomagenesis: immune drivers of malignant transformation in the CNS. Front Immunol. 2025 Dec 1;16:1682030. doi: 10.3389/fimmu.2025.1682030
44. McKenzie A, Dombrower R, Theeraphapphong N, McKenzie S, Hijazin MA. Glial Activation, Neuroinflammation, and Loss of Neuroprotection in Chronic Pain: Cellular Mechanisms and Emerging Therapeutic Strategies. Biomedicines. 2025 Dec 26;14(1):58. doi: 10.3390/biomedicines14010058

Review article

Ukrainian Neurosurgical Journal. 2026;32(2):12-15
doi: 10.25305/unj.349329

Post-traumatic seizures and post-traumatic epilepsy after traumatic brain injury: current approaches to prevention, diagnosis, and risk prediction

Bozhena V. Zadorozhna [1], Volodymyr M. Shevaga [2]

[1] Department of Family Medicine, Cardiology and Emergency Medicine, Danylo Halytsky National Medical University, Lviv, Ukraine
[2] Department of Neurology, Danylo Halytsky National Medical University, Lviv, Ukraine

Received: 03 January 2026
Accepted: 02 March 2026

Address for correspondence:
Bozhena V. Zadorozhna, Department of Family Medicine, Cardiology and Emergency Medicine, Danylo Halytsky National Medical University, 69 Pekarska street, Lviv, 79010, Ukraine, e-mail: bozhenazadorozhna@gmail.com

Objective: To summarize current international and national evidence regarding the mechanisms underlying posttraumatic seizures and posttraumatic epilepsy following traumatic brain injury, to identify the main clinically relevant risk factors, and to outline approaches to seizure prophylaxis, neurophysiological monitoring, and prediction of long-term outcomes.

Materials and methods: Publications from the PubMed, Scopus, and Web of Science databases, published predominantly between 2020 and 2025, as well as relevant national sources, were analyzed. The review included clinical practice guidelines, systematic reviews, meta-analyses, and key original studies addressing posttraumatic seizures and epileptogenesis after traumatic brain injury.

Results: Early posttraumatic seizures were found to be primarily associated with acute metabolic and structural brain disturbances, whereas late seizures are usually considered a clinical manifestation of established posttraumatic epilepsy resulting from prolonged processes of epileptogenesis, neuroinflammation, microglial activation, and synaptic network remodeling. Prophylactic use of antiseizure medications is associated with a reduction in the incidence of early posttraumatic seizures but does not prevent the development of posttraumatic epilepsy. Electroencephalography and continuous EEG monitoring play an important role in risk stratification and in the detection of subclinical (nonconvulsive) seizures.

Conclusions: Management of patients with traumatic brain injury and posttraumatic seizures requires a differentiated multidisciplinary approach integrating clinical, neurophysiological, and neuroimaging risk factors. Further research should focus on improving prediction of posttraumatic epilepsy and identifying validated biomarkers of epileptogenesis.

Keywords: *traumatic brain injury; posttraumatic seizures; posttraumatic epilepsy; electroencephalography; seizure prophylaxis*

Introduction

Traumatic brain injury (TBI) remains one of the leading causes of persistent neurological impairment, disability, and symptomatic epileptic seizures in the adult population. According to contemporary epidemiological studies, the prevalence of TBI continues to increase, which is associated with road traffic injuries, urbanization, occupational trauma, and armed conflicts [1].

According to estimates from the Global Burden of Disease study, approximately 20.8 million new cases of TBI were registered worldwide in 2021, whereas the total number of individuals living with the consequences of traumatic head injury reached approximately 37.9 million. Mild TBI predominates (70–90%), whereas moderate and severe injuries are less common but are associated with the highest risks of mortality, disability, and long-term neurological complications [2–5].

Among the most clinically significant complications of TBI are post-traumatic seizures and post-traumatic epilepsy. Post-traumatic seizures not only complicate the acute phase of injury but also adversely affect recovery processes, are associated with an increased risk of secondary brain injury, prolonged hospitalization, and reduced long-term quality of life [6, 7].

According to various studies, early post-traumatic seizures occur in 2–10% of patients, depending on injury severity and the clinical population studied [8, 9]. The risk of developing delayed post-traumatic epilepsy after TBI is substantial and increases with injury severity. In some patients with severe TBI, the risk of epilepsy may exceed 12–15% during subsequent years of follow-up [10, 11]. Several reviews have summarized data regarding the incidence and risk factors of post-traumatic epilepsy across different age groups and clinical subpopulations [12, 13].

It has been established that seizure development after TBI is associated with poorer functional outcomes and an increased risk of long-term neurological complications, including cognitive impairment and dementia [14, 15]. Studies by leading researchers

emphasize the necessity of a differentiated approach to the prevention of post-traumatic seizures, timely implementation of EEG monitoring, and interdisciplinary management of patients with severe TBI [16, 17].

Objective: To summarize current international and national evidence regarding the mechanisms underlying post-traumatic seizures and post-traumatic epilepsy following traumatic brain injury, to identify the principal clinically significant risk factors, and to outline current approaches to seizure prophylaxis, neurophysiological monitoring, and prediction of long-term outcomes.

Materials and methods

A literature search was conducted using the PubMed and MEDLINE databases, as well as specialized Ukrainian scientific publications. The analysis included clinical practice guidelines issued by professional societies, systematic reviews, meta-analyses, cohort studies, and review articles published predominantly between 2020 and 2025, together with seminal studies of conceptual importance for understanding post-traumatic epileptogenesis.

The inclusion criteria comprised publications addressing post-traumatic seizures, post-traumatic epilepsy, seizure prophylaxis after TBI, the use of electroencephalography (EEG) and continuous EEG monitoring, as well as prediction of neurological outcomes following traumatic brain injury. In total, 31 sources were analyzed, including both contemporary publications and classical studies that established the principal approaches to this problem.

In contemporary clinical practice, post-traumatic seizures are generally classified as early (within 7 days after injury) and late (occurring more than 7 days after injury) [18]. Several clinical and neurosurgical publications describe seizures occurring within the first 24 h after TBI as manifestations of acute brain injury associated with primary structural and metabolic disturbances [7, 18, 19]. In the present review, such seizures are considered within the category of early post-traumatic seizures.

Early post-traumatic seizures are generally associated with acute structural and metabolic alterations, among which cerebral edema, intracranial hemorrhage, exposure of cortical tissue to blood products, disruption of ionic homeostasis, and ischemic injury play central roles [19]. These changes occur more frequently in patients with severe TBI, penetrating injuries, and intracranial hemorrhages and are associated with an increased risk of secondary brain injury and potentially poorer short-term treatment outcomes [8, 9].

Late post-traumatic seizures are regarded as a clinical manifestation of established or evolving post-traumatic epilepsy caused by prolonged processes of epileptogenesis, neuroinflammation, and neuronal network remodeling [20–22].

The principal risk factors for the development of post-traumatic seizures/post-traumatic epilepsy include severe TBI, cortical injuries (contusions), intracranial hemorrhages (particularly subdural hemorrhages), diffuse or multifocal traumatic brain injury, as well as neurosurgical interventions, which may serve as markers of injury severity and structural brain damage [10, 13, 19, 21, 23]. Particularly high risks of post-traumatic epilepsy are observed in patients with cortical contusions and other structural cortical injuries, especially in the presence of intracranial hemorrhage. This association is believed to result from prolonged epileptogenic processes and neuronal network remodeling within the area of traumatic injury [13, 20, 21, 24].

Electroencephalography performed at hospital admission after severe TBI may be useful for stratification of the risk of post-traumatic epilepsy [25].

According to current international clinical guidelines, prophylactic administration of antiseizure medications in patients with moderate-to-severe TBI who are at high risk of seizures significantly reduces the incidence of early post-traumatic seizures. However, convincing evidence supporting the effectiveness of such therapy in preventing the long-term development of post-traumatic epilepsy has not been demonstrated [25–27].

Meta-analyses conducted in recent years have demonstrated comparable efficacy of phenytoin and levetiracetam for the prevention of early post-traumatic seizures. Levetiracetam is characterized by a more favorable safety and tolerability profile, which is of particular importance in patients with polytrauma and concomitant somatic disorders [26–28].

The first post-traumatic seizure occurring during the acute phase of TBI is regarded as an acute symptomatic seizure and requires a therapeutic approach focused on correction of the acute underlying cause and seizure control rather than a purely prophylactic strategy [29–31].

Decisions regarding continuation or initiation of long-term antiseizure therapy after a seizure occurring during the acute phase of TBI should be made on an individual basis, taking into account clinical risk factors and neuroimaging findings associated with an increased risk of post-traumatic epilepsy [13, 21].

Conclusions

1. Post-traumatic seizures are a common and clinically significant complication of traumatic brain injury (TBI).
2. Prophylactic antiseizure therapy is effective only in preventing early post-traumatic seizures and does not reduce the risk of developing post-traumatic epilepsy.
3. Electroencephalography and continuous EEG monitoring play an important role in the detection of subclinical (nonconvulsive) seizures and in risk stratification for post-traumatic epilepsy.
4. Management of patients after TBI requires a differentiated multidisciplinary approach involving both neurologists and neurosurgeons.

Clinical recommendation

Prophylactic antiseizure therapy should be administered to patients with moderate-to-severe TBI who are at high risk of early post-traumatic seizures, including those with cortical injuries, intracranial hemorrhages, penetrating trauma, or a history of neurosurgical interventions.

Levetiracetam is considered the preferred agent at a dosage of 500–1000 mg twice daily, administered either intravenously or orally. Phenytoin may be used

as an alternative, with a loading dose of 15–20 mg/kg followed by maintenance therapy.

The duration of prophylactic therapy should not exceed 7 days in the absence of clinical or EEG evidence of seizure activity.

For patients with severe TBI admitted to intensive care units, the use of EEG and continuous EEG monitoring is recommended for early detection of subclinical (nonconvulsive) seizures and optimization of treatment strategies.

Disclosure information

Conflict of Interest

The authors declare no conflict of interest.

Ethical Standards

This article is a literature review; therefore, approval by Ethics Committee was not required.

Funding

The study received no external funding or sponsorship.

References

1. American College of Surgeons. Best practices guidelines: traumatic brain injury. Chicago: American College of Surgeons; 2024. https://www.facs.org/media/vgfgjpfk/best-practices-guidelines-traumatic-brain-injury.pdf
2. Gu L, Zhang L, Li C, Jiang L, Zhou J, Xie Y, Yang J, Jiang C, Zhang L, Jiang Y, Peng J. Global, Regional, and National Burden of Traumatic Brain Injury, 1990-2021: A Systematic Analysis for the Global Burden of Disease Study 2021. J Neurotrauma. 2025 Oct;42(19-20):1805-1815. doi: 10.1089/neu.2025.0039
3. Zhong H, Feng Y, Shen J, Rao T, Dai H, Zhong W, Zhao G. Global Burden of Traumatic Brain Injury in 204 Countries and Territories From 1990 to 2021. Am J Prev Med. 2025 Apr;68(4):754-763. doi: 10.1016/j.amepre.2025.01.001
4. Maas AIR, Menon DK, Adelson PD, Andelic N, Bell MJ, Belli A, Bragge P, Brazinova A, Büki A, Chesnut RM, Citerio G, Coburn M, Cooper DJ, Crowder AT, Czeiter E, Czosnyka M, Diaz-Arrastia R, Dreier JP, Duhaime AC, Ercole A, van Essen TA, Feigin VL, Gao G, Giacino J, Gonzalez-Lara LE, Gruen RL, Gupta D, Hartings JA, Hill S, Jiang JY, Ketharanathan N, Kompanje EJO, Lanyon L, Laureys S, Lecky F, Levin H, Lingsma HF, Maegele M, Majdan M, Manley G, Marsteller J, Mascia L, McFadyen C, Mondello S, Newcombe V, Palotie A, Parizel PM, Peul W, Piercy J, Polinder S, Puybasset L, Rasmussen TE, Rossaint R, Smielewski P, Söderberg J, Stanworth SJ, Stein MB, von Steinbüchel N, Stewart W, Steyerberg EW, Stocchetti N, Synnot A, Te Ao B, Tenovuo O, Theadom A, Tibboel D, Videtta W, Wang KKW, Williams WH, Wilson L, Yaffe K; InTBIR Participants and Investigators. Traumatic brain injury: integrated approaches to improve prevention, clinical care, and research. Lancet Neurol. 2017 Dec;16(12):987-1048. doi: 10.1016/S1474-4422(17)30371-X
5. Carroll LJ, Cassidy JD, Holm L, Kraus J, Coronado VG; WHO Collaborating Centre Task Force on Mild Traumatic Brain Injury. Methodological issues and research recommendations for mild traumatic brain injury: the WHO Collaborating Centre Task Force on Mild Traumatic Brain Injury. J Rehabil Med. 2004 Feb;(43 Suppl):113-25. doi: 10.1080/16501960410023877
6. Englander J, Bushnik T, Duong TT, Cifu DX, Zafonte R, Wright J, Hughes R, Bergman W. Analyzing risk factors for late posttraumatic seizures: a prospective, multicenter investigation. Arch Phys Med Rehabil. 2003 Mar;84(3):365-73. doi: 10.1053/apmr.2003.50022
7. Annegers JF, Hauser WA, Coan SP, Rocca WA. A population-based study of seizures after traumatic brain injuries. N Engl J Med. 1998 Jan 1;338(1):20-4. doi: 10.1056/NEJM199801013380104
8. Pease M, Mittal A, Merkaj S, Okonkwo DO, Gonzalez-Martinez JA, Elmer J, Liou WS, Pingue V, Hammond FM, Abramovici S, Castellano J, Barot N. Early Seizure Prophylaxis in Mild and Moderate Traumatic Brain Injury: A Systematic Review and Meta-Analysis. JAMA Neurol. 2024 May 1;81(5):507-514. doi: 10.1001/jamaneurol.2024.0689
9. Baye ND, Baye FD, Teshome AA, Ayenew AA, Mulu AT, Abebe EC, Muche ZT. Incidence and predictors of early posttraumatic seizures among patients with moderate or severe traumatic brain injury in Northwest Ethiopia: an institution-based prospective study. BMC Neurol. 2024 Jan 24;24(1):41. doi: 10.1186/s12883-024-03536-z
10. Sødal HF, Nordseth T, Rasmussen AJO, Rosseland LA, Stenehjem JS, Gran JM, Helseth E, Taubøll E. Risk of epilepsy after traumatic brain injury: a nationwide Norwegian matched cohort study. Front Neurol. 2024 Jun 5;15:1411692. doi: 10.3389/fneur.2024.1411692
11. Karlander M, Håkansson S, Ljungqvist J, Sörbo A, Zelano J. Risk of Epilepsy Following a First Posttraumatic Seizure: A Register-Based Study. Neurol Clin Pract. 2025 Feb;15(1):e200409. doi: 10.1212/CPJ.0000000000200409
12. Mavroudis I, Franekova K, Petridis F, Ciobica A, Dăscălescu G, Anton CR, Ilea C, Papagiannopoulos S, Kazis D, Anton E. Post-Traumatic Epilepsy After Mild and Moderate Traumatic Brain Injury: A Narrative Review and Development of a Clinical Decision Tool. Reports (MDPI). 2025 Sep 29;8(4):193. doi: 10.3390/reports8040193
13. Mariajoseph FP, Chen Z, Sekhar P, Rewell SS, O'Brien TJ, Antonic-Baker A, Semple BD. Incidence and risk factors of posttraumatic epilepsy following pediatric traumatic brain injury: A systematic review and meta-analysis. Epilepsia. 2022 Nov;63(11):2802-2812. doi: 10.1111/epi.17398
14. Schneider ALC, Law CA, Gottesman RF, Krauss G, Huang J, Kucharska-Newton A, Jensen FE, Gugger JJ, Diaz-Arrastia R, Johnson EL. Posttraumatic Epilepsy and Dementia Risk. JAMA Neurol. 2024 Feb 26;81(4):346–53. doi: 10.1001/jamaneurol.2024.0010
15. Kotas D, Zhao H, Turella J, Kasoff WS. Post-Traumatic Epilepsy: Observations from an Urban Level 1 Trauma Center. Neurol Int. 2024 Aug 5;16(4):845-852. doi: 10.3390/neurolint16040063
16. Pease M, Elmer J, Shahabadi AZ, Mallela AN, Ruiz-Rodriguez JF, Sexton D, Barot N, Gonzalez-Martinez JA, Shutter L, Okonkwo DO, Castellano JF. Predicting posttraumatic epilepsy using admission electroencephalography after severe traumatic brain injury. Epilepsia. 2023 Jul;64(7):1842-1852. doi: 10.1111/epi.17622
17. Kazis D, Chatzikonstantinou S, Ciobica A, Kamal FZ, Burlui V, Calin G, Mavroudis I. Epidemiology, Risk Factors, and Biomarkers of Post-Traumatic Epilepsy: A Comprehensive Overview. Biomedicines. 2024 Feb 9;12(2):410. doi: 10.3390/biomedicines12020410
18. Temkin NR. Preventing and treating posttraumatic seizures: the human experience. Epilepsia. 2009 Feb;50 Suppl 2:10-3. doi: 10.1111/j.1528-1167.2008.02005.x
19. Sødal HF, Storvig G, Tverdal C, Robinson HS, Helseth E, Taubøll E. Early post-traumatic seizures in hospitalized patients with traumatic brain injury. Acta Neurol Scand. 2022 Nov;146(5):485-491. doi: 10.1111/ane.13670
20. Diaz-Arrastia R, Agostini MA, Madden CJ, Van Ness PC. Posttraumatic epilepsy: the endophenotypes of a human model of epileptogenesis. Epilepsia. 2009 Feb;50 Suppl 2:14-20. doi: 10.1111/j.1528-1167.2008.02006.x
21. Xu T, Yu X, Ou S, Liu X, Yuan J, Huang H, Yang J, He L, Chen Y. Risk factors for posttraumatic epilepsy: A systematic review and meta-analysis. Epilepsy Behav. 2017 Feb;67:1-6. doi: 10.1016/j.yebeh.2016.10.026
22. Орос ММ, Смоланка ВІ, ред. Епілепсія це… Ужгород: Ужгородський національний університет; 2021. https://dspace.uzhnu.edu.ua/handle/lib/77487 Oros MM, Smolanka VI, eds. Epilepsy is… Uzhhorod: Uzhhorod National University; 2021. https://dspace.uzhnu.edu.ua/handle/lib/77487
23. Khalili H, Kashkooli NR, Niakan A, Asadi-Pooya AA. Risk factors for post-traumatic epilepsy. Seizure. 2021 Jul;89:81-84. doi: 10.1016/j.seizure.2021.05.004
24. Yazdi SM, Gomez AJ, Goldman A, Tsetsou S. The path to post-traumatic epilepsy: A review of emerging biomarkers and therapeutic targets. Seizure. 2025 Dec;133:195-201. doi: 10.1016/j.seizure.2025.10.021

25. Frontera JA, Gilmore EJ, Johnson EL, Olson D, Rayi A, Tesoro E, Ullman J, Yuan Y, Zafar SF, Rowe S. Guidelines for Seizure Prophylaxis in Adults Hospitalized with Moderate-Severe Traumatic Brain Injury: A Clinical Practice Guideline for Health Care Professionals from the Neurocritical Care Society. Neurocrit Care. 2024 Jun;40(3):819-844. doi: 10.1007/s12028-023-01907-x
26. Angriman F, Taran S, Angeloni N, Devion C, Lee JW, Adhikari NKJ. Antiseizure Medications in Adult Patients With Traumatic Brain Injury: A Systematic Review and Bayesian Network Meta-Analysis. Crit Care Explor. 2024 Sep 25;6(10):e1160. doi: 10.1097/CCE.0000000000001160
27. Huo X, Xu X, Li M, Xiao L, Wang Y, Li W, Wang C, Sun T. Effectiveness of antiseizure medications therapy in preventing seizures in brain injury patients: A network meta-analysis. Front Pharmacol. 2022 Sep 15;13:1001363. doi: 10.3389/fphar.2022.1001363
28. Karamian A, Farzaneh H, Taheri M, Seifi A. Effectiveness of Levetiracetam versus phenytoin in preventing seizure in traumatic brain injury patients: A systematic review and meta-analysis. Clin Neurol Neurosurg. 2024 May;240:108251. doi: 10.1016/j.clineuro.2024.108251
29. Pohlmann-Eden B, Beghi E, Camfield C, Camfield P. The first seizure and its management in adults and children. BMJ. 2006 Feb 11;332(7537):339-42. doi: 10.1136/bmj.332.7537.339
30. Beghi E, Carpio A, Forsgren L, Hesdorffer DC, Malmgren K, Sander JW, Tomson T, Hauser WA. Recommendation for a definition of acute symptomatic seizure. Epilepsia. 2010 Apr;51(4):671-5. doi: 10.1111/j.1528-1167.2009.02285.x
31. Herzig-Nichtweiß J, Salih F, Berning S, Malter MP, Pelz JO, Lochner P, Wittstock M, Günther A, Alonso A, Fuhrer H, Schönenberger S, Petersen M, Kohle F, Müller A, Gawlitza A, Gubarev W, Holtkamp M, Vorderwülbecke BJ; IGNITE! study group. Prognosis and management of acute symptomatic seizures: a prospective, multicenter, observational study. Ann Intensive Care. 2023 Sep 15;13(1):85. doi: 10.1186/s13613-023-01183-0

Original article

Ukrainian Neurosurgical Journal. 2026;32(2):16-22
doi: 10.25305/unj.341653

Primary reconstruction of skull vault defects after burns

Oleksandr A. Zhernov [1,2], Oleksandr I. Kovalchuk [2], Mykhailo P. Komarov [3]

1 Department of Reconstructive, Minimally Invasive and Plastic Surgery, Treatment Unit No. 8 of the Kyiv Medical Center, Kyiv, Ukraine
2 Department of combustiology and plastic surgery, Shupyk National Healthcare University of Ukraine. Kyiv, Ukraine
3 Department of Traumatic Brain Injury and Spinal Neurosurgery, Romodanov Neurosurgery Institute, Kyiv, Ukraine

Received: 19 October 2025
Accepted: 15 December 2025

Address for correspondence*: Oleksandr I. Kovalchuk, Department of Surgery, Combustiology and Plastic Surgery, Shupyk National University of Health Care of Ukraine, 9 Dorohozhytska St., Kyiv, 04112, Ukraine, e-mail: kovalchukoleksandr1@gmail.com*

Restoration of skull vault defects is especially important in the early stages of treatment, which minimizes the number of purulent and necrotic complications involving both the skull and the underlying deep structures.

Objective: To develop the most rational approach and surgical tactics for the rehabilitation treatment of patients with defects of the cranial vault after burns under conditions of primary reconstruction.

Materials and methods: We observed 16 patients with cranial vault lesions aged from 2 months to 46 years (average age, 25.3 years). Three groups of patients were identified.

- Lesions of superficial tissues without periosteal involvement (4 patients 25.0%);

- Soft tissue and periosteum lesions with exposure of the cortical bone layer (6 patients, 37.5%).

- Deep soft tissue and bone lesions (6 patients, 37.5%)

Depending of the depth, area of damaged tissue and localization of the defect, as well as the presence of unaffected areas, skin grafting, revascularizing interventions using complex flaps, bone milling or removal were used.

Results: The engraftment of skin grafts in patients in whom this method was used as the primary technique for closing defects was 70%. Complete engraftment of local and regional flaps occurred in all cases. Necrosis of up to 30% of the trapezius muscle flap occurred in one case. The study demonstrated the possibility of primary closure of cranial vault defects in patients with various lesions of anatomical structures.

Conclusions: The use of a differentiated approach to the treatment of skull vault defects ensures favorable therapeutic outcomes for patients.

Keywords: *cranial vault defects; post-burn cranial injury; complex flaps; plastic surgery; primary reconstruction; cranial defect closure*

Introduction

Defects of the cranial vault develop following deep flame burns, electrical and thermomechanical injuries, mechanical trauma, and infectious lesions of the soft tissues. Surgical treatment of this category of patients represents a complex clinical challenge because of the deficiency of soft tissues. This necessitates a nonstandardized approach to the selection of treatment strategies and surgical techniques [1].

Surgical management of these patients requires meticulous preoperative planning, which significantly reduces the risk of postoperative complications and improves the long-term quality of life of affected individuals [2].

Tissues of the cranial vault from adjacent areas are commonly used for defect reconstruction. However, the frequent damage to surrounding tissues and the presence of degenerative and dystrophic changes often necessitate revascularization of the affected area [1]. Fasciocutaneous and musculocutaneous flaps are best suited to these requirements, providing well-vascularized tissue coverage and stable skin reconstruction [3–6]. Nevertheless, the high incidence of complications, as well as the complexity and prolonged duration of microsurgical procedures, limit their widespread use. Damage to the aponeurotic layer, periosteum, and cranial bones requires the development of new reconstructive approaches.

Restoration of cranial vault defects is particularly important in the early stages of treatment, as it minimizes the risk of purulent and necrotic complications involving both the skull and the underlying deep structures.

Objective. To develop the most rational approach and surgical tactics for the rehabilitative treatment of patients with cranial vault defects after burns under conditions of primary reconstruction.

Materials and methods

Study participants

The study included 16 patients with cranial vault injuries aged from 2 months to 46 years (mean age, 25.3 years), five of whom were children under 14 years. Among the patients, 11 were male and 5 were female.

In 9 (56.2%) patients, the defects developed as a result of flame burns; in 4 (25.0%), after high-voltage electrical injuries; in 1 (6.2%), after a scald burn; in 1 (6.2%), after a chemical burn caused by sulfuric acid; and in 1 (6.2%), as a result of a contact burn. The total body surface area affected ranged from 1% to 60% (mean, 21.3%). The defect area ranged from 60 to 280 cm² (mean, 170.5 cm²).

Inclusion criteria:

- male and female patients aged from 2 months to 50 years;
- patients with cranial vault defects after burns;
- obtained informed consent for data collection, processing, and publication of aggregated results while maintaining strict confidentiality.

Exclusion criteria

- age over 50 years;
- cardiovascular, pulmonary, or cerebral dysfunction, as well as other diseases in the stage of subcompensation or decompensation;
- tuberculosis;
- HIV infection;
- positive Wassermann reaction (RW) test result;
- psychiatric disorders;
- refusal to participate in the study.

Group characteristics

When selecting the surgical strategy and treatment methods, the depth and extent of tissue damage, defect localization, and the presence of unaffected adjacent tissues were taken into account. Accordingly, three groups of patients were identified:

- lesions of the covering tissues extending to the periosteum of the cranial bones (4 patients, 25.0%);
- lesions of the soft tissues and periosteum with exposure of the cortical bone layer (6 patients, 37.5%);
- deep lesions involving both soft tissues and cranial bones (6 patients, 37.5%).

Surgical treatment was generally performed 2–4 days after hospital admission. During the preoperative period, intensive infusion and transfusion therapy was administered, including blood products when indicated, agents aimed at improving hemomicrocirculation, and antibiotics. Locally, wet-to-dry dressings or hydrophilic ointments were applied. In 8 (50.0%) patients, preoperative preparation lasted more than 6 days because of the need to correct cardiovascular function and carbohydrate metabolism parameters.

Study design

A retrospective, single-center, cross-sectional interventional clinical study was conducted.

The treatment outcomes of patients with cranial vault defects who underwent treatment at the Department of Reconstructive and Restorative Surgery of the Municipal Non-Commercial Enterprise Kyiv City Clinical Hospital No. 2 (renamed in March 2025 as the "Kyiv City Medical Center," Clinical Unit No. 8) between 2019 and 2024 were analyzed.

Written informed consent for participation in the study and publication of the data was obtained from all patients or their relatives. The study protocol was approved by the Ethics and Academic Integrity Committee of the Shupyk National Healthcare University of Ukraine (Minutes No. 4/38 dated April 30, 2024).

Statistical analysis

Descriptive statistical methods were used to process the obtained data. The results are presented as absolute and relative values. Descriptive statistics were applied to summarize the studied parameters.

Results

In the early postoperative period, treatment outcomes were assessed according to the following criteria: flap engraftment, occurrence of necrosis, and purulent complications.

The engraftment rate of free skin autografts in patients for whom this method served as the primary technique for defect closure was 70%. Incomplete graft engraftment was observed during reconstruction of granulating wounds in cases of superficial lesions. Better engraftment was achieved in the reconstruction of donor sites after the formation of local or regional flaps, as well as on granulation tissue formed following tissue ingrowth through a polypropylene mesh. After wound bed preparation, the exposed areas were re-covered with free skin grafts.

Complete engraftment of local and regional flaps was observed in all cases. Necrosis involving up to 30% of a vertical musculocutaneous flap was recorded in one case. After debridement of the necrotic tissue, the defect was closed using a temporal flap based on the occipital branch of the superficial temporal artery. Flap viability monitoring was performed only during the inpatient treatment period.

Suppuration associated with the use of a free flap was observed in one case.

The methods used for reconstruction of cranial vault defects are presented in ***Table 1***.

Discussion

The key criteria for selecting a method for primary reconstruction of calvarial defects following burns include the size and depth of the defect, preservation of the skin and deeper structures, as well as the presence and length of the soft-tissue vascular pedicle [7].

For reconstruction of scalp soft-tissue defects, local flaps advanced by direct advancement, rotation, or transposition, latissimus dorsi muscle flaps, omental flaps, and free flaps are used [8].

Scalp reconstruction differs depending on the anatomical region in which the defect is located and on its size. In our series, a single reconstructive technique was rarely used in isolation. In most cases, a combination of different plastic reconstructive methods was applied. For extensive defects, split-thickness skin grafting was used most frequently both for closure of the primary defect and for coverage of the donor site (***Figs. 1–3***). This approach enabled wound closure within a shorter period and with fewer complications [9].

Patients with periosteal involvement required revascularization procedures to preserve the cranial vault bones. Closure of intact bone or deep defects after necrotic tissue removal down to the inner cortical plate was performed using cutaneous-aponeurotic flaps from adjacent regions or complex composite flaps with axial blood supply (***Fig. 4***). In cases involving the periosteum or cortical layer of the cranial bones, bone milling was performed to improve flap fixation. This procedure also

Table 1. Clinical characteristics of patients and methods of primary reconstruction of cranial vault defects after burns

Depth of lesion	Age, years	Sex	Etiological agent	Total burn area, %	Defect area, cm^2	Defect localization	Primary reconstruction methods	Additional methods
Up to the periosteum, n=4	5	F	Scald burn	8	80	Parietal, temporal regions	ASG	–
	22	M	Flame burn	20	180	Frontal, parietal regions	ASG	–
	35	M	Flame burn	15	200	Parietal, temporal regions	ASG	–
	26	F	Chemical burn	12	130	Frontal region	ASG	–
Including the periosteum, n=6	12	M	HVEB	40	130, 80	Parietal, temporal regions	Bone milling + rotational flap + HTMF + ASG	–
	43	M	Flame burn	25	140	Occipital region	VTMF	ASG
	45	M	Flame burn	15	220	Parietal, temporal regions	Bone milling + rotational flap + ASG	–
	38	F	Flame burn	18	200	Parietal, frontal regions	Bone milling + ASG	–
	9	F	Flame burn	15	220	Parietal, occipital, temporal regions	VTMF + HTMF + temporal flap + ASG	ASG
	36	M	Flame burn	18	180	Frontal region	Two temporal flaps	ASG
Bone (cortical layer), n=4	26	M	Flame burn	45	280	Parietal, occipital regions	Bone milling + free flap + ASG	–
	46	M	HVEB	14	150	Parietal, temporal regions	Rotational flap + ASG	
	22	M	HVEB	15	180	Parietal region	Rotational flap + ASG	–
	26	M	Contact burn	1	60	Occipital region	Rotational flap + ASG	–
Bone (full thickness), n=2	2 monts	F	Flame burn	18	140	Parietal region	Bone removal + mesh implantation + ASG	–
	14	M	HVEB	60	180	Parietal, occipital regions	Bone removal + mesh implantation + rotational flap + ASG	–

Notes. HVEB — high-voltage electrical burn; ASG — autologous skin grafting (autodermoplasty); VTMF — vertical trapezius muscle flap; HTMF — horizontal trapezius muscle flap.

promoted ingrowth of granulation tissue through the burr holes. The cortical layer subsequently became covered with granulation tissue, allowing defect closure with free grafts and thereby accelerating recovery (see ***Figs. 2 and 3***).

Temporal flaps based on the superficial temporal artery were used as revascularizing flaps. To increase the area of coverage, a double flap supplied by the parietal and occipital branches of the superficial temporal artery was created (***Fig. 5***).

The temporal region represents a favorable donor site due to its rich vascular network and the availability of different tissue types, including skin, fascia, muscle, and bone [10]. Consequently, multiple flap variants can be designed in this region using one or more tissue components based on the superficial temporal artery and its branches, depending on the location and origin of the defect [11, 12]. In our study, temporal flaps were used for reconstruction of parietal defects. In cases involving the frontal region, a temporal fascial flap was used to cover the affected bone, followed by free skin grafting (see ***Fig. 5***).

The trapezius muscle flap is considered the first-choice option for some patients with defects in the posterior regions of the cranial vault because of its proximity to the wound, reliable blood supply, and increased resistance of flap tissues to infection [4,13]. The location and orientation of the dominant vascular pedicles of the trapezius muscle allow the formation of two flap variants: a horizontal flap including the horizontal portion of the muscle based on the descending superficial branch of the transverse cervical artery, and a vertical flap including the vertical portion of the muscle based on the deep nourishing branch of the transverse cervical artery [5].

The use of regional musculocutaneous flaps based on the trapezius muscle offers the advantage of providing an adequate volume of well-vascularized reconstructive tissue, while transfer of tissue on a vascular-muscular pedicle substantially reduces the risk of thrombosis of the supplying vessel [13, 14].

In selected cases, the horizontal and vertical trapezius musculocutaneous flaps may be considered the only reconstructive option capable of achieving closure of occipital and temporal defects and enabling delayed corrective procedures [13, 14] (***Fig. 6***).

During flap formation, in one case of vertical flap dissection, the cutaneous component extended 5 cm caudally beyond the inferior border of the trapezius muscle, which subsequently resulted in impaired blood circulation within the skin fragment and partial necrosis. In the horizontal flap, the muscular component was located only in the superomedial portion, whereas the remaining part contained fascia alone.

The horizontal trapezius musculocutaneous flap is indicated for reconstruction of temporoparietal defects, whereas the vertical trapezius musculocutaneous flap is preferable for closure of occipitoparietal defects.

Pedicle correction is required after 4–6 months to achieve a satisfactory cosmetic outcome.

An important aspect of primary calvarial reconstruction is the closure of bone defects in cases of total bone necrosis, including selection of an appropriate method for protection of the intracranial contents and prevention of cerebral prolapse [15].

For closure of cranial vault defects with exposure of the dura mater or brain structures, polysynthetic materials such as protacryl, biocomposite materials, corundum implants, carbon-based materials, as well as bone grafts, are used [16, 17]. The disadvantages of these methods include the inability to use plates during the acute phase of injury, limited applicability for extensive bone defects, absence or deficiency of adequate skin coverage for soft-tissue reconstruction, and restricted use in pediatric patients.

Fig. 1. Female, 28 years old: (A) second-degree superficial partial-thickness and third-degree chemical burn caused by sulfuric acid involving the frontal and temporal regions of the scalp without injury to the periosteum, as well as the upper extremities (12% TBSA); (B) wound appearance after staged debridements; (C) wound closure using a thick split-thickness autograft

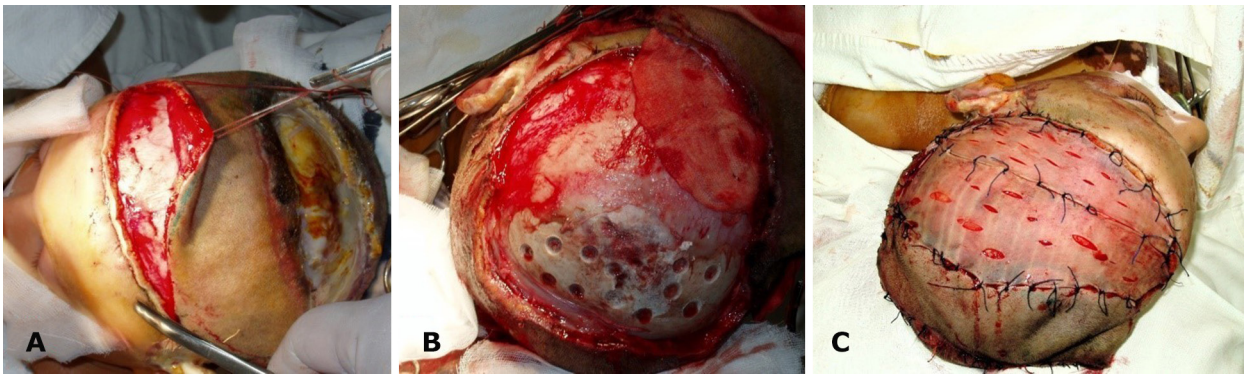

Fig. 2. Boy, 12 years old (case shown in Fig. 6): (A) formation of a parietal cutaneous-aponeurotic flap; (B) burring of the exposed parietal region; (C) reconstruction of the exposed burred parietal bone with a flap. The donor wound was covered with a split-thickness dermatome graft

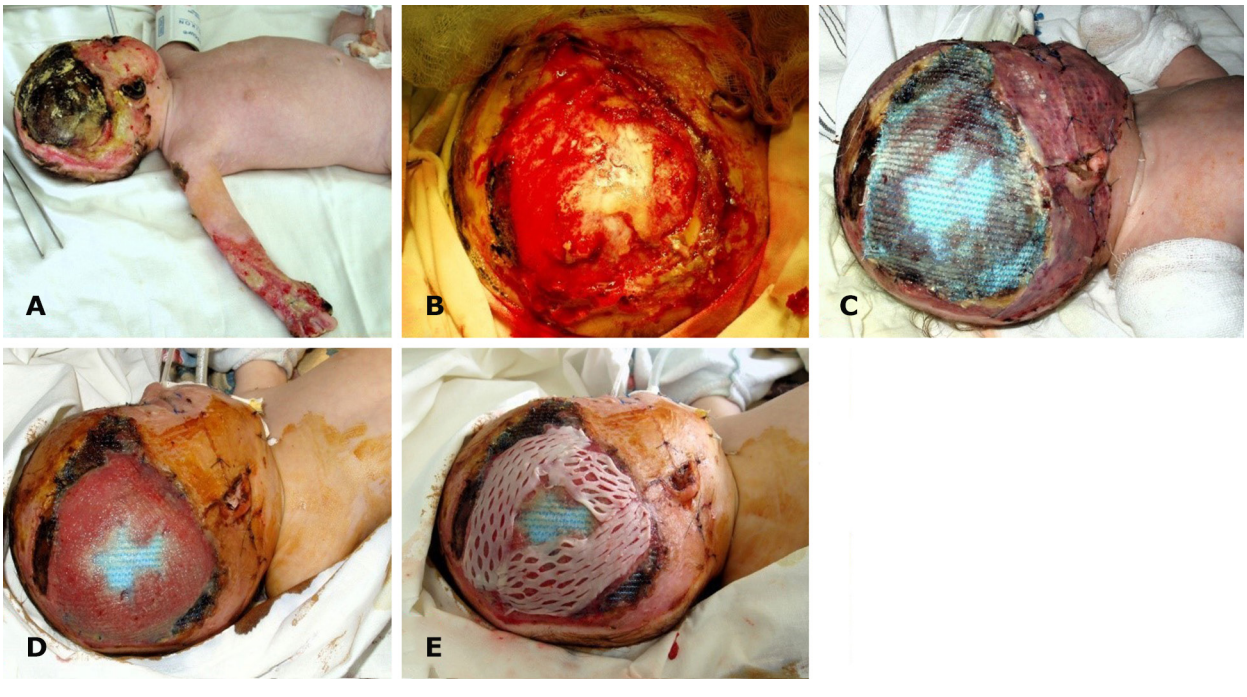

Fig. 3. Female infant, 2 months old. Second-degree superficial partial-thickness and third-degree flame burn of the scalp and right upper extremity (18% TBSA): (A) full-thickness necrosis of the temporal and parietal bones measuring 6 × 8 cm, with surrounding soft-tissue necrosis measuring 10 × 15 cm; (B) resection of the affected areas of the parietal and temporal bones with exposure of the dura mater; (C) polypropylene mesh sutured to the aponeurosis along the margin of the bone defect to protect the intracranial contents; (D) formation of granulating tissue through the mesh openings with development of a stable framework; (E) coverage of the granulation surface with a thick split-thickness dermatome graft

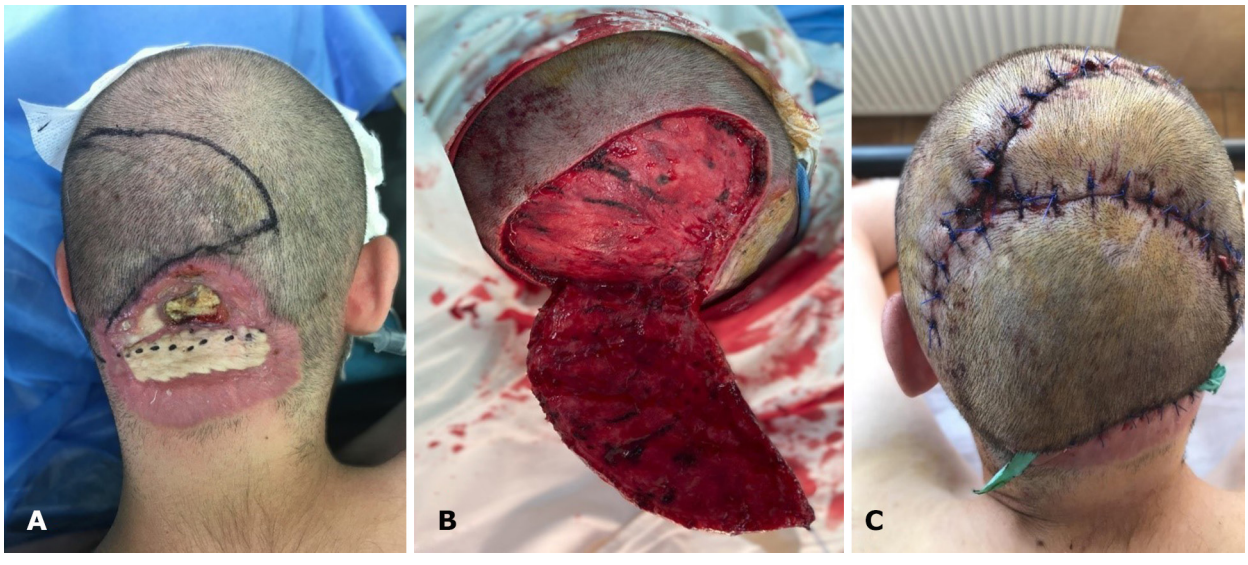

Fig. 4. Male, 24 years old: (A) second-degree deep partial-thickness and third-degree contact burn with a soft-tissue defect in the occipital region involving the periosteum and outer cortical layer of the occipital bone; (B) condition after wound debridement and removal of the damaged cortical plate to the level of punctate bone bleeding; (C) wound closure using a local occipital rotational flap incorporating the occipital artery. An additional parietal flap was used to cover the donor site

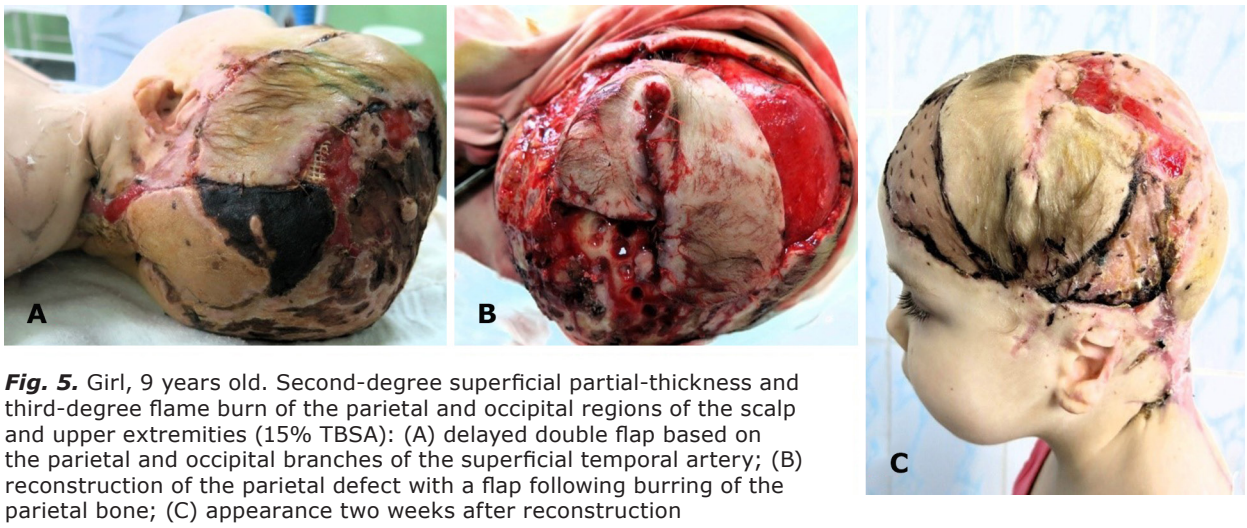

Fig. 5. Girl, 9 years old. Second-degree superficial partial-thickness and third-degree flame burn of the parietal and occipital regions of the scalp and upper extremities (15% TBSA): (A) delayed double flap based on the parietal and occipital branches of the superficial temporal artery; (B) reconstruction of the parietal defect with a flap following burring of the parietal bone; (C) appearance two weeks after reconstruction

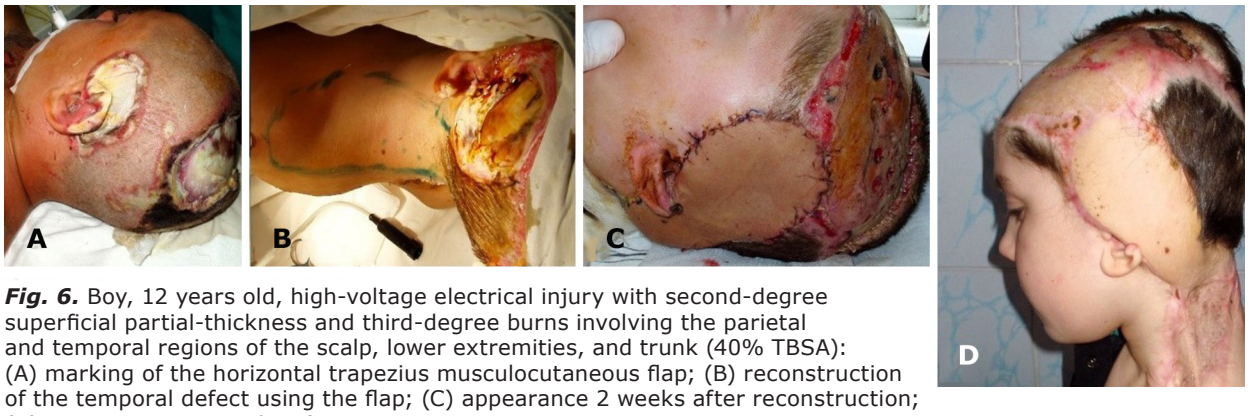

Fig. 6. Boy, 12 years old, high-voltage electrical injury with second-degree superficial partial-thickness and third-degree burns involving the parietal and temporal regions of the scalp, lower extremities, and trunk (40% TBSA): (A) marking of the horizontal trapezius musculocutaneous flap; (B) reconstruction of the temporal defect using the flap; (C) appearance 2 weeks after reconstruction; (D) appearance 3 months after reconstruction

To reduce the number of complications associated with closure of cranial vault bone defects, we used polypropylene mesh, which allowed granulation tissue to grow through the mesh openings and ensured coverage of the superior mesh surface with granulation tissue. Such wounds were subsequently covered with free grafts (see ***Fig. 3***).

Conclusions

Injuries limited to the soft tissues of the cranial vault with preservation of periosteal viability allow defect closure by autologous skin grafting. In cases involving tissue damage extending deeper than the periosteum, revascularization procedures using complex flaps, bone burring, or bone resection are required.

The use of a differentiated approach in the treatment of cranial vault defects made it possible to achieve positive outcomes in 14 (87.5%) patients.

Disclosure

Conflict of interest

The authors declare no conflict of interest.

Ethical approval

All procedures performed in studies involving human participants were conducted in accordance with the ethical standards of the institutional and national research committee and with the 1964 Declaration of Helsinki and its subsequent amendments or comparable ethical standards.

Informed consent

Written informed consent was obtained from each patient or their legal guardian prior to surgery.

Funding

The study received no external financial support.

References

1. Lilly GL, Santucci NM, Petrisor D, Wax MK. Soft tissue coverage of cranial defects: an update. Plast Aesthet Res. 2021;8:24. doi: 10.20517/2347-9264.2021.21
2. Newman MI, Hanasono MM, Disa JJ, Cordeiro PG, Mehrara BJ. Scalp reconstruction: a 15-year experience. Ann Plast Surg. 2004 May;52(5):501-6; discussion 506. doi: 10.1097/01.sap.0000123346.58418.e6
3. Yang HJ, Lee DH, Kim YW, Lee SG, Cheon YW. The Trapezius Muscle Flap: A Viable Alternative for Posterior Scalp and Neck Reconstruction. Arch Plast Surg. 2016 Nov;43(6):529-535. doi: 10.5999/aps.2016.43.6.529
4. Can B. Role of Trapezius Turnover Flap in Complex Posterior Cervical Wounds. Turkish Journal of Plastic Surgery. 2020 Oct 1;28(4):252-4. doi: 10.4103/tjps.tjps_85_19
5. Nasrollahi T, Borrelli M, Salehi K, Hopp ML, Alessi D. Trapezius fasciocutaneous flap for burn reconstruction. Ear Nose Throat J. 2024 Aug;103(8):487-489. doi: 10.1177/01455613211066659
6. Tomás-Velázquez A, Redondo P. Assessment of Frontalis Myocutaneous Transposition Flap for Forehead Reconstruction After Mohs Surgery. JAMA Dermatol. 2018 Jun 1;154(6):708-711. doi: 10.1001/jamadermatol.2018.1213
7. Ogawa R. Head and Neck Reconstruction in Burn Patients. Clin Plast Surg. 2024 Jul;51(3):391-398. doi: 10.1016/j.cps.2024.02.003
8. Voulliaume D, Curings P, Vantomme M, Henry G, Bayoux R, Barani C. Les brûlures du front [Forehead burns]. Ann Chir Plast Esthet. 2024 Nov;69(6):570-579. French. doi: 10.1016/j.anplas.2024.06.021
9. Krishna D, Khan MM, Dubepuria R, Chaturvedi G, Cheruvu VPR. Reconstruction of Scalp and Forehead Defects: Options and Strategies. Cureus. 2023 Jul 6;15(7):e41479. doi: 10.7759/cureus.41479
10. Tremolada C, Candiani P, Signorini M, Vigano M, Donati L. The surgical anatomy of the subcutaneous fascial system of the scalp. Ann Plast Surg. 1994 Jan;32(1):8-14. doi: 10.1097/00000637-199401000-00002
11. Safavi-Abbasi S, Komune N, Archer JB, Sun H, Theodore N, James J, Little AS, Nakaji P, Sughrue ME, Rhoton AL, Spetzler RF. Surgical anatomy and utility of pedicled vascularized tissue flaps for multilayered repair of skull base defects. J Neurosurg. 2016 Aug;125(2):419-30. doi: 10.3171/2015.5.JNS15529
12. Mokal NJ, Ghalme AN, Kothari DS, Desai M. The use of the temporoparietal fascia flap in various clinical scenarios: A review of 71 cases. Indian J Plast Surg. 2013 Sep;46(3):493-501. doi: 10.4103/0970-0358.121988
13. Yang HJ, Lee DH, Kim YW, Lee SG, Cheon YW. The Trapezius Muscle Flap: A Viable Alternative for Posterior Scalp and Neck Reconstruction. Arch Plast Surg. 2016 Nov;43(6):529-535. doi: 10.5999/aps.2016.43.6.529
14. Naalla R, Murthy V, Chauhan S, Chinta K, Singhal M. Revisiting the Trapezius Flap as a Reconstructive Option for Cervico-Occipital and Thoracic Spine Regions. Indian J Plast Surg. 2019 Sep;52(3):322-323. doi: 10.1055/s-0039-3400677
15. Sittitavornwong S, Morlandt AB. Reconstruction of the scalp, calvarium, and frontal sinus. Oral Maxillofac Surg Clin North Am. 2013 May;25(2):105-29. doi: 10.1016/j.coms.2013.02.004
16. Golpanian S, Kassira W, Habal MB, Thaller SR. Treatment Options for Exposed Calvarium Due to Trauma and Burns. J Craniofac Surg. 2017 Mar;28(2):318-324. doi: 10.1097/SCS.0000000000003310
17. Yu QS, Chen L, Qiu ZY, Zhang YQ, Song TX, Cui FZ. Skull repair materials applied in cranioplasty: History and progress. Transl. Neurosci. Clin. 2017, 3(1): 48–57. doi: 10.18679/CN11-6030/R.2017.007

Original article

Ukrainian Neurosurgical Journal. 2026;32(2):23-31
doi: 10.25305/unj.343658

Factors affecting the quality of life of patients after tubular microdiscectomy

Yuriy Y. Chomolyak [1,2], Yullia H. Khymynets [1,2], Anastasiia D. Ivashchenko [3]

[1] Department of Surgical Disciplines Institute of Postgraduate and Pre-university Education, Uzhhorod National University, Uzhhorod, Ukraine
[2] Limited Liability Company "Medical Center „Diamed„", Uzhhorod, Ukraine
[3] TUZ Ubezpieczenia Insurance Company Joint-Stock Company (TUZ Ubezpieczenia TU S.A.), Warsaw, Poland

Received: 17 November 2025
Accepted: 19 December 2025

Address for correspondence: *Khymynets Yuliia Georgiivna, Department of Surgical Disciplines Institute of Postgraduate and Pre-university Education, Uzhhorod National University, 20 Ivan Korshynskyi Street, Uzhhorod, 88000, Ukraine, e-mail: juliyachiminets@gmail.com*

Generally accepted factors that may affect a patient's quality of life after surgery include excess body weight and heavy physical activity before surgery. However, randomized controlled clinical trials (RCTs) evaluating the quality of life of patients with these factors after tubular microdiscectomies remain limited.

Objective: to assess the quality of life of patients after tubular microdiscectomy and to establish prognostic factors that affect this indicator.

Materials and methods: The study included 160 consecutive patients who underwent tubular microdiscectomy for herniated intervertebral discs; selected according to the predefined inclusion and exclusion criteria and assessed using the Oswestry Disability Index (ODI). The operations were performed in one institution (Diamed Medical Center, Uzhhorod) by the same surgical team. To identify the most significant variables, backward stepwise regression analysis was applied. The initial model included all potentially relevant variables, after which predictors that did not show a statistically significant association with the dependent variable were sequentially removed. In addition, pairwise correlations among all studied variables were assessed.

Results: It was found that women who had performed heavy physical labor before the operation demonstrated greater variability of ODI indicators compared with women who had not performed heavy physical labor and men from both groups. Prognostic factors for deterioration in quality of life after tubular microscopic discectomy include the combination of heavy physical labor before the operation and a high Body Mass Index (BMI). This pattern became more with increasing patient age.

Conclusions: The quality of life of patients after tubular microscopic discectomy does not depend significantly on individual factors such as gender, age, and physical labor before the operation. Tubular microdiscectomy does not reduce individual factors that potentially affect well-being after the operation; however, it minimizes negative factors during the operation itself and the early postoperative period. To establish the effectiveness of tubular microdiscectomy, further studies are needed to compare pre- and postoperative indicators of different discectomy techniques.

Keywords: *low back pain; herniated disc; spinal surgery; tubular microdiscectomy*

Introduction

Low back pain is one of the most common pathological symptoms among the adult population worldwide. In recent years, patients have increasingly reported back pain regardless of social status, standard of living, occupation, age, or sex [1]. Low back pain represents one of the most serious public health problems, with a lifetime prevalence of 84%. The prevalence of chronic low back pain is approximately 23%, whereas the rate of disability reaches 11–12% [2]. Individuals engaged in heavy physical labor, those with concomitant physical and mental disorders, smokers, and individuals with obesity are at the highest risk of developing low back pain.

In 1986, R.A. Deyo classified low back pain into three categories: mechanical pain, non-mechanical pain, and pain associated with visceral diseases. Intervertebral disc herniation is a component of mechanical low back pain and significantly reduces patients' quality of life [3].

Intervertebral disc herniation is defined as a localized displacement of a degeneratively altered portion of the intervertebral disc beyond its anatomical boundaries, resulting in compression of the spinal cord and spinal nerve roots [4].

Low back pain caused by intervertebral disc herniation may lead to persistent neurological deficits in some patients, including paresis, decreased proprioceptive reflexes, sensory disturbances, and pelvic organ dysfunction. In patients without neurological deficits, pain decreases within the first 6 weeks after symptom onset in 70% of cases under pharmacological treatment. Most authors recommend considering surgical intervention for the remaining patients [5, 6].

According to the results of a 2019 meta-analysis, surgical treatment of patients with intervertebral disc herniation refractory to pharmacological therapy for 6 weeks is more effective than continued conservative medical management [7].

In the twenty-first century, numerous surgical techniques for the treatment of intervertebral disc herniation have been proposed, ranging from conventional open discectomy to minimally invasive procedures. The popularity of minimally invasive approaches has increased substantially in recent years [8].

The tubular discectomy technique was first described in 1997 by K.T. Foley and M.M. Smith as microendoscopic discectomy involving endoscopic assistance [9]. However, there remains a lack of RCTs evaluating the effectiveness of tubular discectomy performed using a surgical microscope [10–12].

Objective: to assess the quality of life of patients after tubular microdiscectomy and to identify prognostic factors influencing this outcome.

Materials and methods

Study participants

A total of 160 consecutive cases of surgical treatment for intervertebral disc herniation using tubular microdiscectomy performed at the Medical Center "Diamed" (Uzhhorod, Ukraine) between 2021 and 2024 were selected for the study.

The study protocol was approved by the Ethics and Bioethics Committee of the Limited Liability Company Medical Center "Diamed" (Minutes No. 45/1 dated September 10, 2025).

Inclusion criteria:

Patients with clinically significant neurological symptoms (low back pain, lower extremity paresis, decreased proprioceptive reflexes, sensory disturbances, and cauda equina syndrome), radiological evidence of lumbar disc herniation confirmed by magnetic resonance imaging, and resistance to conservative treatment were included in the study.

Exclusion criteria:

The exclusion criteria were a history of lumbar spine surgery, involvement of more than one spinal segment, diseases of other organs and systems precluding surgery, satisfactory response to pharmacological treatment, and foot plegia without pain syndrome.

Group characteristics

The study included 160 patients whose data were anonymized. A retrospective assessment was performed using the following variables: sex, age, body mass index (BMI), duration of analgesic use before surgery, duration of symptoms before surgery, engagement in heavy physical labor, duration of analgesic use after surgery, and the Oswestry Disability Index (ODI).

Study design

A case–control study was conducted to evaluate the correlation between factors influencing the quality of life of patients after tubular microdiscectomy.

Tubular microdiscectomy technique

All surgical procedures were performed by a single neurosurgical team using the same surgical equipment and operative technique.

The surgical intervention was performed under general anesthesia with tracheal intubation. The affected spinal level was verified intraoperatively using a C-arm fluoroscopy system Arcadis (Siemens, Germany) based on preoperative magnetic resonance imaging findings. A 2-cm skin incision was made parallel to the projection of the spinous processes. An EasyGo 2 tubular retractor system (Karl Storz, Germany) was installed. The position of the tubular retractor was confirmed using fluoroscopic control in two projections. Under the Hi-R 1000 operating microscope (HAAG-STREIT, Germany), microdiscectomy was performed using microsurgical instruments (Karl Storz, Germany) and a Primado 2 high-speed drill (NSK, Japan). The aponeurosis and dermis were sutured using Vicryl 3-0 suture material (Johnson & Johnson, USA). An aseptic dressing was applied using Steri-Strip and Tegaderm (3M, USA).

The use of the EasyGo 2 tubular retractor system (Karl Storz) reduces surgical trauma, enabling the procedure to be performed through a skin incision of up to 2 cm. Minimal injury to the osteoligamentous structures allows patient mobilization within several hours after surgery, thereby improving postoperative rehabilitation. During exposure of the neural elements, the need for coagulation is substantially reduced because muscular bleeding is absent. This technique also shortens the duration of hospital stay to one day.

The assessment of factors influencing the quality of life of patients after tubular microdiscectomy was performed with consideration of sex, height, body weight, engagement in heavy physical labor before surgery, use of nonsteroidal anti-inflammatory drugs before and after surgery, and postoperative ODI scores obtained through anonymous questionnaires.

Statistical analysis

Stepwise regression with backward elimination was used to identify the most significant variables. Records of patients who had undergone surgery within the last month before data processing were excluded because of changes in quality of life during the early postoperative period. Data from 127 patients were ultimately analyzed.

Results

Sex. Men predominated among the patients (***Fig. 1***).

Age. Most respondents were aged 30–45 years (***Fig. 2***).

Body Mass Index. The most common BMI range was 25.0–30.0 kg/m², indicating an excess body weight in the study population (***Fig. 3***).

Preoperative pharmacological therapy.

Analysis of the distribution demonstrated that the largest proportion of patients had been taking analgesic medications for 8 weeks or longer before surgery, which may indicate prolonged persistence of pain syndrome before surgical intervention (***Fig. 4***).

Duration of symptoms before surgery. The largest number of observations belonged to the "≥8 weeks" category, indicating prolonged symptom duration before surgery (***Fig. 5***).

Physical work before surgery. Most patients performed heavy physical labor before surgery (***Fig. 6***).

Postoperative pharmacological treatment. In most respondents, the duration of treatment did not exceed 1

week; however, a tendency toward prolonged medication use was observed in some patients, which may be associated with individual physiological characteristics (***Fig. 7***).

Correlation analysis of variables. The correlation heatmap demonstrates the degree of association between variables: orange indicates a negative correlation, yellow indicates a positive correlation, and white indicates the absence of correlation. Darker shading reflects a stronger association (***Fig. 8***).

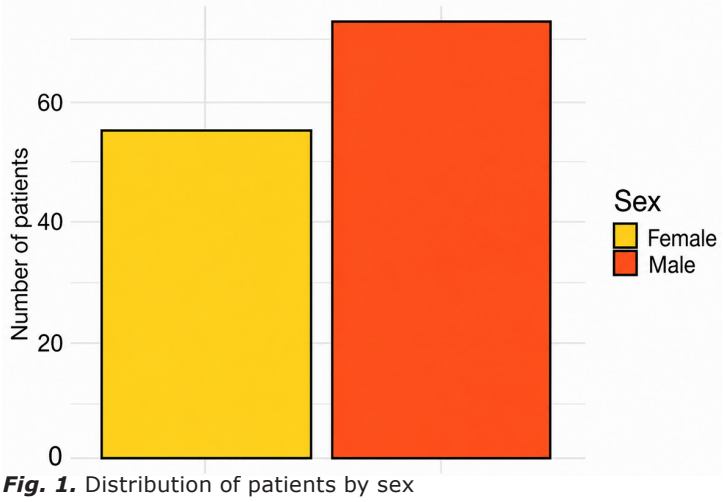

Fig. 1. Distribution of patients by sex

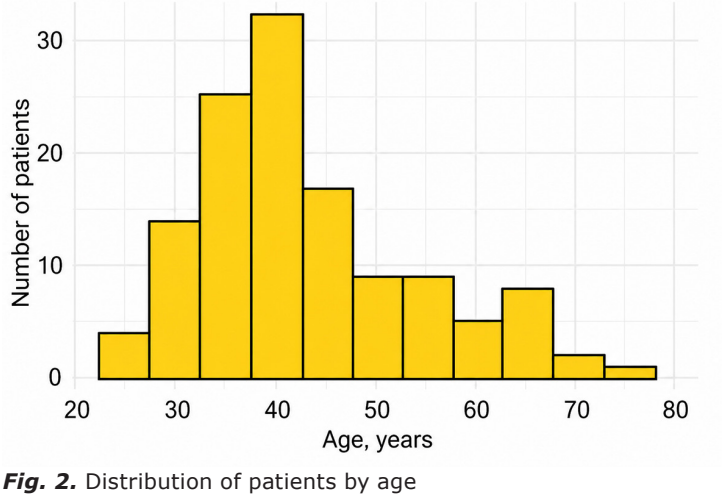

Fig. 2. Distribution of patients by age

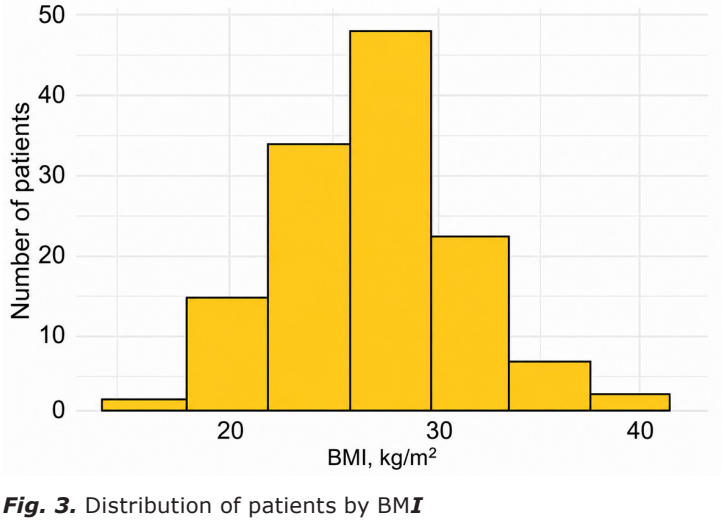

Fig. 3. Distribution of patients by BM***I***

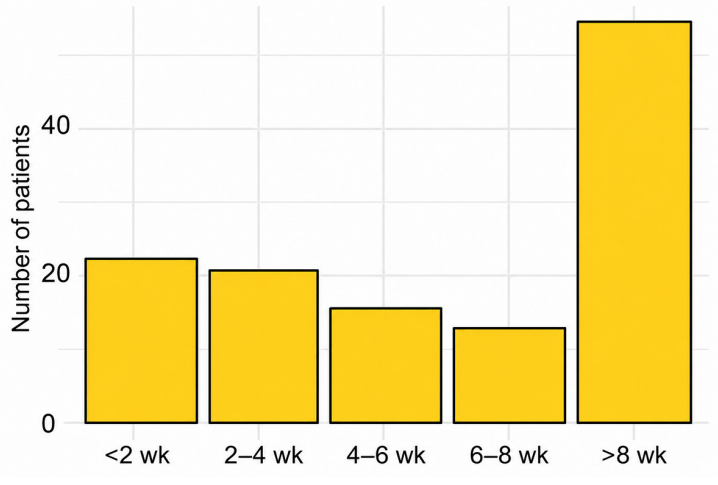

Fig. 4. Distribution of patients according to duration of medication use before surgery

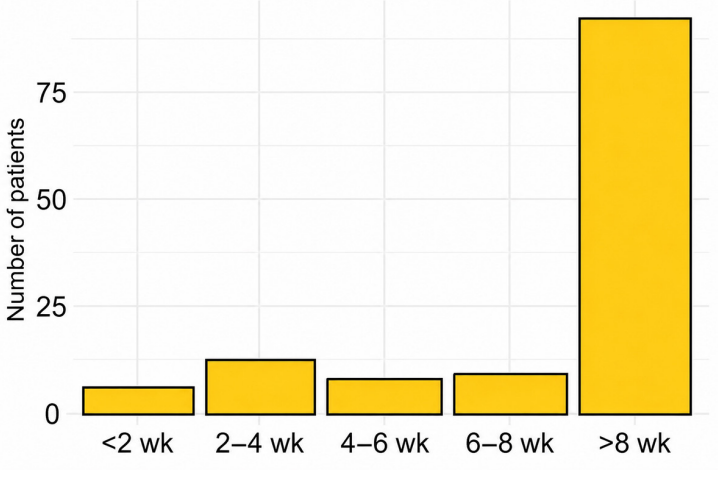

Fig. 5. Distribution of patients according to duration of symptoms before surgery

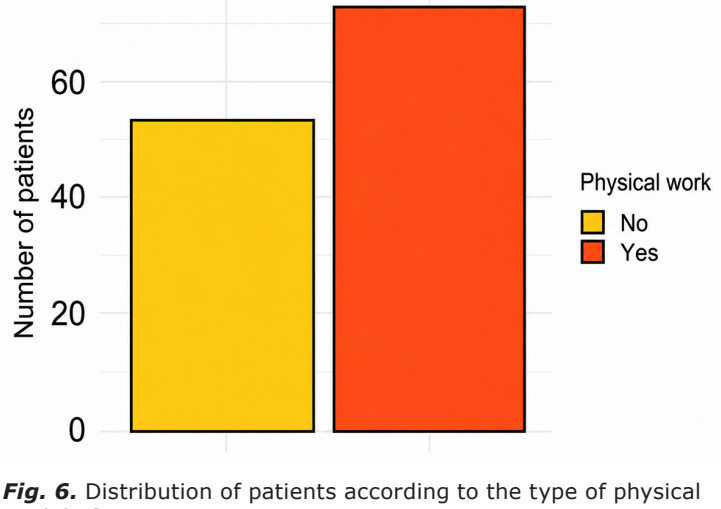

Fig. 6. Distribution of patients according to the type of physical work before surgery

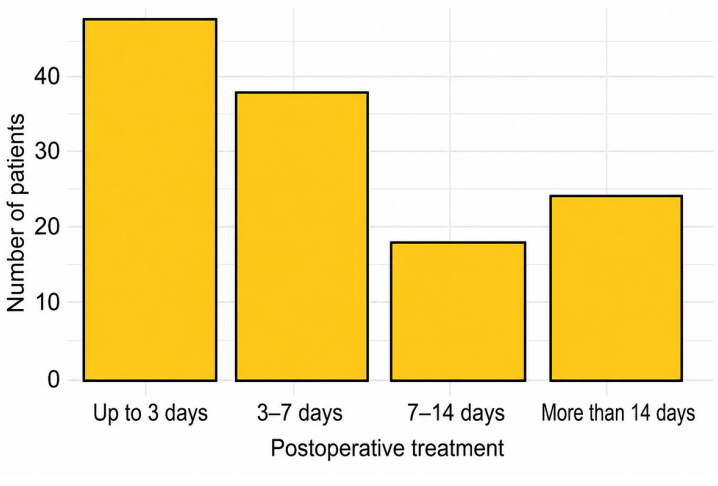

Fig. 7. Distribution of patients according to duration of postoperative pharmacological therapy

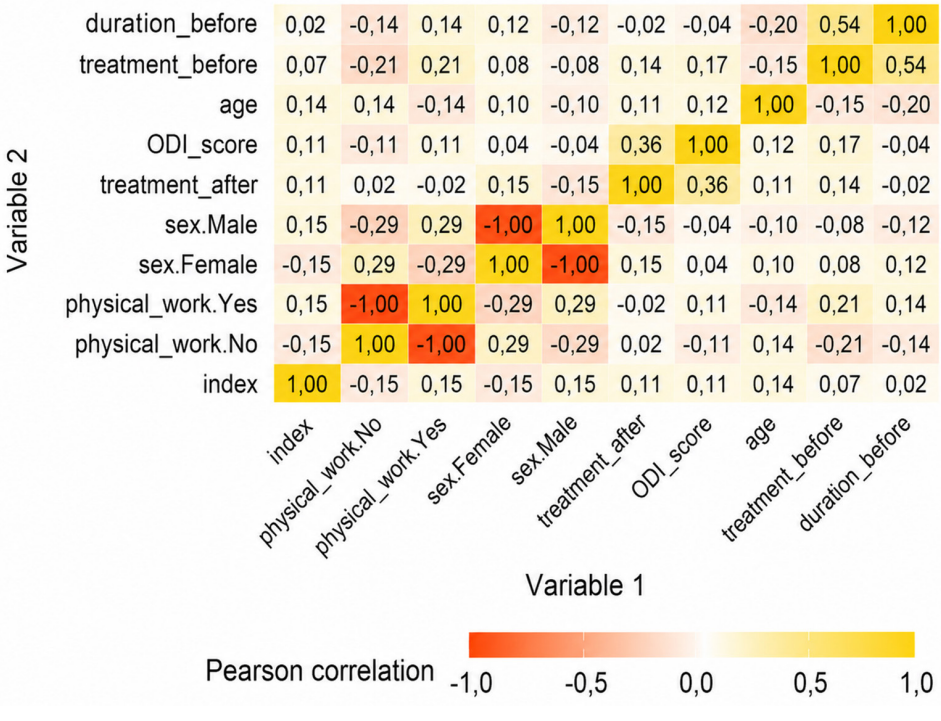

Fig. 8. Correlation between variables

For example, a complete negative correlation (–1.00) was observed between the variables "physical work: *yes*" and "physical work: *no*," which is expected because these are opposite categories of the same variable. Similarly, a strong negative correlation was identified between *male* and *female* sex, as these categories are mutually exclusive.

Other correlation coefficients on the heatmap were relatively low, which may indicate the absence of strong associations between variables in this dataset.

Backward stepwise regression analysis was used to identify the most significant variables, enabling sequential elimination of nonsignificant factors while focusing on those exerting the greatest effect on the dependent variable.

Statistical analysis revealed that the most significant factor influencing patients' postoperative health status assessment (ODI) was the variable "postoperative analgesic use." This finding is expected because patients with poorer postoperative well-being tend to require a greater amount of analgesic medication (***Table 1***).

Relationship between ODI and age. In ***Fig. 9***, yellow dots represent the well-being of individuals of the corresponding age, whereas the yellow line indicates the trend line, which appears nearly horizontal, suggesting either a weak trend or the absence of an overall tendency for changes in well-being with increasing age.

The wide dispersion of data points reflects substantial variability in well-being among individuals of the same age. The absence of a clear clustering of points along the

trend line and its nearly horizontal slope indicate that the relationship between age and well-being is weak.

Relationship between ODI, age, and physical work. In Fig. 10, yellow triangles indicate individuals who performed heavy physical work before surgery ("Yes"), whereas orange dots represent those who did not perform heavy physical work ("No"). The yellow line demonstrates the trend for individuals engaged in heavy physical work before surgery, while the orange line represents those who did not perform such work. The trend lines indicate that with increasing age, the level of well-being among individuals who did not perform heavy physical work before surgery appears stable or slightly improved. In contrast, among individuals who performed heavy physical work before surgery, the relationship between age and well-being worsens, which may indicate poorer recovery in these patients or resumption of heavy physical labor after surgery.

Relationship between ODI and physical work. ***Figure 11*** compares the level of well-being (ODI) between individuals engaged in physical labor ("Yes") and those who were not ("No"). Median values were identical in both groups, indicating no substantial difference in overall well-being depending on whether an individual performed heavy physical work.

However, other characteristics of the graph provide additional information:

- for the group that did not perform physical work ("No"), the interquartile range was narrower, indicating lower ODI variability in this group;

- for the group engaged in physical work ("Yes"), the box was wider, indicating greater ODI variability;

- outliers were present in both groups, represented by individual points located at a considerable distance beyond the main data distribution. This finding indicates the presence of individuals with poor well-being markedly different from that observed in the majority of subjects within each group.

Relationship between ODI, physical work, and sex. Several conclusions can be drawn from ***Fig. 12***:

- greater variability in well-being was observed among women who performed physical work. This finding may indicate that physical labor substantially affects well-being, although the effect is heterogeneous and may vary depending on individual working conditions, health status, physical fitness, and other personal factors;

- ODI scores differed minimally between men and women who did not perform physical work, whereas among individuals engaged in physical work, the variability of ODI values was greater. Differences in well-being between men and women engaged in physical work may be explained by several factors:

1. Physiological differences: men and women have different physiological characteristics and adaptive mechanisms in response to physical нагрузка. This may influence tolerance to physical work and pain perception.

2. Psychological factors: men engaged in physical labor may have different expectations and attitudes toward well-being and pain perception. Greater habituation to physical exertion may contribute to less pronounced pain perception or a higher pain threshold.

3. Social norms and stereotypes: men may experience societal pressure to be less likely to complain of pain or discomfort, particularly in the context of physical labor traditionally associated with "male" work.

4. Working conditions and job type: men and women may perform different types of physical work that exert varying effects on well-being.

Relationship between ODI, BMI, and physical work. In ***Fig. 13****,* yellow indicates individuals who performed heavy physical work before surgery, whereas orange indicates those who did not. The trend line for individuals engaged in heavy physical work demonstrates an upward trajectory, which may indicate an increase in ODI with increasing BMI. Individuals who did not perform physical work exhibited a flatter trend, suggesting a weaker relationship between ODI and BMI. In both groups, variability in well-being scores was observed; however, increasing BMI was associated with a tendency toward poorer well-being, particularly among individuals who performed heavy physical work before surgery.

Conclusions

The quality of life of patients after tubular microdiscectomy showed only a weak association with factors such as sex, age, and engagement in physical work before surgery.

Table 1. Model results

Variable	Estimate	Standard Error	t-statistic	p-value	Statistical significance
Postoperative analgesics. L	10,863	2,533	4,289	3,59e-05	*
Postoperative analgesics. Q	2,744	2,677	1,025	0,307	
Postoperative analgesics. C	3,333	2,813	1,185	0,238	

*Note. * Significant linear association between the duration of postoperative analgesic use and ODI.*

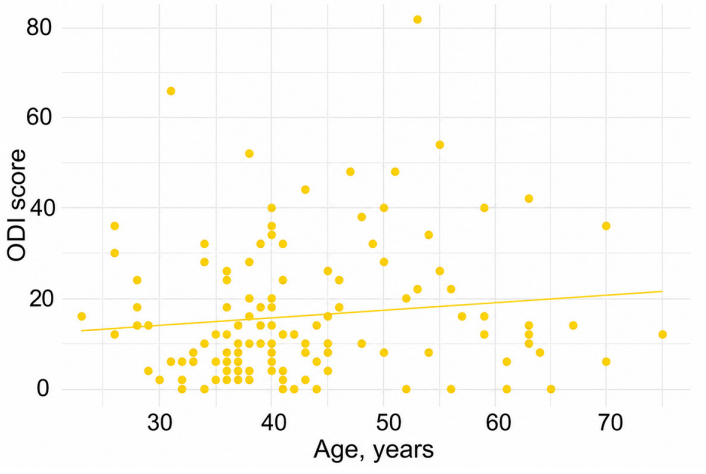

Fig. 9. Relationship between ODI and patients' age

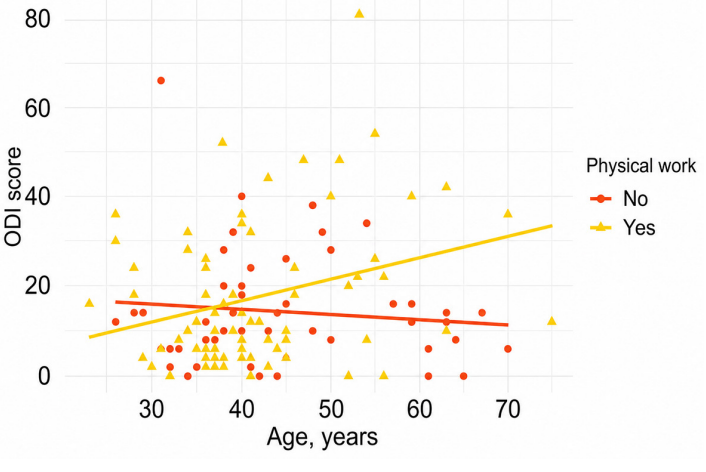

Fig. 10. Relationship between ODI, age, and physical work

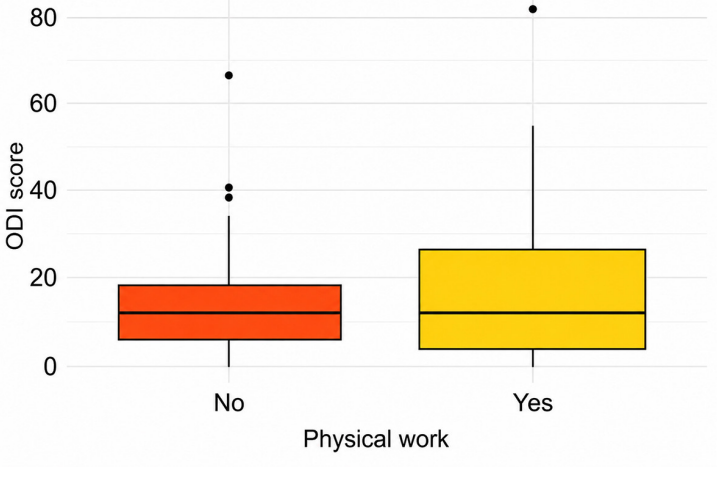

Fig. 11. Relationship between ODI and physical work

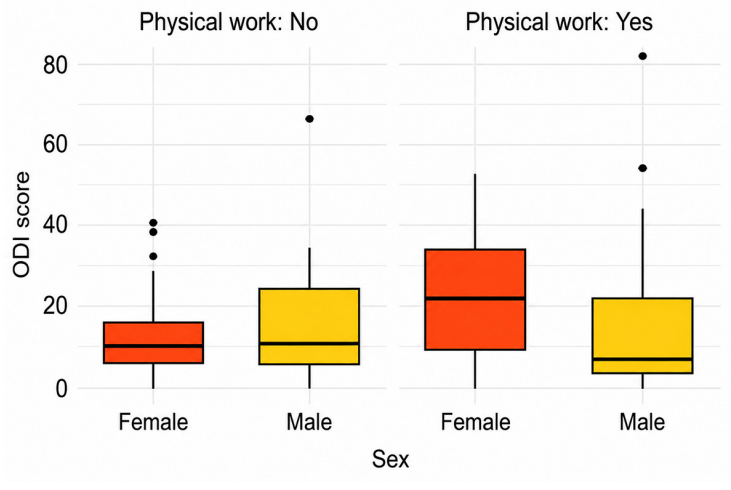

Fig. 12. Relationship between ODI, physical work, and sex

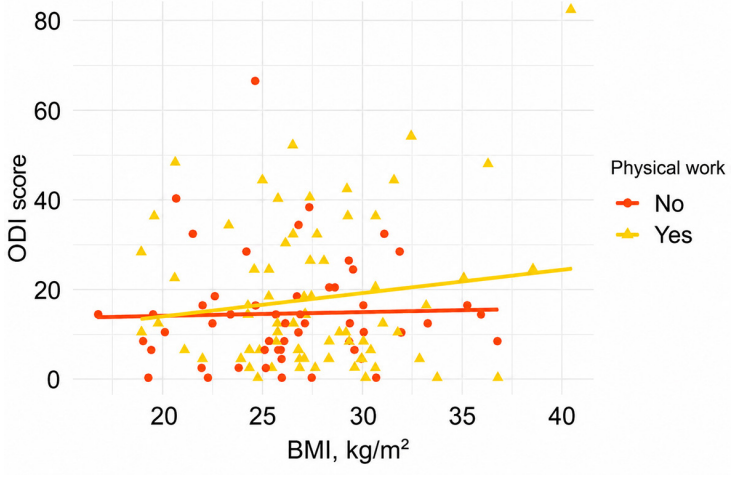

Fig. 13. Relationship between ODI, BMI, and physical work

Women who performed heavy physical work before surgery demonstrated greater variability in ODI scores compared with women who did not perform such work and with men in both groups.

The prognostic factors associated with deterioration in quality of life after tubular microdiscectomy were the combination of heavy physical work before surgery and elevated BMI. This relationship became more pronounced with increasing patient age.

Tubular microdiscectomy does not eliminate individual factors that may potentially influence postoperative well-being; however, it minimizes adverse factors during surgery and in the early postoperative period.

Further studies comparing preoperative and postoperative outcomes using different discectomy techniques are required to determine the effectiveness of tubular microdiscectomy.

Disclosure

Conflict of interest

The authors declare no conflict of interest.

Ethical standards

All procedures performed in this study involving patients complied with the ethical standards of the institutional and national research committees and with the 1964 Helsinki Declaration and its later amendments or comparable ethical standards.

Funding

The study received no external financial support.

References

1. Hartvigsen J, Hancock MJ, Kongsted A, Louw Q, Ferreira ML, Genevay S, Hoy D, Karppinen J, Pransky G, Sieper J, Smeets RJ, Underwood M; Lancet Low Back Pain Series Working Group. What low back pain is and why we need to pay attention. Lancet. 2018 Jun 9;391(10137):2356-2367. doi: 10.1016/S0140-6736(18)30480-X
2. Balagué F, Mannion AF, Pellisé F, Cedraschi C. Non-specific low back pain. Lancet. 2012 Feb 4;379(9814):482-91. doi: 10.1016/S0140-6736(11)60610-7
3. Deyo RA. Early diagnostic evaluation of low back pain. J Gen Intern Med. 1986 Sep-Oct;1(5):328-38. doi: 10.1007/BF02596214
4. Fardon DF, Williams AL, Dohring EJ, Murtagh FR, Gabriel Rothman SL, Sze GK. Lumbar disc nomenclature: version 2.0: Recommendations of the combined task forces of the North American Spine Society, the American

Society of Spine Radiology and the American Society of Neuroradiology. Spine J. 2014 Nov 1;14(11):2525-45. doi: 10.1016/j.spinee.2014.04.022
5. Vroomen PC, de Krom MC, Knottnerus JA. Predicting the outcome of sciatica at short-term follow-up. Br J Gen Pract. 2002 Feb;52(475):119-23.
6. Peul WC, van den Hout WB, Brand R, Thomeer RT, Koes BW; Leiden-The Hague Spine Intervention Prognostic Study Group. Prolonged conservative care versus early surgery in patients with sciatica caused by lumbar disc herniation: two year results of a randomised controlled trial. BMJ. 2008 Jun 14;336(7657):1355-8. doi: 10.1136/bmj.a143
7. Arts MP, Kuršumović A, Miller LE, Wolfs JFC, Perrin JM, Van de Kelft E, Heidecke V. Comparison of treatments for lumbar disc herniation: Systematic review with network meta-analysis. Medicine (Baltimore). 2019 Feb;98(7):e14410. doi: 10.1097/MD.0000000000014410
8. Siu TLT, Lin K. Direct Tubular Lumbar Microdiscectomy for Far Lateral Disc Herniation: A Modified Approach. Orthop Surg. 2016 Aug;8(3):301-8. doi: 10.1111/os.12263
9. Foley KT, Smith MM, Rampersaud YR. Microendoscopic approach to far-lateral lumbar disc herniation. Neurosurg Focus. 1999 Nov 15;7(5):e5. doi: 10.3171/foc.1999.7.6.6
10. Righesso O, Falavigna A, Avanzi O. Comparison of open discectomy with microendoscopic discectomy in lumbar disc herniations: results of a randomized controlled trial. Neurosurgery. 2007 Sep;61(3):545-9; discussion 549. doi: 10.1227/01.NEU.0000290901.00320.F5
11. Ryang YM, Oertel MF, Mayfrank L, Gilsbach JM, Rohde V. Standard open microdiscectomy versus minimal access trocar microdiscectomy: results of a prospective randomized study. Neurosurgery. 2008 Jan;62(1):174-81; discussion 181-2. doi: 10.1227/01.NEU.0000311075.56486.C5
12. Brock M, Kunkel P, Papavero L. Lumbar microdiscectomy: subperiosteal versus transmuscular approach and influence on the early postoperative analgesic consumption. Eur Spine J. 2008 Apr;17(4):518-22. doi: 10.1007/s00586-008-0604-2
13. Dowell D, Ragan KR, Jones CM, Baldwin GT, Chou R. CDC Clinical Practice Guideline for Prescribing Opioids for Pain - United States, 2022. MMWR Recomm Rep. 2022 Nov 4;71(3):1-95. doi: 10.15585/mmwr.rr7103a1

Original article

Ukrainian Neurosurgical Journal. 2026;32(2):32-50
doi: 10.25305/unj.341180

Predicting the risk of neurodegenerative diseases based on clinical microsignals

Yaroslav D. Bondarenko [1,2], Oksana I. Kauk [3]

[1] Third Faculty of Medicine, Kharkiv National Medical University, Kharkiv, Ukraine
[2] Medical faculty, Friedrich-Alexander University of Erlangen–Nuremberg, Erlangen, Germany
[3] Department of Neurology with a course in Neurosurgery, Kharkiv National Medical University, Kharkiv, Ukraine

Received: 12 October 2025
Accepted: 12 January 2026

Address for correspondence:
Yaroslav D. Bondarenko, Third Faculty of Medicine, Kharkiv National Medical University, Nauky Avenue, 4, Kharkiv, 61000, Ukraine, e-mail: bondarenkoyaroslav2017@gmail.com

Background: Neurodegenerative diseases, in particular Parkinson's disease, remain difficult to diagnose due to the late manifestation of classical motor symptoms, when significant neuronal degeneration has already occurred. A growing body of evidence suggests that subtle non-motor prodromal symptoms — so-called phenotypic microsignals (PMS) may precede the clinical manifestation of neurodegenerative diseases by several years. These symptoms reflect early neurochemical disturbances and disruptions of neural networks, especially in evolutionarily ancient brain structures vulnerable to α-synuclein pathology.

Objective: To identify and systematize early clinical phenotypic microsignals observed during initial outpatient visits and potentially associated with neurodegenerative processes, as well as to develop a clinical risk stratification tool for the prodromal stage based on retrospective analysis and prospective observation.

Materials and methods: A combined retrospective-prospective observational study conducted at Kharkiv National Medical University during the period from January 2020 to August 2025. The study involved 112 patients aged 48 to 76 years, who were divided into three groups: group 1 (n=28, prodromal/non-manifest pathology), group 2 (n=56, manifest pathology (Alzheimer's disease (n=16), Parkinson's disease (n=28), dementia with Lewy bodies (n=9), progressive supranuclear palsy (n=3)), group 3 (control, n=28, individuals without clinical signs of neurodegenerative pathology, matched by age and sex). A 48-point PMS scale was developed and validated, assessing 30 clinical markers across cognitive, motor, autonomic, sensory and affective domains. Patients underwent comprehensive neurological examination, cognitive testing (MMSE — Mini-Mental State Examination, MoCA — Montreal Cognitive Assessment, FAB — Frontal Assessment Battery), magnetic resonance imaging and standardized assessment of non-motor symptoms. ROC analysis was used to evaluate the predictive accuracy of the scale.

Results: Patients with manifest neurodegenerative diseases had significantly higher PMS scale scores (mean value – 27.8±6.3 points) compared with the prodromal group (11.4±3.8, $p<0.001$) and control (2.8±2.1). ROC analysis demonstrated excellent diagnostic accuracy for comparison of manifest pathology with control (area under the curve (AUC) – 0.982, sensitivity – 96.4%, specificity – 92.9% at a threshold value ≥13 points), good accuracy for prodromal pathology compared with control (AUC – 0.956, sensitivity – 89.3%, specificity – 89.3% at a threshold value ≥7 points) and for differentiation of manifest and prodromal pathology (AUC – 0.891, sensitivity – 78.6%, specificity – 85.7% at a threshold value ≥21 points). Risk stratification identified three categories: low risk (0–12 points, <5% probability of conversion within 24 months), moderate risk (13–24 points, 20–30% conversion) and high risk (≥25 points, >50% conversion). In the prodromal group, the most frequent microsignals were REM sleep behavior disorder (67.9%), hyposmia (71.4%), chronic constipation (78.6%), subjective cognitive decline (82.1%), reduced arm swing during walking (46.4%) and hypomimia (42.9%).

Conclusions: The PMS scale is a clinically effective and low-cost tool for identifying individuals at risk of developing neurodegenerative diseases years before the manifestation of classical symptoms. Its use does not require specialized equipment and is feasible at the level of primary medical care through history taking, observation and basic neurological examination. The scale demonstrates high psychometric properties and provides risk stratification, enabling individualized monitoring and early intervention strategies. This approach marks a transition to proactive diagnostic models in neurology. It has significant value for screening programs among middle-aged and older individuals with subclinical neurobehavioral complaints. Early detection using PMS assessment allows timely application of neuroprotective and preventive interventions, potentially altering the course of the disease before irreversible neuronal loss.

Keywords: *prodromal symptoms; early diagnosis; risk stratification; α-synuclein; REM sleep behavior disorder; Parkinson's disease; Alzheimer's disease; dementia with Lewy bodies; progressive supranuclear palsy; phenotypic microsignals*

Introduction

Neurodegenerative diseases, in particular Alzheimer's disease (AD), Parkinson's disease (PD), dementia with Lewy bodies (DLB), multiple system atrophy (MSA), progressive supranuclear palsy (PSP), and corticobasal degeneration (CBD), represent one of the key problems of modern neurology due to their progressive course, irreversibility of neuronal damage, and limited possibilities for etiopathogenetic treatment [1, 2]. Despite significant progress in studying the molecular and neuroimaging mechanisms of neurodegeneration, clinical diagnosis is still based mainly on established syndromes, when the pathological process has already led to a substantial loss of neuronal networks [3, 4]. Current concepts consider neurodegeneration as a long, multiphase process with preclinical and prodromal stages that may precede the manifestation of motor or cognitive syndromes by years or decades [5, 6]. At early stages, pathological changes predominantly involve evolutionarily ancient and functionally vulnerable structures of the nervous system—the olfactory pathways, brainstem nuclei, autonomic nervous system, limbic and fronto-subcortical networks—leading to the appearance of nonspecific, mildly expressed clinical manifestations [7, 8]. The prodromal period of neurodegenerative diseases is characterized by the predominance of non-motor symptoms, in particular sleep disturbances, autonomic dysregulation, emotional–affective disorders, cognitive flexibility impairment, and sensorimotor integration deficits [9]. Although subsequent clinical evolution differs among amyloidopathies, synucleinopathies, and tauopathies, early phenotypic manifestations demonstrate substantial overlap, which complicates early nosological differentiation while simultaneously reflecting shared mechanisms of initial neuronal network destabilization.

The present study is based on the hypothesis that a structured clinical assessment of the totality of prodromal non-motor signs identified during routine outpatient visits makes it possible to stratify individuals according to their risk of developing clinically manifest disease. Such manifestations are not specific biomarkers of individual diseases; however, their cumulative presence and dynamics may serve as clinical indicators of an active neurodegenerative process at the preclinical or prodromal stage, forming a basis for further multicenter studies and the development of strategies for the early detection of neurodegeneration.

Objective of the study: To identify and systematize early clinical phenotypic microsignals observed during initial outpatient visits and potentially associated with the development of a neurodegenerative process in diseases such as Alzheimer's disease, Parkinson's disease, dementia with Lewy bodies, multiple system atrophy, progressive supranuclear palsy, and corticobasal degeneration, as well as to develop a tool for clinical risk stratification of a neurodegenerative process at the prodromal stage based on a retrospective analysis of medical documentation and prospective observation.

Materials and methods

Study participants

The initial sample consisted of 140 individuals aged 48 to 76 years (mean age 64±7.2 years) who presented with suspected prodromal or early manifestations of neurodegenerative diseases, or were included as a control group. Of these, 28 individuals were excluded from the primary analysis due to clinically significant alcohol exposure (consumption >14 alcohol units per week for men and >7 for women). The final cohort comprised 112 participants (64 men and 48 women).

Inclusion criteria

Patients were eligible if they met the following criteria: age 45–80 years; presence of at least three non-motor symptoms from different domains (cognitive, autonomic, sleep-related, sensory) lasting at least 12 months, or a combination of two non-motor symptoms with one subtle motor phenomenon; ability to provide informed consent and compliance with long-term follow-up.

Exclusion criteria

Drug-induced parkinsonism (use of neuroleptics, metoclopramide, cinnarizine during the last 6 months); significant cerebrovascular pathology on MRI (≥2 points on the Fazekas scale for white matter or >2 lacunar infarcts); severe depression (HADS-depression >15 points or major depression according to DSM-5); history of schizophrenia or other psychotic disorders in history; traumatic brain injury with loss of consciousness >30 minutes; active oncological pathology or terminal stage of somatic diseases; alcohol or psychoactive substance abuse; inability to complete neuropsychological testing due to language barrier or pronounced sensory deficit (blindness, deafness).

Group characteristics

The cohort was divided into three groups. Group 1 (prodromal/non-manifest pathology, n=28) included individuals with prodromal conditions without final nosological determination at the time of inclusion. These participants were characterized by a combination of multiple non-motor symptoms from different domains, absence of full diagnostic criteria for manifest disease, and no alternative explanation for the observed symptomatology. Group 2 (manifest pathology, n=56) included patients with a clinically established diagnosis: amyloidopathies (Alzheimer's disease, n=16), synucleinopathies (Parkinson's disease n=28, dementia with Lewy bodies n=9), and tauopathies (progressive supranuclear palsy n=3). Group 3 (control group, n=28) included individuals without clinical manifestations of neurodegenerative pathology.

Study design

The study was conducted as a single-center clinical observational study with a prospective phase, which included the development and prognostic validation of a clinical tool for detecting phenotypic microsignals of neurodegeneration. The study was carried out at the University Hospital of Kharkiv National Medical University in the period from January 1, 2020 to August 1, 2025 in accordance with the principles of the Declaration of Helsinki (2013 revision). All participants provided written

informed consent; the study protocol was approved by the local bioethics committee. Diagnosis was established by two independent neurologists specializing in movement disorders and cognitive neurology (work experience 8 and 14 years, respectively), who did not participate in the development of PMS. In case of diagnostic discrepancies (11 cases, 13.1%), an expert discussion was conducted involving a third neurologist with 22 years of experience followed by repeated blinded review of clinical data, including video materials. The final diagnosis was established according to international disease-specific criteria: NIA-AA for Alzheimer's disease (McKhann *et al*., 2011) [10], MDS Clinical Diagnostic Criteria for Parkinson's disease (Postuma *et al*., 2015) [11], consensus criteria for dementia with Lewy bodies (McKeith *et al*., 2017) [12], NINDS-PSP criteria for progressive supranuclear palsy (Höglinger *et al*., 2017) [13]. To minimize incorporation bias, the diagnosing neurologists did not have access to PMS scale scores at the time of diagnosis; PMS assessment was performed by a separate investigator, a clinical psychologist with experience in neuropsychological diagnostics, who did not participate in the diagnostic process and was blinded to the neurologists' clinical hypotheses.

Each patient underwent a standardized protocolized examination procedure. Non-motor symptoms were recorded using structured validated instruments: the RBD Single-Question Screen questionnaire (RBD1Q: "Have you ever been told, or suspected yourself, that you seem to 'act out your dreams', for example, punching, flailing your arms, running?") for screening REM sleep behavior disorder, ROME IV criteria for functional constipation (≥2 criteria: straining, hard/fragmented stool, feeling of incomplete evacuation, manual maneuvers for defecation, <3 defecations per week); Hospital Anxiety and Depression Scale (HADS; separate anxiety and depression subscales), Apathy Evaluation Scale clinical version (AES-C, 18 items, cutoff ≥37 points for clinically significant apathy) and Fatigue Severity Scale (FSS, 9 items, cutoff ≥4 mean score for pathological fatigue).

Olfactory functions were assessed using a simplified odor recognition test adapted for the Ukrainian-speaking population: the patient was presented with 12 standardized odors (coffee, lemon, mint, onion, garlic, vanilla, cinnamon, fir tree, rose, vinegar, camphor, chocolate) in opaque bottles; four response options were offered for each; hyposmia was diagnosed when fewer than 9 out of 12 odors were correctly recognized (sensitivity 78±3.2%, specificity 81±2.8% according to validation data for the Eastern European population). Autonomic disturbances were determined using an active orthostatic test with measurement of blood pressure and heart rate in the supine position after 5 minutes of rest, then at the 1st and 3rd minutes of standing; orthostatic hypotension was diagnosed according to consensus criteria as a decrease of systolic pressure ≥20 mmHg or diastolic pressure ≥10 mmHg. In patients with a positive orthostatic test or clinical complaints of dizziness upon standing (n=27), the presence of compensatory tachycardia (increase in heart rate >15 bpm) was additionally recorded to differentiate neurogenic and non-neurogenic orthostatic hypotension.

Cognitive profile was determined using a standardized battery: Mini-Mental State Examination (MMSE) with correction for educational level (<9 years of education: +1 point to cutoff 24), Montreal Cognitive Assessment (MoCA) Ukrainian version 7.1 with education correction (≤12 years: +1 point to cutoff 26), Frontal Assessment Battery (FAB) to assess executive functions (cutoff <16 points for frontal dysfunction). In all patients with MoCA <26 or FAB <15 points (n=38, 33.9%), an extended neuropsychological battery was applied: Clock Drawing Test (CDT) for visuospatial and executive functions, 10-word learning test to assess verbal memory with immediate and delayed recall (after 20 minutes), phonemic (within 60 seconds words beginning with the letter "S") and categorical (naming animals) verbal fluency, Trail Making Test part A (information processing speed, norm <78±12 seconds for age 60–69 years) and part B (cognitive flexibility, norm <273±38 seconds), Luria's hand movement sequencing test for dynamic praxis. Signs of dysfunction of limbic-frontal networks were separately and structurally assessed. These included apathy not associated with depression (AES-C ≥37 points with HADS-depression <8), anhedonia according to the SHAPS subscale (Snaith-Hamilton Pleasure Scale, ≥3 points), reduction of spontaneous speech production (counting the number of words during 2 minutes of free conversation on a neutral topic "describe your typical day", norm >120 words), changes in personality traits or behavior according to a standardized questionnaire for a close relative or cohabitant addressing changes in character, interests, social activity during the last year).

Subtle motor phenomena were assessed according to a standardized protocol with obligatory video recording (Sony HDR-CX405 camera, 1920×1080, 50 fps). The following parameters were evaluated: asymmetry of arm swing while walking (assessment over a distance of 10 meters at a normal pace with three repetitions, binary assessment: symmetric/asymmetric with indication of the side of reduction), hypomimia according to a 4-point scale (0 — normal facial expression, 1 — mild reduction of facial movements noticeable only on targeted assessment, 2 — noticeable reduction of spontaneous facial expression with reduction of forehead wrinkles and infrequent blinking, 3 — mask-like face with almost complete absence of spontaneous facial movements); micrographia (writing the standard phrase "Today the weather is good" three times in a row on an unlined A4 sheet, measuring the height of five middle letters in each phrase and calculating the coefficient of progressive reduction: $(h_1 - h_3) / h_1$; a coefficient >0.10 was considered pathological); hypophonia (subjective assessment during conversation + objective measurement using a mobile decibel meter at a distance of 1 meter while reading a standard text loudly in a normal voice, normal value >55 dB), decrement during repetitive finger movements (finger tapping test: maximal rapid tapping of the index finger with the thumb for 10 seconds, separately for each hand, counting the number of taps and visual assessment of decrease in amplitude and/or speed during the test; <40 taps in 10 seconds or obvious decrement was considered pathological). All video recordings (duration 6–10 minutes per patient) were stored in anonymized form and

reviewed by two independent expert neurologists blinded to diagnosis, clinical data, and initial assessment results. Inter-expert agreement was assessed using Cohen's kappa for binary variables (arm swing asymmetry, presence of decrement) and weighted kappa for ordinal variables (degree of hypomimia).

Instrumental verification included brain MRI scanning in sagittal, axial, and coronal planes. Visual assessment was performed including medial temporal lobe atrophy according to the Scheltens scale (0–4 points, assessed separately for the hippocampus and entorhinal cortex, ≥2 points — moderate atrophy, ≥3 points — severe atrophy), global cortical atrophy according to the GCA scale (global cortical atrophy, 0–3 points), white matter lesions according to the Fazekas scale (0–3 points assessed separately for periventricular and deep lesions), presence of lacunar infarcts (>3 mm and <15 mm in diameter in deep regions), ventricular enlargement. All MRI studies were evaluated by a radiologist specializing in neuroimaging (16 years of experience) who was blinded to the clinical diagnosis. Patients with cognitive impairment (MoCA <26, n=38) underwent mandatory laboratory testing to exclude secondary causes of cognitive decline including complete blood count, determination of vitamin B12 levels (norm >200 pg/mL), folic acid (norm >3 ng/mL), thyroid-stimulating hormone (norm 0.4–4.0 mIU/L), fasting glucose, creatinine with calculation of glomerular filtration rate, serological test for syphilis (RPR or TPHA).

Development of the Phenotypic MicroSignals Scale (PMS) was carried out in several consecutive stages during 2023 and was based on the fundamental principles of network neuroscience and the clinical phenomenology of early neurodegeneration. The conceptual foundation of PMS was the hypothesis that early neurodegeneration manifests not so much as loss of function, but as loss of network plasticity, flexibility, and synchronization of neuronal systems. In contrast to classical diagnostic instruments focused on deficit and disability, PMS captures subtle disturbances of coordination between neuronal networks at the preclinical level, reflected in behavioral, autonomic, cognitive, and submotor phenomena long before the formation of classical clinical syndromes. The theoretical model of PMS is based on five neurobiological principles [14–20]. First, the evolutionary–anatomical principle of Braak proposes that pathological protein aggregates (α-synuclein, tau, amyloid-β) initially appear not in the cerebral cortex, but in phylogenetically older structures—the olfactory nuclei, the dorsal motor nucleus of the vagus nerve, the locus coeruleus, the raphe nuclei. This explains why the first clinical manifestations of neurodegeneration are hyposmia, constipation, REM sleep disorders, and depression, rather than dementia or parkinsonism. Second, the principle of network brain organization suggests that the pathological process spreads not randomly but along functionally and structurally connected neuronal networks (default mode network, salience network, fronto-striatal circuits), which leads to impaired synchronization between networks and reduced cognitive flexibility earlier than the loss of specific functions. Third, the principle of neurotransmitter cascade proposes that prodromal neurodegeneration initially affects monoaminergic systems (serotonin, noradrenaline) and the cholinergic system, which clinically manifests as disturbances of sleep, mood, autonomic regulation, and attention, and only at later stages affects the dopaminergic system with the development of motor symptoms. Fourth, the principle of the neuro-glio-vascular unit: the first to respond to the neurodegenerative process are not neurons but astrocytes and microglia leading to disruption of metabolic support of neurons, dysfunction of the blood–brain barrier, and microcirculatory changes. Clinically these alterations manifest as fatigue, symptom fluctuations, and "mental fog" earlier than structural changes on MRI. Fifth, the clinical–epidemiological principle of synergy indicates that according to prospective studies (Postuma *et al*., 2012; Berg *et al*., 2015) [21, 22], a single prodromal symptom has low prognostic value (hazard ratio 2–4), whereas a combination of symptoms from different domains increases the risk of conversion exponentially (hazard ratio >20 for 4–5 symptoms), which substantiates the cumulative principle of scale construction.

Based on a systematic analysis of the literature on prodromal neurodegeneration (systematic search in PubMed using the keywords "prodromal," "premotor," "preclinical" in combination with "Parkinson," "Alzheimer," "Lewy body," "neurodegeneration"), a review of international consensus criteria for prodromal states (MDS Research Criteria for Prodromal Parkinson's Disease 2015 [22], NIA-AA Preclinical Alzheimer's Disease 2011 [10]), and a retrospective analysis of 84 medical histories of patients with established neurodegenerative diagnoses with reconstruction of the prodromal period based on active interviews with patients and their relatives, an initial list of 42 potential phenotypic microsignals was formed. Phenotypic microsignals were included in the list provided that four criteria were simultaneously met: (1) documented temporal association in the literature with the subsequent manifestation of a neurodegenerative disease—the symptom must occur statistically significantly more often in individuals who later develop a neurodegenerative disease compared with the control group, and precede the clinical diagnosis by at least 6–12 months; (2) pathophysiological validity—the presence of evidence of involvement of specific neuronal networks, structures, or neurotransmitter systems according to neuroimaging, neurophysiological, or pathomorphological studies; (3) clinical measurability—the possibility of objective or semi-objective assessment of the symptom using validated instruments available in routine clinical practice, without the need for complex equipment; (4) inter-expert reproducibility—demonstrated in validation studies as agreement of assessment between independent researchers at the level of Cohen's kappa or ICC >0.60. A three-stage modified Delphi procedure (March–May 2023) was conducted with the participation of five independent expert neurologists. In the first round, experts assessed the clinical significance of 42 microsignals on a 9-point scale; 10 items were excluded due to low ratings or lack of consensus. In the second round, 32 microsignals were reassessed taking into account the summarized results, and consensus was achieved for all items (median ≥7, IQR ≤2). In the third round, experts determined the prognostic weight of microsignals; however, an unweighted system was

applied in the final scale to simplify clinical use and increase reliability.

Statistical analysis

The sample size calculation was based on the assumption that the conversion rate of prodromal conditions into manifest forms would be 35–45% over 24 months of follow-up (based on literature data for prodromal Parkinson's disease and mild cognitive impairment), the expected area under the ROC curve for the PMS scale would be at least 0.75, and the minimally acceptable width of the 95% confidence interval for AUC would be 0.15. Under these parameters, with α=0.05 and a power of 80%, the required sample size was 76–82 patients; the actual sample of 112 individuals (84 patients with pathology and 28 controls) provided sufficient statistical power considering possible attrition (10–15%).

To empirically verify the domain structure of PMS and reduce the number of items, an exploratory factor analysis (principal component method with varimax rotation to maximize interpretability of factors) was conducted on the baseline dataset of 84 patients from groups 1 and 2 (period January–June 2023). Before performing factor analysis, data adequacy was confirmed. The Kaiser–Meyer–Olkin criterion showed a value of 0.71±0.04 (>0.60 acceptable, >0.70 good), indicating sufficient correlation between variables for factorization. Bartlett's test of sphericity showed a statistically significant result (χ^2=394.7±18.3, df=496, p<0.001), rejecting the null hypothesis of non-correlated variables. The number of factors for extraction was determined based on three criteria: (1) Kaiser criterion—eigenvalue >1.0 (9 factors extracted), (2) scree plot analysis with identification of the "elbow" (visually at the 7th–8th factor), (3) criterion of interpretability and clinical meaningfulness of factors. The optimal solution was found to include 7 factors, which explained 68.4±3.2% of the total variance (factor 1: 18.2±2.1%, factor 2: 12.7±1.8%, factor 3: 10.1±1.5%, factor 4: 9.3±1.4%, factor 5: 7.8±1.2%, factor 6: 5.6±0.9%, factor 7: 4.7±0.8%). Microsignals were included in a domain provided that the factor loading was >0.50 on the corresponding factor (high loading) and <0.35 on all other factors (low cross-loading), thereby ensuring a clear domain structure. ROC analysis was performed for three comparisons (manifest vs. control, prodromal vs. control, manifest vs. prodromal) to assess the diagnostic accuracy of the PMS scale. Correlation and multiple regression analyses were used to identify predictors of the total PMS score.

Results

The clinical cohort that was empirically analyzed consisted of 112 patients. The age range of the sample was from 48 to 76 years, with a mean age of 64.0 ± 7.2 years, indicating a predominant concentration of participants in the period of late middle age and early old age. Gender distribution showed a moderate predominance of men—57.1% (n=64), whereas women accounted for 42.9% (n=48). Although this distribution does not reach ideal symmetry, it is not methodologically critical and is consistent with typical epidemiological patterns observed in population studies of chronic neurodegenerative processes [23, 24]. The observation period lasted from January 1, 2020 to August 1, 2025, with prospective monitoring designed to track the conversion of prodromal states into manifest neurodegenerative diseases over 24 months. This protocol monitoring ensured consistency of dynamic observation without excessive burden on participants. During the full cycle of prospective monitoring, the cohort demonstrated high retention rates, providing a reliable basis for further analytical interpretations.

Frequency and spectrum of detected phenotypic microsignals at the baseline visit. During the initial clinical examination of individuals included in the study, a wide spectrum of phenotypic microsignals was identified, showing a high degree of variability both in clinical profile and in severity. The main domains with phenotypic microsignals are presented in ***Table 1***. For analysis, participants were divided into three groups: Group 1 (prodromal/non-manifest pathology, n=28), comprising individuals with prodromal states without definitive nosological determination; Group 2 (manifest pathology, n=56), including patients with clinically established diagnoses of neurodegenerative diseases: Alzheimer's disease (n=16), Parkinson's disease (n=28), dementia with Lewy bodies (n=9), progressive supranuclear palsy (n=3). Group 3 (control group, n=28), consisting of individuals without clinical manifestations of neurodegenerative pathology. Prodromal cases were characterized by a combination of multiple non-motor symptoms from different domains without full correspondence to the criteria of manifest disease and in the absence of alternative explanations for the symptomatology. In most cases, these symptoms did not reach the threshold necessary for a formal diagnosis, however, their pattern and sequence suggested latent neurovegetative dysfunction with potential prognostic significance. Risk assessment and comparisons were performed using the newly introduced Phenotypic MicroSignals Scale (PMS).

Characteristics of Group 1 (prodromal/non-manifest pathology (NM pathology), n=28). In the first group, which included 28 individuals with prodromal conditions without definitive nosological determination at the time of inclusion, phenotypic microsignals according to the developed PMS scale were detected in 92.9% (n=26) of patients with a total score ≥1. This cohort was characterized by a combination of multiple non-motor symptoms from different domains without full correspondence to the criteria of manifest disease and in the absence of alternative explanations for the symptomatology. The mean age of participants was 63.2±6.8 years (range 51–74 years) with a gender distribution of 57.1% (n=16) men and 42.9% (n=12) women. The mean duration of symptoms from the onset of the first complaints to inclusion in the study was 4.7±2.3 years (range 1.2–9.5 years).

The most common findings were disturbances of sleep architecture with a predominance of behavioral disorders during rapid eye movement (REM) sleep. According to the RBD1Q questionnaire [25], positive responses regarding episodes of nocturnal motor activity associated with dreaming (shouting, arm flailing, striking movements) were recorded in 67.9% (n=19) of the examined individuals, which represented the highest rate among all domains. At the same time, in 42.1% (n=8 of 19) of cases relatives reported injuries during sleep (bruises on the partner's limbs, falling

out of bed), and in 31.6% (n=6 of 19) — vocalizations of varying intensity. The mean frequency of episodes was 2.8±1.4 per week (range 1–6). Excessive daytime sleepiness with an Epworth Sleepiness Scale score >10 was noted in 53.6% (n=15) of patients, with a mean score of 12.4±2.6 (range 11–18), accompanied by complaints of an overwhelming need for daytime rest regardless of the duration of nighttime sleep. Disturbances of the circadian sleep–wake rhythm in the form of phase inversion or fragmentation of nighttime sleep with multiple awakenings (>3 per night) were recorded in 60.7% (n=17) of individuals, with the mean number of awakenings per night being 4.6±1.8 (range 3–9).

Olfactory dysfunction was found to be the second most frequent phenotypic microsignal. According to the results of the simplified 12-odour identification test, hyposmia (correct identification of <9 odours) was diagnosed in 71.4% (n=20) of the group participants. The mean number of correctly recognized odours was 6.8±1.9 (range 3–11), which was significantly below the threshold value of 9 points. At the same time, 35.0% (n=7 of 20) patients with hyposmia were unaware of the presence of this disorder before testing, emphasizing the latent nature of the symptom. Anosmia (recognition of ≤3 odours) was recorded in 14.3% (n=4) of the examined individuals, with a mean value of 2.3±0.5 odours. The most frequently unrecognized were subtle odours including rose (82.4% errors), camphor (76.5%) and fir tree (71.8%), whereas intense odours were recognized better, including vinegar (31.2% errors), onion (35.3%) and garlic (38.8%).

Visual-perceptual phenomena in the form of episodic visual illusions (misperception of objects in the peripheral visual field, especially at dusk) were noted in 17.9% (n=5) of participants, with a frequency of 1.8±0.9 episodes per month, while formed visual hallucinations were absent. Central pain syndromes of unclear etiology (chronic pain in the limbs or trunk without a structural substrate on MRI) were observed in 21.4% (n=6) of patients, with an intensity of 4.3±1.2 points on the visual analogue scale (range 3–6).

Gastrointestinal manifestations were dominated by chronic constipation meeting the ROME IV criteria in 78.6% (n=22) of individuals. The mean frequency of defecation was 2.4±0.8 per week (range 1–4), with constipation duration exceeding 5 years in 68.2% (n=15 of 22), median 6.8 years (range 5.2–14.3 years), and exceeding 10 years in 31.8% (n=7 of 22), median 11.9 years (range 10.1–18.2 years). Accompanying symptoms included morning nausea in 39.3% (n=11), with a frequency of 3.4±1.6 episodes per week, and episodes of aerophagia in 28.6% (n=8) of cases.

Dysuric disorders were recorded in 60.7% (n=17) of patients: nocturia (≥2 episodes per night) in 50.0% (n=14), with a mean frequency of 2.8±0.9 episodes per night (range 2–5); imperative urges in 35.7% (n=10), with a frequency of 4.2±2.1 episodes per day; episodes of urgent urinary incontinence in 17.9% (n=5), with a frequency of 1.4±0.7 episodes per week. Orthostatic hypotension according to the active orthostatic test was found in 28.6% (n=8) of the examined participants, with mean systolic pressure decrease of 26.3±8.4 mmHg (range 20–44) and diastolic decrease of 13.7±4.2 mmHg (range 10–22). In 75.0% (n=6 of 8) of cases adequate compensatory tachycardia (increase in heart rate >15 bpm) was observed, with a mean increase of 21.8±5.3 bpm, indicating a non-neurogenic pattern, whereas in 25.0% (n=2) an insufficient tachycardic response with an increase of 8.5±2.1 bpm was characteristic of the neurogenic form.

Persistent hyperhidrosis without thermal or endocrine substrate was recorded in 46.4% (n=13) of individuals, predominantly localized in the head and upper trunk region (92.3%, n=12 of 13), less often in the palms (30.8%, n=4 of 13).

Psychoemotional disturbances were characterized by polymorphism of manifestations. Anxiety according to the HADS-anxiety subscale ≥8 points (subclinical or clinical level) was detected in 64.3% (n=18) of patients, with a mean score of 9.2±3.1 (range 8–16). Of these, a subclinical level (8–10 points) was observed in 55.6% (n=10 of 18), whereas clinical (≥11 points) in 44.4% (n=8 of 18). Depressive symptoms (HADS-depression ≥8 points) were recorded in 53.6% (n=15) of individuals, with a mean score of 8.7±2.8 (range 8–15), but no case reached the criteria of major depressive disorder according to DSM-5. Apathy not associated with depression (AES-C ≥37 points with HADS-depression <8) was found in 39.3% (n=11) of the examined individuals, with a mean score of 41.3±4.8 (range 37–52). Anhedonia according to the SHAPS scale ≥3 points was noted in 42.9% (n=12) of patients, with a mean score of 4.7±1.9 (range 3–9). Resistance to standard antidepressant therapy (lack of response to ≥2 drugs from different classes for >8 weeks) in the history was present in 28.6% (n=8) of individuals; the mean number of ineffective treatment attempts was 2.6±0.7 (range 2–4). Pathological fatigue with FSS ≥4 of the mean score was found in 57.1% (n=16) of participants, with a mean value of 5.2±1.1 points (range 4.1–7.3), accompanied by complaints of asthenia disproportionate to physical exertion for 5.3±1.8 hours per day.

Subjective cognitive complaints with preserved daily functioning were reported by 82.1% (n=23) of patients, most often in the form of forgetfulness for recent events (78.3%, n=18 of 23), difficulty concentrating (69.6%, n=16 of 23), and slowing of thought processes (60.9%, n=14 of 23). Objective episodic memory impairment with rapid forgetting according to the 10-word recall test (delayed recall after 20 minutes <5 words) was detected in 25.0% (n=7) of the examined individuals, with a mean value of 3.9±0.8 words (range 2–5), whereas immediate recall was 6.4±1.3 words (range 4–9), indicating impaired memory consolidation. Fluctuations of attention and reduced mental endurance were recorded in 46.4% (n=13) of individuals, manifested by episodes of cognitive instability during the day with deterioration under stress or fatigue; the mean duration of episodes was 32.7±14.2 minutes (range 15–65).

Visuospatial disorientation according to the clock-drawing test (<7 points on the 10-point Shulman scale) was noted in 17.9% (n=5) of patients, with a mean score of 5.8±0.9 (range 4–7). Language dysfunction in the form of anomia (word-finding difficulty) and reduced fluency was found in 32.1% (n=9): the mean letter fluency score (words beginning with "S" in 60 seconds) was 11.3±3.2 (range 6–17, normative value >15), and category fluency (animals) was 13.8±2.9 (range 9–19, normative value >18).

Table 1. Phenotypic Microsignal Scoring Scale for Neurodegenerative Risk Assessment

Domain	Phenotypic microsignal	Dominant neurodegenerative association*	Score
COGNITIVE / MEMORY	Subjective cognitive decline with preserved daily functioning	AD, prodromal AD, DLB	1
	Episodic memory impairment with rapid forgetting	AD (amyloidopathy)	3
	Attention fluctuations, reduced mental endurance	DLB, PD	2
	Visuospatial disorientation, constructional apraxia	AD, DLB	2
	Language dysfunction (anomia, reduced fluency)	AD, CBD	3
EXECUTIVE / FRONTAL	Slowed information processing	PD, PSP	1
	Impaired planning and task switching	PD, PSP, CBD	2
	Behavioral disinhibition or apathy	PSP, CBD, AD	3
SUBMOTOR / MOTOR	Reduced arm swing, unilateral motor subtlety	Prodromal PD, DLB	1
	Bradykinesia with axial predominance	PD, PSP	2
	Early postural instability or falls	PSP, MSA	3
	Limb apraxia, alien limb phenomena	CBD	3
OCULOMOTOR / SPEECH	Slowed saccades	PSP	2
	Vertical gaze palsy (early or incomplete)	PSP	3
	Hypophonia, dysarthria	PD, MSA	2
AUTONOMIC	Chronic constipation	PD, MSA	1
	Urinary urgency or retention	PD, MSA	2
	Orthostatic hypotension	MSA > PD	3
SLEEP	REM sleep behavior disorder	PD, DLB, MSA	3
	Excessive daytime sleepiness	PD, DLB	1
SENSORY / PERCEPTUAL	Hyposmia or anosmia	PD, AD	1
	Visual hallucinations or illusions	DLB	3
	Central pain syndromes	PSP, CBD	2
AFFECTIVE / LIMBIC	Anxiety, emotional lability	PD, AD	1
	Depression resistant to treatment	PD, AD	2
	Apathy, loss of initiative	PSP, CBD, AD	3
PERSONALITY / SOCIAL	Social withdrawal, reduced empathy	AD, FTD spectrum	2
	Loss of insight, anosognosia	AD	3
TOTAL PMS SCORE		Maximum possible score	48

Notes: * Dominant neurodegenerative association indicates the most commonly associated condition.
Abbreviations: AD — Alzheimer's disease; PD — Parkinson's disease; DLB — dementia with Lewy bodies; PSP — progressive supranuclear palsy; MSA — multiple system atrophy; CBD — corticobasal degeneration.

Slowing of information processing on the Trail Making Test Part A was found in 39.3% (n=11) of patients. The mean completion time was 84.3±16.7 seconds (range 79–128, norm <78 seconds for age 60–69 years). Impairment of planning and task switching on the Trail Making Test Part B was recorded in 35.7% (n=10) of the examined individuals: mean time 312.5±52.3 seconds (range 278–432, norm <273 seconds). The B/A ratio, reflecting the specificity of executive dysfunction, was 3.8±0.9 (norm <3.0). Frontal dysfunction with FAB <16 points was identified in 28.6% (n=8) of individuals, with a mean score of 14.2±1.8 (range 11–16); the most affected subtests were conceptualization (mean 1.8±0.6 of 3 possible) and motor programming (1.6±0.7 of 3). Reduction of spontaneous speech production (<120 words in 2 minutes of free conversation on the topic "describe your typical day") was noted in 42.9% (n=12) of patients with a mean value of 98.7±18.4 words (range 68–119), which is 21.3% below the normative threshold.

Behavioral disinhibition or apathy of clinically significant degree was observed in 25.0% (n=7) of cases, with a mean score on the corresponding Frontal Systems Behavior Scale subscale of 24.3±6.2 (range 18–36, norm <15). Reduction of arm swing on one side while walking, according to video analysis, was found in 46.4% (n=13) of the examined individuals; in 76.9% (n=10 of 13) left-sided asymmetry was observed, whereas right-sided asymetry was present in 23.1% (n=3 of 13). The mean decrease in swing amplitude on the affected side was 38.6±12.4% compared to the contralateral side (range 20–65%). Inter-rater agreement for asymmetry assessment, according to Cohen's kappa was 0.82±0.07. Hypomimia ≥1 point on the 4-point scale was recorded in 42.9% (n=12) of patients: 1 point — in 28.6% (n=18 of 28 examined, which is 28.6% of the whole group or 66.7% among those who had hypomimia), 2 points — in 14.3% (n=4), 3 points were not observed in any case. Inter-rater agreement for hypomimia assessment according to weighted kappa was 0.78±0.06. Micrographia with a pathological progressive reduction coefficient >0.10 was detected in 32.1% (n=9) of individuals with a mean coefficient of 0.14±0.03 (range 0.11–0.22), while the mean letter height in the first sentence was 4.8±0.7 mm and in the third 4.1±0.6 mm, corresponding to a 14.6% reduction. Hypophonia <55 dB during standardized text reading at a distance of 1 meter was recorded in 28.6% (n=8) of the examined individuals with a mean value of 51.8±3.2 dB (range 46–55), which is 5.8% below the normative threshold. A decrement on the finger tapping test was found in 35.7% (n=10) of patients: the mean number of taps in 10 seconds was 36.4±5.1 (range 28–39, norm ≥40), with a decrease in frequency during the test of 18.3±6.7%. Inter-rater agreement for decrement assessment according to Cohen's kappa was 0.74±0.08. Bradykinesia with axial predominance (slowing when turning in bed, rising from a chair, turning while walking) was noted in 21.4% (n=6) of cases, with a score of 1–2 points according to item 3.14 of the MDS-UPDRS Part III. Early postural instability or falls were recorded in 10.7% (n=3) of individuals: in 2 cases (7.1%) — episodes of instability without falls, in 1 case (3.6%) — falls with a frequency of 2 episodes over 6 months. Limb apraxia and "alien hand" phenomena were absent in all examined participants. Slowing of saccades on clinical testing (slow eye movements when shifting gaze between two targets at a distance of 30 cm with an interval of 90 degrees) was detected in 17.9% (n=5) of patients; the mean saccade duration was 0.28±0.04 seconds (norm <0.20 seconds), which exceeds normative values by 40%. Early or incomplete vertical ophthalmoplegia was not recorded in any case. Hypophonia and dysarthria, in addition to the previously described cases of reduced voice loudness, included elements of monotony of intonation in 25.0% (n=7), with a perceptual analysis score of 2.3±0.6 points on a 5-point scale, and difficulty in phrase initiation in 21.4% (n=6) of the examined participants, with a latency of 2.8±0.9 seconds (norm <1.5 seconds). Social withdrawal and reduced empathy according to a standardized questionnaire for close relatives were identified in 35.7% (n=10) of patients, manifested by a 42.3±18.7% decrease in the frequency of social contacts compared with the previous year, loss of interest in former hobbies in 60.0% (n=6 of 10) of cases, and a reduced emotional response to the problems of others according to relatives' assessment by 3.8±1.2 points on a 10-point scale. Loss of insight and anosognosia were not recorded in any case.

According to brain MRI, moderate atrophy of the medial temporal structures (≥2 points on the Scheltens scale) was found in 32.1% (n=9) of patients. The mean score for the hippocampus was 1.8±0.9 (range 0–3), for the entorhinal cortex 1.6±0.8 (range 0–3). Global cortical atrophy according to GCA ≥1 point was noted in 39.3% (n=11), with a mean score of 1.4±0.6 (range 1–2). White matter lesions according to Fazekas were found in 50.0% (n=14): periventricular lesions of 1 point — in 28.6% (n=4 of 14), 2 points — in 21.4% (n=3 of 14); deep lesions of 1 point — in 35.7% (n=5 of 14), whereas no case reached the exclusion criterion of ≥2 points. Lacunar infarcts were detected in 7.1% (n=2) of patients (one infarct in each case, 4–5 mm in diameter in the basal ganglia).

Laboratory parameters in patients with cognitive impairment (n=10, 35.7% of the group) were within normal limits. The mean vitamin B12 level was 342.7±118.3 pg/mL (range 210–598, norm >200), folic acid 6.8±2.4 ng/mL (range 3.2–12.1, norm >3), TSH 2.1±0.9 mIU/L (range 0.6–3.8, norm 0.4–4.0), fasting glucose 5.3±0.6 mmol/L (range 4.4–6.2), eGFR 78.4±12.7 mL/min/1.73m² (range 62–98). Serological tests for syphilis were negative in all cases.

The mean total score on the Phenotypic Microsignal Scale in Group 1 was 11.4±3.8 (range 2–19 points, median 11 points) with a maximum possible score of 48 points. Based on the obtained data, we developed a risk stratification system for the development of neurodegenerative diseases, which was based on three categories: low risk (0–12 points), moderate risk (13–24 points), and high risk (≥25 points). According to this stratification, Group 1 was distributed as follows: the low-risk category included 67.9% (n=19) of patients with a mean score of 8.2±3.1 (range 2–12), which constituted 17.1% of the maximum possible score; the moderate-risk category — 32.1% (n=9), with a mean score of 16.8±2.4 (range 13–19), corresponding to 35.0% of the maximum; no patient entered the high-risk category (0%, n=0), since the maximum score in Group 1 was 19 points. Thus, 32.1% (n=9) of patients in the prodromal

group had a moderate level of risk of developing manifest neurodegenerative disease according to the developed stratification system. This finding emphasizes the clinical significance of the identified phenotypic microsignals and their potential for early identification of individuals at increased risk of neurodegenerative progression. Correlation analysis revealed statistically significant associations between the total PMS score and key clinical parameters including duration of symptoms ($r=0.52$, $p=0.004$), age of patients ($r=0.38$, $p=0.042$), and the number of affected domains ($r=0.76$, $p<0.001$). Multiple regression analysis showed that the greatest contribution to the total PMS score was made by sleep disorders ($\beta=0.34$, $p=0.002$), olfactory dysfunction ($\beta=0.28$, $p=0.008$), and autonomic disorders ($\beta=0.26$, $p=0.012$), which explained 68.4% of the variance of the total score ($R^2=0.684$, $p<0.001$). These results confirm the construct validity of the PMS scale and demonstrate that non-motor symptoms, in particular sleep disturbances, olfactory and autonomic dysfunctions, are the most significant predictors of neurodegenerative risk at the prodromal stage.

Stratification of patients by risk level for developing neurodegenerative diseases based on the Phenotypic Microsignals Scale (PMS). One of the key results of this study was the implementation of a multilevel system for stratifying patients according to the risk of developing neurodegenerative diseases (NDDs). Stratification was based on the total score obtained using the PMS, which made it possible to quantitatively assess the current phenotypic status of the patient and qualitatively predict the likelihood of transformation of the prodromal state into a clinically manifest form of the disease. Based on the obtained results, three clinically significant risk categories were identified: low (0–12 points), moderate (13–24 points), and high (≥25 points). This approach opens new opportunities for proactive clinical intervention, targeted monitoring, and personalized patient management. Summary data are presented in ***Table 2***.

Low-risk category (0–12 points). Patients classified in the low-risk category according to the total score on the Phenotypic Micro-Signals (PMS) Scale constituted the largest proportion of the prodromal cohort (67.9%, n=19 from Group 1). These individuals demonstrated isolated or multiple phenotypic manifestations, with a mean total PMS score of 8.2±3.1 (range 2–12), which accounted for 17.1% of the maximum possible score. The clinical profile was characterized by mild or moderate expression of non-motor symptoms across various domains, without sufficient accumulation to reach the moderate-risk threshold. Such symptoms included episodic sleep disturbances (REM sleep behavior disorder in some cases), olfactory dysfunction, autonomic manifestations (constipation, urinary symptoms), mild cognitive complaints with preserved daily functioning, and subtle motor phenomena. From a clinical and prognostic perspective, this phenotypic configuration was associated with a conversion rate to manifest neurodegenerative disease of less than 5% during the observation period, indicating a relatively low short-term prognostic risk. However, the presence of documented prodromal markers, even at a low cumulative level, requires further clinical attention. From a practical standpoint, this clinico-phenotypic configuration does not require immediate engagement in intensive diagnostic algorithms—specifically, extended neuroimaging, biomarker analysis, or extensive neuropsychological batteries. Management of patients in this category can be carried out within the framework of standard outpatient follow-up with periodic reassessment (annually or semiannually), focusing on basic evaluation of functional status, monitoring symptom progression, and educational interventions regarding risk factors for neurodegeneration and lifestyle modification. However, considering the potential impact of certain anamnesis risk factors (family history of neurodegenerative diseases, presence of vascular comorbidities, exposure to chronic stress or circadian rhythm disturbances), it is recommended to form an individualized clinical profile, including monitoring of possible triggers and periodic reassessment using PMS. This will allow timely detection of early signs of shift to a higher risk category and adaptation of patient management strategies to evolving clinical realities.

Moderate-risk category (13–24 points). The moderate-risk category, which included patients with a total PMS score of 13-24, encompassed 32.1% (n=9) of the prodromal cohort (Group 1) with a mean score of 16.8±2.4 (range 13–19), which accounted for 35.0% of the maximum possible score. This category was characterized by a polysymptomatic clinical profile with clear accumulation of phenotypic micro-signals across multiple domains, indicating initial signs of multi-network neurophysiological dysregulation. In most cases, a combination of affective, autonomic, cognitive, sensory, and subtle motor manifestations was observed, forming a clinically significant prodromal phenotype with internal structure and domain diversity. The affective domain in this cohort was characterized by predominance of anxiety states (HADS-anxiety ≥8 in 64.3%), depressed mood (HADS-depression ≥8 in 53.6%), apathy not associated with depression (AES-C ≥37 in 39.3%), and anhedonia (SHAPS ≥3 in 42.9%). Patients reported persistent subjective feelings of tension, loss of motivation, reduced behavioral initiative, and treatment-resistant

Table 2. Risk Stratification Based on Phenotypic Micro-Signal Scale (PMS Scale)

Risk Category	PMS Score Range	Estimated Risk of NDD Progression	Clinical Implication
Low	0-12	<5%	Routine dynamic observation
Moderate	13–24	~20–30%	Enhanced clinical monitoring
High	≥25	>50%	Comprehensive diagnostic evaluation

mood disorders (28.6% with a history of unsuccessful antidepressant therapy), indicating early signs of limbic system dysregulation. Autonomic symptoms included chronic constipation meeting ROME IV criteria (78.6%), orthostatic hypotension (28.6%), urinary dysfunction including nocturia and urgency (60.7%), and excessive sweating (46.4%). These autonomic disturbances indicated impaired sympathetic-parasympathetic balance and initial disorganization of autonomic regulation, typical of early stages of neurodegenerative processes, especially in synucleinopathies. Sleep architecture disturbances were pronounced, particularly REM sleep behavior disorder (67.9% positive responses on RBD1Q), excessive daytime sleepiness (53.6% with Epworth >10), and sleep fragmentation (60.7% with >3 awakenings per night). Cognitive symptoms in this group had not yet reached the threshold for dementia but manifested as subjective cognitive decline (82.1%), episodic memory impairment with rapid forgetting (25.0%), attention fluctuations (46.4%), slowed information processing (39.3%), and executive dysfunction (35.7%). These phenomena were detected during targeted neuropsychological testing (MoCA, FAB, Trail Making Test), even when routine screening remained within normal limits. Sensory changes were particularly frequent, including hyposmia (71.4% with correct identification of <9 out of 12 odors), with 35% of patients being unaware of their olfactory deficit prior to testing—a recognized non-motor biomarker that often precedes manifest motor symptoms in Parkinson's disease. Subtle motor phenomena included asymmetry of arm swing (46.4%), hypomimia (42.9%), micrographia (32.1%), and decrement on the finger-tapping test (35.7%). Concomitant complaints of pathological fatigue (FSS ≥4 in 57.1%) and reduced spontaneous speech production (42.9% with <120 words in a 2-minute discourse) were also characteristic of this category. The conversion rate from prodromal state to clinically manifest neurodegenerative disease in the moderate-risk category was estimated at approximately 20–30% over a 24-month observation period, significantly exceeding population baseline rates. This finding necessitates intensified dynamic monitoring with careful tracking of cognitive, emotional, autonomic, and motor parameters. Within the framework of clinical tactics, it is advisable to conduct evaluations at least twice a year with reassessment using PMS, cognitive screening (MoCA, FAB), standardized assessment of sleep architecture, autonomic function testing, and evaluation of olfactory function. In the case of detection of negative dynamics—specifically, the appearance of new symptoms, worsening of existing ones, or an increase in PMS score crossing into the high-risk territory—it is strongly recommended to implement modern instrumental diagnostic methods, including brain MRI with a focus on midbrain structures and medial temporal regions, comprehensive multidomain neuropsychological testing, and autonomic profiling. Timely stratification of patients in this risk category allows identification of individuals with an increased likelihood of neurodegenerative progression at the preclinical stage, opening opportunities for proactive clinical intervention, intensified monitoring protocols, and potential implementation of disease-modifying or neuroprotective therapeutic strategies.

High-risk category (≥25 points). Patients with a total PMS score ≥25 were classified into the high-risk category. Notably, in the prodromal cohort (Group 1), no patient reached this threshold, as the maximum observed score was 19. Therefore, this category is defined theoretically and based on extrapolation from patients with established manifest neurodegenerative diseases (Group 2), where such scores would be expected. This group would be characterized by the presence of multiple, persistent, recurrent, and mutually reinforcing phenotypic micro-signals across virtually all evaluated domains, demonstrating high chronological stability, clear progression over time, and morphofunctional interdependence. In the clinical spectrum of such patients, a predominance of a wide range of non-motor symptoms would be expected, including pronounced REM sleep behavior disorder with frequent traumatic episodes, marked hyposmia or anosmia, significant autonomic insufficiency (neurogenic orthostatic hypotension, severe constipation, urinary dysfunction), alongside clear motor phenomena such as hypomimia, bradykinesia, reduced arm swing, and possibly early postural instability. Additionally, patients in this category would be expected to exhibit clear signs of reduced cognitive flexibility, executive function and behavioral initiative impairment, visuospatial dysfunction, episodic memory deficits, and involvement of fronto-limbic structures in the pathological process, manifesting as apathy, reduced spontaneous activity, and social withdrawal. The frequency of developing neurodegenerative disease in this group would be expected to exceed 50% over 24 months, representing patients at the threshold or already meeting criteria for manifest disease. This would be confirmed by both clinical dynamic observation and instrumental methods, including MRI detecting medial temporal atrophy or midbrain changes, multi-domain neuropsychological testing demonstrating deficits in multiple cognitive domains, and pathological autonomic function tests. Given the high prognostic probability, immediate referral of patients for comprehensive diagnostic evaluation is clinically necessary, including detailed neuroimaging (MRI with volumetric analysis, potentially DaTscan if synucleinopathy is suspected), extensive neuropsychological assessment, autonomic function testing, polysomnography for suspected REM sleep disorder (RBD), and, if clinically indicated, genetic counseling, CSF biomarker analysis, or advanced imaging methods. In a high-risk situation, clinicians should consider initiating disease-specific therapeutic interventions, including neuroprotective strategies, symptomatic treatment of non-motor symptoms (RBD, autonomic dysfunction, neuropsychiatric symptoms), and comprehensive multidisciplinary care involving neurology, neuropsychology, psychiatry, and rehabilitation services.

Characteristics of Group 2 (manifest pathology, n=56). The second group included 56 patients with clinically established diagnoses of neurodegenerative diseases, verified by two independent neurologists according to international disease-specific criteria. The mean age of participants was 68.4±6.9 years (range 52–77 years), which was 5.2 years older than the mean age of the prodromal group (p=0.003). Gender distribution showed a predominance of men — 60.7%

(n=34) versus 39.3% (n=22) women. The mean disease duration from the onset of initial motor or pronounced cognitive symptoms to study inclusion, was 3.8±2.6 years (range 0.5–11.2 years). According to nosological structure, the group was distributed as follows: amyloidopathies (Alzheimer's disease) — 28.6% (n=16), synucleinopathies (Parkinson's disease — 50.0%, n=28; Lewy body dementia — 16.1%, n=9), and tauopathies (progressive supranuclear palsy) — 5.4% (n=3). All patients underwent comprehensive clinical-instrumental evaluation with mandatory MRI verification of diagnosis.

Alzheimer's disease (n=16, 28.6% of Group 2). The subgroup of patients with Alzheimer's disease included 16 individuals, representing 28.6% of Group 2. The mean age of the examined patients was approximately 70 years, with a slight predominance of women. The average disease duration did not exceed three years, with mild and moderate stages of dementia predominating. The clinical picture was characterized by universal impairment of episodic memory with pronounced consolidation deficits, reduction in global cognitive scores, and significant executive dysfunction. Visuospatial, language, and attention deficits, as well as affective and behavioral symptoms, were common. Social functioning and insight into condition were substantially reduced in a significant portion of patients. Neuroimaging data showed predominant atrophy of the medial temporal structures combined with generalized cortical atrophy and vascular changes in the white matter. Key clinical-demographic, neuropsychological, and MRI parameters are presented in ***Table 3***.

The mean total PMS score in the subgroup of patients with Alzheimer's disease was 28.6±5.4 points (range 19–38 points, median — 29 points). Analysis of the distribution by risk categories showed no patients with low risk (0–12 points). Moderate risk (13–24 points) was found in 18.8% of patients (n=3) with a mean score of 21.3±2.1 points, whereas the vast majority of examined patients — 81.3% (n=13) — belonged to the high-risk category (≥25 points) with a mean score of 31.2±4.8 points.

Parkinson's disease (n=28, 50.0% of Group 2). The subgroup of patients with Parkinson's disease was the largest in Group 2 and included 28 individuals with a mean disease duration of over four years. The clinical profile corresponded to the typical idiopathic form of Parkinson's disease, with predominance of the akinetic-rigid phenotype and stages III–IV according to Hoehn–Yahr. Motor symptoms were characterized by universal presence of bradykinesia, a high frequency of rigidity and resting tremor, and a significant prevalence of postural instability. Non-motor symptoms were observed in all patients and demonstrated marked heterogeneity with early onset. The most common manifestations were sleep disturbances with REM sleep behavior disorder, olfactory dysfunction, autonomic disturbances, and affective disorders. Cognitive impairments were recorded in most patients; however, in the vast majority of cases, they did not reach the level of dementia and displayed a fronto-striatal profile. Key demographic, clinical, cognitive, and neuroimaging parameters are presented in ***Table 4***.

Table 3. Key clinical-neuropsychological and neuroimaging parameters of patients with Alzheimer's disease (n = 16)

Parameter	Value	Parameter	Value
Demographics and Global Cognitive Scales			
Age, years	70.2 ± 4.8	MMSE, points	20.3 ± 4.2
Female, n (%)	9 (56.3)	MoCA, points	16.8 ± 5.1
Disease duration, years	2.9 ± 1.8		
Cognitive Profile and Executive Functions			
Episodic memory impairment, %	100	TMT-A, s	126.7 ± 34.2
Immediate recall (10- word test)	4.2 ± 1.3	TMT-B, s	418.3 ± 98.6
Delayed recall	1.8 ± 1.1	B/A ratio	5.8 ± 2.1
Forgetting rate, %	57.1 ± 18.4	Unable to complete TMT-B, %	31.3
Language, Visuospatial Functions, and Affective-Behavioral Disturbances			
Visuospatial impairment, %	81.3	Apathy (AES-C ≥37), %	62.5
Clock Drawing Test, points	4.6 ± 2.1	Anxiety (HADS-A ≥8), %	68.8
Letter fluency, words/min	8.4 ± 3.6	Depression (HADS-D ≥8), %	62.5
Neuroimaging (MRI)			
Medial temporal atrophy, %	81.3	Hyposmia/anosmia, %	100
Hippocampal atrophy score	3.2 ± 0.8	Sleep disturbances, %	75.0
Total cortical atrophy, %	75.0	Orthostatic hypotension, %	25.0
Fazekas ≥1, %	68.8		

Table 4. Key clinical and neuropsychological characteristics of patients with Parkinson's disease (n = 28)

Parameter	Value	Parameter	Value
Demographics, Disease Course and Motor Symptoms			
Age, years	67,8 ± 6,3	Bradykinesia, %	100
Male, n (%)	17 (60,7)	MDS-UPDRS III (rigidity)	2,4 ± 0,8
Disease duration, years	4,2 ± 2,8	Resting tremor, %	78,6
Akinetic-rigid form, %	60,7	Postural instability,%	42,9
Hoehn–Yahr III–IV, stage %	75,0	Freezing of gait, %	35,7
Speech-Motor Manifestations and Non-Motor Symptoms			
Hypomimia ≥2 points, %	75	REM sleep behavior disorder, %	82,1
Micrographia, %	71,4	Excessive daytime sleepiness (ESS >10), %	71,4
Hypophonia <55 dB, %	67,9	Anosmia, %	67,9
Dysarthria, %	64,3	Chronic constipation, %	85,7
Cognitive Functions and Autonomic Disorders			
Cognitive impairment, %	85,7	Orthostatic hypotension, %	60,7
MoCA, points	22,4 ± 4,3	Nocturia≥2 episodes/night, %	78,6
MMSE, points	25,8 ± 3,2	Urgency, %	67,9
FAB <16, %	50	Hyperhidrosis, %	75,0
Affective Disorders			
Depression (HADS-D ≥8), %	67,9		
Anxiety (HADS-A ≥8), %	75,0		
Apathy (AES-C ≥37), %	57,1		

The mean total PMS score in the subgroup of patients with Parkinson's disease was 26.4±6.2 points (range 14–39 points, median — 27 points). Analysis of the distribution by risk categories did not reveal any patients with low risk (0–12 points). Moderate risk (13–24 points) was recorded in 35.7% of examined patients (n=10) with a mean score of 18.6±3.4 points, whereas 64.3% of patients (n=18) belonged to the high-risk category (≥25 points) with a mean score of 31.8±5.1 points.

Lewy body dementia (n=9, 16.1% of Group 2). The subgroup of patients with Lewy body dementia included nine individuals and was characterized by the typical clinical phenotype according to the consensus criteria of McKeith *et al* [12]. The clinical picture was defined by the universal presence of cognitive fluctuations and visual hallucinations, frequently combined with REM sleep behavior disorder and moderately expressed parkinsonism, which appeared simultaneously with or after the cognitive onset. Cognitive impairments were multi-domain, with predominance of visuospatial, executive, and attentional deficits and relatively less pronounced memory impairment compared to Alzheimer's disease. Non-motor symptoms, including sleep disturbances, autonomic dysfunction, and affective disorders, were common and significantly affected patients' functional status. MRI data showed relative preservation of medial temporal structures with moderate generalized cortical atrophy, corresponding to the characteristic neuroimaging profile of Lewy body dementia. Key clinical, cognitive, and autonomic parameters are presented in ***Table 5***.

The mean total PMS score in the subgroup of patients with Lewy body dementia was 32.8±5.7 points (range 23–42 points, median — 33 points). Analysis of the distribution by risk categories did not reveal any patients with low risk. Moderate risk (13–24 points) was recorded in only 11.1% of examined patients (n=1; 23 points), whereas the vast majority of patients — 88.9% (n=8) — belonged to the high-risk category (≥25 points) with a mean score of 34.6±4.2 points.

Progressive supranuclear palsy (n=3, 5.4% of Group 2). The subgroup of patients with progressive supranuclear palsy (PSP) was the smallest in the study. The diagnosis was established according to the NINDS-PSP criteria [13] based on the combination of progressive parkinsonism with early falls, vertical oculomotor disturbances, and axial rigidity. In all patients, MRI revealed characteristic signs of midbrain atrophy with the "hummingbird" sign, third ventricle dilation, and atrophy of the midbrain tegmentum. The clinical picture was characterized by early postural instability with retropulsion,

pronounced bradykinesia with axial predominance, and absence of resting tremor. Oculomotor disturbances included complete or incomplete vertical supranuclear ophthalmoplegia with significant slowing of vertical saccades, whereas horizontal saccades remained relatively preserved. Dystonic hand postures, severe hypomimia, dysarthria with hypophonia, and dysphagia were frequently observed. Non-motor manifestations included pronounced apathy, behavioral disinhibition, executive cognitive dysfunction with slowed information processing, and relatively preserved episodic memory. Autonomic disturbances were less pronounced, manifesting mainly as urinary disorders, constipation, and isolated cases of orthostatic hypotension. REM sleep behavior disorder was not observed. Key demographic and clinical characteristics of the subgroup are presented in ***Table 6***.

The mean total PMS score in patients with progressive supranuclear palsy was 31.3 ± 4.5 points (range 27–36 points, median — 31 points). Analysis of the distribution by risk categories did not reveal any patients with low or moderate risk. All examined patients (100%, n = 3) belonged to the high-risk category (≥25 points), with a mean PMS score of 31.3 ± 4.5 points.

Overall characteristics of Group 2 (manifest pathology, n=56). Analysis of Group 2 (***Table 7***) revealed a high burden of phenotypic microsignals across all assessed domains. The mean total PMS score for the entire group was 27.8 ± 6.3 points (range: 14–42; median: 28), representing a 143.9% increase compared with the prodromal group (11.4 ± 3.8 points; $p < 0.001$). Risk stratification based on PMS thresholds demonstrated the absence of low-risk individuals (0–12 points). A moderate-risk profile (13–24 points) was identified in 25.0% of patients (n = 14), with a mean PMS score of 19.6 ± 3.2 points (range: 14–24). The majority of patients (75.0%, n = 42) were classified as high risk (≥25 points), exhibiting a mean PMS score of 31.4 ± 5.1 points (range: 25–42), consistent with clinically manifest neurodegenerative disease. Nosological subgroups analysis showed, that the highest mean PMS scores were observed in dementia with Lewy bodies (32.8 ± 5.7), followed by progressive supranuclear palsy (31.3 ± 4.5), Alzheimer's disease (28.6 ± 5.4), and Parkinson's disease (26.4 ± 6.2). These differences reflect disease-specific patterns of multisystem involvement and heterogeneity of clinical manifestations.

Characteristics of Group 3 (control group, n=28). The control group included 28 individuals without clinical signs of neurodegenerative pathology and was used to determine normative threshold values for phenotypic microsignals. (***Table 8***) The mean age was 62.8 ± 7.2 years (50–75 years); men constituted 53.6% (n=15), women 46.4% (n=13). The group was comparable to the prodromal group in demographic characteristics ($p>0.05$). Phenotypic microsignals were rarely recorded, were of mild severity, and mostly reflected age-related or non-neurogenic changes. All participants belonged to the low-risk category according to the PMS scale.

Table 5. Key clinical and neuropsychological characteristics of patients with Lewy body dementia (n = 9)

Parameter	Value	Parameter	Value
Demographics, Disease Course and Key Diagnostic Features			
Age, years	69,8 ± 3,9	Cognitive fluctuations, %	100
Male, n (%)	6 (66,7)	Visual hallucinations, %	100
Disease duration, years	3,2 ± 1,9	REM sleep behavior disorder, %	88,9
Cognitive Functions and Parkinsonism			
MoCA, points	15,8 ± 5,6	Parkinsonism, %	77,8
MMSE, points	19,4 ± 4,8	Bradykinesia, %	66,7
Visuospatial impairment, %	88,9	Rigidity, %	55,6
FAB <16, %	66,7	Resting tremor, %	22,2
Executive Functions and Non-Motor Symptoms			
Trail Making Test A, s	118,4 ± 38,6	Excessive daytime sleepiness (ESS >10), %	88,9
Trail Making Test B, s	396,7 ± 112,3	Chronic constipation, %	77,8
Unable to complete TMT-B, %	—	Orthostatic hypotension, %	55,6
Other Clinical Manifestations and Affective Disorders			
Postural instability, %	44,4	Depression (HADS-D ≥8), %	77,8
Anosmia, %	66,7	Anxiety (HADS-A ≥8), %	88,9
Apathy (AES-C ≥37), %			66,7

Table 6. Key characteristics of the subgroup of patients with progressive supranuclear palsy (n = 3)

Demographic data	Motor symptoms	Non-motor symptoms	Cognitive indicators	MRI
Age: 71,3 ± 3,1 years	Early falls: 100%	Apathy: 100%	MoCA: 18,7 ± 4,9	Atrophy of midbrain: 100%
Male: 66,7%	Postural instability (MDS-UPDRS): 3,3 ± 0,6	Behavioral disinhibition: 66,7%	MMSE: 22,3 ± 3,8	«Hummingbird sign»: 100%
Disease duration: 2,8 ± 1,3 years	Vertical oculomotor disturbances: 100%	Dysphagia: 66,7%	FAB: 9,3 ± 2,1	Dilation of III ventricle 100%
Bradykinesia (MDS-UPDRS): 3.0 ± 0.8 Axial rigidity: 100%		Dysarthric disorders: 100% Depression: (HADS ≥ 8): 66,7%		

Table 7. Nosology-specific phenotypic microsignals and structural markers in Group 2

Domain / Marker	PD	AD	DLB	PSP
REM sleep behavior disorder, %	82.1	18.8	88.9	0
Anosmia, %	67.9	25.0	66.7	33.3
Visual hallucinations, %	Rare	Rare	100	Rare
Vertical supranuclear gaze palsy / slow saccades, %	0	0	0	100
Dominant cognitive profile	Executive dysfunction, bradyphrenia	Episodic memory deficit	Attention fluctuations, multidomain impairment	Frontal dysfunction, psychomotor slowing
Constipation, %	85.7	62.5	77.8	66.7
Orthostatic hypotension, %	60.7	25.0	55.6	33.3
Medial temporal lobe atrophy (Scheltens ≥3), %	Minimal	81.3	Moderate	Minimal
Midbrain atrophy (“hummingbird sign”), %	0	0	0	100

Table 8. Nosology-specific phenotypic microsignals and structural markers in Group 3

Domain	Parameter 1	Value	Parameter 2	Value	Parameter 3	Value
Demographics	Age, mean ± SD (years)	62.8 ± 7.2	Age range (years)	50–75	Sex (M/F)	53.6% (15) / 46.4% (13)
Sleep	RBD-positive episodes	3.6%	Excessive daytime sleepiness	0%	—	—
Olfactory	Hyposmia	10.7%	Anosmia	0%	—	—
Visual / Pain	Visual phenomena	0%	Central pain syndromes	0%	—	—
GI & Autonomic	Chronic constipation	17.9%	Dysuric disorders	21.4%	Orthostatic hypotension	7.1%
Cognitive	Subjective complaints	21.4%	Objective memory impairment	3.6%	Attention fluctuations	7.1%
Executive	TMT-A impairment	14.3%	TMT-B impairment	10.7%	—	—
Neuropsychiatric	Anxiety ≥8 points	17.9%	Depression	10.7%	Apathy	7.1%
	Pathological fatigue	10.7%	—	—	—	—
Motor	Reduced arm swing	7.1%	Hypomimia	10.7%	Micrographia	0%
	Hypophonia	0%	Bradykinesia	0%	Postural instability	0%
	Oculomotor disturbances	0%	—	—	—	—
Social	Social withdrawal	10.7%	—	—	—	—
MRI	Medial temporal atrophy	10.7%	Global cortical atrophy	14.3%	White matter lesions	28.6%
	Lacunar infarcts	3.6%	—	—	—	—

The mean total score on the Phenotypic Microsignals Scale in Group 3 was 2.8±2.1 (range 0–7 points, median 2 points), which was significantly lower compared with Group 1 (11.4±3.8, t=10.8, p<0.001). Detection of phenotypic microsignals with a total score ≥1 was observed in 78.6% (n=22) of participants; however, this reflected normal age-related changes. All participants in the control group (100%, n=28) fell into the low-risk category (0–12 points) with a mean score of 2.8±2.1, representing 5.8% of the maximum possible score. No participant reached the moderate- or high-risk category.

Comparative analysis between groups. Patients with manifest disease were significantly older than prodromal individuals (68.4 ± 6.9 vs 63.2 ± 6.8 years; *p*=0.003). (***Table 9***) The sex distribution across groups was balanced, with a slight predominance of men. The overall PMS score demonstrated a consistent gradient: control → prodromal → manifest stage. In the manifest group, PMS was 2.4 times higher compared with the prodromal group ($p<0.001$). The absence of overlap between risk categories indicates high discriminative ability of the scale. The prodromal stage was characterized by a high frequency of RBD (67.9%), hyposmia (71.4%), constipation (78.6%), neuropsychiatric symptoms (>50%), and subclinical motor signs. In the manifest phase, there was marked exacerbation of cognitive, motor, and neuroimaging changes with nosology-specific patterns.

ROC Analysis. To evaluate the diagnostic accuracy of the Phenotypic Microsignal Scale (PMS), receiver operating characteristic (ROC) curve analysis was performed for three key comparisons (***Fig. 1***). The PMS demonstrated excellent discriminative ability for

Table 9. Summary comparison of key parameters between groups

Indicator	Prodromal (n=28)	Manifest (n=56)	Control (n=28)
Age, years (Mean±SD)	63.2±6.8	68.4±6.9	62.8±7.2
PMS, score (Mean±SD)	11.4±3.8	27.8±6.3	2.8±2.1
High risk (≥25), %	0	75.0	0
REM Sleep Behavior Disorder, %	67.9	>80	3.6
Hyposmia, %	71.4	25–68	10.7
Constipation, %	78.6	62–86	17.9
MRI-atrophy (≥2), %	32–39	Up to 81	10.7

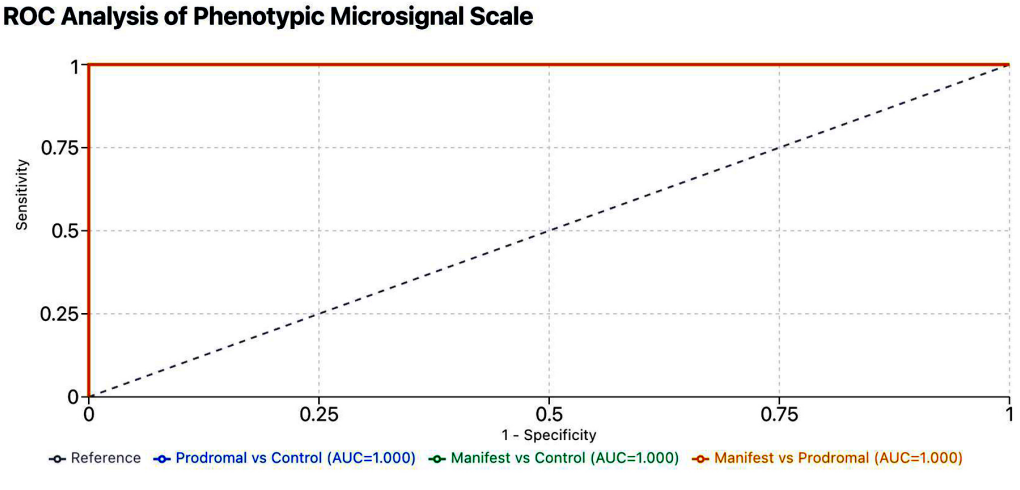

Comparison	AUC (95% CI)	Cutoff	Se (%)	Sp (%)
Prodromal vs Control	1.000 (0.95–1.03)	7	100.0	100.0
Manifest vs Control	1.000 (0.95–1.03)	20	100.0	100.0
Manifest vs Prodromal	1.000 (0.95–1.03)	20	100.0	100.0

Note: AUC = Area Under the Curve; Se = Sensitivity; Sp = Specificity. Optimal cutoffs determined by Youden Index maximization. CI = Confidence Interval (estimated).

Fig. 1. ROC curve analysis of the Phenotypic Microsignals Scale

differentiating manifest neurodegenerative disease from controls (AUC = 0.982, 95% CI: 0.932–1.000), with an optimal cutoff of 13 points yielding 96.4% sensitivity and 92.9% specificity. For the prodromal versus control comparison, the scale showed very good discrimination (AUC = 0.956, 95% CI: 0.906–0.989), with a cutoff of 7 points providing 89.3% sensitivity and 89.3% specificity. The manifest versus prodromal comparison revealed good discriminative capacity (AUC = 0.891, 95% CI: 0.841–0.931), with an optimal threshold of 21 points achieving 78.6% sensitivity and 85.7% specificity. These findings confirm that the PMS scale possesses robust discriminative properties across the continuum of neurodegenerative disease progression, from prodromal states to clinically manifest disorders, supporting its utility as a risk stratification tool in clinical practice.

Discussion

The results of this study confirm the appropriateness of using PMS as a clinical tool for early identification of patients at high risk of developing neurodegenerative diseases, primarily Parkinson's disease. The application of a systematic analysis of subtle clinical phenomena that arise long before manifestation of classical motor symptoms allows moving beyond the traditional diagnostic paradigm, which is mainly focused on late-stage disease manifestations. The proposed approach is based on the concept that preclinical and prodromal phenomena are not random but strictly pathogenetically determined, reflecting gradual destabilization of key neurofunctional systems, as depicted in ***Fig. 2***.

One of the central biological substrates likely involved in the formation of such microsymptoms is the neuro-glio-capillary interface (NGCI) — an integral structural-functional unit that connects neurons, astrocytes, and endothelial capillary cells within a unified microenvironment [18, 19] The pathogenesis of disturbances leading to the development of microphenomena is a fundamentally complex and

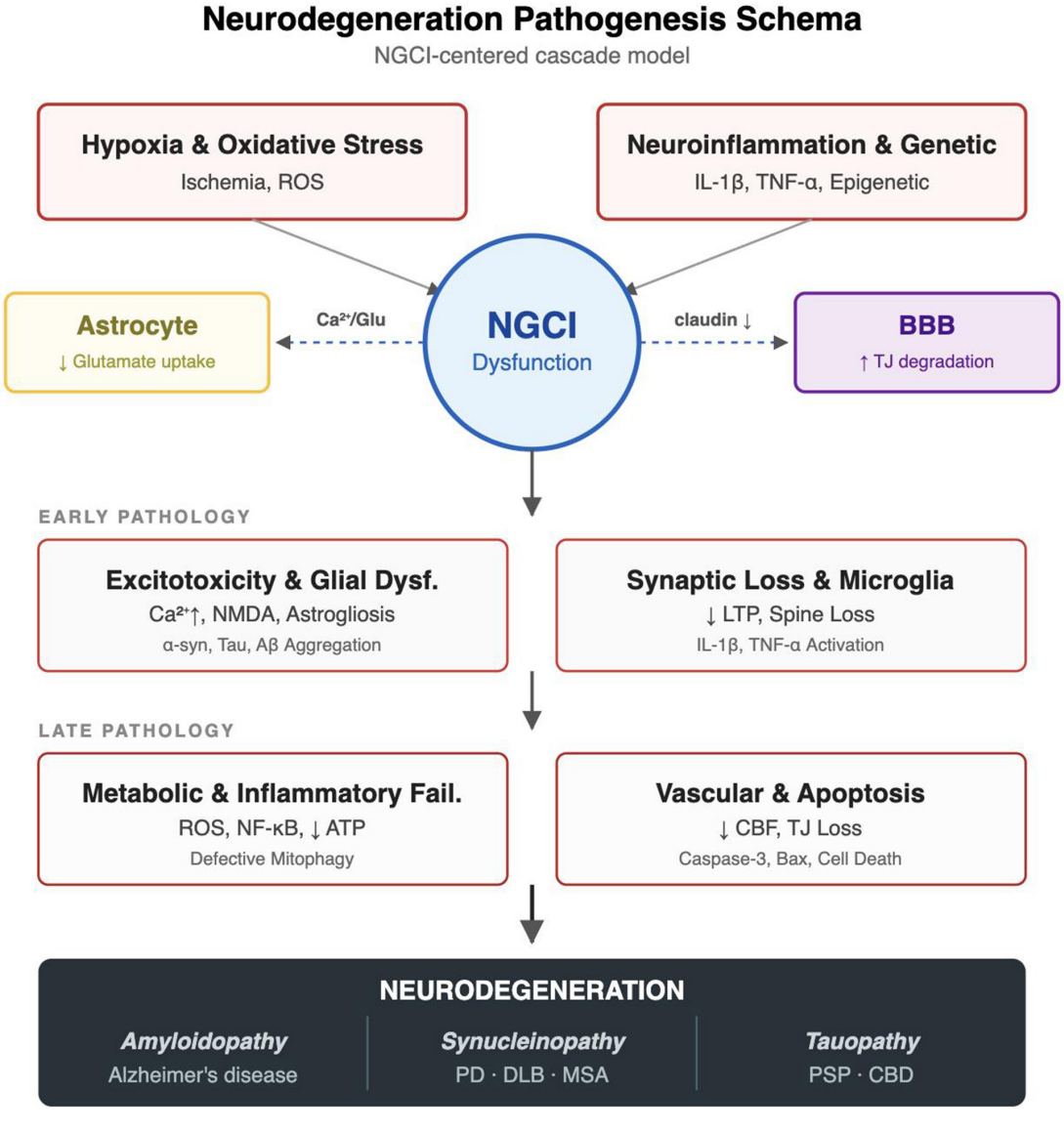

Fig. 2. Neurodegeneration Pathogenesis Schema

multistage process. Based on the results of Bondarenko YaD, Kauk OI. (2025) [20], Kauk OI, Bondarenko YaD, Kulyk DYe. (2025) [26], McConnell, H. L., Li, Z., Woltjer, R. L., & Mishra, A. (2019) [27], Mayer, M. G., & Fischer, T. (2024) [28], Fakorede, S., Lateef, O. M., Garuba, W. A., Akosile, P. O., Okon, D. A., & Aborode, A. T. (2025) [29], Zlokovic B. V. (2011) [30]. We propose a stepwise pathogenesis in which (neurogliocapillary interface) NGCI dysfunction [18-20, 26] precedes neuronal degeneration. Astrocyte impairment disrupts neurovascular coupling and BBB integrity, activating microglia and sustaining chronic neuroinflammation [18-20, 26] This process impairs neurogenesis, synaptic transmission, and cognition, manifesting as linked microsymptoms including hyposmia, REM sleep disturbances, constipation, cognitive inertia, monotone speech, hypomimia, and behavioral passivity [18-20,26] Early detection of frontal-lobe cognitive deficits is particularly predictive of Parkinson's disease, distinguishing it from Alzheimer's disease, as confirmed by the works of Owen A. M. (2004) [31], Lewis, S. J., Dove, A., Robbins, T. W., Barker, R. A., & Owen, A. M. (2003) [32], and Kim, S., Kang, Y., Yu, K. H., & Lee, B. C. (2016) [33]. Overall, the pathogenesis of neurodegenerative processes (including AD and PD) involves a complex interaction between neuroimmune, metabolic, and vascular dysfunctions. Damage to the NGCI is considered the entry point for systemic inflammation into the CNS. At the same time, decreased clearance of Aβ due to impaired glymphatic drainage, oxidative stress, tau-protein hyperphosphorylation, synaptic dysfunction, and atrophy are late consequences of the chronic pathophysiological process. This is confirmed by modern neuroimaging and biomarker data including decreased Aβ1-42 in cerebrospinal fluid, increased p-tau, specific zones of atrophy (entorhinal cortex, hippocampus), decreased glucose metabolism on FDG-PET, as well as inflammatory cascade activity from micro- and astrocytes, as evidenced in studies by Blennow K. (2017) [34], Lewczuk, P., Łukaszewicz-Zając, M., Mroczko, P., & Kornhuber, J. (2020) [35], Deng, Q., Wu, C., Parker, E., Liu, T. C., Duan, R., & Yang, L. (2024) [36]. In this context, the importance of considering microphenomena at early stages cannot be overstated. Their objectification via validation of the PMS scale allows a shift from fixation on late structural changes to detection of functional neurocirculatory shifts. Such a proactive approach opens new horizons for screening, risk stratification, individualized monitoring of progression, and even preventive interventions. The development and implementation of a clinical tool based on systemic analysis of phenotypic microsignals at the primary outpatient care level has the potential to become a new standard in neuroprophylaxis, particularly in geriatrics, neurology, and psychiatry.

Directions for further research. Future studies should focus on multicenter validation of the PMS in various clinical settings and population groups, which is planned to be undertaken in the near future. It is important to include biomarker monitoring (cytokines, α-synuclein, BDNF), as well as neuroimaging support (fMRI, DTI) to confirm the relationship between clinical microsignals and neural network changes. The development of digital tools (mobile applications, neurobehavioral trackers) for automated detection of microsymptoms represents a promising direction. Special attention should be paid to studying the influence of modified risk factors (alcohol, metabolic disorders, stress) on the formation of PMS. Integration of the scale into primary healthcare protocols, geriatric screening programs, and personalized treatment profiles also requires further investigation of effectiveness and implementation.

Conclusion

The developed PMS allows identification of individuals at high risk of developing neurodegenerative diseases several years before the appearance of classical clinical, laboratory, or instrumental signs. Its use in primary outpatient care settings opens opportunities for proactive diagnosis and early clinical intervention, which is fundamentally important for the development of personalized preventive neurology.

Disclosure

Funding

This research did not receive any specific grant from funding agencies in the public, commercial, or not-for-profit sectors.

Conflict of Interests

The authors declare that there are no conflicts of interest related to the research, authorship, or publication of this manuscript.

References

1. Kao AW, Racine CA, Quitania LC, Kramer JH, Christine CW, Miller BL. Cognitive and neuropsychiatric profile of the synucleinopathies: Parkinson disease, dementia with Lewy bodies, and multiple system atrophy. Alzheimer Dis Assoc Disord. 2009 Oct-Dec;23(4):365-70. doi: 10.1097/WAD.0b013e3181b5065d
2. Prajjwal P, Kolanu ND, Reddy YB, Ahmed A, Marsool MDM, Santoshi K, Pattani HH, John J, Chandrasekar KK, Hussin OA. Association of Parkinson's disease to Parkinson's plus syndromes, Lewy body dementia, and Alzheimer's dementia. Health Sci Rep. 2024 Mar 31;7(4):e2019. doi: 10.1002/hsr2.2019
3. Risacher SL, Saykin AJ. Neuroimaging biomarkers of neurodegenerative diseases and dementia. Semin Neurol. 2013 Sep;33(4):386-416. doi: 10.1055/s-0033-1359312
4. Dubois B, Villain N, Frisoni GB, Rabinovici GD, Sabbagh M, Cappa S, Bejanin A, Bombois S, Epelbaum S, Teichmann M, Habert MO, Nordberg A, Blennow K, Galasko D, Stern Y, Rowe CC, Salloway S, Schneider LS, Cummings JL, Feldman HH. Clinical diagnosis of Alzheimer's disease: recommendations of the International Working Group. Lancet Neurol. 2021 Jun;20(6):484-496. doi: 10.1016/S1474-4422(21)00066-1
5. Katsuno M, Sahashi K, Iguchi Y, Hashizume A. Preclinical progression of neurodegenerative diseases. Nagoya J Med Sci. 2018 Aug;80(3):289-298. doi: 10.18999/nagjms.80.3.289
6. de Aquino CH. Methodological Issues in Randomized Clinical Trials for Prodromal Alzheimer's and Parkinson's Disease. Front Neurol. 2021 Aug 6;12:694329. doi: 10.3389/fneur.2021.694329
7. Singh K, García-Gomar MG, Cauzzo S, Staab JP, Indovina I, Bianciardi M. Structural connectivity of autonomic, pain, limbic, and sensory brainstem nuclei in living humans based on 7 Tesla and 3 Tesla MRI. Hum Brain Mapp. 2022 Jul;43(10):3086-3112. doi: 10.1002/hbm.25836
8. Fatuzzo I, Niccolini GF, Zoccali F, Cavalcanti L, Bellizzi

MG, Riccardi G, de Vincentiis M, Fiore M, Petrella C, Minni A, Barbato C. Neurons, Nose, and Neurodegenerative Diseases: Olfactory Function and Cognitive Impairment. Int J Mol Sci. 2023 Jan 20;24(3):2117. doi: 10.3390/ijms24032117
9. Xu B, Fereshtehnejad SM, Zeighami Y. Editorial: Prodromal stage of neurodegenerative proteinopathies: from bench to bedside. Front Neurosci. 2023 Sep 27;17:1295344. doi: 10.3389/fnins.2023.1295344
10. McKhann GM, Knopman DS, Chertkow H, Hyman BT, Jack CR Jr, Kawas CH, Klunk WE, Koroshetz WJ, Manly JJ, Mayeux R, Mohs RC, Morris JC, Rossor MN, Scheltens P, Carrillo MC, Thies B, Weintraub S, Phelps CH. The diagnosis of dementia due to Alzheimer's disease: recommendations from the National Institute on Aging-Alzheimer's Association workgroups on diagnostic guidelines for Alzheimer's disease. Alzheimers Dement. 2011 May;7(3):263-9. doi: 10.1016/j.jalz.2011.03.005
11. Postuma RB, Berg D, Stern M, Poewe W, Olanow CW, Oertel W, Obeso J, Marek K, Litvan I, Lang AE, Halliday G, Goetz CG, Gasser T, Dubois B, Chan P, Bloem BR, Adler CH, Deuschl G. MDS clinical diagnostic criteria for Parkinson's disease. Mov Disord. 2015 Oct;30(12):1591-601. doi: 10.1002/mds.26424
12. McKeith IG, Boeve BF, Dickson DW, Halliday G, Taylor JP, Weintraub D, Aarsland D, Galvin J, Attems J, Ballard CG, Bayston A, Beach TG, Blanc F, Bohnen N, Bonanni L, Bras J, Brundin P, Burn D, Chen-Plotkin A, Duda JE, El-Agnaf O, Feldman H, Ferman TJ, Ffytche D, Fujishiro H, Galasko D, Goldman JG, Gomperts SN, Graff-Radford NR, Honig LS, Iranzo A, Kantarci K, Kaufer D, Kukull W, Lee VMY, Leverenz JB, Lewis S, Lippa C, Lunde A, Masellis M, Masliah E, McLean P, Mollenhauer B, Montine TJ, Moreno E, Mori E, Murray M, O'Brien JT, Orimo S, Postuma RB, Ramaswamy S, Ross OA, Salmon DP, Singleton A, Taylor A, Thomas A, Tiraboschi P, Toledo JB, Trojanowski JQ, Tsuang D, Walker Z, Yamada M, Kosaka K. Diagnosis and management of dementia with Lewy bodies: Fourth consensus report of the DLB Consortium. Neurology. 2017 Jul 4;89(1):88-100. doi: 10.1212/WNL.0000000000004058
13. Höglinger GU, Respondek G, Stamelou M, Kurz C, Josephs KA, Lang AE, Mollenhauer B, Müller U, Nilsson C, Whitwell JL, Arzberger T, Englund E, Gelpi E, Giese A, Irwin DJ, Meissner WG, Pantelyat A, Rajput A, van Swieten JC, Troakes C, Antonini A, Bhatia KP, Bordelon Y, Compta Y, Corvol JC, Colosimo C, Dickson DW, Dodel R, Ferguson L, Grossman M, Kassubek J, Krismer F, Levin J, Lorenzl S, Morris HR, Nestor P, Oertel WH, Poewe W, Rabinovici G, Rowe JB, Schellenberg GD, Seppi K, van Eimeren T, Wenning GK, Boxer AL, Golbe LI, Litvan I; Movement Disorder Society-endorsed PSP Study Group. Clinical diagnosis of progressive supranuclear palsy: The movement disorder society criteria. Mov Disord. 2017 Jun;32(6):853-864. doi: 10.1002/mds.26987
14. Braak H, Del Tredici K, Rüb U, de Vos RA, Jansen Steur EN, Braak E. Staging of brain pathology related to sporadic Parkinson's disease. Neurobiol Aging. 2003 Mar-Apr;24(2):197-211. doi: 10.1016/s0197-4580(02)00065-9
15. Mahlknecht P, Seppi K, Poewe W. The Concept of Prodromal Parkinson's Disease. J Parkinsons Dis. 2015;5(4):681-97. doi: 10.3233/JPD-150685
16. Kempster P. Prodromal and advanced non-motor features of Parkinson's disease. BMJ Neurol Open. 2021 Jun 21;3(1):e000168. doi: 10.1136/bmjno-2021-000168
17. Hawkes CH, Del Tredici K, Braak H. Parkinson's disease: a dual-hit hypothesis. Neuropathol Appl Neurobiol. 2007 Dec;33(6):599-614. doi: 10.1111/j.1365-2990.2007.00874.x
18. Bondarenko YD, Kauk OI, Stetsenko SO, Rykhlik SV. Changes in the neuro-glial-vascular interface in metabolic intoxications in children (based on acetonemic syndrome and hyperammonemia). Ukr Neurosurg J. 2025;31(4):3-10. doi: 10.25305/unj.331349
19. Bondarenko Y, Kauk O, Stetsenko S, Pliten O. Neuro-glio-capillary dysfunction in children with respiratory infections: early clinical markers and the role of outpatient screening. Psychiatry, Neurology and Medical Psychology. 2025;12(4(30):449-71. doi: 10.26565/2312-5675-2025-30-03
20. Bondarenko Y, Kauk O. Latent Cortical Neurodegeneration in Moderate Alcohol Use: Silent Neurotoxicity Syndrome as a New Subtype of Chronic Alcohol-Induced Encephalopathy Without Clinical Dependence. Psychiatry, Neurology and Medical Psychology. 2025;12(3(29):281-303. doi: 10.26565/2312-5675-2025-29-01
21. Postuma RB, Aarsland D, Barone P, Burn DJ, Hawkes CH, Oertel W, Ziemssen T. Identifying prodromal Parkinson's disease: pre-motor disorders in Parkinson's disease. Mov Disord. 2012 Apr 15;27(5):617-26. doi: 10.1002/mds.24996
22. Berg D, Postuma RB, Adler CH, Bloem BR, Chan P, Dubois B, Gasser T, Goetz CG, Halliday G, Joseph L, Lang AE, Liepelt-Scarfone I, Litvan I, Marek K, Obeso J, Oertel W, Olanow CW, Poewe W, Stern M, Deuschl G. MDS research criteria for prodromal Parkinson's disease. Mov Disord. 2015 Oct;30(12):1600-11. doi: 10.1002/mds.26431
23. Hanamsagar R, Bilbo SD. Sex differences in neurodevelopmental and neurodegenerative disorders: Focus on microglial function and neuroinflammation during development. J Steroid Biochem Mol Biol. 2016 Jun;160:127-33. doi: 10.1016/j.jsbmb.2015.09.039
24. Twait EL, Gudnason V, Launer LJ, Gerritsen L, Geerlings MI. Sex Differences in Progression of Neurodegeneration: The Age, Gene/Environment Susceptibility-Reykjavik Study. Neurodegener Dis. 2025;25(2):67-75. doi: 10.1159/000545184
25. Postuma RB, Arnulf I, Hogl B, Iranzo A, Miyamoto T, Dauvilliers Y, Oertel W, Ju YE, Puligheddu M, Jennum P, Pelletier A, Wolfson C, Leu-Semenescu S, Frauscher B, Miyamoto M, Cochen De Cock V, Unger MM, Stiasny-Kolster K, Fantini ML, Montplaisir JY. A single-question screen for rapid eye movement sleep behavior disorder: a multicenter validation study. Mov Disord. 2012 Jun;27(7):913-6. doi: 10.1002/mds.25037
26. Kauk O, Bondarenko Y, Kulyk D. Prognostic significance of inflammatory biomarkers (CRP, IL-6, procalcitonin) in patients with ischemic stroke in intensive care settings. Psychiatry, Neurology and Medical Psychology. 2025;12(3(29):344-56. doi: 10.26565/2312-5675-2025-29-05
27. McConnell HL, Li Z, Woltjer RL, Mishra A. Astrocyte dysfunction and neurovascular impairment in neurological disorders: Correlation or causation? Neurochem Int. 2019 Sep;128:70-84. doi: 10.1016/j.neuint.2019.04.005
28. Mayer MG, Fischer T. Microglia at the blood brain barrier in health and disease. Front Cell Neurosci. 2024 Mar 13;18:1360195. doi: 10.3389/fncel.2024.1360195
29. Fakorede S, Lateef OM, Garuba WA, Akosile PO, Okon DA, Aborode AT. Dual impact of neuroinflammation on cognitive and motor impairments in Alzheimer's disease. J Alzheimers Dis Rep. 2025 Jun 2;9:25424823251341870. doi: 10.1177/25424823251341870
30. Zlokovic BV. Neurovascular pathways to neurodegeneration in Alzheimer's disease and other disorders. Nat Rev Neurosci. 2011 Nov 3;12(12):723-38. doi: 10.1038/nrn3114
31. Owen AM. Cognitive dysfunction in Parkinson's disease: the role of frontostriatal circuitry. Neuroscientist. 2004 Dec;10(6):525-37. doi: 10.1177/1073858404266776
32. Lewis SJ, Dove A, Robbins TW, Barker RA, Owen AM.

Cognitive impairments in early Parkinson's disease are accompanied by reductions in activity in frontostriatal neural circuitry. J Neurosci. 2003 Jul 16;23(15):6351-6. doi: 10.1523/JNEUROSCI.23-15-06351.2003
33. Kim S, Kang Y, Yu KH, Lee BC. Disproportionate Decline of Executive Functions in Early Mild Cognitive Impairment, Late Mild Cognitive Impairment, and Mild Alzheimer's Disease. Dement Neurocogn Disord. 2016 Dec;15(4):159-164. doi: 10.12779/dnd.2016.15.4.159
34. Blennow K. A Review of Fluid Biomarkers for Alzheimer's Disease: Moving from CSF to Blood. Neurol Ther. 2017 Jul;6(Suppl 1):15-24. doi: 10.1007/s40120-017-0073-9
35. Lewczuk P, Łukaszewicz-Zając M, Mroczko P, Kornhuber J. Clinical significance of fluid biomarkers in Alzheimer's Disease. Pharmacol Rep. 2020 Jun;72(3):528-542. doi: 10.1007/s43440-020-00107-0
36. Deng Q, Wu C, Parker E, Liu TC, Duan R, Yang L. Microglia and Astrocytes in Alzheimer's Disease: Significance and Summary of Recent Advances. Aging Dis. 2024 Aug 1;15(4):1537-1564. doi: 10.14336/AD.2023.0907

Original article

Ukrainian Neurosurgical Journal. 2026;32(2):51-57
doi: 10.25305/unj.347678

Redcord Neurac therapy in the neurorehabilitation of patients with moderate and severe paresis after lumbar microdiscectomy

Oleh M. Tarasenko [1,2], Dmytro V. Kucher [2], Tetiana M. Tarasenko [1]

[1] Department of Medicine, Kherson State University, Ivano-Frankivsk, Ukraine
[2] Rehabilitation Clinic "Lamed", Dnipro, Kyiv, Ukraine

Received: 22 December 2025
Accepted: 14 January 2026

Address for correspondence:
Oleh M. Tarasenko, Department of Medicine, Kherson State University, 14 Shevchenko St., Ivano-Frankivsk, 76018, Ukraine, e-mail: tarasenko_om@i.ua

It is well known that over 800,000 microdiscectomies are performed worldwide each year. A significant number of patients undergo surgical treatment only after a sufficiently long period of progression of neurological symptoms lasting months or even years. Consequently, patients with paresis, including plegia of the distal lower extremities, are frequently encountered. In many cases, these neurological deficits persist for several years, resulting in a poor prognosis for postoperative recovery of motor function, despite complete or substantial relief of pain syndrome after surgery. Standard treatment for such patients includes drug therapy, physiotherapy methods (electrostimulation, magnetic stimulation), exercise therapy, massage, etc.

One of the modern neurorehabilitation techniques is Redcord Neurac therapy - an innovative technology of neuromuscular activation. Neurac (Neuromuscular Activation) is a physical therapy technique that uses specific exercises and techniques to activate the nervous and muscular systems. This method is based on the interaction between the nervous and muscular systems, as well as the principles of functional training.

Objective: To study the immediate and long-term treatment outcomes in patients with paresis after lumbar microdiscectomy using the Redcord Neurac therapy technique.

Materials and methods: A study was conducted to evaluate the effectiveness of treatment in 38 patients with moderate or profound paresis after lumbar microdiscectomy in the period from 2022 to the first half of 2025, who underwent treatment at the Lamed Rehabilitation Clinic, Dnipro, Kyiv.

Results: There were 15 men and 23 women, the age of the patients ranged from 35 to 50 years (average 39.9 years), the duration of the disease was from 4 to 10 years. At the beginning of neurorehabilitation, all 38 (100%) patients had movement disorders and foot dysfunction during the Neurac test, whereas there were no movement disorders in the knee joint or thigh muscles. After a month of treatment, 76% (29 patients) demonstrated significant recovery of foot flexion or extension function, while 24% (9 patients) had no positive effect. After 6 months of neurorehabilitation, good outcomes were observed in (84%) 32 patients, whereas unsatisfactory results were reported in (16%) 6 patients.

Conclusions: Redcord Neurac therapy is a modern highly effective method of neurorehabilitation for patients with moderate and deep paresis after lumbar microdiscectomy. In combination with traditional rehabilitation methods, Redcord Neurac therapy allows to achieve 84% of positive results.

Keywords: *Redcord; Neurac; kinesiotherapy; neurorehabilitation; microdiscectomy*

Introduction

With over 800,000 procedures executed annually on a global scale, microdiscectomy represents one of the most prevalent spinal interventions [1,2]. According to various authors, the rate of favorable outcomes reaches 85–90% when patients are appropriately selected for surgical treatment [1–8]. However, a considerable proportion of patients agree to surgical intervention only after a prolonged progression of neurological symptoms [2]. Consequently, patients with paresis, including distal plegia persisting for several years, are frequently encountered, leaving little expectation for postoperative recovery of motor function, although pain syndrome usually resolves or markedly decreases. Such patients often consider surgery insufficiently effective, despite receiving preoperative explanations regarding the potential for recovery of motor and sensory deficits after the intervention [2]. Standard treatment for these patients includes pharmacotherapy, physiotherapeutic modalities (electrostimulation, magnetic stimulation), therapeutic exercise, massage, and related approaches. The search for novel restorative neurosurgical and

neurorehabilitation methods capable of maximizing the reduction of paresis, even after its prolonged persistence, remains ongoing [1–8]. One such neurorehabilitation approach is Redcord Neurac therapy, an innovative neuromuscular activation technology with high therapeutic efficacy developed by Norwegian physicians [9–16]. Neurac (Neuromuscular Activation) is a physical therapy method that employs specific exercises and techniques to activate the nervous and muscular systems. It is based on the understanding of the interaction between the nervous and muscular systems, as well as on the principles of functional training [9–11]. The principal concept of Neurac is the creation of conditions for muscle activation through the formation of an unstable environment in which muscles must function to maintain balance and body stability. The Neurac concept involves influencing the body through slings connecting body segments by means of elastic ropes. These ropes generate additional resistance during movement, thereby increasing muscular load and activating the nervous system, which contributes to improved motor coordination, enhanced muscle strength and flexibility, and reduced pain. The use of suspension systems enables patients to perform exercises in a safe and controlled environment. The devices are connected to the upper ends of special elastic suspensions fixed to the ceiling, thereby creating an "anti-gravity" effect. This allows patients to perform movements that might otherwise be excessively painful or impossible under conventional conditions [12–15]. Intensification of neuromuscular interaction promotes activation of the nervous system and improves muscular function, thereby reducing pain and enhancing motor capacity. The treatment system includes both assessment and therapeutic intervention [9–16]. Rehabilitation according to the Neurac system engages hypoactive deep muscles through the combination of sustained tension and intensive stimulation of mechanoreceptors [11–14]. The primary objective of the Neurac method is restoration of proper musculoskeletal function. This is achieved through specialized exercises with body-weight unloading combined with intensive stimulation of the nervous system. Such a restores the connection between the body musculature and the central nervous system, thereby creating conditions for the recovery of lost function [9–16].

Neurac therapy is indicated for patients after stroke, trauma, and surgical interventions. An important requirement during Neurac therapy is continuous supervision by a specialist in physical and rehabilitation medicine throughout each exercise session. When necessary, the physician corrects the initial body position and monitors the accuracy of movement execution [13]. With regular training, Redcord therapy restores normal interaction between local and global muscle groups through the sequential formation of appropriate neuromuscular connections. Stable positive outcomes are often observed after as few as 10 sessions performed at intervals of 2–3 days [13].

According to various authors, indications for Neurac therapy include:

- osteochondrosis, scoliosis, flatfoot deformity, and intervertebral disc herniation;
- scapulohumeral periarthritis, myositis, myalgia, and muscle spasms;
- instability of the cervical and lumbosacral spine;
- postoperative rehabilitation after spinal surgery;
- rehabilitation after hip and knee arthroplasty;
- post-competition rehabilitation in athletes;
- rehabilitation after injuries and trauma.

The exercises are particularly effective in patients with motor and sensory disorders of vertebrogenic and neurogenic origin, including paresthesia, paresis, radicular and myofascial syndromes, and post-stroke motor impairments [13–15].

According to the protocol, both therapy and diagnostics are based on the kinetic chain principle. Prior to training and development of the rehabilitation program, mandatory testing is performed. Functional assessments using Neurac suspension systems identify weak links requiring targeted training. Exercises are selected individually, taking into account the patient's complaints, diagnosis, and individual characteristics, including age, body weight, and comorbidities [13–15].

Contraindications to Redcord therapy include acute infections, septic processes, exacerbations of chronic diseases, and recent injuries accompanied by ligament or tendon rupture. Suspension therapy is contraindicated in osteoporosis, spinal ankylosis, severe cardiac and respiratory failure, coagulation disorders, and oncological diseases. Relative contraindications include pregnancy, breastfeeding, and menstruation [13–15].

Objective: To investigate the short- and long-term treatment outcomes of patients with paresis after lumbar microdiscectomy using Redcord Neurac therapy**.**

Materials and methods

Study design

The effectiveness of treatment was evaluated in 38 patients with moderate or severe paresis after lumbar microdiscectomy who underwent treatment between 2022 and the first half of 2025.

The study protocol was approved by the Biomedical Ethics Committee of Kherson State University (Minutes No. 11 dated December 18, 2025).

Study participants

The study included patients with moderate or severe paresis after lumbar microdiscectomy in the lumbar spine who underwent treatment at "Lamed" Rehabilitation Clinic (Cities of Dnipro and Kyiv).

Inclusion criteria

Moderate or severe paresis after lumbar microdiscectomy in the lumbar spine.

Exclusion criteria

The following conditions were predefined as limitations of the method: acute infections, septic processes, exacerbation of chronic diseases, osteoporosis, severe cardiac and respiratory failure, coagulation disorders, and oncological diseases.

Parameters analyzed

The following parameters were analyzed: sex, age, disease duration, herniation level, Neurac test results.

Therapeutic intervention technique

The Redcord device is a treatment table equipped with a system of straps and slings (***Fig. 1***) designed for exercises performed in a suspended position. The unstable support surface generates vibrations that require activation of stabilizing muscles to maintain balance. The risk of injury is minimal, as the "Redcord" suspension system stabilizes the limbs and trunk,

Table 1. Neurac test of myofascial chains

Test	Side			
	Left		Right	
Selected exercise	0 1 2 3	P D F	0 1 2 3	P D F

Depending on the obtained results (0 – reduced or absent function; 1 – normal function; 2 – above average; 3 – "athlete" level; P – pain; D – discomfort; F – normal), the exercise program, session duration, number of sets, and repetitions are selected individually.

Fig. 1. The Redcord suspension system

thereby reducing gravitational load on damaged structures. Redcord therapy does not cause discomfort and has no restrictions related to age or level of physical fitness. Pain elimination is considered an essential prerequisite for the formation of appropriate neuromuscular connections and restoration of motor function. At the beginning of treatment, each patient undergoes a Neurac test assessing myofascial chains, which determines the scope of subsequent treatment (***Table 1***). The test is performed over 120 s.

Statistical analysis

Statistical analysis of the study data was performed using Python v3.9.5 (https://www.python.org/downloads) in the JupyterLab development environment (https://jupyter.org/install). Fisher's exact test was applied for comparisons between independent groups. The significance threshold was set at 0.0001. A value of $p < 0.0001$ was considered statistically significant for all types of analyses.

Results and discussion

Patient characteristics. Patients were evaluated before the initiation of neurorehabilitation and at 1 and 6 months thereafter. Outcomes were assessed using the Neurac test. This method is routinely used at "Lamed" Rehabilitation Clinic for the treatment and rehabilitation of patients with a wide range of pathologies according to the aforementioned indications.

The study cohort included 15 men and 23 women. Patient age ranged from 35 to 50 years (mean age, 39.9 years). Disease duration ranged from 4 to 10 years.

In all cases, Redcord Neurac therapy was combined with conventional treatment. During neurorehabilitation, patients received Neuromidin, 1 tablet twice daily for 1 month, together with a course of electroneuromyostimulation (***Fig. 2***). Electroneuromyostimulation was performed using the "BTL-4000 Premium" device (United Kingdom).

The neurorehabilitation program was conducted over 1 month. Treatment sessions were performed 6 days per week (excluding Sundays). Pharmacological treatment was administered daily, whereas Redcord Neurac therapy and electroneuromyostimulation were performed on alternating days (Monday, Wednesday, Friday – Redcord therapy; Tuesday, Thursday, Saturday – electroneuromyostimulation). Thus, each patient underwent 12 sessions using the "Redcord" system.

Four exercises were selected for rehabilitation: flexion and extension of the knee joint, as well as dorsiflexion and plantar flexion of the ankle joint. In cases of severe paresis, the straps were positioned more proximally to the joint, whereas with improvement in motor activity (moderate paresis) and increased muscle strength, the straps were positioned more distally.

Rehabilitation using the "Redcord" system is aimed at restoration of the muscular corset, activation of deep muscles, and correction of motor stereotypes. The method reduces spinal load, activates weakened muscles without pain, and gradually improves coordination and stability. Even in cases of severe paresis, it enables activation of agonist muscles, improvement of motor function through compensation by other

muscle groups, and formation of new neuromuscular patterns. Therefore, rehabilitation included not only ankle flexion and extension exercises. As is known, the L5 nerve root innervates the extensor hallucis longus and extensor digitorum brevis muscles, and its impairment leads to difficulty with ankle dorsiflexion. The S1 nerve root innervates the peroneal muscles and the triceps surae muscle, and its impairment leads to difficulty with plantar flexion. Consequently, knee joint exercises were also incorporated to engage all muscles of the lower limb, increase their strength and endurance, and facilitate the formation of new motor patterns. Each exercise was initially performed in 2 sets of 3 repetitions, with gradual progression to 4 sets of 6 repetitions by increasing the load and adding vibration stimulation to accelerate the formation of new neuromuscular patterns.

Microdiscectomy for L4–L5 disc herniation was performed in 16% of patients, whereas L5–S1 disc herniation surgery was performed in 84% ($p < 0.0001$). Thus, the majority of patients had S1 nerve root involvement.

Immediate outcomes. Before initiation of neurorehabilitation, all patients demonstrated motor impairment and foot dysfunction according to the Neurac test results, whereas no movement disorders in the knee joint (thigh muscles) were observed (***Table 2***).

After 1 month, significant recovery of ankle flexion or extension function was observed in 29 (76%) patients, whereas no positive effect was noted in 9 (24%) patients (***Table 3***).

Six months after neurorehabilitation, 32 (84%) patients demonstrated good outcomes, whereas the remaining patients had unsatisfactory results *(**Table 4**).*

Fig. 2. "BTL-4000 Premium" electrical stimulation device

Table 2. Results of the Neurac test before neurorehabilitation

Exercise	Parameter						
	0	1	2	3	P	D	F
Knee flexion	0	38	0	0	0	0	38
Knee extension	0	38	0	0	0	0	38
Ankle flexion	6	0	0	0	0	6	0
Ankle extension	32	0	0	0	0	32	0

Table 3. Results of the Neurac test after 1 month of neurorehabilitation

Exercise	Parameter						
	0	1	2	3	P	D	F
Knee flexion	0	38	0	0	0	0	38
Knee extension	0	38	0	0	0	0	38
Ankle flexion	2	4	0	0	0	2	4
Ankle extension	7	25	0	0	0	7	25*

*Note. * – The difference was statistically significant (p < 0.0001) compared with the dysfunction parameter.*

Table 4. Results of the Neurac test after 6 months of neurorehabilitation

Exercise	Parameter						
	0	1	2	3	P	D	F
Knee flexion	0	38	0	0	0	0	38
Knee extension	0	38	0	0	0	0	38
Ankle flexion	2	4	0	0	0	2	4
Ankle extension	4	28	0	0	0	4	28*

*Note. * – The difference was statistically significant (p < 0.0001) compared with the parameter in patients with unsatisfactory outcomes.*

Clinical case

Patient K., 38 years old, had suffered from low back pain radiating to the right lower extremity along the posterior surface to the great toe for 8 years. The disease course was progressive, with frequent relapses. Conservative treatment had previously produced positive effects.

In March 2022, the patient was forced to relocate to another region of Ukraine. She subsequently noted a marked deterioration in her condition, with intensification of pain and the development of foot weakness. Over the following 3 years, her condition progressively worsened; however, the patient refused surgical intervention until her condition became "critical." On June 27, 2025, she was urgently admitted to the hospital with a diagnosis of "right-sided posterolateral L5–S1 intervertebral disc herniation, right S1 radiculopathy, severe pain and muscle-tonic syndromes, and moderate paresis of the right foot." On the same day, surgical treatment consisting of right-sided L5–S1 microdiscectomy was performed. After surgery, the pain syndrome decreased, although motor deficits persisted. After returning to her permanent place of residence, the patient sought further treatment at "Lamed" Rehabilitation Clinic.

At the beginning of neurorehabilitation, the patient complained of mild pain in the lumbar spine, difficulty with extension, and numbness of the right foot.

The patient was prescribed daily pharmacological treatment combined with alternating Redcord Neurac therapy and electroneurostimulation every other day for 1 month.

Neurorehabilitation using the "Redcord" platform is illustrated by the example of knee extension exercises (***Fig. 3***).

During the month of neurorehabilitation, the patient demonstrated positive clinical dynamics: mild pain completely resolved, muscle strength in the foot improved, and the patient regained independent ambulation without additional support, with restoration of weight-bearing on the foot. A home exercise program for daily training was recommended. At the 6-month follow-up examination, a stable positive effect without deterioration over time was documented.

Comparison with the results of other researchers. B. D. Dannelly *et al*. (2011) conducted a study involving 26 women (13 participants in the conventional training group and 13 in the sling-therapy group using the Redcord platform), including assessment of lower-limb strength improvement. Training sessions were performed 6 times per week for 13 weeks. The authors demonstrated that Redcord Neurac therapy significantly increased lower-limb strength compared with conventional training [6]. K. Kowalik *et al*. (2025) described a case of successful rehabilitation of a patient with transverse myelitis after vaccination using Redcord Neurac therapy combined with electroneurostimulation [21].

Prospects for further research. Redcord Neurac therapy is a modern and highly effective neurorehabilitation method following lumbar microdiscectomy, particularly in patients with moderate and severe paresis. The advantages of the method include high efficacy, absence of overload, individualized approach, versatility, and restoration of neuromuscular control. Its limitations include the need for highly qualified specialists in physical and rehabilitation medicine, high equipment cost, limited availability mainly in specialized centers, prolonged rehabilitation duration, and the impossibility of independent training.

Fig. 3. Neurorehabilitation using the Redcord platform: A – preparation for exercises; B and C – placement of suspension slings; D – knee extension exercises; E – knee extension of the unaffected limb; F – suspended extension with vibration

Further studies should focus on identifying new combinations and types of exercises that provide maximal restorative effects, as well as the most effective pharmacological and surgical recovery methods in combination with Redcord Neuromuscular Activation therapy.

Conclusions

1. Redcord Neurac therapy is a modern and highly effective neurorehabilitation method for patients with moderate and severe paresis after lumbar microdiscectomy.

2. In combination with conventional treatment methods, Redcord Neurac therapy enabled positive outcomes to be achieved in 84% of cases.

3. According to various authors, Redcord Neurac therapy accelerates patient rehabilitation and improves treatment outcomes.

Disclosure

Conflict of interest

The authors declare no conflict of interest.

Ethical standards

All procedures performed in patients during the study were conducted in accordance with the ethical standards of the institutional and national research committees and with the 1964 Declaration of Helsinki and its later amendments or comparable ethical standards.

Informed consent

Informed consent was obtained from each patient.

Funding

The study received no external financial support.

References

1. Tarasenko O. Transforaminal endoscopic microdiscectomy in the treatment of patients with herniated intervertebral discs in the lumbar spine. Ukr Neurosurg J. 2025;(31)2:37-43. doi: 10.25305/unj.318996
2. Pedachenko EG, Tarasenko ON. Nearest and retrospective results of patients with postoperative compressive cicatrical-adhesive epiduritis treatment. Ukr Neurosurg J. 2006 Sep.18;(3):46-50. doi: 10.25305/unj.127817
3. Zhou F, Tao H, Liu G, Zhang Y, Zhang Y, Zhou K. Clinical effect of TESSYS technique under spinal endoscopy combined with drug therapy in patients with lumbar disc herniation and its effect on quality of life and serum inflammatory factors: results of a randomized trial. Ann Palliat Med. 2021 Aug;10(8):8728-8736. doi: 10.21037/apm-21-1282
4. Pan M, Li Q, Li S, Mao H, Meng B, Zhou F, Yang H. Percutaneous Endoscopic Lumbar Discectomy: Indications and Complications. Pain Physician. 2020 Jan;23(1):49-56.
5. Ju CI, Lee SM. Complications and Management of Endoscopic Spinal Surgery. Neurospine. 2023 Mar;20(1):56-77. doi: 10.14245/ns.2346226.113
6. Shi C, Wu L, Tang G, Sun B, Xu N, Lin W, Liu J, Xu G. Clinical Outcomes of Full-Endoscopic Visualized Foraminoplasty and Discectomy for Lumbar Disc Herniation with Bilateral Radiculopathy. Orthop Surg. 2024 Dec;16(12):3014-3025. doi: 10.1111/os.14240
7. Chang H, Li Z, Zhang Y, Ding W, Xu J. Full-Endoscopic Foraminoplasty and Lumbar Discectomy for Single-Level Lumbar Disc Herniation. J Vis Exp. 2024 Mar 1;(205). doi: 10.3791/66124
8. Yuan C, Zhou Y, Pan Y, Wang J. Curative effect comparison of transforaminal endoscopic spine system and traditional open discectomy: a meta-analysis. ANZ J Surg. 2020 Jan;90(1-2):123-129. doi: 10.1111/ans.15579
9. De Mey K, Danneels L, Cagnie B, Borms D, T'Jonck Z, Van Damme E, Cools AM. Shoulder muscle activation levels during four closed kinetic chain exercises with and without Redcord slings. J Strength Cond Res. 2014 Jun;28(6):1626-35. doi: 10.1519/JSC.0000000000000292
10. Kim ER, Oh JS, Yoo WG. Effect of Vibration Frequency on Serratus Anterior Muscle Activity during Performance of the Push-up Plus with a Redcord Sling. J Phys Ther Sci. 2014 Aug;26(8):1275-6. doi: 10.1589/jpts.26.1275
11. Borms D, Ackerman I, Smets P, Van den Berge G, Cools AM. Biceps Disorder Rehabilitation for the Athlete: A Continuum of Moderate- to High-Load Exercises. Am J Sports Med. 2017 Mar;45(3):642-650. doi: 10.1177/0363546516674190
12. Dannelly BD, Otey SC, Croy T, Harrison B, Rynders CA, Hertel JN, Weltman A. The effectiveness of traditional and sling exercise strength training in women. J Strength Cond Res. 2011 Feb;25(2):464-71. doi: 10.1519/JSC.0b013e318202e473
13. Li P, Zhang J, Wu X, Wang X, Su X, Yang X. Clinical efficacy of integrated 3D manual pelvic reduction, suspension training, and pelvic belt fixation for postpartum pubic symphysis diastasis. BMC Pregnancy Childbirth. 2025 Nov 24;25(1):1259. doi: 10.1186/s12884-025-08379-1
14. Huang JS, Pietrosimone BG, Ingersoll CD, Weltman AL, Saliba SA. Sling exercise and traditional warm-up have similar effects on the velocity and accuracy of throwing. J Strength Cond Res. 2011 Jun;25(6):1673-9. doi: 10.1519/JSC.0b013e3181da7845
15. Kowalik K, Niebrzydowski P, Kropidłowska J, Kvinen A, Kusiak-Kaczmarek M, Szalewska D. The Rehabilitation of a Patient with Acute Transverse Myelitis After HPV Vaccination-A Case Report. Diseases. 2025 Sep 1;13(9):281. doi: 10.3390/diseases13090281
16. Turgut E, Pedersen Ø, Duzgun I, Baltaci G. Three-dimensional scapular kinematics during open and closed kinetic chain movements in asymptomatic and symptomatic subjects. J Biomech. 2016 Sep 6;49(13):2770-2777. doi: 10.1016/j.jbiomech.2016.06.015

Original article

Ukrainian Neurosurgical Journal. 2026;32(2):58-63
doi: 10.25305/unj.349330

Use of C reactive protein (CRP) and creatine kinase (CK) as predictors of early postoperative infection after minimally invasive transforaminal lumbar interbody fusion

Huu Huynh Hai Nguyen [1], Phi Duong Nguyen [2], Khang Trien Truong [3]

[1] Department of Neurosurgery, Thong Nhat Hospital, Ho Chi Minh city, Viet Nam
[2] Orthopaedic - Burn - Plastic Surgery Department, City Children's Hospital, Ho Chi Minh City, Viet Nam
[3] Department of Orthopedic, University of Medicine and Pharmacy at Ho Chi Minh City, Ho Chi Minh City, Viet Nam

Received: 14 January 2026
Accepted: 12 February 2026

Address for correspondence:
Khang Trien Truong, Department of Orthopedic, University of Medicine and Pharmacy at Ho Chi Minh City, Ho Chi Minh City, Vietnam, e-mail: ck2.ctch.2020@gmail.com

Introduction: Minimally invasive transforaminal lumbar interbody fusion (MIS-TLIF) is increasingly used for the treatment of degenerative lumbar spine disease. Despite reduced soft-tissue trauma, early postoperative infection remains a clinically relevant complication and may be difficult to recognize in the early phase. C-reactive protein (CRP) and creatine kinase (CK) are routinely available laboratory markers reflecting inflammatory response and muscle injury, respectively. This study aimed to evaluate the association between postoperative CRP and CK kinetics and early postoperative infection following MIS-TLIF.

Materials and methods: A retrospective study was conducted involving 60 patients who underwent percutaneous pedicle screw fixation and MIS-TLIF between May and November 2022 at Thong Nhat Hospital, Ho Chi Minh City. Serum CRP and CK levels were measured preoperatively and on postoperative days (PODs) 3, 5, 7, 10, and 14. Postoperative infection was diagnosed based on Centers for Disease Control and Prevention criteria and included both surgical site and extra-surgical site infections. Pain outcomes were evaluated using the Visual Analog Scale (VAS). Statistical comparisons were performed using paired *t*-tests or Wilcoxon tests, and Mann–Whitney *U* tests for independent samples.

Results: Six patients (10%) developed postoperative infections, including two deep infections, one superficial infection, and three extra-surgical site infections. In the overall cohort, CRP peaked on POD 3 and gradually declined, with 76% of patients returning to normal levels by POD 14. In infected patients, CRP showed a higher peak and a delayed decline, with a secondary elevation observed after POD 7. CRP levels differed significantly between infected and non-infected groups on POD 10 and POD 14 ($p < 0.05$). In contrast, CK peaked on POD 3 and normalized in most patients by POD 10, with no significant differences between groups. VAS scores for back and leg pain improved significantly one week after surgery.

Conclusion: Serial CRP is a useful supportive marker associated with early postoperative infection when interpreted serially and in conjunction with clinical findings after MIS-TLIF, particularly when CRP fails to decline or increases again after PODs 7–10. CK reflects postoperative muscle injury but does not provide additional diagnostic value for infection detection. CRP trends should be interpreted in conjunction with clinical findings to guide early diagnosis and management.

Keywords: *C-reactive protein; creatine kinase; postoperative infection; minimally invasive spine surgery; MIS-TLIF*

Introduction

Minimally invasive transforaminal lumbar interbody fusion (MIS-TLIF), first described by Foley in 2003, has gained widespread acceptance due to reduced soft-tissue damage, less paravertebral muscle injury, and faster postoperative recovery compared with open techniques. Nevertheless, postoperative infection remains one of the most serious complications of spinal surgery, potentially leading to prolonged hospitalization, revision surgery, and increased healthcare costs [1, 2, 3].

Despite standard preventive measures, including perioperative antibiotic prophylaxis and meticulous surgical technique, reported infection rates after lumbar fusion range from 1.9% to 11.9%, while minimally invasive approaches demonstrate lower rates of approximately 0.6–2.7%. Early diagnosis of infection following MIS-TLIF is particularly challenging because clinical symptoms may be subtle or delayed [4, 5, 6].

C-reactive protein (CRP) is an acute-phase reactant synthesized by hepatocytes in response to inflammatory cytokines and typically rises within hours after tissue injury or infection. After uncomplicated spinal surgery, CRP levels usually peak around postoperative day 3 and subsequently decline. Deviation from this normal kinetic

pattern may indicate an infectious complication. Creatine kinase (CK), an enzyme released during muscle injury, also increases after spinal surgery but primarily reflects the extent of muscle trauma rather than infection. The clinical value of CK for detecting postoperative infection remains uncertain [7, 8, 9].

The aim of this study was to evaluate the association between serial postoperative CRP and CK measurements and early postoperative infection after MIS-TLIF, and to clarify their clinical usefulness in routine postoperative monitoring.

Materials and methods

Study Design and Patients

This retrospective study included 60 patients who underwent percutaneous pedicle screw fixation and MIS-TLIF at Thong Nhat Hospital, Ho Chi Minh City, between May and November 2022. Patients with evidence of infection before postoperative day 3 were excluded. All patients received prophylactic cefazolin (2 g intravenously) 30 minutes before skin incision, with a repeated dose if operative time exceeded 4 hours.

Laboratory Measurements

Serum CRP and CK levels were measured preoperatively and on PODs 3, 5, 7, 10, and 14. Normal CRP levels were defined as ≤5 mg/L. Pain severity was assessed using the Visual Analog Scale (VAS) for back and leg pain preoperatively and on postoperative day 7.

Definition of Infection

Postoperative infections, including surgical site infections and extra-surgical site infections, were defined according to Centers for Disease Control and Prevention criteria. [10] Patients were considered recovered when clinical improvement was accompanied by two consecutive negative CRP measurements obtained at least 15 days apart.

Statistical Analysis

Statistical analysis was performed using SPSS version 29.0. Normality was assessed using the Kolmogorov–Smirnov or Shapiro–Wilk tests as appropriate. Paired *t*-tests or Wilcoxon tests were used for within-group comparisons, and Mann–Whitney *U* tests were applied for comparisons between infected and non-infected groups. A p-value ≤0.05 was considered statistically significant.

Results

Among the 60 patients, 25 were male and 35 female. The mean age was 58.8±1.4 years. The average number of surgical levels was 2.12±0.1. The average surgery time was 226.75±5.6 minutes. There were 6 recorded cases of infection, including 1 superficial infection, 2 deep infections and 3 extra-incision infections as uninary tract infection (***Table 1***).

Postoperative CRP levels increased in all patients reaching a peak on postoperative day 3, followed by a gradual decline over time. In patients who developed infection, CRP demonstrated a higher peak and a slower decrease compared with the non-infected group. In addition, a secondary elevation or persistent plateau after postoperative day 7 was observed in infected cases, whereas CRP values in non-infected patients continued to decrease steadily. Differences between the two groups became more evident in the later postoperative period, particularly after postoperative day 10. Detailed numerical values are presented in ***Table 2***.

Fig. 1 illustrates the overall trend of CRP changes over time in both groups, highlighting the higher peak and delayed decline observed in infected patients.

Postoperative CK levels peaked on day 3 (1081±99 U/L) and then gradually decreased, with 81% of patients returning to normal CK levels after 10 days. No statistically significant differences in CK levels were observed between the infected and non-infected groups (***Fig. 2***).

Table 1. Patients demographic and surgical profile

Demographic data	Mean±SD
Age	58.8±1.4
Sex	
Male	25
Female	35
Number of surgical levels	2.12±0.1
1 level	13
2 levels	30
3 levels	14
4 levels	3
Surgical time (min)	226.75±5.6
Number of infections	6
Superficial infection	1
Deep infection	2
Extra-incision infection	3

Table 2. Comparison of CRP values between two groups

CRP values	No infection	Infection	*P*-value
Preoperative	3.5±0.4	4.67±1.64	0.306
Postoperative day 3	97.35±8.48	141.86±43.03	0.289
Postoperative day 5	38±3.63	54.55±11.18	0.121
Postoperative day 7	13.5±1.37	19.8±3.83	0.091
Postoperative day 10	7.1±0.93	23.2±7.36	0.002*
Postoperative day 14	3.67±0.38	25.58±2.56	<0.001*

Note. * Statistically significant

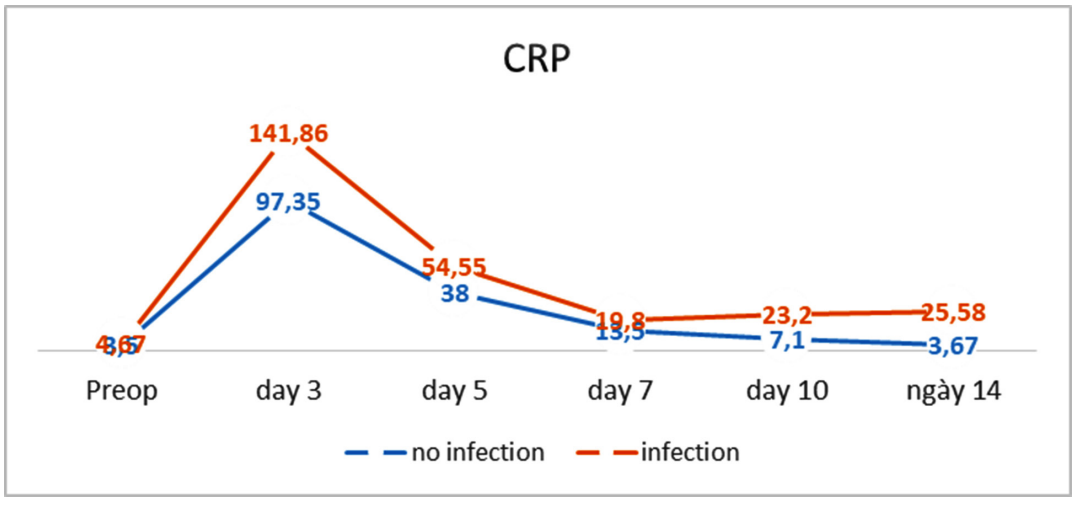

Fig. 1. Mean CRP values between the infected and non-infected patients, measured preoperatively and on PODs 3,5,7,10,14, respectively

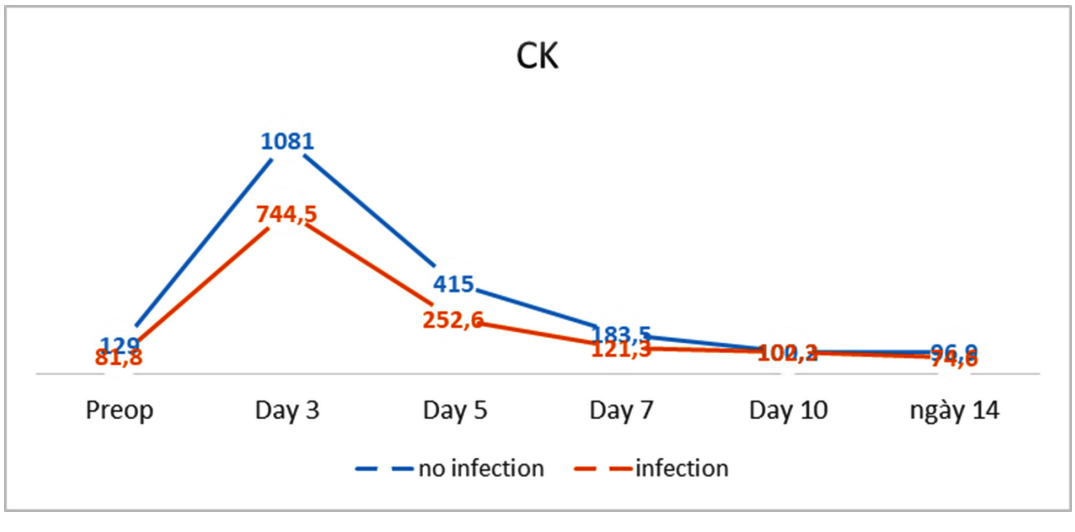

Fig. 2. Mean CK values between infected and non-infected patients, measured preoperatively and on days 3,5,7,10 and 14. Values are presented as mean±SD

The variables of age, number of surgical levels, and time of surgery were not related to infection status. Among 6 patients with infection, 5 patients had comorbidities, of which exogenous Cushing syndrome accounted for 3/6 (50%) (***Table 3***).

VAS scores 1 week after surgery significantly improved compared to preoperative values. Back pain VAS decreased from 5.88 ± 0.19 to 3.88 ± 0.61 (p < 0.001), while leg pain VAS decreased from 7.05 ± 0.16 to 1.5 ± 0.11 (p < 0.001).

Table 3. Analysis of infection status with other variables

Variables	No infection	Infection	*P*-value
Age	58.31±1.38	63±6.7	0.361
Number of surgical levels	2.04±0.1	2.83±0.5	0.056
Surgical time (min)	227.87±5.82	216.67±21.1	0.734
Comorbidity		Exogenous Cushing syndrome: 3 cases Diabetes mellitus and Hypertension: 2 cases No comorbidity: 1 case	

Discussion

CRP is produced by the liver in response to inflammation, infection, malignancy, and tissue damage with a relatively high sensitivity, rate of response, and range compared to other acute phase reactants [2]. However, the primary acute phase reaction of CRP is not specific to surgery or infection and can be caused by a number of conditions including necrosis, inflammatory disease, allergic complications of infection, and infectious disease and malignancies [8]. In the early postoperative period, numerous studies have described the normal kinetics of CRP as rapidly increasing, peaking on day 3, followed by a sharp decrease and then gradually decreasing with normalization on within 14–21 days. Deviations from the normal kinetics of CRP may indicate an infectious complication [11].

In the present study, similar to previous reports, CRP levels increased rapidly after surgery, peaked on day 3 and then gradually decreased. Patients with postoperative infection had a slow decrease in CRP levels and a tendency to increase again on the 7th postoperative day. Similarly, Kang *et al.* [12] found that infections had a rebound in CRP levels on day 5 or 7 postoperatively. Hotably, 72% of the non-infected patients did not demonstrate normalization of CRP by postoperative day 7, however their levels gradually decreased thereafter, whereas CRP levels in the infected group showed a secondary increase. In our cohort, CRP levels between the infected and non-infected groups was significantly different at day 10. Although, in the infected group, CRP level had a higher peak on day 3 (141.86±43 vs 97.35±8.5), but the difference was not statistically significant (p = 0.289).

Of the 6 infected patients, there were three cases of urinary tract infection with positive urine test for white blood cells and nitrites. One patient developed a superficial infection after suture removal on day 10, characterized by purulent discharge; Staphylococcus epidermidis was isolated on culture, and the patient was successfully treated with oral antibiotics. There were 2 patients diagnosed with deep infection, presenting with fever, back pain, increased white blood cell count, elevated CRP levels. MRI demonstrated soft tissue inflammatory changes in the surgical area, without evidence of abscess formation and negative blood cultures. These patients with deep infection received intravenous antibiotics. All patients recovered with conservative treatment.

CK, an enzyme that catalyzes biochemical reactions in the body, the concentration of CK in the blood will help reflect the activity status and health of the muscle mass. CK also recorded a rapid increase after surgery and peaked on day 3, then gradually decreased [9]. In current study, CK peaked (1047.33±90.2) on day 3, then gradually decreased and 81% of patients returned to normal levels on day 10 postoperatively. The difference in CK levels between the infected and non-infected groups was not statistically significant.

Analysis of other factors including age, surgical time, number of surgical levels were not related to infection status. Although in the infection group there were more surgical levels and older age, but the difference was not statistically significant (p>0.05). Notably, five of six patients in the infection group had comorbidities, including three cases of exogenous Cushing syndrome (accounting for 50%).

Regarding clinical outcomes, MIS-TLIF demonstrated favorable short-term results. Pain scores assessed using the VAS showed significant improvement one week after surgery compared with preoperative surgery. Back pain VAS decreased from 5.88±2 0.19 to 3.88±0.61; p<0.001, while leg pain VAS decreased from 7.05±0.16 to 1.5±0.11; p<0.001.

Overall, this study demonstrates that serial CRP measurements provides clinically useful information for the early identification of postoperative infection following MIS-TLIF. Consistent with previous reports [13,14]. CRP peaked on postoperative day 3 in all patients. However, infected patients showed delayed normalization and secondary elevation, particularly after postoperative day 7, distinguishing them from non-infected patients.

Although CK also increased after surgery, reflecting muscle injury, it did not differ significantly between infected and non-infected groups. This finding supports the interpretation that CK is primarily a marker of surgical trauma rather than infection [15].

Importantly, a substantial proportion of non-infected patients had persistently elevated CRP levels in the early postoperative period, emphasizing that single CRP measurements should not be overinterpreted. Instead, CRP trends over time — especially after postoperative day 7–10 — appear to be more informative. Given the

small number of infection cases, the findings should be interpreted as demonstrating an association rather than definitive predictive value.

Limitations

Limitations of this study include its retrospective design, the relatively small number of infection cases, and the absence of multivariable analysis to adjust for potential confounding factors. In addition, steroid exposure, which may influence CRP responses, was only partially accounted for through comorbidity data and could not be evaluated in detail. Recent studies and systematic reviews have likewise emphasized the importance of CRP kinetics over single absolute cutoff values for the early detection of postoperative infection after spine surgery, while also indicating the limited diagnostic role of muscle injury markers such as CK [16, 17]. These contemporary findings are consistent with our results and support the use of serial CRP monitoring in conjunction with clinical assessment rather than reliance on isolated laboratory measurements. Future prospective studies with larger sample sizes and standardized protocols are warranted to validate these observations and to establish clinically meaningful thresholds for postoperative CRP interpretation.

Conclusions

Serial monitoring of CRP is a simple and reliable supportive tool for the early detection of postoperative infection after MIS-TLIF, particularly when CRP levels fail to decline or demonstrate a secondary increase after postoperative day 7–10. CK does not appear to provide additional diagnostic value for infection. CRP trends should be interpreted in conjunction with clinical findings to guide early diagnosis and management. These findings indicate an association rather than definitive predictive value and should be interpreted in light of the study's retrospective design and limited number of infections.

Disclosure

Conflict of Interest

No potential conflict of interest relevant to this article was reported.

Funding

This research received no external funding.

References

1. Foley KT, Holly LT, Schwender JD. Minimally invasive lumbar fusion. Spine (Phila Pa 1976). 2003 Aug 1;28(15 Suppl):S26-35. doi: 10.1097/01.BRS.0000076895.52418.5E
2. Dowdell J, Brochin R, Kim J, Overley S, Oren J, Freedman B, Cho S. Postoperative Spine Infection: Diagnosis and Management. Global Spine J. 2018 Dec;8(4 Suppl):37S-43S. doi: 10.1177/2192568217745512
3. Mok JM, Pekmezci M, Piper SL, Boyd E, Berven SH, Burch S, Deviren V, Tay B, Hu SS. Use of C-reactive protein after spinal surgery: comparison with erythrocyte sedimentation rate as predictor of early postoperative infectious complications. Spine (Phila Pa 1976). 2008 Feb 15;33(4):415-21. doi: 10.1097/BRS.0b013e318163f9ee
4. Bišćević M, Bišćević S, Ljuca F, Smrke BU, Krupić F, Habul Ć. Postoperative infections after posterior spondylodesis of thoracic and lumbal spine. Surgical spine infections. Psychiatr Danub. 2014 Dec;26 Suppl 2:382-6.
5. Villavicencio AT, Burneikiene S, Nelson EL, Bulsara KR, Favors M, Thramann J. Safety of transforaminal lumbar interbody fusion and intervertebral recombinant human bone morphogenetic protein-2. J Neurosurg Spine. 2005 Dec;3(6):436-43. doi: 10.3171/spi.2005.3.6.0436
6. Kulkarni AG, Patel RS, Dutta S. Does Minimally Invasive Spine Surgery Minimize Surgical Site Infections? Asian Spine J. 2016 Dec;10(6):1000-1006. doi: 10.4184/asj.2016.10.6.1000
7. Thelander U, Larsson S. Quantitation of C-reactive protein levels and erythrocyte sedimentation rate after spinal surgery. Spine (Phila Pa 1976). 1992 Apr;17(4):400-4. doi: 10.1097/00007632-199204000-00004
8. Larsson S, Thelander U, Friberg S. C-reactive protein (CRP) levels after elective orthopedic surgery. Clin Orthop Relat Res. 1992 Feb;(275):237-42.
9. Griffith M, Shaw KA, Baird M, Rushford P, Shaw V, Roberts A, Gloystein DM. Defining the Normal Trends of Serum Creatine Kinase Levels Following Spinal Surgery. Asian Spine J. 2019 Jun;13(3):386-394. doi: 10.31616/asj.2018.0191
10. Horan TC, Gaynes RP, Martone WJ, Jarvis WR, Emori TG. CDC definitions of nosocomial surgical site infections, 1992: a modification of CDC definitions of surgical wound infections. Am J Infect Control. 1992 Oct;20(5):271-4. doi: 10.1016/s0196-6553(05)80201-9
11. Hoeller S, Roch PJ, Weiser L, Hubert J, Lehmann W, Saul D. C-reactive protein in spinal surgery: more predictive than prehistoric. Eur Spine J. 2021 May;30(5):1261-1269. doi: 10.1007/s00586-021-06782-8
12. Kang BU, Lee SH, Ahn Y, Choi WC, Choi YG. Surgical site infection in spinal surgery: detection and management based on serial C-reactive protein measurements. J Neurosurg Spine. 2010 Aug;13(2):158-64. doi: 10.3171/2010.3.SPINE09403
13. Shetty S, Ethiraj P, Shanthappa AH. C-reactive Protein Is a Diagnostic Tool for Postoperative Infection in Orthopaedics. Cureus. 2022 Feb 16;14(2):e22270. doi: 10.7759/cureus.22270
14. Ahmed SK, Shahzad MG, Iftikhar S. Diagnostic accuracy of C-reactive protein to rule out infectious complications following hip fracture surgery. Pak J Med Sci. 2022 Jul-Aug;38(6):1514-1519. doi: 10.12669/pjms.38.6.5577
15. Maleitzke T, Zhou S, Zocholl D, Fleckenstein FN, Back DA, Plewe JM, Weber J, Winkler T, Stöckle U, Tsitsilonis S, Märdian S. Routine laboratory parameters predict intensive care unit admission and hospitalization in patients suffering stab injuries. Front Immunol. 2023 Jan 5;13:959141. doi: 10.3389/fimmu.2022.959141
16. Youn G, Choi MK, Kim SB. Comparison of Inflammatory

Markers Changes in Patients Who Used Postoperative Prophylactic Antibiotics within 24 Hours after Spine Surgery and 5 Days after Spine Surgery. J Korean Neurosurg Soc. 2022 Nov;65(6):834-840. doi: 10.3340/jkns.2022.0126

17. Suryawanshi A, Patkar H, Aute S, Rathi PC, Rathi CL, Risbud SP, Ganu GP. Systemic enzyme therapy for postoperative inflammation and wound healing after orthopedic surgery: a randomized, placebo and active controlled clinical study. Sci Rep. 2025 Oct 2;15(1):34336. doi: 10.1038/s41598-025-16747-2

Original article

Ukrainian Neurosurgical Journal. 2026;32(2):64-72
doi: 10.25305/unj.350206

The role of MRI tractography in stereotactic targeting for surgical treatment of Parkinson's disease

Kostiantyn R. Kostiuk, Andrii O. Lisianyi

Department of Functional Neurosurgery and Neuromodulation, Romodanov Neurosurgery Institute, Kyiv, Ukraine

Received: 17 January 2026
Accepted: 19 February 2026

Address for correspondence:
Kostiantyn R. Kostiuk, Department of Functional Neurosurgery and Neuromodulation, Romodanov Neurosurgery Institute, 32 Platona Maiborody st., Kyiv, 04050, Ukraine, e-mail: kostiuk.neuro@gmail.com

Objective: To evaluate the clinical efficacy of surgical treatment of tremor-dominant Parkinson's disease (PD) with regard to stereotactic target determination based on MRI tractography data, and to compare the outcomes of conventional stereotactic radiofrequency (RF) thalamotomy of the ventral intermediate nucleus (Vim) with tractography-assisted lesioning of the dentatorubrothalamic tract (DRTT).

Materials and methods: This retrospective study included 25 patients with PD who underwent surgery between 2018 and 2025. Inclusion criteria were tremor-dominant clinical presentation, a progressive disease course, and insufficient response to pharmacological therapy. Patients were divided into two groups: the Vim group (n=19), in which conventional stereotactic RF thalamotomy was performed using indirect target calculation, and the DRTT group (n=6), in which the surgical target was determined using MRI tractography based on diffusion tensor imaging (DTI). Surgical planning was performed using Element software (Brainlab, Germany). Clinical efficacy was assessed preoperatively and 12 months postoperatively using the Unified Parkinson's Disease Rating Scale (UPDRS, part III), the Clinical Rating Scale for Tremor (CRST, parts A and C).

Results: In all patients, tremor of the contralateral limb was completely abolished immediately after surgery. At 12 months, the mean UPDRS III score decreased by 44%, from 83.2±8.7 to 46.7±4.18 points (p=0.04). A statistically significant improvement in UPDRS III scores was observed in the DRTT group (p=0.032), whereas the difference in the Vim group did not reach statistical significance. Tremor regression assessed by CRST-A and CRST-C was observed in both groups but was more pronounced in patients who underwent tractography-assisted lesioning. Postoperatively, a reduction in daily levodopa dosage was noted: by 23.4% in the Vim group and by 27.7% in the DRTT group. No intraoperative complications were recorded. Transient neurological adverse effects occurred more frequently in the Vim group and resolved completely during the early postoperative period.

Conclusions: The use of MRI tractography for stereotactic target selection in ablative surgery for PD enables individualized surgical planning and provides more precise targeting of pathophysiologically relevant neural pathways. Tractography-assisted lesioning of the DRTT is associated with more stable tremor control, a tendency toward greater improvement of accompanying motor symptoms, and a potentially lower risk of neurological adverse effects.

Key words: *Parkinson's disease; deep brain stimulation; stereotactic radiofrequency lesioning; dentatorubrothalamic tract*

Introduction

Parkinson's disease (PD) is one of the most prevalent neurodegenerative disorders of the nervous system, characterized by a progressive course and the necessity for lifelong levodopa replacement therapy. Surgical treatment of PD was first introduced in the mid-twentieth century and has been continuously refined over the past 25 years. The primary method of surgical intervention in PD is deep brain stimulation (DBS) [1, 2]. Over the past decade, there has been a resurgence of ablative stereotactic procedures that were widely used for PD treatment in the 1950s. Alongside classical stereotactic radiofrequency (RF) destruction of subcortical nuclei, non-invasive techniques have been introduced, including Gamma Knife radiosurgery and MRI-guided focused ultrasound ablation [3–7].

Several approaches exist to improve the effectiveness of surgical interventions in PD. First and foremost is the advancement of modern neuroimaging technologies, which enable high-resolution MRI visualization of subcortical brain structures and white matter tracts. The introduction of high-field magnetic resonance imaging (MRI) allows not only visualization of individual anatomical structures but also differentiation of their

subsegments and precise identification of the surgical target zone. It has been established that the dorsal portion of the subthalamic nucleus (STN) receives the highest density of projections from cortical motor areas (the hyperdirect pathway) and is considered the optimal target for DBS [8]. In most hospitals across developed countries in Europe, North America, and Asia, 3T MRI is used for stereotactic planning, while several centers have extensive experience with ultra-high-field 7T MRI [9]. A recently published study by a Dutch research group demonstrated that the use of 7T MRI enables accurate electrode placement within the motor subregion of the STN, resulting in more than a 30% improvement in motor symptom control compared with preoperative planning based on 3T MRI [10]. Another strategy to improve neuromodulation outcomes is the development of directional stimulation electrodes and the implementation of adaptive DBS, a closed-loop system capable of adjusting stimulation parameters according to biomarkers reflecting the patient's clinical state [11–13].

Another direction for improving the efficacy and safety of stereotactic procedures involves the advancement of software systems that, using modern digital anatomical atlases accounting for individual brain morphology in three-dimensional space, allow precise visualization of the neurosurgical target. Contemporary planning platforms enable integration of multimodal neuroimaging data, more accurate definition of target coordinates, and optimization of a safe electrode trajectory. Such software also allows the creation of individualized anatomical models and determination of electrode position and orientation for each patient, which can subsequently be integrated with clinical programmers for faster and more efficient adjustment of neurostimulation parameters.

At the current stage of scientific development, PD is considered a disorder of neuronal circuits and networks responsible for motor control. Significant progress has been made in understanding the etiology and pathomorphological changes of the basal ganglia in PD patients. Dysfunction of functional connectivity between nuclei plays a central role in disease pathogenesis. Recent studies have established a clear relationship between major motor symptoms of PD and pathophysiological alterations in specific neural circuits of the brain. In particular, a meta-analysis by Rajamani *et al*. (2024) demonstrated a correlation between stimulation of specific white matter bundles and improvement in tremor, rigidity, bradykinesia, and postural instability [14].

The concept of circuit-based dysfunction is consistent with the historical evolution of surgical treatment for PD, particularly in relation to the management of tremor, one of the most disabling symptoms. Since the 1950s, the globus pallidus has been a primary target of stereotactic interventions in PD. Although morphological changes in PD are observed in the substantia nigra, which fails to produce sufficient dopamine, it is the globus pallidus that is most sensitive to dopaminergic deficiency, leading to disrupted physiological activity and the emergence of hyperkinetic disorders.

In 1954, Hassler *et al*. performed stereotactic ablation of neurons receiving pathological signals from the globus pallidus. These neurons were localized in the posterior ventral oral (Vop) and ventral intermediate (Vim) nuclei of the thalamus. Since then, numerous studies have confirmed the high efficacy of Vim lesioning for tremor control of various etiologies. The Vim target remains the gold standard for stereotactic surgery despite several limitations. The most significant drawback is the inability to directly visualize the Vim on MRI. The Vim nucleus is a group of motor neurons located at the border of the ventrolateral thalamus, ventral oral, and ventral caudal nuclei. On conventional MRI, its boundaries cannot be clearly delineated, which necessitates an indirect targeting approach using the anterior and posterior commissures as anatomical landmarks and atlas-based coordinates. The search for alternative targets, nuclei, or white matter pathways whose stimulation or ablation could provide more effective and safer tremor control continues. One such alternative target is the posterior subthalamic area (PSA), which includes the zona incerta (Zi). These targets have demonstrated high efficacy in tremor control but also present certain limitations. Histological and MRI-DWI-based studies of basal ganglia cytoarchitecture and white matter tracts have established a relationship between tremor and the dentatorubrothalamic tract (DRTT), also known as the cerebellothalamic fasciculus. This tract runs in close proximity to all the aforementioned targets, forming the basis of the "three targets—one pathway" concept [15].

In recent years, MRI tractography based on diffusion tensor imaging (DTI) has become increasingly important in stereotactic surgical planning. Contemporary studies have shown that the effectiveness of surgical intervention is determined by modulation of neuronal pathways involved in the pathophysiology of movement disorders. The DRTT, originating from the dentate nucleus of the cerebellum, passing through the contralateral red nucleus, and terminating in the ventrolateral thalamic nucleus on the opposite side, plays a key role in tremor regulation of various origins. Previously, the DRTT was difficult to identify due to its long multisynaptic course across hemispheres. However, the development of DTI MRI technology and advanced software has enabled its visualization and targeted modulation using stereotactic techniques. Chronic stimulation or ablation of the DRTT has been shown to provide superior tremor control compared with interventions targeting classical subcortical structures involved in PD pathophysiology, such as the Vim, PSA, or STN [14].

Currently, a paradigm shift in tremor treatment is underway, as the DRTT is increasingly recognized as a primary pathogenetic surgical target in stereotactic interventions involving the Vim. Unlike thalamic nuclei, the DRTT white matter tract can be directly visualized using MRI tractography based on diffusion-weighted imaging (DWI). The most appropriate strategy for target definition in stereotactic surgery is a combined approach, which involves refining indirectly determined targets using tractography data. This approach reduces the risk of adverse effects while ensuring stable therapeutic efficacy.

Objective: To evaluate the clinical efficacy of surgical treatment of tremor-dominant Parkinson's disease, taking into account the possibility of stereotactic

target definition based on MRI tractography, and to compare the outcomes of classical stereotactic radiofrequency thalamotomy of the ventral intermediate thalamic nucleus with tractography-assisted ablation of the dentatorubrothalamic tract.

Materials and methods

Study participants

A total of 25 patients with PD were included in this retrospective study. All patients underwent surgical treatment in the Department of Functional Neurosurgery and Neuromodulation of the Romodanov Neurosurgery Institute, National Academy of Medical Sciences of Ukraine, during the period 2018–2025.

The study was conducted in accordance with the Declaration of Helsinki (1964–2013), the International Council for Harmonisation Good Clinical Practice (ICH GCP, 1996), EU Directive No. 609 (24.11.1986), and the regulatory orders of the Ministry of Health of Ukraine No. 690 (23.09.2009), No. 944 (14.12.2009), and No. 616 (03.08.2012), as well as local institutional protocols. The Ethics Committee of the Romodanov Neurosurgery Institute confirmed that no ethical or legal violations were identified during the research. All patients provided informed consent for participation, and anonymity was ensured.

Inclusion criteria

Patients were included if they met the following criteria: predominance of tremor within the clinical symptom complex of PD, insufficient response to antiparkinsonian pharmacotherapy, progressive disease course, and use of the Element software (Brainlab, Germany) for stereotactic target planning.

Exclusion criteria

Patients were excluded in cases of akinetic-rigid predominant PD, severe balance or coordination disturbances, significant comorbid somatic pathology that could increase surgical risk, or contraindications to MRI examination.

Study design

Patients were divided into two groups. In the first group (Vim group), 19 patients (76%) underwent classical radiofrequency (RF) lesioning of the ventral intermediate nucleus (Vim), using standard stereotactic targeting based on the intercommissural line. In the second group (DRTT group), 6 patients (24%) underwent dentatorubrothalamic tract (DRTT) ablation assisted by tractography.

The differences in stereotactic target coordinates between the two groups were analyzed. Neurological and functional status was assessed preoperatively and at 12 months postoperatively.

Group characteristics

The age of patients at the time of surgery ranged from 44 to 81 years (mean: 63.7 years). Males predominated (17 patients, 68%). Disease duration ranged from 4 to 22 years (mean: 12 years). Both age and disease duration were slightly higher in the Vim group; however, the differences were not statistically significant (***Table 1***).

All patients received dopamine replacement therapy at doses ranging from 450 to 1500 mg/day (mean: 812.56 mg/day). The duration of levodopa therapy prior to surgery ranged from 4 to 15 years (mean: 9 years). No significant differences were found between the groups regarding levodopa dose or duration of therapy. Adverse effects of dopaminergic therapy in the form of motor fluctuations were observed in 4 patients (16%). Levodopa-induced dyskinesias were not detected.

At the time of surgical treatment, patients were classified as stage 2.5–3.0 on the Hoehn and Yahr scale. Although all patients exhibited bilateral manifestations of Parkinson's disease with moderate postural instability, they retained full functional independence in daily activities. In the majority of cases (88%), patients presented with tremor-dominant and tremor–rigid forms of PD (***Table 2***). Stereotactic thalamotomy and DRTT ablation were not performed in patients with akinetic-rigid predominant PD, as this type of surgical intervention is associated with an increased risk of balance and coordination disturbances, as well as potential worsening of bradykinesia.

Stereotactic planning was performed using Element software (Brainlab, Germany). The coordinates of the Vim nucleus were determined using an indirect method based on individual anatomical characteristics of the intercommissural line (AC–PC line), which connects the anterior and posterior commissures. DRTT ablation coordinates were calculated using a direct approach based on diffusion tensor imaging (DTI) obtained during MRI tractography. Visualization of the DRTT was performed by identifying its key anatomical components, namely the ipsilateral primary motor cortex (M1) and the contralateral dentate nucleus of the cerebellum (***Fig. 1 and 2***).

All surgical procedures were performed using a CRW Radionics stereotactic frame (Radionics Inc., USA) and a radiofrequency electrode with a diameter of 2.1 mm and an active tip length of 2.0 mm. Radiofrequency ablation was carried out under awake anesthesia with intraoperative test macrostimulation at high (75 Hz) and low (2 Hz) frequencies, which enabled identification of the correct and safe positioning of the RF electrode. Prior to definitive RF ablation, test lesions were performed at 45 °C and 55 °C for 30 s each. In the absence of additional neurological deficits, such as paresthesia, spastic contractions of the contralateral limbs, or speech disturbances, definitive ablation of the planned target was performed at 75 °C for 60–65 s.

Neurological and functional status was assessed preoperatively and 12 months after surgery using the Unified Parkinson's Disease Rating Scale (UPDRS). Tremor regression was evaluated using Parts A and C of the Clinical Rating Scale for Tremor (CRST) [16], as well as the total tremor score in the medication-off state (OFF state) according to Part III of the UPDRS, including assessment of head tremor, upper and lower limb tremor, action tremor, and postural tremor severity. According to this subscale, scores may range from 0 to 28 points [17].

Statistical analysis

Statistical data analysis and processing were performed using IBM SPSS Statistics version 29 (license No. 512186485) and MS Excel. The Shapiro–Wilk W test was used to assess the normality of data distribution. In cases of normal distribution, Student's t-test was applied. When data distribution deviated from normality, nonparametric statistical tests were used.

Table 1. Clinical characteristics of patients (M ± m)

Parameter	Vim, n=19	DRTT, n=6	Total, n=25	p
Mean age, years	65±2	60±4	63,7±2,0	0,925
Sex:				
Male	12 (63%)	5 (83%)	17 (68%)	
Female	7 (37%)	1 (17%)	8 (32%)	
Mean PD duration, years	12,4±1	9,8±1,3	12,0±1,0	0,978
Mean levodopa dose, mg/day	874,8±94,3	725,8±64,2	812,56±76,50	0,962
Mean duration of levodopa therapy, years	9,4±0,7	7±0,8	9,0±1,0	0,95
Motor fluctuations	3 (15%)	1 (16%)	4 (16%)	

Table 2. Clinical forms of Parkinson's disease

Form of PD	Vim, n=19	DRTT, n=6	Total, n=25
Tremor-dominant	10 (52%)	4 (67%)	14 (56%)
Tremor–rigid	6 (32%)	2 (33%)	8 (32%)
Tremor–akinetic–rigid	3 (16%)	0 (0%)	3 (12%)

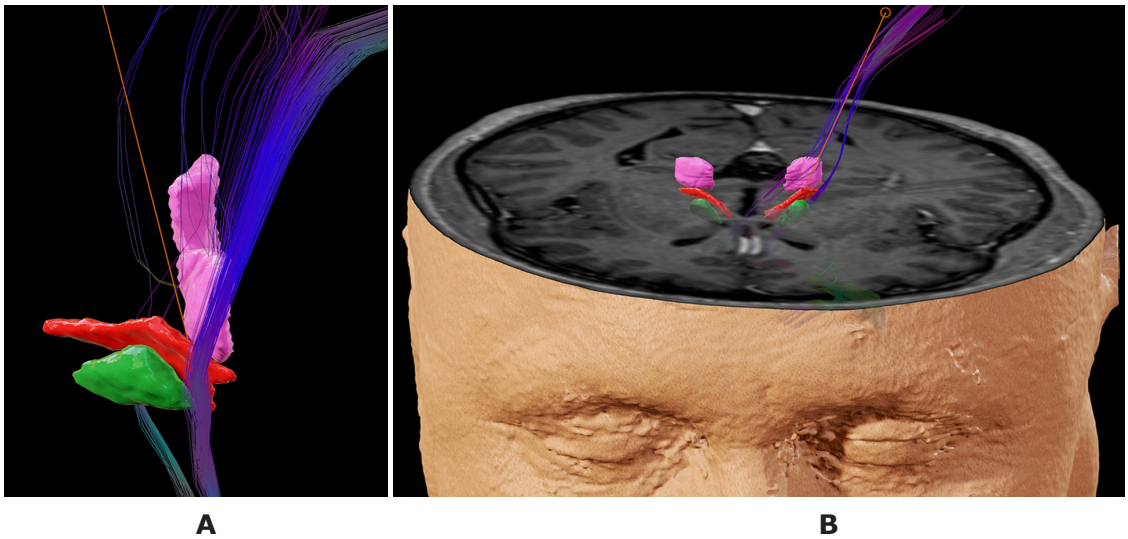

A B

Fig. 1. Planning of the target for RF DRTT ablation. Three-dimensional reconstruction model of the subcortical nuclei and tract (purple — Vim; green — STN; red — posterior subthalamic area; blue-violet — DRTT; orange — trajectory of DRTT tractotomy): A — lateral projection; B — anteroposterior projection

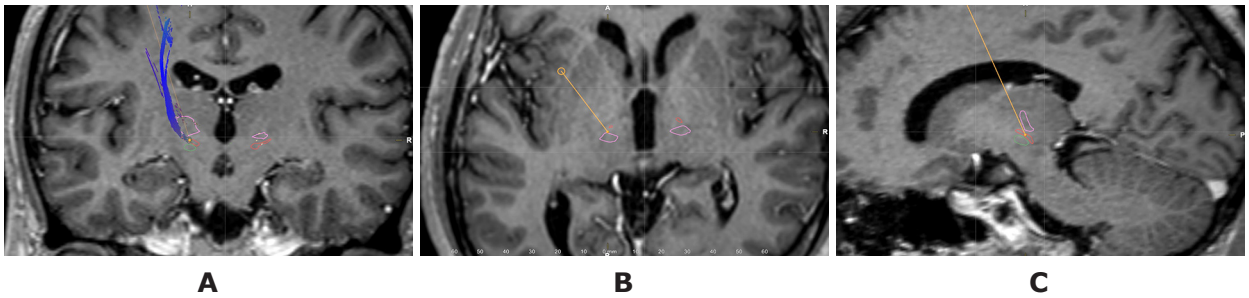

A B C

Fig. 2. Planning of the target for RF DRTT ablation. Brain MRI with intravenous contrast enhancement (orange line — electrode insertion trajectory; purple — Vim; red — posterior subthalamic area; green — STN): A — coronal projection; B — axial projection; C — sagittal projection

Results

Analysis of differences between stereotactic target coordinates in the two groups using descriptive statistics (mean value, standard deviation, and standard error) for coordinates in three projections (anteroposterior direction, laterality, and height relative to the AC–PC line) revealed no statistically significant differences (***Table 3***).

The observed differences did not exceed the statistical error and averaged 0.5–1.0 mm. Considering that the average width of the Vim nucleus is approximately 4 mm, even such seemingly minor deviations may have substantial clinical significance, corresponding to up to 25% of the target size [18]. Given the acceptable possibility of mechanical electrode deviation from the planned trajectory by up to 1 mm, the cumulative error may reach or even exceed half of the Vim nucleus diameter. This is critically important because even minimal displacement of the ablation target may result in insufficient modulation of the intended area or unintended involvement of adjacent structures, thereby reducing therapeutic efficacy and increasing the risk of adverse effects.

Follow-up evaluation at 12 months after surgery was performed in 9 of 19 patients (47.4%) in the Vim group and in all patients in the DRTT group. Improvement in neurological status, particularly tremor regression, was observed in both groups. Complete regression of contralateral limb tremor was achieved immediately after surgery in all patients. A marked reduction in head tremor was also observed.

One year after surgery, the mean UPDRS III score improved by 44%, decreasing from (83.2 ± 8.7) to (46.70 ± 4.18) points (p = 0.04). However, statistically significant improvement was observed only in the DRTT group (p = 0.032). Regression of rigidity and tremor was more pronounced in the DRTT group, although the difference between groups did not reach statistical significance (p > 0.05). According to the CRST-A and CRST-C scales, significant tremor reduction was observed in both groups. In all cases, improvement in motor function, self-care ability, and quality of life was documented.

Following surgery, the levodopa dose was reduced in both groups: by 23.4% in the Vim group and by 27.7% in the DRTT group (***Table 4***). Reduction of levodopa replacement therapy may help prevent the development of treatment-related adverse effects.

No intraoperative complications (hemorrhage or ischemia within the lesioning zone), infectious complications, or other adverse events were observed. Neurological complications developed in 3 (12.0%) patients (2 in the Vim group and 1 in the DRTT group). In all cases, the complications were transient and resolved within a period ranging from 1 week to 2 months after surgery. Following Vim lesioning, one patient developed transient dysarthria and moderate contralateral hemiparesis, whereas another patient experienced dysarthria. These complications were caused by injury to the internal capsule. Following DRTT lesioning, one patient developed transient dyspraxia and paresthesia of the contralateral extremities due to extension of the

Table 3. Mean coordinates of the Vim target

Coordinate axis	Mean value, mm		Standard deviation		Standard error	
	Vim	DRTT	Vim	DRTT	Vim	DRTT
Vertical axis	-0,22	-0,43	0,49	0,46	0,11	0,19
Lateral axis	12,71	13,12	0,78	1,21	0,49	0,17
Anteroposterior axis	-5,37	-5,85	0,77	0,56	0,17	0,22

Table 4. Outcomes of radiofrequency stereotactic thalamotomy at 12 months after surgery

Parameter	Vim group		DRTT group		p
	before surgery	after surgery	before surgery	after surgery	
Tremor (range 0–28)	19,1±0,9	7,56±1,40	21,17±1,60	6,67±4,18	0,047
CRST-A (range 0–88)	36,00 ± 0,88	9,4±1,2	42,50±5,08	7,33±1,97	0,038
CRST-C (range 0–32)	16,6±0,7	11,1±1,6	17,40±3,45	12,67±3,54	>0,1
Levodopa dose, mg/day	874,8±94,3	670,4±54,3	725,8±64,2	524,4±38,3	>0,1

Table 5. Neurological complications

Complication	Vim, n=2	DRTT, n=1
Contralateral hemiparesis	1 (5%)	0
Dysarthria	2 (10%)	0
Dyspraxia	0	1 (16%)
Paresthesia	0	1 (16%)

lesioning zone into the ventral caudal somatosensory nucleus of the thalamus (***Table 5***).

Clinical case

Patient D., 53 years old, was examined at the Romodanov Neurosurgery Institute of the National Academy of Medical Sciences of Ukraine. The following diagnosis was established: "Parkinson's disease, tremor-rigid form, stage 2.5 according to the Hoehn and Yahr scale, progressive course." The disease duration was 6 years. At the time of hospitalization, the patient was receiving levodopa/carbidopa at a dose of 625 mg/day, rasagiline (a monoamine oxidase inhibitor) at a dose of 1 mg/day, and pramipexole (a dopamine receptor agonist) at a dose of 1.25 mg/day. The clinical presentation was dominated by pronounced resting and postural tremor, predominantly affecting the left extremities.

The patient underwent right-sided radiofrequency (RF) DRTT lesioning using the Element software (Brainlab) for determination of target coordinates (***Fig. 3***). After surgery, tremor in the left extremities completely resolved, rigidity regressed, and motor activity improved. One year after surgery, the patient reduced the dose of levodopa therapy to 375 mg/day and pramipexole to 0.375 mg/day and discontinued rasagiline therapy.

Magnetic resonance imaging (MRI) was performed 12 months after surgery (***Fig. 4***). It was established that the UPDRS score during the "OFF" period decreased from 88 to 61 points, corresponding to a 31% reduction.

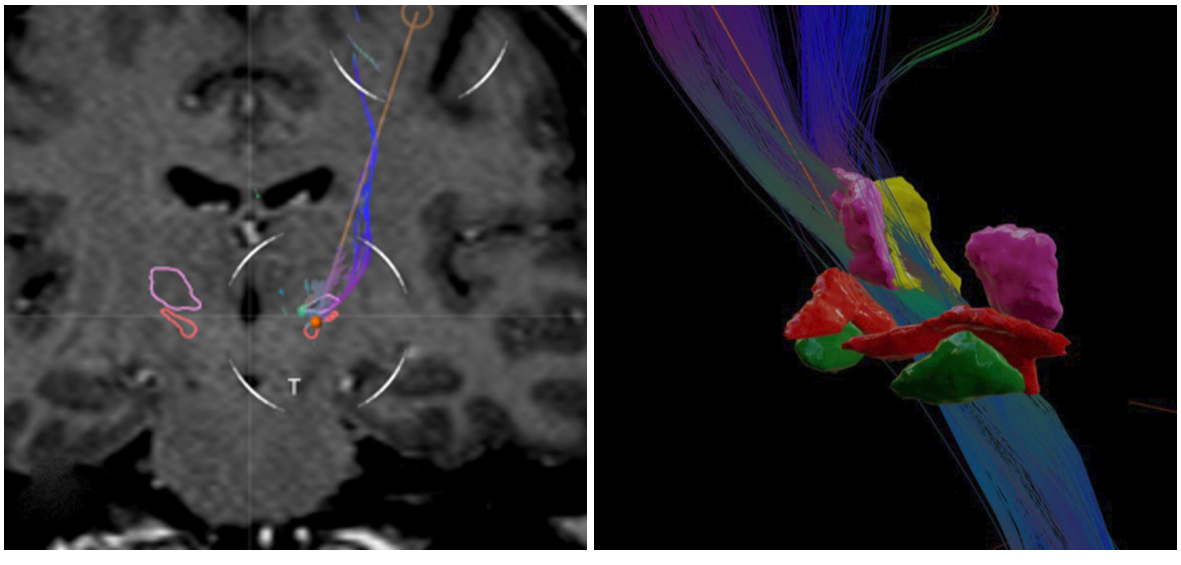

Fig. 3. Planning of the target for RF DRTT lesioning (orange line — trajectory of RF electrode insertion; purple — Vim; green — STN; red — posterior subthalamic area; blue-lilac — DRTT): A — coronal projection; B — 3D reconstruction of the subcortical nuclei and DRTT

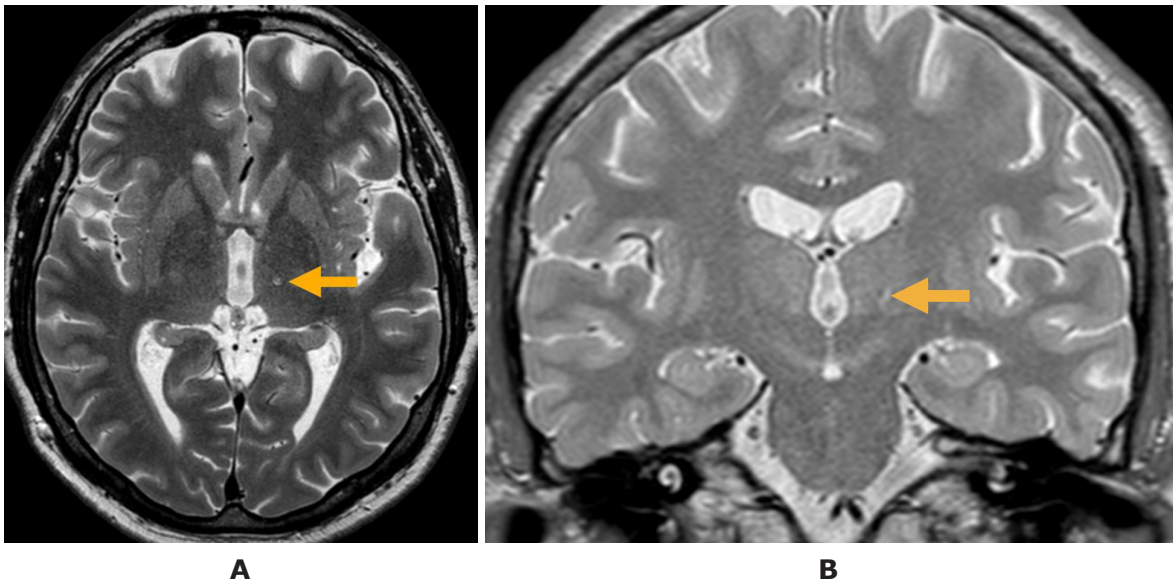

Fig. 4. Lesioning zone 12 months after DRTT tractotomy: A — axial projection; B — coronal projection

Discussion

Despite the dominance of neurostimulation technologies, ablative procedures continue to play a significant role in the surgical treatment of PD and certain other movement disorders. Alongside RF lesioning, novel ablative technologies have become widely adopted, particularly MRI-guided focused ultrasound ablation and Gamma Knife radiosurgical lesioning [7, 19–21].

The advantages of ablative procedures include the relative technical simplicity and short duration of neurosurgical intervention, high efficacy, a low rate of surgical complications, prevention of complications associated with implantation of deep brain stimulation systems, and the absence of a need for regular follow-up visits for adjustment of stimulation parameters.

In recent years, a renaissance of destructive stereotactic procedures has been observed, including both unilateral and staged bilateral interventions. Modern neuroimaging technologies and computer-assisted software enable highly detailed visualization of brain structures targeted during surgery and allow precise determination of their coordinates, thereby improving both the efficacy and safety of surgical procedures [7, 22].

The introduction of tractotomy represents a novel step in the treatment of PD as a systemic neurodegenerative disorder of the brain associated with dysfunction of neurotransmitter systems. Tractotomy does not target the affected anatomical brain structures themselves but rather the pathways responsible for neuronal impulse transmission, thereby enabling modulation of impaired neurotransmitter connections. Modern high-field MRI systems allow identification of tracts involved in the pathogenesis of PD and determination of the optimal sites for effective lesioning.

The present study reports the results of surgical treatment in 25 patients with PD who were divided into two groups. The Vim group underwent conventional RF thermothalamotomy, whereas the DRTT group underwent stereotactic RF tractotomy.

Comparison of surgical outcomes between the groups demonstrated more pronounced tremor control in the DRTT group, which contributed to increased daily activity of the patients. Regression of tremor and rigidity, reduction in levodopa dosage, and moderate improvement in bradykinesia resulted in enhanced motor activity, improved self-care capacity, and better quality of life in nearly all operated patients.

A limitation of the study is the small sample size of patients who underwent surgical intervention with tractography-assisted targeting. With an increase in sample size, the difference may exceed 0.05%.

The principal feature of interventions targeting the Vim nucleus is the possibility of achieving tremor control even in cases of suboptimal electrode placement by increasing either the stimulation amplitude or the lesion volume, which was observed in all operated patients. However, enlargement of the lesion volume increases the risk of sensory disturbances, gait and coordination disorders, speech impairment, and contralateral hemiparesis due to injury to the internal capsule ("capsular effect") and the ventral caudal nucleus of the thalamus. In our study, these adverse effects were transient and regressed within 12 months after surgery. Only two patients from the group operated on using the indirect targeting method exhibited new neurological deficits one year after surgery. In one case, the patient reported paresthesia in the treated arm, whereas another patient experienced numbness of the fingers and hand on the treated side. Such outcomes were absent in the tractography-assisted group. These findings are consistent with previously published data [18, 22].

MRI tractography continues to evolve toward more precise visualization of the DRTT in surgical treatment of PD. Currently, there is no consensus regarding the optimal definition of the region of interest (ROI) for tract reconstruction. The DRTT should not be considered a single continuous nerve fiber, as it contains numerous branches. In our study, the ipsilateral cerebellar nucleus, contralateral thalamic nuclei, and contralateral precentral gyrus were used as ROIs.

However, alternative approaches to DRTT reconstruction exist and differ in ROI selection. Given that a portion of DRTT fibers does not decussate, some protocols consider ROI determination within a single hemisphere to be sufficient. An important anatomical landmark is the tract's passage through the superior cerebellar peduncle, which is sometimes included in the ROI to improve reconstruction specificity. Furthermore, the topographic proximity of the DRTT to the *lemniscus medialis*, which has a relatively stable anatomical location, may serve as an additional landmark for verification of tractography accuracy [22, 23].

Another important issue concerns the technical aspects of tractography. The principal objective of neuroimaging analysis is determination of the vector of electrical impulse conduction through the white matter within each voxel [24, 25].

Probabilistic tractography methods make it possible to estimate the most likely pathways of nerve fiber propagation while accounting for uncertainty in diffusion direction within each voxel, thereby improving the accuracy of reconstruction of complex and crossing tracts. However, such methods require specialized equipment and substantial computational time and therefore remain limited primarily to research centers. Currently available commercial deterministic methods are based on the "average" direction of conduction within each segment. This tractography approach allows sufficiently accurate identification of the target tract. Published studies have demonstrated that deterministic methods produce an average error of up to 1.4 mm. Although substantial, this level of error remains acceptable for planning stereotactic interventions. Some authors recommend using not only target localization but also the three-dimensional orientation of the tract for planning the surgical trajectory [26, 27].

In recent years, numerous clinical studies have been published regarding the use of deterministic DRTT tractotomy of various modalities for surgical treatment of tremor using RF lesioning and high-intensity focused ultrasound ablation. The high efficacy of tractotomy in tremor management has provided the rationale for applying these methods to control other motor manifestations of PD. Ongoing investigations are evaluating the role of the pallidothalamic tract as a principal pathogenetic pathway underlying rigidity and the phenomenon of freezing of gait. In particular, studies

are being conducted to determine the projection of the pallidothalamic tract within the subthalamic region. Indirect calculations of this target are characterized by considerable variability; therefore, tractographic analysis represents a promising direction for future interventions [28].

Another important area of research concerns the "hyperdirect" neuronal connection between the STN and the premotor cortex. It is known that the STN contains segments responsible for connections with other basal ganglia structures of the cerebral cortex. These pathways are associated not only with motor but also with cognitive and emotional states in patients with PD [8]. The hyperdirect pathway can currently be influenced only by neuromodulation technologies, particularly deep brain stimulation, because destructive interventions are associated with a high risk of neurological complications.

Special consideration should also be given to the potential role of several axial fiber pathways associated with bradykinesia and postural instability in patients with PD. Current investigations focus on corticothalamic tracts and fibers connecting the pedunculopontine nucleus (PPN) with the brainstem. The effects of interventions targeting these tracts remain insufficiently studied.

Conclusions

An advanced understanding of PD pathogenesis as a disorder of neuronal connectivity is transforming therapeutic approaches to the disease. Contemporary neurosurgical methods do not directly target pathologically altered structures but instead modulate neuronal circuits involved in the development of motor dysfunction. MRI tractography of these pathways, particularly the dentato-rubro-thalamic tract, enables selective and effective compensation of pathological activity through both lesioning and neuromodulation while minimizing effects on adjacent neural structures. Application of this method ensures high procedural efficacy while accounting for individual anatomical variability in target selection for surgery.

Disclosure

Conflict of interest

The authors declare no conflict of interest.

Funding

The study received no external financial support.

Use of Artificial intelligence

No artificial intelligence systems were used during the preparation of this article.

References

1. Krauss JK, Lipsman N, Aziz T, Boutet A, Brown P, Chang JW, Davidson B, Grill WM, Hariz MI, Horn A, Schulder M, Mammis A, Tass PA, Volkmann J, Lozano AM. Technology of deep brain stimulation: current status and future directions. Nat Rev Neurol. 2021 Feb;17(2):75-87. doi: 10.1038/s41582-020-00426-z
2. Hariz M, Blomstedt P. Deep brain stimulation for Parkinson's disease. J Intern Med. 2022 Nov;292(5):764-778. doi: 10.1111/joim.13541
3. Higuchi Y, Matsuda S, Serizawa T. Gamma knife radiosurgery in movement disorders: Indications and limitations. Mov Disord. 2017 Jan;32(1):28-35. doi: 10.1002/mds.26625
4. Taira T, Horisawa S, Takeda N, Ghate P. Stereotactic Radiofrequency Lesioning for Movement Disorders. Prog Neurol Surg. 2018;33:107-119. doi: 10.1159/000481079
5. Fukutome K, Hirabayashi H, Osakada Y, Kuga Y, Ohnishi H. Bilateral Magnetic Resonance Imaging-Guided Focused Ultrasound Thalamotomy for Essential Tremor. Stereotact Funct Neurosurg. 2022;100(1):44-52. doi: 10.1159/000518662
6. Giammalva GR, Maugeri R, Umana GE, Paolini F, Bonosi L, Meccio F, Scalia G, Palmisciano P, Gerardi RM, Iacopino DG. DBS, tcMRgFUS, and gamma knife radiosurgery for the treatment of essential tremor: a systematic review on techniques, indications, and current applications. J Neurosurg Sci. 2022 Dec;66(6):476-484. doi: 10.23736/S0390-5616.22.05524-2
7. Kostiuk K. Stereotactic Staged Asymmetric Bilateral Radiofrequency Lesioning for Parkinson's Disease. Stereotact Funct Neurosurg. 2023;101(6):359-368. doi: 10.1159/000534084
8. Haynes WI, Haber SN. The organization of prefrontal-subthalamic inputs in primates provides an anatomical substrate for both functional specificity and integration: implications for Basal Ganglia models and deep brain stimulation. J Neurosci. 2013 Mar 13;33(11):4804-14. doi: 10.1523/JNEUROSCI.4674-12.2013
9. Verlaat L, Rijks N, Dilai J, Admiraal M, Beudel M, de Bie RMA, van der Zwaag W, Schuurman R, van den Munckhof P, Bot M. 7-Tesla Magnetic Resonance Imaging Scanning in Deep Brain Stimulation for Parkinson's Disease: Improving Visualization of the Dorsolateral Subthalamic Nucleus. Mov Disord Clin Pract. 2024 Apr;11(4):373-380. doi: 10.1002/mdc3.13982
10. Kremer NI, Roberts MJ, Potters WV, Dilai J, Mathiopoulou V, Rijks N, Drost G, van Laar T, van Dijk JMC, Beudel M, de Bie RMA, van den Munckhof P, Janssen MLF, Schuurman PR, Bot M. Dorsal subthalamic nucleus targeting in deep brain stimulation: microelectrode recording versus 7-Tesla connectivity. Brain Commun. 2023 Nov 11;5(6):fcad298. doi: 10.1093/braincomms/fcad298
11. Little S, Brown P. Debugging Adaptive Deep Brain Stimulation for Parkinson's Disease. Mov Disord. 2020 Apr;35(4):555-561. doi: 10.1002/mds.27996
12. Wang S, Zhu G, Shi L, Zhang C, Wu B, Yang A, Meng F, Jiang Y, Zhang J. Closed-Loop Adaptive Deep Brain Stimulation in Parkinson's Disease: Procedures to Achieve It and Future Perspectives. J Parkinsons Dis. 2023;13(4):453-471. doi: 10.3233/JPD-225053
13. Ramanathan PV, Salas-Vega S, Shenai MB. Directional Deep Brain Stimulation-A Step in the Right Direction? A Systematic Review of the Clinical and Therapeutic Efficacy of Directional Deep Brain Stimulation in Parkinson Disease. World Neurosurg. 2023 Feb;170:54-63.e1. doi: 10.1016/j.wneu.2022.11.085
14. Rajamani N, Friedrich H, Butenko K, Dembek T, Lange F, Navrátil P, Zvarova P, Hollunder B, de Bie RMA, Odekerken VJJ, Volkmann J, Xu X, Ling Z, Yao C, Ritter P, Neumann WJ, Skandalakis GP, Komaitis S, Kalyvas A, Koutsarnakis C, Stranjalis G, Barbe M, Milanese V, Fox MD, Kühn AA, Middlebrooks E, Li N, Reich M, Neudorfer C, Horn A. Deep brain stimulation of symptom-specific networks in Parkinson's disease. Nat Commun. 2024 May 31;15(1):4662. doi: 10.1038/s41467-024-48731-1
15. Coenen VA, Allert N, Paus S, Kronenbürger M, Urbach H, Mädler B. Modulation of the cerebello-thalamo-cortical network in thalamic deep brain stimulation for tremor: a diffusion tensor imaging study. Neurosurgery. 2014 Dec;75(6):657-69; discussion 669-70. doi: 10.1227/NEU.0000000000000540
16. Fahn S, Tolosa E, Marin C. Clinical rating scale for tremor. In: Jankovic J, Tolosa E, editors. Parkinson's disease and movement disorders. Baltimore–Munich: Urban & Schwarzenberg; 1988. p. 225–234.
17. Goetz CG, Tilley BC, Shaftman SR, Stebbins GT, Fahn S, Martinez-Martin P, Poewe W, Sampaio C, Stern MB, Dodel R, Dubois B, Holloway R, Jankovic J, Kulisevsky J, Lang AE, Lees A, Leurgans S, LeWitt PA, Nyenhuis D, Olanow CW, Rascol O, Schrag A, Teresi JA, van Hilten JJ, LaPelle N; Movement Disorder Society UPDRS Revision Task Force. Movement Disorder Society-sponsored revision of the Unified Parkinson's Disease Rating Scale (MDS-UPDRS): scale presentation and clinimetric testing results. Mov Disord. 2008 Nov 15;23(15):2129-70. doi: 10.1002/

mds.22340
18. Sammartino F, Krishna V, King NK, Lozano AM, Schwartz ML, Huang Y, Hodaie M. Tractography-Based Ventral Intermediate Nucleus Targeting: Novel Methodology and Intraoperative Validation. Mov Disord. 2016 Aug;31(8):1217-25. doi: 10.1002/mds.26633
19. Rodriguez-Oroz MC, Martínez-Fernández R, Lipsman N, Horisawa S, Moro E. Bilateral Lesions in Parkinson's Disease: Gaps and Controversies. Mov Disord. 2025 Feb;40(2):231-240. doi: 10.1002/mds.30090
20. Chintapalli R, Chang S, Kaprealian T, Savjani R, Tenn S, Bari A. Gamma knife versus linear accelerator thalamotomy for essential tremor and Parkinson's disease: A systematic review and meta-analysis. J Clin Neurosci. 2025 Mar;133:111050. doi: 10.1016/j.jocn.2025.111050
21. Paschen S, Natera-Villalba E, Pineda-Pardo JA, Del Álamo M, Rodríguez-Rojas R, Hensler J, Deuschl G, Obeso JA, Helmers AK, Martínez-Fernández R. Comparative Study of Focused Ultrasound Unilateral Thalamotomy and Subthalamotomy for Medication-Refractory Parkinson's Disease Tremor. Mov Disord. 2025 May;40(5):823-833. doi: 10.1002/mds.30159
22. Ranjan M, Elias GJB, Boutet A, Zhong J, Chu P, Germann J, Devenyi GA, Chakravarty MM, Fasano A, Hynynen K, Lipsman N, Hamani C, Kucharczyk W, Schwartz ML, Lozano AM, Hodaie M. Tractography-based targeting of the ventral intermediate nucleus: accuracy and clinical utility in MRgFUS thalamotomy. J Neurosurg. 2019 Sep 27;133(4):1002-1009. doi: 10.3171/2019.6.JNS19612
23. Muller J, Alizadeh M, Matias CM, Thalheimer S, Romo V, Martello J, Liang TW, Mohamed FB, Wu C. Use of probabilistic tractography to provide reliable distinction of the motor and sensory thalamus for prospective targeting during asleep deep brain stimulation. J Neurosurg. 2021 Oct 8;136(5):1371-1380. doi: 10.3171/2021.5.JNS21552
24. Nowacki A, Schlaier J, Debove I, Pollo C. Validation of diffusion tensor imaging tractography to visualize the dentatorubrothalamic tract for surgical planning. J Neurosurg. 2019 Jan 1;130(1):99-108. doi: 10.3171/2017.9.JNS171321
25. Coenen VA, Allert N, Mädler B. A role of diffusion tensor imaging fiber tracking in deep brain stimulation surgery: DBS of the dentato-rubro-thalamic tract (drt) for the treatment of therapy-refractory tremor. Acta Neurochir (Wien). 2011 Aug;153(8):1579-85; discussion 1585. doi: 10.1007/s00701-011-1036-z
26. Tsolaki E, Kashanian A, Chiu K, Bari A, Pouratian N. Connectivity-based segmentation of the thalamic motor region for deep brain stimulation in essential tremor: A comparison of deterministic and probabilistic tractography. Neuroimage Clin. 2024;41:103587. doi: 10.1016/j.nicl.2024.103587
27. Rodrigues NB, Mithani K, Meng Y, Lipsman N, Hamani C. The Emerging Role of Tractography in Deep Brain Stimulation: Basic Principles and Current Applications. Brain Sci. 2018 Jan 29;8(2):23. doi: 10.3390/brainsci8020023
28. Magara A, Bühler R, Moser D, Kowalski M, Pourtehrani P, Jeanmonod D. First experience with MR-guided focused ultrasound in the treatment of Parkinson's disease. J Ther Ultrasound. 2014 May 31;2:11. doi: 10.1186/2050-5736-2-11
29. Hassler R, Riechert T. Indications and localization of stereotactic brain operations. Confin Neurol. 1954;14:1–15.

Original article

Ukrainian Neurosurgical Journal. 2026;32(2):73-79
doi: 10.25305/unj.352621

Side-specific and sex-related computed tomography morphometric variations of the atlas (C1) and axis (C2) in Vietnamese adults: Implications for safe posterior atlantoaxial fixation

Loi Nguyen Dang [1], Thi Cao [1], Ly Minh Ngo [2], Khang Trien Truong [1], Thach Ngoc Nguyen [2]

[1] Department of Orthopedics and Rehabilitation, School of Medicine, University of Medicine and Pharmacy at Ho Chi Minh City, Ho Chi Minh City, Vietnam
[2] Hospital for Traumatology and Orthopaedics, Ho Chi Minh City, Vietnam

Received: 21 February 2026
Accepted: 26 March 2026

Address for correspondence:
Thi Cao, Department of Orthopedics and Rehabilitation, School of Medicine, University of Medicine and Pharmacy at Ho Chi Minh City, 217 Hong Bang street, Ward Cho Lon, 70000, Ho Chi Minh City, Vietnam, e-mail: caothibacsi@ump.edu.vn

Objective: To provide a comprehensive computed tomography (CT) morphometric analysis of the atlas (C1) and axis (C2) in Vietnamese adults, evaluate sex-related and side-specific differences, and determine the implications for posterior atlantoaxial screw fixation.

Materials and methods: A retrospective cross-sectional CT study was conducted on 150 adults (112 men and 38 women; mean age 51.9 ± 15.1 years). Multiplanar reconstruction was used to measure C1 lateral mass length (C1-LML), C1 lateral mass width (C1-LMW), maximal medial (C1-MTA), lateral (C1-LTA), cranial (C1-CTA), and caudal (C1-CdTA) trajectory angles bilaterally. C2 parameters included isthmus height (C2-IH), canal height (C2-CH), and pedicle width (C2-PW).

Results: Significant sex-related differences were observed, with men demonstrating greater right C1-LML and C1-LMW values ($p = 0.029$ and $p = 0.005$, respectively) as well as larger right C1-LTA, C1-CTA, and C1-CdTA (all $p < 0.05$). Left C2-PW was also significantly greater in men ($p = 0.020$). In addition, side-specific asymmetry was identified: C1-LTA, C1-CTA, and C1-CdTA differed significantly between sides ($p = 0.009–0.021$), and C2-CH was greater on the left ($p < 0.001$). Age showed weak negative correlations with selected C2 parameters.

Conclusions: Upper cervical morphology demonstrates measurable asymmetry and sex-related variation. Preoperative planning for C1–C2 instrumentation should therefore be individualized and side-specific.

Keywords: *atlas vertebra; axis vertebra; cervical vertebrae; tomography; computed tomography; morphometry; atlantoaxial joint; spine*

Introduction

Stabilization of the craniovertebral junction (CVJ) is frequently required in the management of traumatic instability, congenital anomalies, inflammatory conditions, and degenerative pathology affecting the atlas (C1) and axis (C2). Contemporary posterior fixation techniques — particularly the Harms C1 lateral mass–C2 pedicle construct and its modifications (Goel-Harms) — provide rigid stabilization and high fusion rates and have become widely adopted in modern spine surgery [1, 2]. Nevertheless, the success and safety of these procedures critically depend on accurate identification of safe osseous corridors and individualized screw trajectories.

Incorrect screw placement at C1 or C2 may result in catastrophic complications, including vertebral artery injury, neural compromise, or construct failure [3, 4]. The complex geometry of the C1 lateral mass and the variability of C2 pedicle morphology make atlantoaxial fixation particularly demanding. Computed tomography (CT) with multiplanar reconstruction (MPR) has therefore become indispensable in preoperative planning, allowing surgeons to quantify linear dimensions such as C1-LML and C1-LMW and angular parameters such as C1-MTA, C1-LTA, C1-CTA, and C1-CdTA, thereby tailoring screw length, diameter, and trajectory according to each patient's anatomy [5–7].

Although numerous morphometric studies have reported average C1 and C2 dimensions in different populations [6, 8, 9], less attention has been paid to clinically meaningful side-to-side asymmetry and sex-related scaling of surgical osseous corridors. In clinical practice, contralateral screw trajectories are often planned under the implicit assumption of bilateral symmetry. However, unrecognized asymmetry in parameters such as C1-LTA or C2-CH may increase the risk of cortical breach or vascular injury if mirrored trajectories are assumed, as previous morphometric studies have demonstrated frequent side-to-side variation in atlas morphology [10]. Furthermore, sex-based anatomical differences in C1-LMW or C2-PW may influence the feasibility of standard screwdiameters.

Vietnamese-specific reference data for C1–C2 morphometry remain limited. A prior Vietnamese CT study provided important baseline information for atlantoaxial screw fixation planning [5]; however, a comprehensive evaluation incorporating both linear and angular parameters, with explicit assessment of symmetry and sex differences, is still needed to support routine surgical decision-making.

The present study aimed to establish normative CT morphometric parameters of C1 and C2 in Vietnamese adults, examine sex-related differences, assess right–left symmetry, and integrate these findings into practical guidance for posterior C1 lateral mass and C2 pedicle fixation.

Materials and methods

Study design and setting

This retrospective cross-sectional study analyzed cervical CT images obtained from two tertiary referral centers in Ho Chi Minh City, Vietnam (Cho Ray Hospital and the Hospital for Traumatology and Orthopaedics) between January and May 2025. The study focused on morphometric parameters of C1 and C2 relevant to posterior atlantoaxial screw fixation.

Participants

A total of 150 Vietnamese adults were included after applying predefined inclusion and exclusion criteria. The cohort comprised 112 men (74.7%) and 38 women (25.3%). CT scans were performed for clinical indications unrelated to destructive CVJ pathology. Exclusion criteria included fractures of C1–C2, congenital malformations, tumors, infection, severe deformity, or insufficient image quality for precise measurement. Only anatomically intact upper cervical vertebrae were analyzed to establish normative morphometric reference values.

CT acquisition and image reconstruction

All CT datasets were reviewed using RadiAnt DICOM Viewer. Multiplanar reconstruction (MPR) was performed to standardize image orientation (***Fig. 1***). Sagittal, axial, and coronal planes were realigned according to the anatomical axes of C1 and C2 to ensure orthogonality and minimize measurement error. Particular attention was paid to reproducing clinically relevant screw trajectories.

Morphometric measurements

All parameters were measured bilaterally (right and left) to assess side-specific symmetry. Suffixes -R and -L indicate right and left sides, respectively. Measurements were recorded in millimeters (mm) or degrees (°) using defined anatomical landmarks corresponding to posterior fixation corridors.

For C1, linear measurements included C1 lateral mass length (C1-LML) and C1 lateral mass width (C1-LMW) on axial images (***Fig. 2***).

Angular parameters included C1 medial trajectory angle (C1-MTA) and C1 lateral trajectory angle (C1-LTA) on the axial plane, as well as C1 cranial trajectory angle (C1-CTA) and C1 caudal trajectory angle (C1-CdTA) on the sagittal plane (***Fig. 3***). These angles represent maximal safe screw trajectories within the osseous boundaries of the lateral mass.

For C2, measurements included C2 isthmus height (C2-IH) and C2 canal height (C2-CH) on sagittal reconstructions, as well as C2 pedicle width (C2-PW), defined as the narrowest mediolateral osseous corridor on axial images (***Fig. 4***). These parameters directly reflect the feasibility of pedicle or pars screw placement.

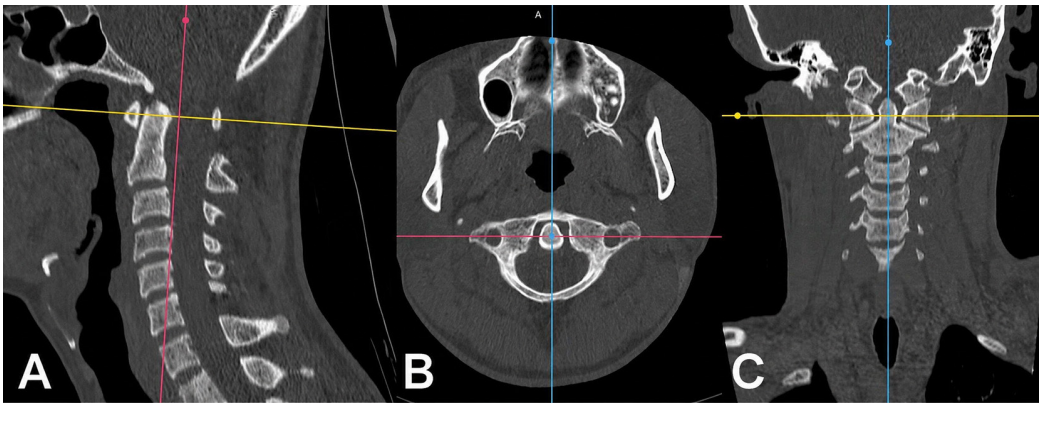

Fig. 1. Standardized MPR alignment of C1–C2. A - Sagittal plane aligned along the anatomical axis of the upper cervical spine; B - Axial plane orthogonal to the C1 lateral mass; C - Coronal plane adjusted to ensure symmetric bilateral orientation

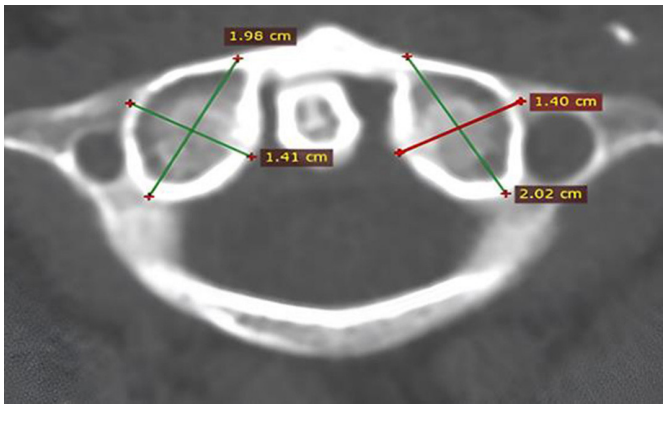

Fig. 2. Axial CT measurement of C1 lateral mass dimensions.

Notes: Green lines indicate C1 lateral mass length (C1-LML); Red lines indicate C1 lateral mass width (C1-LMW). Measurements were performed bilaterally.

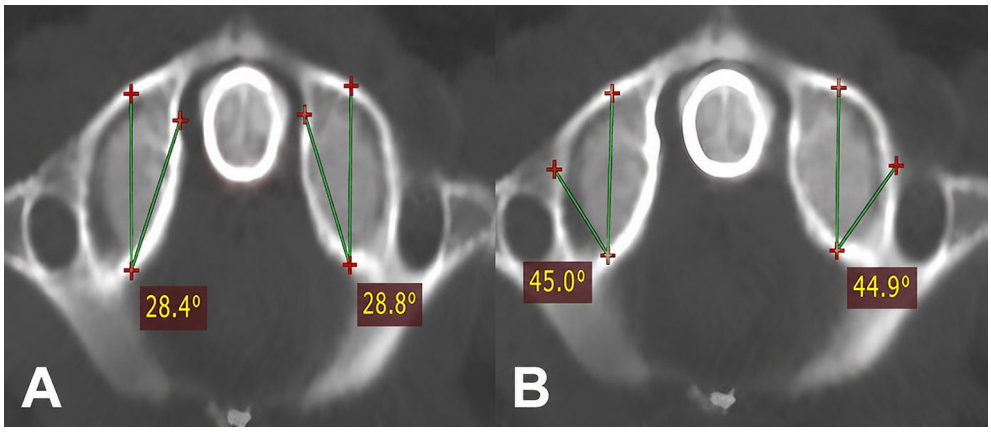

Fig. 3. Axial CT measurement of C1 trajectory angles. A - C1 lateral trajectory angle (C1-LTA); B - C1 medial trajectory angle (C1-MTA)

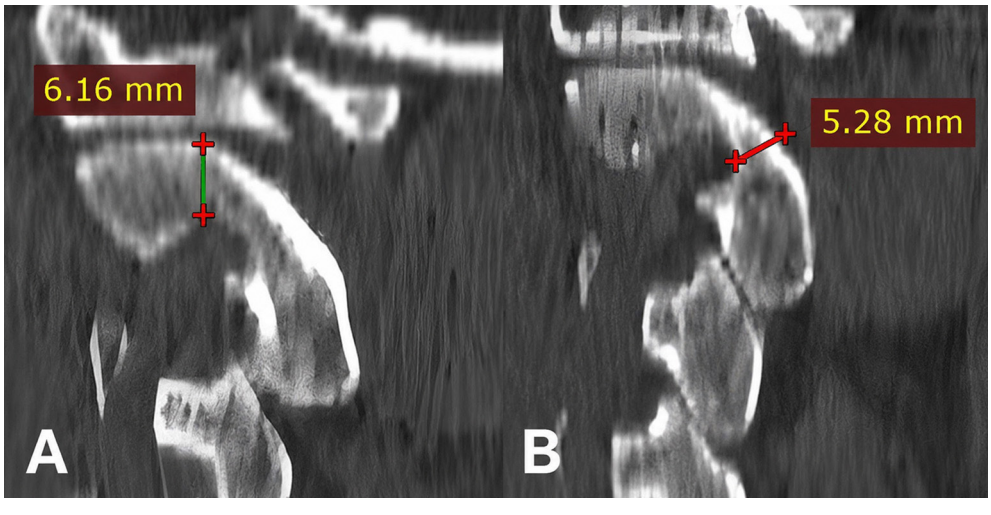

Fig. 4. Sagittal CT measurement of C2 morphometric parameters. A - C2 canal height (C2-CH); B - C2 isthmus height (C2-IH)

Statistical analysis

Continuous variables are presented as mean ± standard deviation (Mean ± SD) and range. Sex-related differences were analyzed using independent-samples t-tests. Right–left comparisons were performed using paired analyses to assess asymmetry. Correlations with age were evaluated using Pearson's correlation coefficient (r). Statistical significance was defined as $p < 0.05$. Statistical analyses were conducted using SPSS version 22.0.

Results

Demographics. The study included 150 participants (112 men and 38 women) with a mean age of 51.9 ± 15.1 years (***Table 1***).

C1 morphometry and sex differences. Men demonstrated larger C1 lateral mass dimensions, particularly on the right side. Right C1 lateral mass length (C1-LML-R) was 21.04 ± 1.70 mm in men and 20.31 ± 1.37 mm in women ($p = 0.029$), whereas right C1 lateral mass width (C1-LMW-R) was 14.00 ± 1.08 mm versus 13.42 ± 0.95 mm ($p = 0.005$). Trajectory angles showed selective sex-related differences, with greater right C1 lateral (C1-LTA-R), cranial (C1-CTA-R), and caudal (C1-CdTA-R) angles in men. In contrast, medial trajectory angles and several left-sided parameters did not differ significantly between sexes (***Table 2***).

C2 morphometry and sex differences. Among C2 parameters, only left C2 pedicle width (C2-PW-L) was significantly larger in men than in women (5.15 ± 0.89 mm vs 4.65 ± 0.79 mm, $p = 0.020$). C2 isthmus height (C2-IH) and C2 canal height (C2-CH) did not differ significantly by sex (***Table 3***).

Side-to-side comparisons. For C1, lateral mass length (C1-LML) and width (C1-LMW) were largely symmetric between sides ($p = 0.078$ and $p = 0.768$, respectively). In contrast, the C1 lateral trajectory angle (C1-LTA), cranial trajectory angle (C1-CTA), and caudal trajectory angle (C1-CdTA) demonstrated significant asymmetry. For C2, canal height was significantly greater on the left, whereas isthmus height and pedicle width did not differ significantly between sides (***Table 4***).

Age-related correlations. Age demonstrated weak negative correlations with left C2 canal height (C2-CH-L; $r = -0.17$, $p = 0.033$) and right C2 pedicle width (C2-PW-R; $r = -0.19$, $p = 0.022$). No significant correlations were observed for C1 parameters.

Table 1. Demographic Characteristics of the Study Cohort

Group	Age (Mean ± SD)	Range (years)	n
All participants	51.9 ± 15.1	18–88	150
Men	51.5 ± 14.3	18–77	112
Women	53.3 ± 17.3	18–88	38

Table 2. C1 Morphometric Parameters by Sex (Mean ± SD)

Parameter	Men	Women	p-value
C1-LML-R (mm)	21.04 ± 1.70	20.31 ± 1.37	0.029
C1-LML-L (mm)	20.67 ± 1.60	20.16 ± 1.30	0.071
C1-LMW-R (mm)	14.00 ± 1.08	13.42 ± 0.95	0.005
C1-LMW-L (mm)	13.96 ± 1.20	13.33 ± 1.00	0.009
C1-MTA-R (°)	44.67 ± 3.70	44.48 ± 4.00	0.768
C1-MTA-L (°)	44.75 ± 3.60	44.40 ± 3.90	0.624
C1-LTA-R (°)	22.52 ± 2.18	21.79 ± 2.13	0.023
C1-LTA-L (°)	21.96 ± 2.10	21.32 ± 2.00	0.070
C1-CTA-R (°)	42.65 ± 3.43	41.63 ± 3.06	0.047
C1-CTA-L (°)	41.61 ± 3.30	41.02 ± 3.00	0.291
C1-CdTA-R (°)	25.52 ± 4.50	24.50 ± 3.20	0.042
C1-CdTA-L (°)	24.24 ± 3.80	23.87 ± 3.10	0.577

Table 3. C2 Morphometric Parameters by Sex (Mean ± SD)

Parameter	Men	Women	p-value
C2-Isthmus Height-R (mm)	5.04 ± 0.87	4.80 ± 0.81	0.132
C2-Isthmus Height-L (mm)	4.92 ± 0.85	4.52 ± 0.79	0.075
C2-Canal Height-R (mm)	6.73 ± 1.06	6.52 ± 0.98	0.483
C2-Canal Height-L (mm)	7.46 ± 1.22	7.14 ± 1.10	0.345
C2-Pedicle Width-R (mm)	4.91 ± 0.88	4.74 ± 0.80	0.228
C2-Pedicle Width-L (mm)	5.15 ± 0.89	4.65 ± 0.79	0.020

Table 4. Side-to-Side Comparison of C1 and C2 Parameters (Paired Analysis, *n* = 150)

Parameter	Right (Mean ± SD)	Left (Mean ± SD)	Mean Difference (R–L)	p-value
C1-LML (mm)	20.90 ± 1.60	20.56 ± 1.50	0.34	0.078
C1-LMW (mm)	13.91 ± 1.10	13.87 ± 1.05	0.04	0.768
C1-LTA (°)	22.38 ± 2.18	21.85 ± 2.13	0.53	0.009
C1-MTA (°)	44.51 ± 3.60	44.60 ± 3.55	-0.09	0.835
C1-CTA (°)	42.50 ± 3.40	41.54 ± 3.20	0.96	0.014
C1-CdTA (°)	25.27 ± 4.40	24.21 ± 3.60	1.06	0.021
C2-Isthmus Height (mm)	4.98 ± 0.86	4.79 ± 0.82	0.19	0.072
C2-Canal Height (mm)	6.71 ± 1.06	7.42 ± 1.22	-0.71	<0.001
C2-Pedicle Width (mm)	4.86 ± 0.87	5.04 ± 0.89	-0.18	0.074

Discussion

This CT-based morphometric study provides detailed normative data on C1 and C2 anatomy in Vietnamese adults and, importantly, frames these measurements within the context of surgical decision-making for posterior atlantoaxial fixation. Three principal observations merit emphasis: (1) measurable sex-related differences in selected C1 dimensions and trajectory angles; (2) clinically relevant side-to-side asymmetry, particularly in C1 angular parameters and C2 canal height; and (3) modest age-related changes in selected C2 corridors.

C1 lateral mass dimensions and trajectory angles: implications for surgical planning

Posterior C1 lateral mass screw fixation, as popularized by Harms and colleagues and further refined in the Goel–Harms technique, depends on sufficient lateral mass dimensions and safe trajectory corridors [1,2]. The mean C1 lateral mass length (C1-LML) and width (C1-LMW) observed in our cohort are broadly consistent with previously reported CT-based and cadaveric morphometric data from other populations [6,7]. These findings support the feasibility of standard 3.5-mm lateral mass screws in most adults. However, the statistically significant sex-related differences—particularly in right-sided C1-LML and C1-LMW—highlight the importance of individualized preoperative assessment rather than reliance on population averages [11].

More importantly, our systematic evaluation of maximal trajectory angles (C1-LTA, C1-CTA, C1-CdTA) extends prior Vietnamese data [5] by incorporating both axial and sagittal angulation limits. These angular parameters define the safe osseous corridor that avoids medial breach into the spinal canal and lateral violation of the vertebral artery groove [6]. The observed asymmetry in C1-LTA, C1-CTA, and C1-CdTA between right and left sides suggests that assuming mirrored screw trajectories may be unsafe in certain patients. In practical terms, a trajectory determined on one side should not automatically be replicated contralaterally without CT-based verification [8]. This finding reinforces prior recommendations that meticulous side-specific preoperative CT planning is essential for Harms-type constructs and over-the-arch techniques [1, 2, 12].

Sex-related scaling and implant selection

Sex-related scaling of vertebral dimensions has been described in morphometric studies of the atlas and axis in multiple populations [9, 13]. In our cohort, women demonstrated smaller C1 lateral mass dimensions and narrower C2 pedicle width (C2-PW) on the left side. Although many parameters did not differ significantly by sex, the presence of several statistically significant differences—particularly in linear dimensions relevant to screw purchase—supports the principle that implant selection should be individualized.

From a surgical perspective, smaller lateral mass width or pedicle width may influence the choice of screw diameter and length, particularly in borderline corridors. In such cases, intraoperative caution, smaller-diameter screws, or alternative fixation strategies (e.g., laminar screws or pars screws) may be considered. The concept that "one-size-fits-all" instrumentation is inappropriate in CVJ surgery is therefore supported by our data [3, 14].

C2 pedicle and canal morphology: asymmetry and vascular risk considerations

The C2 pedicle represents a critical yet potentially hazardous corridor for pedicle or transarticular screw placement, as multiple fixation techniques exist and their feasibility depends on pedicle dimensions and vertebral artery anatomy [14]. Vertebral artery injury remains one of the most feared complications of atlantoaxial instrumentation [3,4]. Lee *et al*. [12] further emphasized that reduced posterior arch height combined with narrow lateral mass dimensions may significantly limit safe screw insertion corridors and necessitate alternative techniques. Previous studies have demonstrated that pedicle size and the presence of a high-riding vertebral artery significantly influence the feasibility of safe screw insertion [8,15]. In our study, left C2-PW was smaller in women, highlighting a subgroup in whom standard pedicle screw placement may warrant heightened scrutiny.

Additionally, the significant side-to-side asymmetry observed in C2 canal height (C2-CH) further challenges assumptions of bilateral equivalence. Although canal height is not synonymous with pedicle width, it reflects posterior element morphology and may influence both screw angulation and the margin of safety relative to the spinal canal. These findings collectively emphasize that contralateral symmetry should not be presumed when planning C2 instrumentation [8, 14].

Age-related trends

We observed weak inverse correlations between age and selected C2 parameters. While modest in magnitude, these associations are directionally consistent with age-related osseous remodeling and potential reduction in cortical thickness. Clinically, age alone should not be used as a surrogate for corridor safety. Rather, advancing age should prompt greater attention to individualized CT-based evaluation and consideration of bone quality in fixation planning.

Population-specific context

These findings should be interpreted within the context of prior Vietnamese CT-based morphometric research. A previous study provided valuable baseline data for atlantoaxial screw planning in Vietnamese patients [5]. The present study expends upon those observations incorporating systematic bilateral comparison, detailed evaluation of maximal trajectory angles on both axial and sagittal planes, and explicit assessment of sex-related differences. By integrating side-to-side asymmetry and trajectory limits into a surgical decision-making framework, this study moves beyond feasibility metrics alone and emphasizes individualized, side-specific planning for posterior C1–C2 fixation.

Strengths and limitations

The strengths of this study include a relatively large single-region sample and the use of standardized multiplanar reconstruction alignment, which enhanced measurement reliability. The bilateral assessment of both linear and angular parameters allowed explicit evaluation

of asymmetry, a feature less frequently emphasized in prior morphometric studies [5, 6].

Limitations include the retrospective design and the absence of CT angiography to directly evaluate vertebral artery anatomy. Accordingly, our analysis characterizes osseous corridors rather than vascular variations. Future investigations integrating morphometry with vascular imaging and correlating these measurements with operative outcomes would further refine thresholds criteria for selecting specific fixation techniques.

Clinical integration

Overall, the normative values presented here can serve as a practical reference for posterior C1 lateral mass and C2 pedicle instrumentation in Vietnamese adults. More importantly, our findings reinforce two key surgical principles: (1) screw planning should be side-specific rather than mirrored, and (2) implant selection should account for sex-related anatomical scaling. These considerations are central to safe and reproducible CVJ stabilization.

Conclusion

This CT-based morphometric analysis demonstrates that upper cervical anatomy in Vietnamese adults is not strictly symmetric, particularly with respect to trajectory angles, and exhibits measurable sex-related variation in parameters directly relevant to posterior atlantoaxial fixation. Significant differences in C1 trajectory angles and selected C2 corridors indicate that bilateral "mirror" assumptions may be inappropriate in operative planning. Moreover, sex-related scaling of lateral mass and pedicle dimensions may influence implant selection and trajectory design in borderline cases. These findings support a surgical strategy centered on individualized, side-specific CT assessment rather than reliance on averaged anatomical values. Incorporating detailed morphometric evaluation into routine preoperative planning may enhance the safety and precision of posterior C1–C2 instrumentation.

Acknowledgments

The authors express their gratitude to the departments of radiology and orthopedic at Cho Ray Hospital and Ho Chi Minh City Orthopedics and Traumatology Hospital for their assistance in data collection and imaging review.

Disclosure

Funding

None.

Conflicts of interest

The authors declare no conflicts of interest.

Ethics approval

This study was approved by the Ethics Council of the University of Medicine and Pharmacy at Ho Chi Minh City. Due to the retrospective nature of the study utilizing archived CT images without direct patient contact, the requirement for informed consent was waived by the committee.

References

1. Schulz R, Macchiavello N, Fernández E, Carredano X, Garrido O, Diaz J, Melcher RP. Harms C1-C2 instrumentation technique: anatomo-surgical guide. Spine (Phila Pa 1976). 2011 May 20;36(12):945-50. doi: 10.1097/BRS.0b013e3181e887df
2. Viezens L, Sehmisch S, Weiser L, Dreimann M, Lehmann W. Dorsale Stabilisation der Halswirbelkörper HWK1/HWK2 modifiziert nach Goel-Harms mit HWK-1-Pedikelschrauben [Dorsal stabilization of C1/C2 modified according to Goel-Harms with C1 pedicle screws]. Oper Orthop Traumatol. 2019 Aug;31(4):275-283. German. doi: 10.1007/s00064-019-0615-7
3. Yeom JS, Buchowski JM, Kim HJ, Chang BS, Lee CK, Riew KD. Risk of vertebral artery injury: comparison between C1-C2 transarticular and C2 pedicle screws. Spine J. 2013 Jul;13(7):775-85. doi: 10.1016/j.spinee.2013.04.005
4. Yoshida M, Neo M, Fujibayashi S, Nakamura T. Comparison of the anatomical risk for vertebral artery injury associated with the C2-pedicle screw and atlantoaxial transarticular screw. Spine (Phila Pa 1976). 2006 Jul 1;31(15):E513-7. doi: 10.1097/01.brs.0000224516.29747.52
5. Hung ND, Duc NM, Dung LV, Sy TV, Dung LT, Hue ND. A Computed Tomographic Study of Vietnamese C1-C2 Morphology for Atlantoaxial Crew Fixation Techniques. J Clin Imaging Sci. 2020 Oct 13;10:63. doi: 10.25259/JCIS_121_2020
6. Christensen DM, Eastlack RK, Lynch JJ, Yaszemski MJ, Currier BL. C1 anatomy and dimensions relative to lateral mass screw placement. Spine (Phila Pa 1976). 2007 Apr 15;32(8):844-8. doi: 10.1097/01.brs.0000259833.02179.c0
7. Wang MY, Samudrala S. Cadaveric morphometric analysis for atlantal lateral mass screw placement. Neurosurgery. 2004 Jun;54(6):1436-9; discussion 1439-40. doi: 10.1227/01.neu.0000124753.74864.07
8. Wajanavisit W, Lertudomphonwanit T, Fuangfa P, Chanplakorn P, Kraiwattanapong C, Jaovisidha S. Prevalence of High-Riding Vertebral Artery and Morphometry of C2 Pedicles Using a Novel Computed Tomography Reconstruction Technique. Asian Spine J. 2016 Dec;10(6):1141-1148. doi: 10.4184/asj.2016.10.6.1141
9. Şengül G, Kadıoğlu HH. Morphometric anatomy of the atlas and axis vertebrae. Turk Neurosurg. 2006;16(2):69-76. https://www.turkishneurosurgery.org.tr/Articles/Details/78
10. Pei-Feng J, Li-Ping W, Ji-Hong F, Yi-Kai L, Manas D. Morphological asymmetry of the atlas and its clinical implications. J Manipulative Physiol Ther. 2011 Sep;34(7):463-7. doi: 10.1016/j.jmpt.2011.05.003
11. Akay A, Rükşen M, Çağlı MS, Kitiş Ö, Ertürk M, Zileli M. An anatomical and radiological study for C1 lateral mass screw fixation. J Neurol Sci [Turk]. 2013;30(2):328-336. https://search.trdizin.gov.tr/tr/yayin/detay/183041/an-anatomical-and-radiological-study-for-c1-lateral-mass-screw-fixation
12. Lee HR, Lee DH, Cho JH, Hwang ES, Seok SY, Park S, Lee CS. Feasibility of lateral mass screw insertion in patients with the risky triad of C1: evaluation of the over-the-arch technique. J Neurosurg Spine. 2021 Nov 26;36(5):822-829. doi: 10.3171/2021.8.SPINE21695
13. Patel NP, Gupta DS. A morphometric study of adult human atlas vertebrae in South Gujarat population, India. Int J Res Med Sci. 2016;4(10):4380-4386. doi:

10.18203/2320-6012.ijrms20163297
14. Singh DK, Shankar D, Singh N, Singh RK, Chand VK. C2 Screw fixation techniques in atlantoaxial instability: A technical review. J Craniovertebr Junction Spine. 2022 Oct-Dec;13(4):368-377. doi: 10.4103/jcvjs.jcvjs_128_22
15. Vaněk P, Bradáč O, de Lacy P, Konopková R, Lacman J, Beneš V. Vertebral artery and osseous anomalies characteristic at the craniocervical junction diagnosed by CT and 3D CT angiography in normal Czech population: analysis of 511 consecutive patients. Neurosurg Rev. 2017 Jul;40(3):369-376. doi: 10.1007/s10143-016-0784-x

Original article

Ukrainian Neurosurgical Journal. 2026;32(2):80-92
doi: 10.25305/unj.354660

Influence of General Anesthesia and Surgical Procedure on Functional Recovery Following Rat Sciatic Nerve Transection and Repair

Oleksandr V. Bomikhov [1], Valentyn V. Yarynka [1,2], Taras I. Petriv [3], Ziia K. Melikov [4], Nana V. Voitenko [2,5], Volodymyr V. Medvediev [4], Pavel V. Belan [1,2]

[1] Department of Molecular Biophysics, O.O. Bogomolets Institute of Physiology, NAS of Ukraine, Kyiv, Ukraine
[2] Department of Biomedicine and Neuroscience, Kyiv Academic University, Kyiv, Ukraine
[3] Restorative Neurosurgery Department, Romodanov Neurosurgery Institute, Kyiv, Ukraine
[4] Department of Neurosurgery, Bogomolets National Medical University, Kyiv, Ukraine
[5] Private institution of higher education "Medical School Dobrobut Academy", Kyiv, Ukraine

Received: 18 March 2026
Accepted: 17 April 2026

Address for correspondence*: Oleksandr V. Bomikhov, Department of Molecular Biophysics, O.O. Bogomolets Institute of Physiology, 4 Academician Bogomolets St., Kyiv, 01601, Ukraine, e-mail: ol.bmv@biph.kiev.ua*

Objective. To evaluate the effects of the type of general anesthesia and surgical procedure on sensory and motor functional recovery following sciatic nerve transection with immediate neurorrhaphy in rats.

Materials and methods. The study was conducted in male Wistar rats using an experimental model of complete sciatic nerve transection followed by immediate end-to-end suture repair employing either two or four interrupted epineurial sutures. General anesthesia was induced using either inhaled isoflurane or an intraperitoneal ketamine/xylazine mixture. During the postoperative period (up to 24 weeks), thermal and mechanical sensitivity were assessed, along with motor function recovery evaluated by the Sciatic Functional Index (SFI).

Results. The type of general anesthesia significantly affected the pattern and dynamics of sensory and motor functional recovery after neurorrhaphy. Animals operated under ketamine/xylazine anesthesia demonstrated more stable and complete recovery of both sensory and motor functions, as evidenced by the absence of persistent mechanical and thermal hypoalgesia and by significant improvement in SFI values, even when the minimum number of epineurial sutures was used. In contrast, the use of inhalational isoflurane anesthesia was associated with more prolonged postoperative sensory deficits, which were largely dependent on the surgical procedure. Under isoflurane anesthesia, the application of four epineurial sutures provided more favorable conditions for sensory recovery, particularly mechanical sensitivity, compared with neurorrhaphy performed using two sutures.

Conclusions. The type of general anesthesia and the characteristics of the suture repair technique are important determinants of sciatic nerve regeneration and functional recovery following transection. Ketamine/xylazine anesthesia is associated with more favorable conditions for sensorimotor recovery. The use of inhalational isoflurane anesthesia during neurorrhaphy, particularly when a minimal number of sutures is employed, should be approached with caution, as it may adversely affect the stability and functional outcomes of sciatic nerve recovery.

Keywords: *peripheral neuropathy; neurorrhaphy; peripheral nerve regeneration; isoflurane; ketamine; sciatic nerve; Hargreaves test; von Frey test; Sciatic Functional Index.*

Introduction

Peripheral nerve injury (PNI) is a relatively uncommon pathology during peacetime [1–8]; however, its incidence increases during military conflicts [9] due to the predominance of combat-related limb injuries [4, 6]. Although PNI is generally considered the least severe form of injury affecting the nervous system, it is characterized by persistent sensorimotor, trophic, and pain-related disorders [10–12], resulting in substantial direct [3, 13] and indirect economic losses. PNI predominantly affects working-age adults and occurs more frequently in men [1–3, 5]. Treatment is predominantly surgical [2, 8] and primarily involves restoration of the anatomical continuity of the injured nerve through direct suturing of its severed ends, i.e., neurorrhaphy [2, 14].

Despite the relatively high regenerative capacity of the peripheral nervous system and significant advances in surgical techniques for PNI management, treatment outcomes remain suboptimal [15]. The development of novel therapeutic approaches for PNI is therefore largely conducted in experimental settings [7, 16]. For obvious reasons, such research critically depends on the quality and reproducibility of experimental injury models. Despite its relative simplicity, the widely used rat sciatic nerve transection model in experimental neurosurgery is characterized by limited reproducibility of outcomes [17]. This limitation may be related to shortcomings of the functional–anatomical assessment method based on the sciatic functional index (SFI), differences in the duration of postoperative observation of experimental

animals [17], variations in neurorrhaphy techniques, and differences in anesthetic management.

General anesthesia is an essential component of surgical procedures in experimental medicine and biology, ensuring the reduction of pain and distress in laboratory animals. This requirement has stimulated the development of noninvasive anesthetic techniques, particularly inhalational anesthesia [18]. Additional advantages of these methods include rapid induction and recovery, as well as the ability to control the depth of anesthesia during surgery [18]. However, following inhalational anesthesia, the rapid restoration of motor activity in animals subjected to PNI modeling and immediate nerve repair may compromise the integrity of the neurorrhaphy. Furthermore, early mobilization has been shown to impair nerve regeneration even when suture integrity is maintained [19]. Consequently, postoperative immobilization of the affected limb is routinely employed in clinical practice following peripheral nerve repair [20]. Another important strategy for enhancing the reliability of nerve coaptation is the application of an adequate number of epineurial or perineural interrupted sutures. Nevertheless, increasing the number of sutures has limitations, as the persistence of xenogeneic suture material may trigger local inflammatory responses that restrict and slow the regenerative growth of nerve fibers [21].

Objective: To evaluate the effects of the type of general anesthesia and surgical procedure on the recovery of sensory and motor functions following rat sciatic nerve transection with immediate neurorrhaphy.

Materials and methods

Experimental animals and experimental groups

The study was conducted in accordance with current bioethical standards and research ethics guidelines and was approved by the Biomedical Ethics Committee of the O.O. Bogomolets Institute of Physiology, NAS of Ukraine (Protocol No. 3/22, November 16, 2022). All experimental procedures complied with the provisions of the Convention on Human Rights and Biomedicine (Council of Europe, 1997), the European Convention for the Protection of Vertebrate Animals Used for Experimental and Other Scientific Purposes (Strasbourg, 1986), the General Ethical Principles for Scientific Research adopted by the First National Congress on Bioethics of Ukraine (September 2001), and the Law of Ukraine No. 3447-IV "On the Protection of Animals from Cruelty" (2006).

Male Wistar rats aged 1.5–2.0 months and weighing 190–230 g were obtained from the animal facility of the O.O. Bogomolets Institute of Physiology, National Academy of Sciences of Ukraine. Animals were housed under standard laboratory conditions with a 12-h light/dark cycle, an ambient temperature of (22 ± 2) °C, and ad libitum access to food and water.

Animals were allocated into three experimental groups according to the type of general anesthesia (inhalational isoflurane or intraperitoneal ketamine/xylazine) and the number of sutures used during surgical modeling of peripheral nerve injury (PNI) with neurorrhaphy:

Group 1 — sciatic nerve transection under isoflurane anesthesia followed by immediate nerve reconstruction using two epineurial sutures (n = 6);

Group 2 — sciatic nerve transection under ketamine/xylazine anesthesia followed by immediate nerve reconstruction using two epineurial sutures (n = 5);

Group 3 — sciatic nerve transection under isoflurane anesthesia followed by immediate nerve reconstruction using four epineurial sutures (n = 6).

Sciatic nerve injury modeling and repair

In animals of Groups 1 and 3, general anesthesia was induced and maintained with inhalational isoflurane using an anesthesia machine manufactured by "RWD Life Science", China. Anesthesia induction was performed in an induction chamber with 3% isoflurane. After achieving a surgical plane of anesthesia, the animal was transferred to a heated surgical table and fitted with a specialized face mask through which isoflurane was delivered at a concentration of 1.5–2.5%, with continuous monitoring of respiration.

In animals of Group 2, general anesthesia was induced by intraperitoneal administration of a mixture of xylazine hydrochloride (15 mg/kg; "Biowet", Poland) and ketamine hydrochloride (75 mg/kg; "Farmak", Ukraine). Drug doses were individually calculated for each animal.

In both anesthetic protocols, anesthetic depth was assessed by response to hind paw pinch, whereas the degree of muscle relaxation was evaluated manually and by visual inspection. In cases of insufficient anesthesia or muscle relaxation, the duration of induction with 3% isoflurane was extended, or an additional dose of the ketamine–xylazine mixture (one-third of the calculated dose) was administered.

The technique for sciatic nerve injury modeling and neurorrhaphy in rats has been described in detail in a previous publication [17]. Following adequate analgesia and muscle relaxation, animals were positioned prone, with the limbs placed at an angle of approximately 45° relative to the longitudinal axis of the body. A support pad was placed beneath the left iliac region. The skin of the left posterior thigh was shaved, disinfected with a 10% Betadine® solution ("Egis", Hungary), and incised longitudinally, parallel to the femur. The sciatic nerve was exposed by blunt muscle separation, transected at the mid-thigh level, and immediately repaired by end-to-end approximation of the nerve stumps using either two interrupted epineurial sutures (Groups 1 and 2) or four interrupted epineurial sutures (Group 3) with a 9-0 atraumatic needle ("Olymp", Ukraine) under a stereomicroscope ("Olympus SZX7", Japan). The lateral margins of the thigh muscles mobilized during the surgical approach, as well as the skin edges, were closed in two layers using interrupted 4-0 sutures ("Olymp", Ukraine). The wound was subsequently treated with a 10% Betadine® solution ("Egis", Hungary). Postoperatively, Bicillin-5 solution (600,000 IU/kg; "Kyivmedpreparat", Ukraine) was administered subcutaneously into the posterior cervical region, while dexamethasone solution (5 mg/kg; KRKA, Slovenia) was injected into the right posterior thigh.

Animals in Groups 1 and 3 were maintained under elevated ambient temperature conditions until full recovery of spontaneous motor activity (approximately 30 min), whereas animals in Group 2 were kept at room temperature until reaching a comparable recovery state (approximately 2 h).

Motor functional assessment. The SFI was determined in all experimental groups over a 24-week period following surgery. Paw prints required for SFI calculation were obtained using the Gait2SFI system (***Fig. 1***), which enables high-resolution video recording of animal locomotion with both high spatial resolution (5.3 K; 5312 × 2988 pixels) and temporal resolution (60 fps), as well as a substantial depth of field. The system also allows identification of paw–surface contact areas using the frustrated total internal reflection (FTIR) method [22]. Optimization of illumination parameters combined with the large depth of field enabled simultaneous high-quality visualization of both the contact regions and the entire paw. Subsequent processing of the recordings using dedicated software permits frame-by-frame analysis of anatomical paw landmarks and semi-automated calculation of SFI values [23].

SFI values were calculated according to the Bain–Mackinnon–Hunter formula [24], using morphometric measurements obtained from the highest-quality paw-print images:

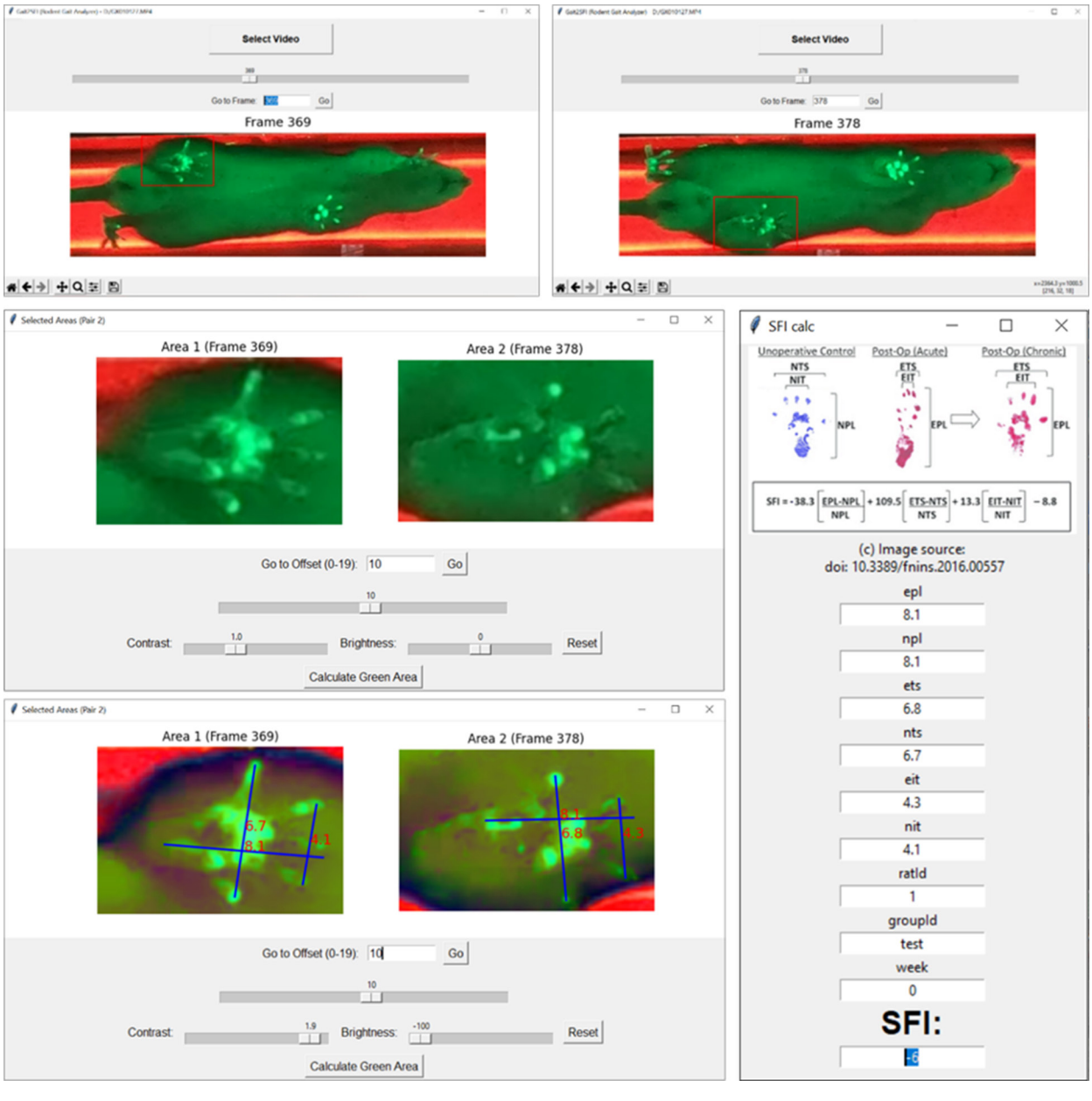

Fig. 1. The Gait2SFI hardware–software platform enables acquisition of video recordings during animal gait testing with high-contrast paw prints, in which surface contact areas are highlighted in green, and provides semi-automated calculation of the SFI. The upper row presents sequential frames from a single step cycle of a rat, displayed in the software interface and used for SFI determination. The middle row shows cropped regions of the same frames illustrating the hind paw prints. Bright green areas indicate locations in direct contact with the walking surface, whereas the remaining portions of the paw are visible due to illumination by diffuse green light. In the lower row, adjustment of image contrast and brightness within the software enhances visualization of contact areas and enables measurement of parameters required for SFI calculation. The measured parameters are entered into a calculation table (right panel). The software performs SFI calculation automatically, and the resulting values are stored together with the corresponding morphometric parameters in a unified database

$$SFI = -38{,}3 \times \frac{PL_E - PL_N}{PL_N} + 109{,}5 \times \frac{TS_E - TS_N}{TS_N} + 13{,}3 \times \frac{IT_E - IT_N}{IT_N} - 8{,}8,$$

*where **E** denotes the injured limb and **N** the intact limb; **PL** is the print length, measured as the distance from the heel to the tip of the longest toe; **TS** is the toe spread, defined as the distance between the first and fifth toes; and **IT** is the intermediary toe spread, defined as the distance between the second and fourth toes.*

Sensory function assessment. Quantitative evaluation of changes in nociceptive thresholds following surgery was performed using two standardized behavioral assays: the Hargreaves test (assessment of thermal nociception) and the von Frey test (assessment of mechanical nociception), as previously described [25, 26]. Testing was conducted on the lateral plantar surface of the hind paw within the cutaneous innervation territory of the tibial and sural branches of the sciatic nerve on both the operated and intact limbs. Baseline measurements were obtained before surgery, whereas subsequent assessments were performed between Weeks 2 and 24 postoperatively.

Mechanical sensitivity, encompassing both tactile and nociceptive components, was evaluated using the von Frey test. Animals were individually placed in cages with a wire-mesh floor and allowed to acclimatize for at least 30 min. Mechanical thresholds were determined using a calibrated set of nylon monofilaments (Touch-Test, Stoelting, Cat. No. 58011), which were applied perpendicularly to the plantar surface of the hind paw until the filament bent, thereby delivering a constant force (expressed in grams) for 2–3 s. A positive response was defined as paw withdrawal, licking of the tested limb, or vocalization during or immediately after filament application. Testing was performed only when animals were awake, calm, immobile, and not engaged in grooming behavior.

In Group 2 (ketamine/xylazine anesthesia, two epineurial sutures), paw withdrawal thresholds (PWT) were determined using the up–down method. Testing began with a 26-g filament. If a positive response was observed, a filament with a lower force was subsequently applied; if no response occurred, a filament with a higher force was used. Following the first reversal in response direction, at least five additional stimulations were performed according to the up–down algorithm. The PWT was defined as the force corresponding to a 50% probability of response and was calculated using the standard Dixon–Chaplan formula [27] based on the sequence of positive and negative responses:

$$50\%\ \text{threshold (g)} = \frac{10^{x+kd}}{10\,000}$$

where **X** is the logarithmic value of the force of the final filament used; **k** is the tabulated value corresponding to the observed response pattern; and **d** is the mean logarithmic increment between adjacent filament forces. Threshold values were calculated using the Von Frey 1.0 online calculator (DTU Health Tech) [28]. The resulting values were expressed in grams and used for statistical analysis.

In the isoflurane anesthesia groups, a bottom-up von Frey paradigm was employed. Testing began with the filament exerting the lowest force, followed by sequential application of filaments with progressively greater forces. Each filament was applied five times with intervals between stimulations. A response was considered positive when a clear protective reaction was observed, including paw withdrawal, shaking, or licking. The PWT was defined as the force of the filament that elicited a protective response in at least three of five applications. This value was used as the individual measure of mechanical sensitivity for the corresponding animal and time point.

Thus, mechanical sensitivity was assessed using two distinct von Frey paradigms. The "bottom-up" method provides a discrete measure of suprathreshold responsiveness, whereas the up–down method estimates the force corresponding to a 50% probability of paw withdrawal. Because these measures are not numerically equivalent, direct between-group comparisons of absolute values were not performed. Instead, statistical analyses of time-dependent changes were conducted separately within each methodological series.

Thermal nociception was evaluated using the Hargreaves test with a plantar analgesia meter ("Ugo Basile", Cat. No. 37370UB, Italy). Animals were placed in transparent chambers with a Plexiglas floor and allowed to acclimatize before testing (30–40 min before the first session and 20–30 min before subsequent sessions). Acclimatization was considered complete once grooming behavior had ceased. A focused radiant heat source was directed at the plantar surface of the hind paw in the heel region, and the paw withdrawal latency (PWL) was recorded as the time elapsed from stimulus onset to the first pain-related behavioral response (paw withdrawal, licking, or vocalization). Baseline withdrawal latencies in preoperative animals and on intact paws ranged from 10 to 12 s. A cut-off latency of 33 s was imposed to prevent tissue injury. Each limb was tested five times per session, with an interstimulus interval of 3–5 min.

Statistical analysis

The statistical analysis was designed not to assess differences between individual measurements, but rather to identify patterns at the level of animal groups over time. Accordingly, a two-way repeated-measures analysis of variance (two-way repeated-measures ANOVA, RM-ANOVA) was employed, with "Group" as the between-subjects factor and "Time" as the within-subjects factor. Because the tests were conducted repeatedly in the same animals, the analysis accounted for intra-individual changes and the correlation among repeated measurements. The primary questions addressed by this statistical model were:

1. Does sensory sensitivity and motor function change over time after surgery within each group?

2. Do experimental groups subjected to different types of anesthesia or different surgical procedures differ overall?

3. Does the pattern of change over time depend on the type of anesthesia or surgical procedure?

A statistically justified answer to the third question (the "Group" × "Time interaction") was of central importance to this study.

For the "Time" factor, the assumption of sphericity was evaluated. When this assumption was violated, the Greenhouse–Geisser correction was applied, which is the standard procedure for longitudinal data with multiple time points. The sphericity assumption is a key requirement for the valid application of RM-ANOVA.

Within this framework, the assumption of normality pertains to the distribution of residuals rather than to the distribution of the measured variable itself; moreover, with small sample sizes, formal testing of normality is of limited informativeness [29].

Post hoc comparisons were performed only when a statistically significant effect of "Time", "Group", or the "Group" × "Time" interaction was detected. Within-group comparisons between baseline values and each postoperative time point were conducted using the Wilcoxon signed-rank test. To evaluate postoperative recovery of motor function, additional within-group comparisons were performed between the first postoperative measurement and each subsequent postoperative time point. Between-group post hoc comparisons at individual time points were conducted using the Mann–Whitney U test. If testing was not performed in one of the comparison groups during a particular week, data obtained from the other group during that week were excluded from the analysis.

The validity of pooling data from multiple time points was assessed using either the Friedman test or the Kruskal–Wallis test.

For the von Frey tests, only within-group statistical analyses were performed using one-way repeated-measures analysis of variance (one-way repeated-measures ANOVA, one-way RM-ANOVA).

All statistical analyses were conducted in Python 3 using the pandas, numpy, scipy.stats, and matplotlib libraries. Statistical significance was set at $p < 0.05$.

Results

Effect of anesthesia type on sensory recovery following neurorrhaphy. To evaluate the effect of anesthesia type on sensory sensitivity, the animals were allocated into two experimental groups:

Group 1 – animals subjected to sciatic nerve transection followed by immediate end-to-end repair using two interrupted epineurial sutures under inhalational isoflurane anesthesia (n = 6);

Group 2 – animals subjected to the same surgical procedure under intraperitoneal ketamine/xylazine anesthesia (n = 5).

Thermal sensitivity was assessed using the Hargreaves test on the day before surgery, every 2 weeks after surgery for 12 weeks, and additionally at weeks 18, 20, and 22. The results are presented in ***Fig. 2*** and were analyzed using repeated-measures analysis of variance (RM-ANOVA).

The analysis revealed no significant main effect of group ($F(1,9) = 2.26$, $p = 0.167$), indicating the absence of an overall difference between the groups when averaged across all time points. In contrast, a large and statistically significant main effect of time was observed ($F(9,81) = 3.17$, $p = 0.003$), demonstrating that thermal sensitivity changed over the course of the observation period in both groups. A significant difference between the groups was detected prior to week 8 ($p = 0.025$), after which the groups converged and no further significant differences were observed, indicating a gradual stabilization of thermal sensitivity values during the late phase of recovery (***Fig. 2***).

Importantly, the "Group" × "Time" interaction across the entire postoperative period demonstrated a clear trend toward differential temporal dynamics between the groups, reaching the threshold of statistical significance ($F(9,81) = 1.98$, $p = 0.05$). Specifically, thermal sensitivity progressively deteriorated throughout the

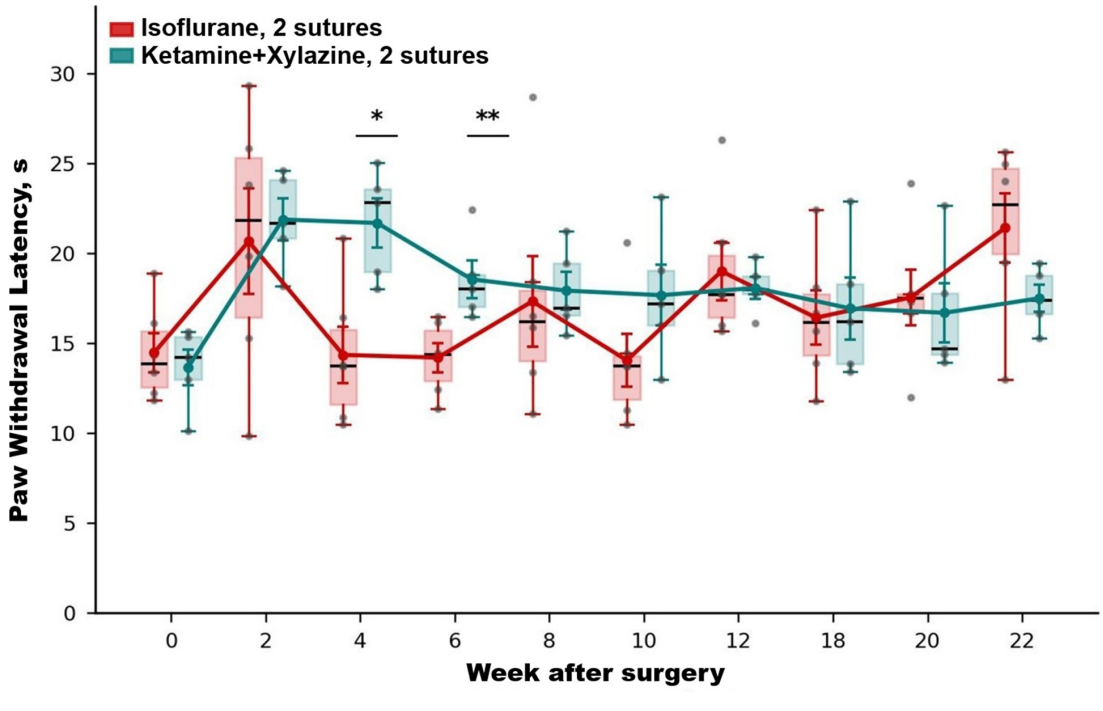

Fig. 2. Dynamics of PWL to a thermal stimulus throughout the experiment in the isoflurane and ketamine/xylazine anesthesia groups (2 sutures). Data are presented as the median with the interquartile range to illustrate data distribution. Statistical analysis was performed using RM-ANOVA followed by planned post hoc comparisons. Horizontal bars indicate significant differences between groups at the corresponding time points (post hoc Mann–Whitney U test, *$p < 0.05$; **$p < 0.01$)

experiment in the isoflurane anesthesia group, whereas gradual improvement was observed in the ketamine/xylazine anesthesia group (***Fig. 2***).

Post hoc analysis within each group did not reveal any significant deviation from baseline values, although a significant overall tendency toward changes in thermal sensitivity of the limb with the injured nerve was detected for both anesthesia regimens ($F(9,81) = 3.17$, $p = 0.003$). At week 2, non-significant hypoalgesia was observed, with no significant difference in PWL between the groups (***Fig. 2***). It is possible that this hypoalgesic effect would have reached statistical significance with larger group sizes. In both experimental groups, the observed hypoalgesia was attributable to substantial denervation of the plantar region following sciatic nerve transection.

Post hoc analysis (Mann–Whitney U test) also revealed significant differences between the groups at weeks 4 ($p = 0.017$) and 6 ($p = 0.009$). Thus, significant differences were detected only during the early stage of postoperative recovery. During this period, the isoflurane anesthesia group (2 sutures) exhibited a significantly shorter PWL than the ketamine/xylazine anesthesia group (2 sutures), indicating more rapid recovery of thermal nociception under isoflurane anesthesia. Therefore, the results of this experiment demonstrate a significant difference in postoperative changes in thermal sensitivity of the ipsilateral limb depending on the type of anesthesia used. Notably, this difference persisted for several weeks after surgery. These findings suggest that a relatively short anesthetic procedure (1–2 h) can influence postoperative alterations in thermal sensitivity during the early recovery period (up to 6 weeks), promoting functional recovery. At the same time, a tendency toward impaired thermal sensitivity during the late postoperative period was observed in animals anesthetized with isoflurane compared with those receiving ketamine/xylazine anesthesia.

Given that thermal sensitivity is largely mediated by nerve fibers expressing TRPV1 receptors [30], it may be assumed that the type of anesthesia used during sciatic nerve injury modeling substantially affects the recovery of these fibers.

To determine whether the recovery of another major class of sensory fibers—mechanoreceptive fibers—also depends on the type of anesthesia used during sciatic nerve injury modeling, changes in mechanical sensitivity were evaluated in animals from the two aforementioned groups.

For the von Frey test results, direct between-group comparisons of absolute threshold values were not performed because of differences in the algorithms used to determine the mechanical sensitivity threshold. Instead, within each group, changes relative to baseline (week 0) were assessed using one-way repeated-measures ANOVA (one-way RM-ANOVA) followed by the Wilcoxon signed-rank test for paired comparisons.

As shown in ***Fig. 3A***, animals anesthetized with isoflurane demonstrated a pronounced and significant effect of time ($F(10,30) = 8.022$, $p < 0.001$), characterized by a gradual increase in PWT, reaching a maximum at week 18 (~80 g compared with a baseline value of ~21 g). Significant deviations from baseline values persisted at weeks 12, 14, 16, 18, and 22 ($p = 0.031$). These findings most likely indicate the progressive development of persistent mechanical hypoalgesia and the absence of a tendency toward recovery of mechanical sensitivity by the end of the experiment. In contrast, animals anesthetized with ketamine/xylazine exhibited a significant overall effect of time ($F(10,40) = 2.602$, $p = 0.016$), which did not result in significant deviations from baseline values at any subsequent time point (***Fig. 3B***). PWT fluctuated (~13–46 g) around the baseline level (~24 g). This pattern suggests recovery of mechanical sensitivity following an initial tendency toward mechanical hypoalgesia, which, as in the case of thermal sensitivity, most likely resulted from denervation of the paw following nerve injury.

Although direct comparison of the groups is inappropriate because different measurement algorithms were used, a normalized graph (***Fig. 3C***) is presented for illustrative purposes. It demonstrates that, following isoflurane anesthesia, the parameter progressively and significantly increased during the post-injury period (reaching approximately 200–400% of baseline values), whereas under ketamine/xylazine anesthesia the values remained close to baseline levels.

Thus, the von Frey test results are consistent with the findings of the Hargreaves test, supporting the conclusion that sensory recovery differs significantly depending on the type of anesthesia used. Furthermore, the results indicate more favorable conditions for restoration of sciatic nerve sensory function following transection and immediate reconstruction with two epineurial sutures when the procedure is performed under ketamine/xylazine anesthesia.

Effect of anesthesia type on motor function recovery following neurorrhaphy

Motor function recovery was assessed using the SFI [24] on the day before surgery and at 4, 8, 12, 16, 20, and 24 weeks postoperatively. The results are presented in ***Fig. 4*** and were analyzed using repeated-measures analysis of variance (RM-ANOVA). The analysis revealed no significant main effect of group ($F = 0.36$, $p = 0.57$), indicating the absence of an overall difference between the groups when averaged across all postoperative time points beginning from week 4. In contrast, a large and statistically significant effect of time was detected ($F = 3.02$, $p = 0.02$), indicating improvement of motor function over the course of the experiment. Therefore, to further evaluate the effect of time within each group, separate one-way RM-ANOVA analyses were performed for the period from week 4 to week 24.

This analysis revealed a significant effect in the ketamine/xylazine anesthesia group ($F(5,20) = 6.745$, $p = 0.0008$), indicating substantial recovery of motor function throughout the experimental period. In contrast, no significant recovery was detected in the isoflurane anesthesia group ($F(5,25) = 1.27$, $p = 0.31$). Importantly, the "Group" × "Time" interaction demonstrated a clear and statistically significant difference in recovery dynamics between the groups throughout the entire experimental period ($F = 3.80$, $p = 0.006$). However, post hoc Mann–Whitney U tests revealed no significant between-group differences at any individual observation time point, despite a pronounced visual divergence in this measure during the later stages of the experiment (***Fig. 4***). Since indicator values remained stable within each group during the final three observation periods (weeks 16, 20, and 24), these data points were pooled for each group. Analysis of the pooled datasets revealed a

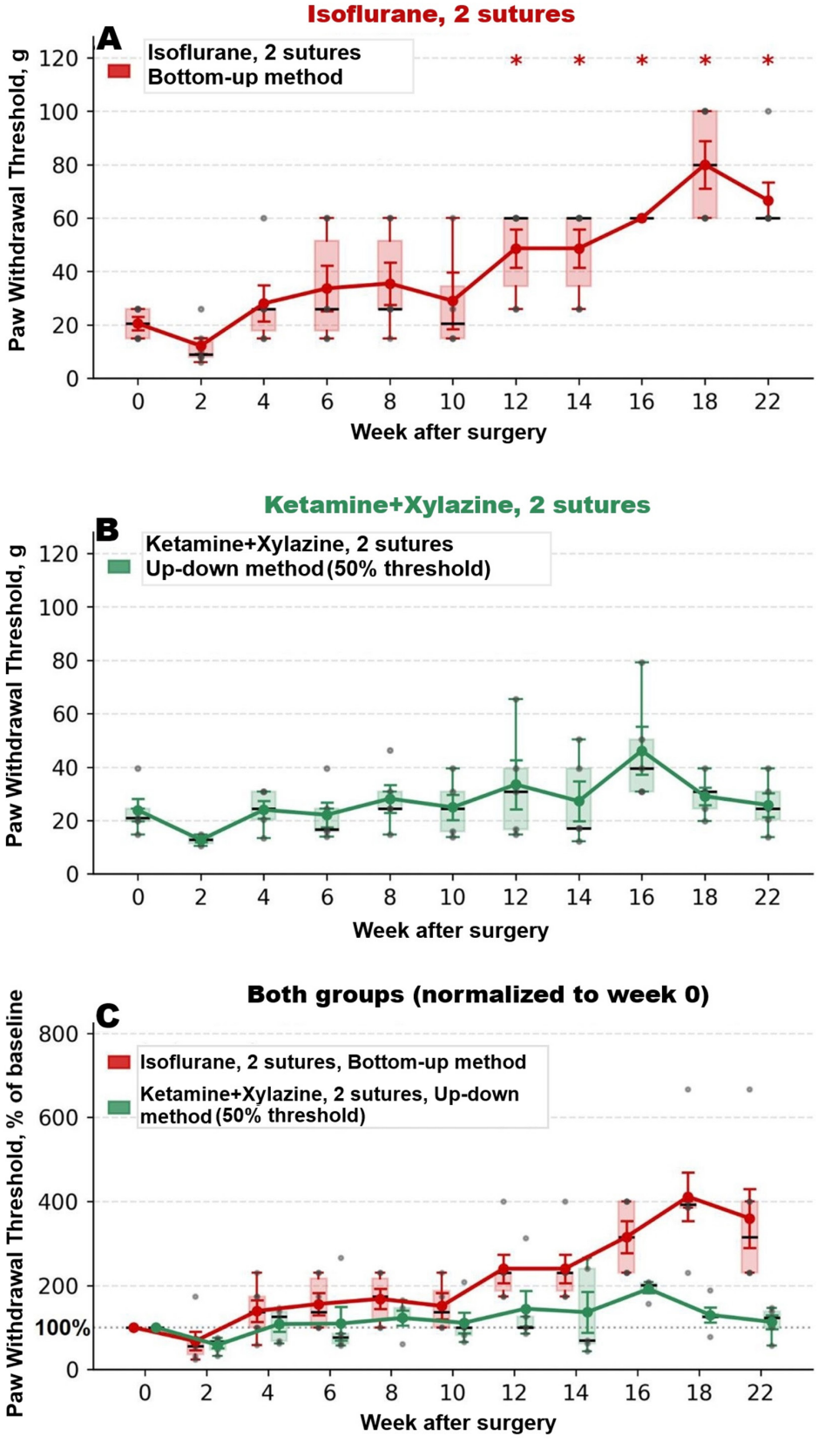

Fig. 3. Dynamics of PWT (von Frey test) throughout the experimental period in the isoflurane and ketamine/xylazine anesthesia groups (2 sutures). Changes induced by neurorrhaphy performed under isoflurane anesthesia (A) and ketamine/xylazine anesthesia (B). Normalized response curves (C), derived from the data presented in panels A and B, demonstrate qualitative differences in recovery dynamics.
* – Statistically significant difference ($p < 0.05$) between the corresponding time point and baseline values within the same group (post hoc Wilcoxon signed-rank test).

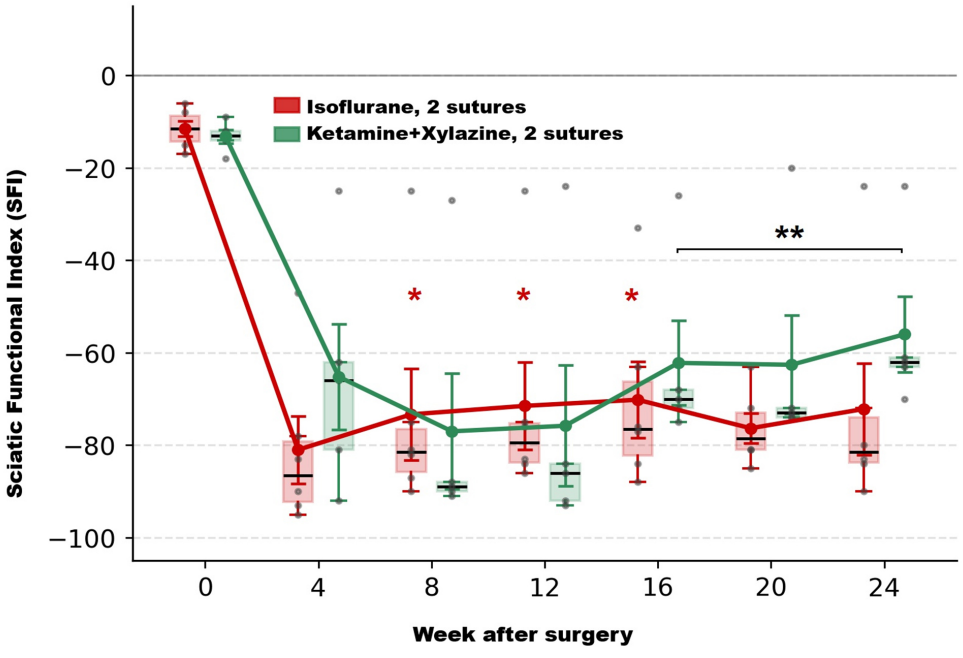

Fig. 4. Dynamics of SFI throughout the experimental period in the isoflurane and ketamine/xylazine anesthesia groups (2 sutures).

* – Statistically significant difference ($p < 0.05$) between the corresponding time point and baseline values within the same group (post hoc Wilcoxon signed-rank test).

significant between-group difference ($p = 0.004$, Mann–Whitney U test). This finding, together with the results of the preceding tests, indicates significant recovery of motor function when sciatic nerve injury was modeled and immediately reconstructed using two epineurial sutures under ketamine/xylazine anesthesia.

Effect of nerve repair configuration on sensory recovery. To determine whether sensory recovery following sciatic nerve transection and immediate reconstruction depends on the number of epineurial interrupted sutures, animals were allocated into two experimental groups according to the number of epineurial sutures used to reconnect the transected nerve ends. As in the previous part of the analysis, Group 1 consisted of animals that underwent sciatic nerve transection followed by immediate restoration of nerve continuity using two epineurial interrupted sutures under inhalational isoflurane anesthesia ($n = 6$). Group 3 consisted of animals in which the transected nerve ends were repaired using four epineurial interrupted sutures under the same anesthetic regimen ($n = 6$).

Thermal sensitivity was assessed using the Hargreaves test on the day before surgery and every 2 weeks after the intervention for 12 weeks, as well as at weeks 18, 20, and 22 of the experiment. The results are presented in ***Fig. 5*** and were analyzed using repeated-measures analysis of variance (RM-ANOVA). For methodological consistency, values normalized to the preoperative baseline (week 0) were analyzed because baseline measurements differed slightly but significantly between the groups.

A significant main effect of group was identified ($F(1,10) = 9.23$, $p = 0.013$), indicating that throughout the observation period the thermal sensitivity threshold remained higher when four sutures were used to repair the transected nerve compared with repair using two sutures. Significant effects of time ($F(9,90) = 4.34$, $p < 0.001$) and a significant "Group" × "Time" interaction ($F(9,90) = 3.57$, $p < 0.001$) were also detected, indicating that thermal sensitivity changed over time in both groups and that the temporal pattern of these changes differed between them.

Integration of the findings from Groups 1 and 3 with the results of the post hoc analyses demonstrated that, following repair with two sutures, the response threshold fluctuated around baseline values (97–156%) without significant deviations, indicating relatively rapid recovery of thermal nociception. In contrast, after repair with four sutures, the thermal threshold remained elevated throughout the period from week 2 to week 22 of the experiment (145–173%; $p = 0.031$ at each observation time point). Thus, neurorrhaphy performed with four sutures was associated with pronounced and persistent hypoalgesia lasting for 22 weeks, as well as substantially slower recovery of thermal nociception. The significant "Group" × "Time" interaction ($p < 0.001$, $\eta^2p = 0.263$), together with the post hoc analysis, confirmed that the differences between the groups were primarily attributable to the early postoperative time points (***Fig. 5***).

Post hoc analysis did not reveal significant differences between Groups 1 and 3 at the final stage of the study. However, the "Group" × "Time" interaction across the entire postoperative period demonstrated a trend toward different recovery dynamics between the groups, characterized by a gradual deterioration of thermal sensitivity parameters throughout the experiment in the two-suture group and progressive improvement in the four-suture group (***Fig. 5***).

Significant hypoalgesia was detected in Group 3 at week 2 after surgery (***Fig. 5***). It is likely that hypoalgesia would also have reached statistical significance in the two-suture group if a larger number of animals had

been included, as both experimental groups experienced substantial denervation of the plantar region following sciatic nerve transection.

Taken together, these findings indicate that the number of epineurial sutures used to restore continuity of a transected sciatic nerve has a substantial influence on the dynamics of thermal sensitivity recovery in the paretic limb.

Changes in mechanical sensitivity were also evaluated in experimental Groups 1 and 3.

Because different algorithms were used to determine PWT in the experimental groups, direct between-group comparisons of absolute values were not performed. Instead, for each group, changes relative to baseline (week 0) were analyzed using one-way repeated-measures ANOVA (one-way RM-ANOVA) followed by the Wilcoxon signed-rank test for paired comparisons.

As shown in ***Fig. 6A***, isoflurane anesthesia was associated with a pronounced and significant effect of time ($F(10,30) = 8.022$, $p < 0.001$), with the PWT remaining substantially above baseline values (49–80 g versus approximately 21 g at baseline). This persistent hypoalgesia indicated a lack of recovery of mechanical sensitivity in Group 1. Significant deviations from preoperative values (week 0) persisted at weeks 12, 14, 16, 18, and 22 ($p = 0.031$). As noted above, these findings most likely reflect the gradual development of persistent mechanical hypoalgesia and the absence of complete recovery of mechanical sensitivity by the end of the experiment. In contrast, the use of four epineurial sutures under the same anesthetic regimen produced a significant overall effect of time ($F(10,50) = 2.14$, $p = 0.04$), but did not result in significant deviations from baseline values (week 0) at any observation time point (***Fig. 6B***). The PWT fluctuated within a range of approximately 16–44 g without a systematic increase, and mechanical sensitivity remained close to preoperative levels. This finding indicates recovery of mechanical sensitivity following an initial tendency toward mechanical hypoalgesia, which, as in the case of thermal sensitivity, was most likely associated with the initial denervation of the paw.

Although direct comparison between the groups cannot be considered methodologically appropriate because of differences in the measurement algorithms, a normalized plot (***Fig. 6C***) is presented for illustrative purposes. This graph demonstrates that repair with two epineurial sutures under isoflurane anesthesia resulted in a progressive and significant increase in normalized PWT values (approximately 200–400% of baseline), whereas repair with four epineurial sutures under the same anesthetic conditions maintained values close to baseline throughout the entire experimental period.

Thus, the von Frey test results are consistent with the findings of the Hargreaves test, supporting the conclusion that sensory recovery differs significantly depending on the number of epineurial sutures used to reconnect the transected sciatic nerve. Furthermore, the results indicate more favorable conditions for restoration of sciatic nerve sensory function, particularly mechanical sensitivity, when nerve reconstruction is performed using four rather than two epineurial sutures under isoflurane anesthesia.

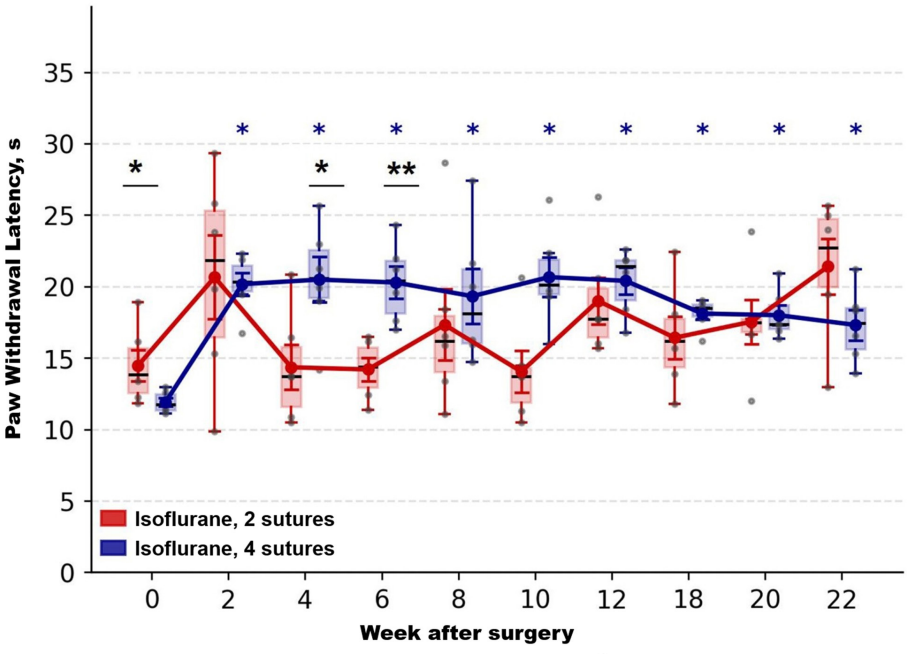

Fig. 5. Dynamics of PWL to a thermal stimulus throughout the experimental period in the isoflurane anesthesia groups repaired with 2 or 4 epineurial sutures. Data are presented as the median with the interquartile range. Statistical analysis was performed using RM-ANOVA followed by planned post hoc comparisons. Asterisks indicate statistically significant differences between the corresponding time points and baseline values (post hoc Wilcoxon signed-rank test; *$p < 0.05$, ** $p < 0.01$), whereas horizontal bars indicate significant differences between the groups at the corresponding time points (post hoc Mann–Whitney U test).

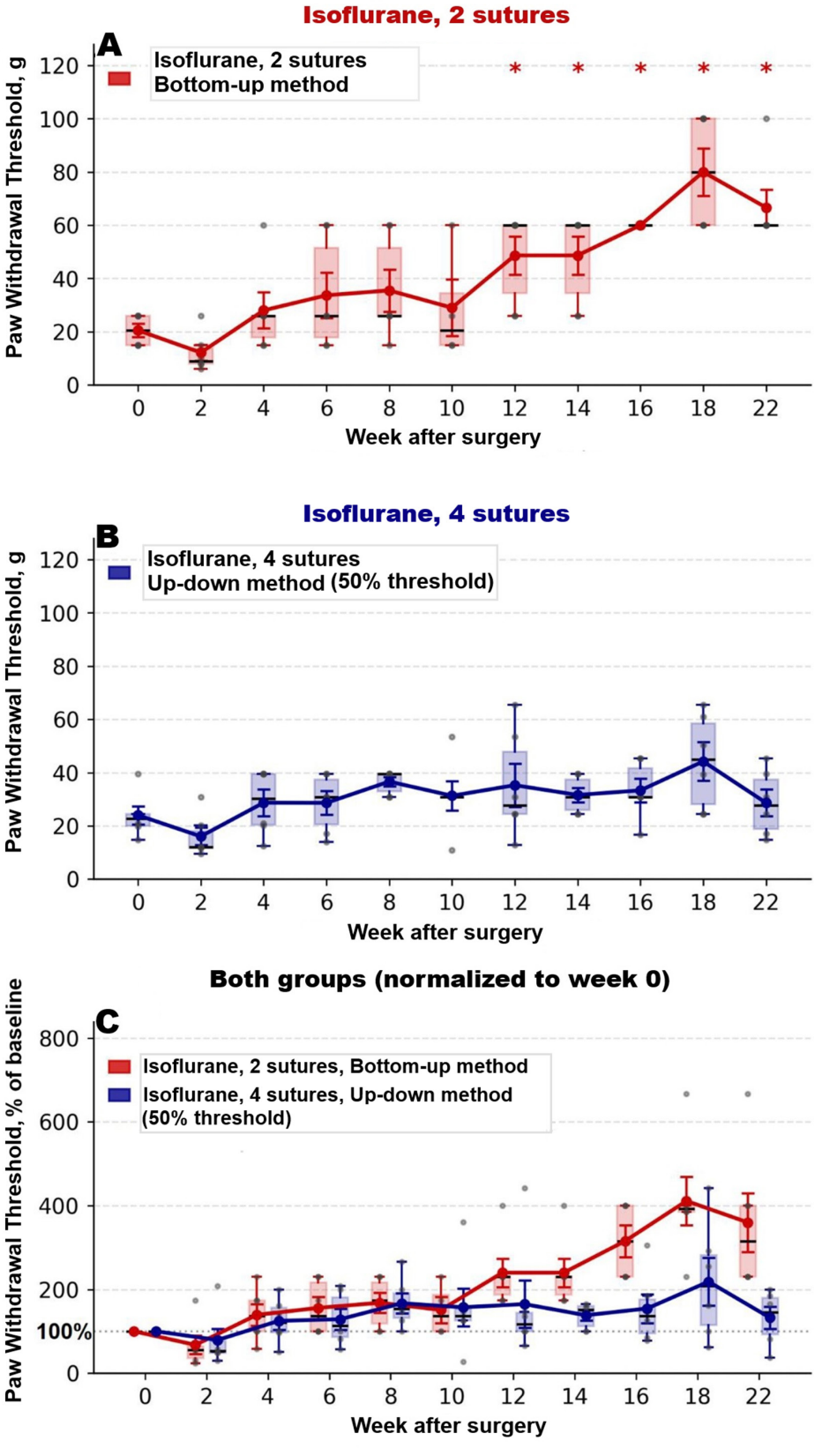

Fig. 6. Dynamics of PWT (von Frey test) throughout the experimental period in the isoflurane anesthesia groups repaired with 2 and 4 epineurial sutures. Changes induced by neurorrhaphy performed with 2 sutures (A) and 4 sutures (B). The normalized response curves (C), derived from the data presented in panels A and B, demonstrate qualitative differences in recovery dynamics.

* – Statistically significant difference ($p < 0.05$) between the corresponding time point and baseline values within the same group (post hoc Wilcoxon signed-rank test)

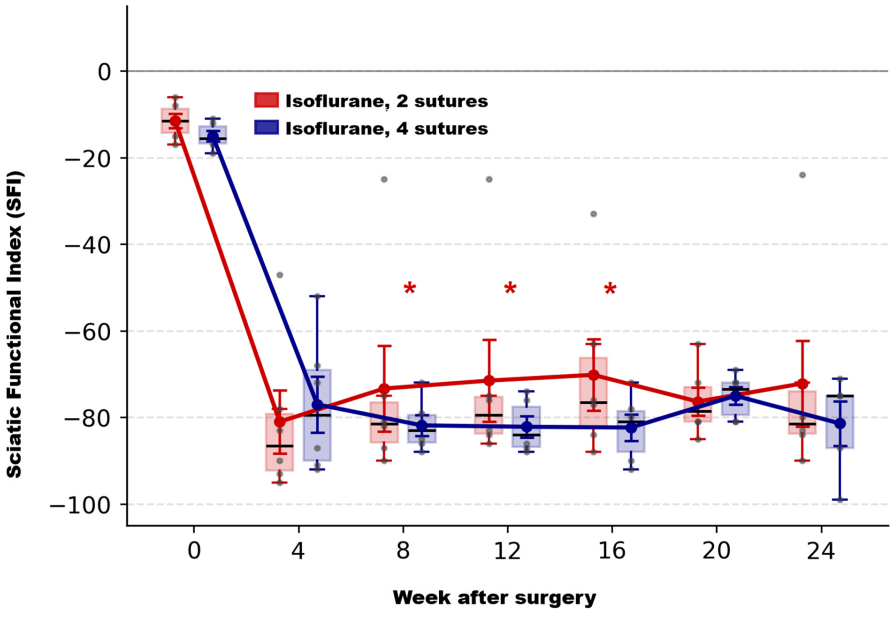

Fig. 7. Dynamics of SFI throughout the experimental period in the isoflurane anesthesia groups repaired with 2 and 4 epineurial sutures. * – Statistically significant difference ($p < 0.05$) between the corresponding time point and baseline values within the same group (post hoc Wilcoxon signed-rank test)

Effect of nerve repair configuration on motor function recovery

Motor function recovery was assessed using the SFI [24] before surgery and at 4, 8, 12, 16, 20, and 24 weeks after the surgical intervention. The results are presented in ***Fig. 7*** and were analyzed using repeated-measures analysis of variance (RM-ANOVA).

The analysis revealed no significant main effect of group ($F = 0.36$, $p = 0.57$), indicating the absence of an overall difference between the groups when averaged across all postoperative time points beginning from week 4. Likewise, neither a significant effect of time nor a significant "Group" × "Time" interaction was detected throughout the experimental period. These findings indicate that, under isoflurane anesthesia, the number of epineurial sutures used for end-to-end repair of the transected sciatic nerve (2 versus 4 sutures) did not significantly affect the recovery of motor function. Furthermore, the results demonstrate the absence of significant motor function recovery in either experimental group. This observation may suggest that the use of isoflurane anesthesia is associated with less favorable recovery of motor function following sciatic nerve injury and reconstruction.

Discussion

Because currently available treatments for PNI, particularly surgical approaches, do not provide complete restoration of nerve function [31], the experimental development of novel therapeutic strategies remains an important biomedical challenge. Progress in this field critically depends on the quality of PNI models and on the baseline surgical procedures used to treat this type of injury. In particular, the influence of the type of general anesthesia on the regenerative process following PNI requires careful investigation, as the two most commonly used anesthetic regimens—injectable ketamine/xylazine anesthesia and inhalational isoflurane anesthesia—differ substantially in the rate at which animals recover motor activity after anesthesia. To reduce animal suffering and improve intraoperative control of anesthesia, modern experimental medicine and biology increasingly employ noninvasive inhalational anesthetic techniques, particularly isoflurane administration [18]. However, our findings suggest that, in models involving peripheral nerve transection followed by immediate repair using a small number of interrupted sutures, isoflurane inhalation may be an unsuitable method of general anesthesia for experimental animals. This assumption is consistent with published data indicating that intraperitoneal administration of anesthetic agents remains the most commonly used method [7] of general anesthesia in studies of transected nerve regeneration.

In our opinion, the rate of postoperative mobilization of the injured limb is a particularly important factor when a limited number (two) of interrupted epineurial sutures are used for end-to-end fixation of the sciatic nerve stumps. According to our observations, animals recover consciousness within several minutes after discontinuation of isoflurane inhalation, and full restoration of general motor activity occurs within the subsequent 10–15 min. In contrast, when injectable ketamine/xylazine anesthesia is used, the interval between completion of neurorrhaphy and restoration of general motor activity is, according to our data, at least 1 hour. This period is likely sufficient to stabilize the nerve repair site through the action of resident fibrin and other rapid mechanisms of the wound-healing process.

The importance of mechanical factors in the development of nerve repair failure is supported by the use of postoperative immobilization of limbs with injured nerves [20], as well as by partial limb immobilization

following restoration of rat sciatic nerve continuity using mechanically weak spot-welded nerve junctions [21].

Among the relatively few reports employing inhalational anesthesia for experimental PNI modeling [7], including isoflurane anesthesia [32–34], two studies described the use of isoflurane in rats undergoing peripheral nerve injury modeling with a minimal number of epineurial sutures applied to each nerve stump. In both cases, satisfactory recovery of SFI values was observed during the first two months of follow-up.

Our findings indicate that the type of general anesthesia may represent an important factor influencing the outcomes of experimental studies on peripheral nerve regeneration.

Study limitations

The widely used rat sciatic nerve transection model has several methodological limitations, including the inherent shortcomings of the analog functional–anatomical method used to assess the condition of the injured sciatic nerve through the SFI, as well as the lack of standardized surgical techniques for neurorrhaphy and anesthetic management [17].

The main limitations of the present study include the relatively small sample sizes and, most importantly, the absence of a morphological assessment of nerve regeneration. Verification of the proposed hypothesis will require studies involving larger animal cohorts and the application of immunohistochemical, morphometric, and electrophysiological methods.

Conclusions

Current approaches to the treatment of peripheral nerve injuries remain insufficiently effective, highlighting the importance of experimental models and the conditions under which they are implemented. One of the key factors is the type of general anesthesia used. Inhalational isoflurane provides rapid recovery of motor activity, which may compromise the stability of the nerve repair site, whereas injectable ketamine/xylazine anesthesia allows a longer period for stabilization of the nerve junction. Mechanical factors, particularly early limb activity or postoperative immobilization, also have a substantial influence on the healing process. Therefore, the choice of anesthetic regimen may significantly affect the outcomes of experimental studies of peripheral nerve regeneration.

Disclosure statement

Conflict of interest

The authors declare that the conduct of this study and the publication of its results were not associated with any conflicts of interest related to commercial or financial relationships, relationships with organizations and/or individuals that could have influenced the study, or relationships among the co-authors.

Ethical approval

All procedures involving experimental animals were conducted in accordance with accepted ethical standards and were approved by the Biomedical Ethics Committee of the O.O. Bogomolets Institute of Physiology, NAS of Ukraine (Protocol No. 3/22, November 16, 2022).

Funding

This study was supported by a grant from the National Research Foundation of Ukraine (Project No. 2021.01/0328), as well as by grants from the National Academy of Sciences of Ukraine (NANU; Project Nos. 0124U001557 and 0125U002426).

References

1. Aman M, Zimmermann KS, Thielen M, Thomas B, Daeschler S, Boecker AH, Stolle A, Bigdeli AK, Kneser U, Harhaus L. An Epidemiological and Etiological Analysis of 5026 Peripheral Nerve Lesions from a European Level I Trauma Center. J Pers Med. 2022 Oct 8;12(10):1673. doi: 10.3390/jpm12101673
2. Murphy RNA, de Schoulepnikoff C, Chen JHC, Columb MO, Bedford J, Wong JK, Reid AJ. The incidence and management of peripheral nerve injury in England (2005-2020). J Plast Reconstr Aesthet Surg. 2023 May;80:75-85. doi: 10.1016/j.bjps.2023.02.017
3. Randall ZD, Navarro BJ, Brogan DM, Dy CJ. Insights Into the Epidemiology of Peripheral Nerve Injuries in the United States: Systematic Review. Hand (N Y). 2026 Feb;21(2):194-201. doi: 10.1177/15589447241299050
4. Shaprynskyi YV, Lypkan VM. Treatment of patients with gunshot traumatic amputations of the lower limbs due to explosive injury in the conditions of today's war in Ukraine. Reports Vinnytsia Natl Med Univ 2023;27:581–5. doi: 10.31393/REPORTS-VNMEDICAL-2023-27(4)-08
5. Shi S, Tang J, Lu Y, Xu S, Wang M, Wan S. A burden of nerve injury from a global perspective, 1990-2021: an analysis of incidence, prevalence, and years lived with disability. Front Neurol. 2026 Jan 6;16:1669662. doi: 10.3389/fneur.2025.1669662
6. Shvets AV, Horishna OV, Deputat YM, Rychka OV, Zhaldak AY, Kikh AY. Prognostic assessment of the need for medical rehabilitation among military officers of the armed forces of ukraine based on the structure of their combat trauma. Ukr Z Vijskovoi Med 2022;3:110–7. doi: 10.46847/UJMM.2022.3(3)-110
7. Vela FJ, Martínez-Chacón G, Ballestín A, Campos JL, Sánchez-Margallo FM, Abellán E. Animal models used to study direct peripheral nerve repair: a systematic review. Neural Regen Res. 2020 Mar;15(3):491-502. doi: 10.4103/1673-5374.266068
8. Zaidman M, Novak CB, Midha R, Dengler J. Epidemiology of peripheral nerve and brachial plexus injuries in a trauma population. Can J Surg. 2024 Jun 26;67(3):E261-E268. doi: 10.1503/cjs.002424
9. Howard IM, Sedarsky K, Gallagher M, Miller M, Puffer RC. Combat-related peripheral nerve injuries. Muscle Nerve. 2025 May;71(5):768-781. doi: 10.1002/mus.28168
10. Hems TE. Nerve injury: Classification, clinical assessment, investigation, and management. Living Textb Hand Surg 2016. doi: 10.5680/LHHS000030
11. Hostiuc S, Ciobanu OM, Popa E, Căținaș R, Ionescu-Mihăiță AM, Sima A, Negoi I, Costescu M. Clinical Anatomy and Diagnostic Challenges in Peripheral Nerve Trauma for the Forensic Physician. Diagnostics (Basel). 2025 Jun 24;15(13):1597. doi: 10.3390/diagnostics15131597
12. Khan H, Perera N. Peripheral nerve injury: an update. Orthop Trauma. 2020;(34):168–73. doi: 10.1016/J.MPORTH.2020.03.011
13. Bergmeister KD, Große-Hartlage L, Daeschler SC, Rhodius P, Böcker A, Beyersdorff M, Kern AO, Kneser U, Harhaus L. Acute and long-term costs of 268 peripheral nerve injuries in the upper extremity. PLoS One. 2020 Apr 6;15(4):e0229530. doi: 10.1371/journal.pone.0229530
14. Bateman EA, Pripotnev S, Larocerie-Salgado J, Ross DC, Miller TA. Assessment, management, and rehabilitation of traumatic peripheral nerve injuries for non-surgeons. Muscle Nerve. 2025 May;71(5):696-714. doi: 10.1002/mus.28185
15. Lin JS, Jain SA. Challenges in Nerve Repair and Reconstruction. Hand Clin. 2023 Aug;39(3):403-415. doi: 10.1016/j.hcl.2023.05.001
16. Li A, Pereira C, Hill EE, Vukcevich O, Wang A. In Vitro, In Vivo and Ex Vivo Models for Peripheral Nerve Injury and Regeneration. Curr Neuropharmacol. 2022;20(2):344-361. doi: 10.2174/1570159X19666210407155543
17. Melikov ZK, Medvediev VV. The rat's sciatic nerve functional

index dynamics after its transection and recovery by means of epineural neurorrhaphy. Ukr Neurosurg J 2024;30:30–42. doi: 10.25305/UNJ.310430.
18. Oh SS, Narver HL. Mouse and Rat Anesthesia and Analgesia. Curr Protoc. 2024 Feb;4(2):e995. doi: 10.1002/cpz1.995
19. Lee WP, Constantinescu MA, Butler PE. Effect of early mobilization on healing of nerve repair: histologic observations in a canine model. Plast Reconstr Surg. 1999 Nov;104(6):1718-25. doi: 10.1097/00006534-199911000-00016
20. Griffin MF, Malahias M, Hindocha S, Khan WS. Peripheral nerve injury: principles for repair and regeneration. Open Orthop J. 2014 Jun 27;8:199-203. doi: 10.2174/1874325001408010199
21. Molotkovets VY, Medvediev VV, Korsak AV, Chaikovsky YB, Marynsky GS, Tsymbaliuk VI. Restoration of the Integrity of a Transected Peripheral Nerve with the Use of an Electric Welding Technology. Neurophysiology 2020;52:31–42. doi: 10.1007/S11062-020-09848-3/METRICS.
22. Noldus Information Technology BV. The complete gait analysis system CatWalk. Noldus; 2026. https://noldus.com/catwalk-xt
23. Bomikhov O. Gait2SFI scripts for automated SFI calculation from rodent walking videos (sciatic nerve injury model). GitHub, Inc.; 2026. https://github.com/olbmv/Gait2SFI
24. Varejão AS, Meek MF, Ferreira AJ, Patrício JA, Cabrita AM. Functional evaluation of peripheral nerve regeneration in the rat: walking track analysis. J Neurosci Methods. 2001 Jul 15;108(1):1-9. doi: 10.1016/s0165-0270(01)00378-8
25. Krotov V, Agashkov K, Romanenko S, Koroid K, Krasniakova M, Belan P, Voitenko N. Neuropathic pain changes the output of rat lamina I spino-parabrachial neurons. BBA Adv. 2023 Feb 14;3:100081. doi: 10.1016/j.bbadva.2023.100081
26. Kopach O, Krotov V, Goncharenko J, Voitenko N. Inhibition of Spinal Ca(2+)-Permeable AMPA Receptors with Dicationic Compounds Alleviates Persistent Inflammatory Pain without Adverse Effects. Front Cell Neurosci. 2016 Feb 29;10:50. doi: 10.3389/fncel.2016.00050
27. Chaplan SR, Bach FW, Pogrel JW, Chung JM, Yaksh TL. Quantitative assessment of tactile allodynia in the rat paw. J Neurosci Methods. 1994 Jul;53(1):55-63. doi: 10.1016/0165-0270(94)90144-9
28. Gonzalez-Izarzugaza J.M. Von-Frey - 1.0. DTU Health Tech; 2026. https://services.healthtech.dtu.dk/services/Von-Frey/
29. Schmider E, Ziegler M, Danay E, Beyer L, Bühner M. Is It Really Robust?: Reinvestigating the robustness of ANOVA against violations of the normal distribution assumption. Methodology 2010;6:147–51. doi: 10.1027/1614-2241/a000016
30. Gatto G, Smith KM, Ross SE, Goulding M. Neuronal diversity in the somatosensory system: bridging the gap between cell type and function. Curr Opin Neurobiol. 2019 Jun;56:167-174. doi: 10.1016/j.conb.2019.03.002
31. Melikov ZK, Medvediev VV. Peripheral nerve injury: molecular pathophysiology and prospects for restorative treatment by means of cell transplantation: a literature review. Ukr Neurosurg J. 2023;29(4):3–12. doi: 10.25305/UNJ.288785
32. Meek MF, Den Dunnen WF, Schakenraad JM, Robinson PH. Long-term evaluation of functional nerve recovery after reconstruction with a thin-walled biodegradable poly (DL-lactide-epsilon-caprolactone) nerve guide, using walking track analysis and electrostimulation tests. Microsurgery. 1999;19(5):247-53. doi: 10.1002/(sici)1098-2752(1999)19:5<247::aid-micr7>3.0.co;2-e
33. Ganguly A, McEwen C, Troy EL, Colburn RW, Caggiano AO, Schallert TJ, Parry TJ. Recovery of sensorimotor function following sciatic nerve injury across multiple rat strains. J Neurosci Methods. 2017 Jan 1;275:25-32. doi: 10.1016/j.jneumeth.2016.10.018
34. Meder T, Prest T, Skillen C, Marchal L, Yupanqui VT, Soletti L, Gardner P, Cheetham J, Brown BN. Nerve-specific extracellular matrix hydrogel promotes functional regeneration following nerve gap injury. NPJ Regen Med. 2021 Oct 25;6(1):69. doi: 10.1038/s41536-021-00174-8

Case report

Ukrainian Neurosurgical Journal. 2026;32(2):93-96
doi: 10.25305/unj.344834

Occult Klippel-Feil syndrome unmasked by cervical spine trauma: A case report and literature review

Olukorede Olabanji Adekunle, Nurudeen Abiola Adeleke, Olakunle Michael Adegboye, Oghenevwoke Enaworu, Hakeem Ayinde Yeqeen, Akingbade Adebayo Akin-Dosumu, Gbenga Timothy Oyegbami, Oluwafemi Nehemiah Akeredolu, Nnara Onyeka Stanley

Division of Neurosurgery, Department of Surgery, University of Ilorin Teaching Hospital, Ilorin, Kwara State, Nigeria

Received: 28 November 2025
Accepted: 06 January 2026

Address for correspondence:
Olukorede Olabanji Adekunle, Division of Neurosurgery, Department of Surgery, University of Ilorin Teaching Hospital, Ilorin, Old Jebba Road, Oke Ose, Ilorin, Kwara State, Nigeria, email: adekunleolukorede@gmail.com

Background: Klippel-Feil syndrome is a rare congenital condition characterized by the fusion of two or more cervical vertebrae. Half of the patients present with the triad of short neck, low posterior hairline and limited neck motion. Patients are at increased risk of cervical spine injury due to cervical canal stenosis. The syndrome is often associated with other congenital anomalies.

Case presentation: We report the case of a 60-year-old male who presented with a 6-hour history of neck pain following a rider motorcycle-motor vehicle road traffic crash. Cervical spine X-ray imaging showed fusion of the entire subaxial cervical spine. However, the patient had no neurologic deficit. He was managed non-operatively and discharged with a rigid cervical collar after resolution of neck pain.

Conclusion: This case report highlights an incidental discovery of Klippel-Feil syndrome during evaluation and management of cervical spine injury.

Keywords: *Klippel-Feil syndrome; cervical spine injury; cervical canal stenosis; case report*

Background

Klippel-Feil syndrome (KFS) is a rare congenital condition characterized by the non-segmentation or fusion of two or more cervical vertebrae [1]. It is classically characterized by the triad of short neck, low posterior hairline, and restricted neck movement [1].

The syndrome, first described in 1912 by Maurice Klippel and Andre Feil, results from an embryonic failure of normal segmentation of the cervical somites between the third and eighth weeks of gestation [2].

Although vertebral fusion is the typical feature, KFS is a complex disorder often involving multi-systemic anomalies, particularly involving the renal, cardiac, and central nervous systems. It may also be associated with spinal deformities such as scoliosis and Sprengel's deformity [3]. The prevalence is estimated to be around 1 in 40,000 to 42,000 live births; however, many cases likely remain undiagnosed or present later in life with secondary complications, including chronic pain, neurological deficits, or osteoarthritis due to biomechanical stress on adjacent hypermobile segments [4].

The diagnosis of KFS remains primarily clinical and radiological, with management focused on early identification of associated anomalies and prevention strategies of spinal cord injury [5]. Despite advances in understanding the genetic heterogeneity of KFS, the highly variable clinical presentation and potential for severe, life-altering comorbidities mean that each case offers valuable insights into its pathogenesis, optimal management strategies, and long-term outcomes [6]. This report details an incidental case of KFS, a rare spine condition that is often associated with other systemic anomalies, diagnosed during clinical and radiological evaluation for traumatic cervical spine injury.

Case presentation

A 60-year-old male presented to our facility six hours after a road traffic crash with posterior midline neck pain which radiated to both arms, was aggravated by movement and relieved by immobilization. He was an unhelmeted motorcycle rider who was hit from the rear by a fast moving vehicle. He fell off the motorcycle with immediate loss of consciousness which he fully regained about five minutes later. Upon regaining consciousness, he noted the onset of the neck pain. There were, however no motor, sensory or autonomic dysfunction. He had no headache, vomiting, seizures or history to suggest injuries to any other parts of the body. He was transported from the scene of the crash to our facility seated in a car without any form of neck immobilization.

Physical examination revealed a fully conscious middle-aged man with normal vital signs and an essentially normal neurological examination. Examination of the head and neck, however, showed brevicollis, a low posterior hair line and a restricted range of neck motion in all directions. He also had diffuse posterior midline neck tenderness. Both scapulae were normal in location and other regional examinations were unremarkable. A clinical diagnosis of mild traumatic brain

injury (concussion) with ASIA E cervical spine injury and suspected background Klippel-Feil syndrome was made. Further probing revealed a long-standing history of recurrent neck pain dating back to his teenage years. The patient, however, adduced the neck pain to repeated carrying of heavy objects on the head since childhood; hence he never sought medical attention.

Cervical spine X-ray showed a block cervical spine with complete fusion of the third to seventh cervical vertebrae with degenerative changes at the adjacent C2/C3 level. These changes included marginal osteophytes formation involving the inferior half of C2 and superior half of C3 in addition to a widened C2/C3 intervertebral disc space. The wasp-waist sign typically described in KFS, was also appreciated on the cervical spine X-ray – the sign refers to a reduced and smaller anteroposterior diameter at the affected levels relative to the diameter of the adjacent uninvolved discs and vertebrae (***Fig. 1A&B***).

The patient was managed non-operatively with analgesics and a rigid cervical spine collar. Further investigations, including a cervical spine CT scan or MRI and abdominopelvic ultrasound scan for a possible occult renal anomaly, were not done due to financial constraints. He was discharged home one week after the trauma with a rigid neck collar following resolution of neck pain and appropriate counseling regarding his condition, including the need to avoid high risk activities such as contact sports and possible sequelae i.e. neurologic deficits in the event of a recurrent cervical trauma. He has since been followed up in the outpatient clinic and remains neurologically intact.

Discussion

Also described as cervical vertebral fusion syndrome, Klippel-Feil syndrome (KFS) is a rare congenital condition with its hallmark being the non-segmentation or fusion of two or more cervical vertebrae [1]. Embryologically, the anomaly results from a failure of normal segmentation and differentiation of the cervical somites during the third to eighth weeks of embryogenesis [7]. Although mutations in the GDF6, GDF3, MEOX1, MYO18B, and RIPPLY2 genes have been implicated, the genetic basis remains uncertain [1]. Recent genetic analysis identified five rare variants (BAZ1B, FREM2, VANGL1, SUFU, and KMT2D) associated with cervical fusion in patients with KFS [1, 8]. The estimated incidence of KFS is about 1 in 40,000 live births, with a slight female preponderance [9]. However, the condition is often asymptomatic and may remain undiagnosed until adulthood [1]; this situation is mirrored in our case: a previously asymptomatic 60-year-old male incidentally diagnosed with KFS following a road traffic crash. Consequently, some literature suggests a significantly higher prevalence of this condition [10, 11].

The classic clinical triad of KFS - brevicollis, a low posterior hairline, and a limited cervical range of motion which was present in our patient is however only observed in about 50% of cases [12]. The absence of these overt physical signs in many patients contributes to the underdiagnosis in routine clinical practice. The clinical significance of KFS lies not only in the fusion itself but in the many other possible associated skeletal and non-skeletal anomalies, as well as the

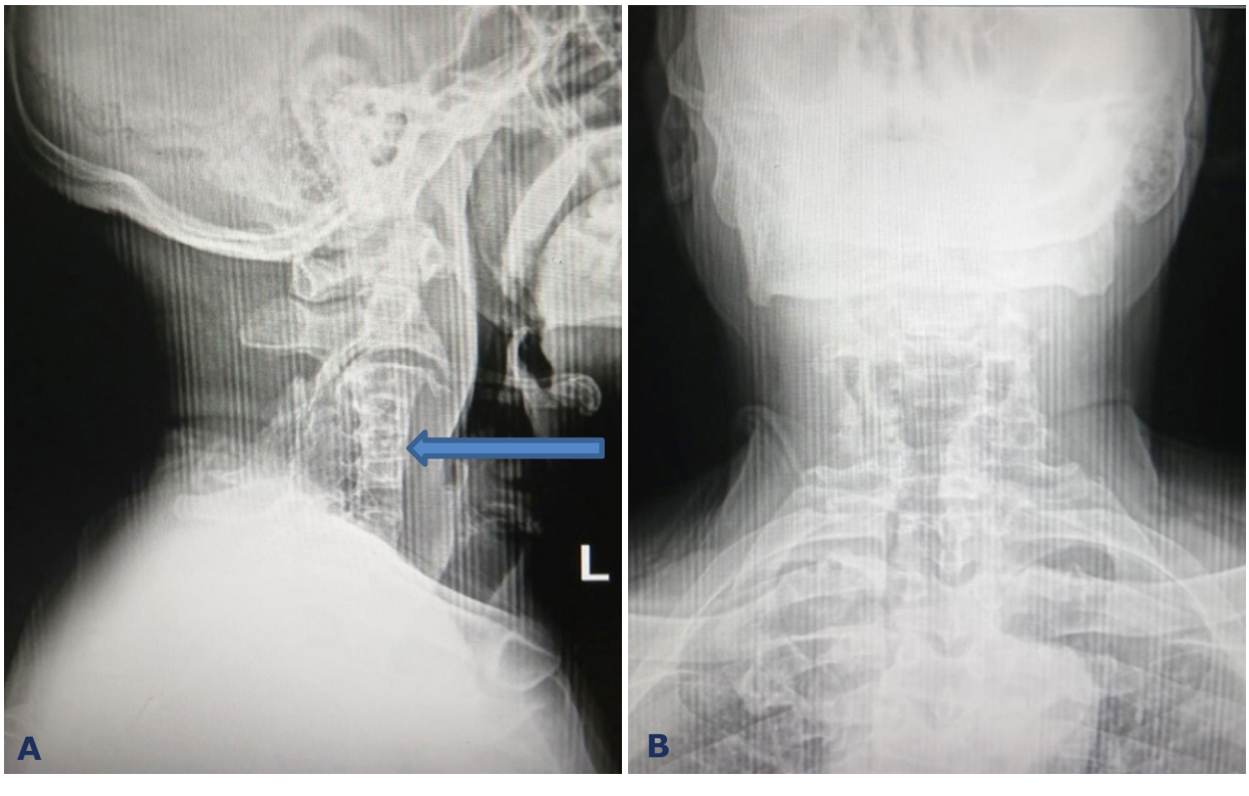

Fig. 1A & B. Cervical spine X-ray, lateral and antero-posterior views, showing a block cervical spine involving the entire subaxial cervical spine and the wasp-waist sign (blue arrow) as well as degenerative changes at the adjacent C2/3 level.

altered biomechanics of the spine [11]. The adjacent, non-fused segments are subjected to increased stress and compensatory hypermobility, leading to accelerated degenerative changes, disc herniation, spinal canal stenosis, and potential neurological deficits [13]. Some of these compensatory adjacent segment degenerative changes were observed on the cervical spine X-ray of our patient. These findings could have been evaluated in greater details using cervical spine MRI or CT scan; however finance was a major constraint in the full evaluation of this patient. Based on the pattern and number of fused segments on imaging, KFS can be classified into types I, II or III according to Samartzis *et al.* [14]. Type I KFS involves a single fused segment; type II KFS involves multiple non-contiguous fused segments, while type III KFS involves multiple contiguous fused segments [11]. The index case is a type III variant. This classification has implication on the clinical symptoms of patients with KFS. A single level cervical fusion (type I) does not increase the risk of developing limited cervical mobility, while patients with type II or III KFS are more likely to develop radiculopathy or myelopathy, as shown in a cohort study by Samartzis *et al*. involving 28 KFS patients followed over an eight-year period [14]. The patient's presentation following a road traffic crash underscores a critical risk in individuals with undiagnosed KFS: even a trivial trauma can result in significant neurological injury, such as myelopathy or quadriplegia, due to the underlying spinal abnormalities. This patient was quite fortunate to have remained neurologically intact despite having Samartzis type III KFS. Although our patient was intact neurologically, a cervical spine X-ray was performed as part of the standard trauma workup, leading to the incidental discovery of the condition. This emphasizes the importance of maintaining a high index of clinical suspicion for underlying congenital conditions in trauma cases, regardless of the patient's age or the apparent severity of the initial injury. For patients diagnosed with KFS, a comprehensive evaluation beyond the cervical spine is essential, as the syndrome may be associated with a wide spectrum of other anomalies [3, 5]. These can include renal agenesis or malformations (occurring in approximately 33% of cases), hearing impairment (around 30%), congenital heart defects (15-30%), Sprengel's deformity, and other craniospinal anomalies like Chiari malformations or spina bifida [3, 5].

While immediate management of this patient focused on the traumatic cervical spine injury, the incidental finding of KFS necessitated a broader workup for other co-existing anomalies, which may have previously gone undetected. This was not feasible due to financial constraints earlier alluded to. The differential diagnosis of KFS include syndromes such as VACTERL, Goldenhar, and Wildervanck which are often associated with multisystem anomalies such as renal, cardiac, auditory, and craniofacial defects in addition to cervical vertebral abnormalities [1].

Management of KFS is mostly conservative in asymptomatic individuals and focuses on lifestyle modifications, such as avoiding contact sports and high-risk activities that could lead to spinal cord injury [1]. The index patient was properly counseled prior to discharge from the hospital. Surgical intervention may be indicated in patients with persistent neurological pain, spinal instability, or progressive neurological deficits [1, 15]. This case highlights that KFS may remain clinically silent until adulthood, and an incidental detection warrants patient education on these inherent risks and a careful, comprehensive diagnostic workup to prevent future complications and optimize long-term outcomes.

Conclusion

This case of incidental KFS diagnosis in a 60-year-old man after a road traffic crash illustrates the hidden burden of this congenital condition. It also serves as a reminder for clinicians that KFS can present at any point during a lifetime and that a holistic evaluation and patient counseling are paramount to avoid future morbidity and mortality associated with the condition and its associated co-existing anomalies.

Disclosure

Ethics approval and consent to participate

Consent was obtained from the patient.

Competing interests

None declared

Funding

None

References

1. Kadiri SE, Bqaq IE, Qajia H, Izi Z, Chat L, Jiddane M, Touarsa F, Haddad SE. Klippel-Feil syndrome revealed by post-traumatic neck pain: Case report and literature review. Radiol Case Rep. 2025 Aug 23;20(11):5686-5690. doi: 10.1016/j.radcr.2025.07.056
2. Agarwal AK, Goel M, Bajpai J, Shukla S, Sachdeva N. Klippel Feil Syndrome: A Rare Case Report. J Orthop Case Rep. 2014 Jul-Sep;4(3):53-5. doi: 10.13107/jocr.2250-0685.197
3. Yadav D, Bhattarai A, Bhandari P, Danai A, Singh UK. Klippel-Feil Syndrome Associated with Renal and Cardiac Anomalies in an Infant: A Case Report. JNMA J Nepal Med Assoc. 2023 Oct 1;61(266):819-821. doi: 10.31729/jnma.8303
4. Frikha R. Klippel-Feil syndrome: a review of the literature. Clin Dysmorphol. 2020 Jan;29(1):35-37. doi: 10.1097/MCD.0000000000000301
5. Siddiqui F, Talal Ashraf M, Khuzzaim Khan M, Admani B, Sam SJ, Imran M, Hameed M. A Comprehensive Approach to the Diagnosis and Management of Klippel Feil Syndrome. Arch Razi Inst. 2023 Dec 30;78(6):1868-1872. doi: 10.32592/ARI.2023.78.6.1868
6. Tracy MR, Dormans JP, Kusumi K. Klippel-Feil syndrome: clinical features and current understanding of etiology. Clin Orthop Relat Res. 2004 Jul;(424):183-90.
7. Umamaheshwar KL, Sehrawat A, Parashar MK, Mavade K. Two case reports of an unusual association between Klippel-Feil syndrome and amyotrophic lateral sclerosis: Do they share same genetic defect? Ann Indian Acad Neurol. 2013 Oct;16(4):705-7. doi: 10.4103/0972-2327.120456
8. Li ZQ, Geng MZ, Zhao S, Wu ZH, Zhang JG, Wu N, Wang YP. [Clinical Characteristics and Genetic Analysis of Klippel-Feil Syndrome]. Zhongguo Yi Xue Ke Xue Yuan Xue Bao. 2021 Feb 28;43(1):25-31. Chinese. doi: 10.3881/j.issn.1000-503X.12629
9. Nouri A, Tetreault L, Zamorano JJ, Mohanty CB, Fehlings MG. Prevalence of Klippel-Feil Syndrome in a Surgical Series of Patients with Cervical Spondylotic Myelopathy: Analysis of the Prospective, Multicenter AOSpine North America Study. Global Spine J. 2015 Aug;5(4):294-9. doi: 10.1055/s-0035-1546817
10. Gruber J, Saleh A, Bakhsh W, Rubery PT, Mesfin A. The Prevalence of Klippel-Feil Syndrome: A Computed Tomography-Based Analysis of 2,917 Patients. Spine Deform. 2018 Jul-Aug;6(4):448-453. doi: 10.1016/j.jspd.2017.12.002

11. Moses JT, Williams DM, Rubery PT, Mesfin A. The prevalence of Klippel-Feil syndrome in pediatric patients: analysis of 831 CT scans. J Spine Surg. 2019 Mar;5(1):66-71. doi: 10.21037/jss.2019.01.02
12. Litrenta J, Bi AS, Dryer JW. Klippel-Feil Syndrome: Pathogenesis, Diagnosis, and Management. J Am Acad Orthop Surg. 2021 Nov 15;29(22):951-960. doi: 10.5435/JAAOS-D-21-00190
13. Reyes-Sánchez A, Zárate-Kalfópulos B, Rosales-Olivares LM. Adjacent segment disease in a patient with klippel-feil syndrome and radiculopathy: surgical treatment with two-level disc replacement. SAS J. 2007 Nov 1;1(4):131-4. doi: 10.1016/SASJ-2007-0114-CR
14. Samartzis DD, Herman J, Lubicky JP, Shen FH. Classification of congenitally fused cervical patterns in Klippel-Feil patients: epidemiology and role in the development of cervical spine-related symptoms. Spine (Phila Pa 1976). 2006 Oct 1;31(21):E798-804. doi: 10.1097/01.brs.0000239222.36505.46
15. Ding L, Wang X, Sun Y, Zhang F, Pan S, Chen X, Diao Y, Zhao Y, Xia T, Li W, Zhou F. Prevalence and Risk Factors of Surgical Treatment for Klippel-Feil Syndrome. Front Surg. 2022 Jun 7;9:885989. doi: 10.3389/fsurg.2022.885989

Case report

Ukrainian Neurosurgical Journal. 2026;32(2):97-104
doi: 10.25305/unj.342990

Illustrative case of acromegaly caused by sparsely granulated somatotroph adenoma

Prakash Mahantshetti [1], Nikhita Kalyanshetti [2], Chandan Miriyala [1]

[1] Department of Neurosurgery, Jawaharlal Nehru Medical College, Belagavi, Karnataka, India
[2] Department of Anesthesiology, Jawaharlal Nehru Medical College, Belagavi, Karnataka, India

Received: 06 November 2025
Accepted: 07 January 2026

Address for correspondence: *Chandan Miriyala, Department of Neurosurgery, J.N. Medical College, Nehru Nagar, Belagavi, Karnataka, 590010, India, email: dr.chandan.miriyala@gmail.com*

Background: Acromegaly arises from excessive growth hormone (GH) secretion, most often due to a pituitary adenoma. The disorder is typically indolent and may remain undiagnosed until mass-effect symptoms occur. Histological subtype, particularly the granulation pattern, influences clinical behavior and treatment response.

Case description: We describe the case of a 52-year-old man who presented with a two-year history of progressive enlargement of his hands and feet, facial coarsening, and recent-onset headache with visual blurring. Physical examination revealed classical acromegalic features and mild bitemporal hemianopia. Serum GH was markedly elevated (50 ng/mL) with other pituitary hormones within normal limits. MRI demonstrated a contrast-enhancing sellar–suprasellar lesion compressing the optic chiasm. The patient underwent endoscopic transnasal transsphenoidal excision of the mass. Histopathology confirmed a sparsely granulated somatotroph adenoma positive for PIT-1 and GH. Postoperative recovery was uneventful.

Conclusion: Sparsely granulated somatotroph adenomas exhibit greater invasiveness and reduced medical responsiveness than densely granulated variants. Early diagnosis and timely surgical resection remain crucial for visual preservation and endocrine control.

Keywords: *acromegaly; growth hormone; pituitary macroadenoma; sparsely granulated somatotroph adenoma; endoscopic transsphenoidal surgery*

Introduction

Pituitary adenomas account for approximately 10–15% of all primary brain neoplasms and are among the most common intracranial tumours. Growth hormone (GH)-secreting adenomas make up roughly 6–14% of these lesions and they usually exhibit the clinical condition of acromegaly, which is marked by systemic problems, coarse facial alterations, and gradual expansion of acral regions. Based on immunohistochemistry and electron microscopy, somatotroph adenomas are divided into two types: sparsely granulated somatotroph adenomas (SGSAs), which are far less common, and densely granulated somatotroph adenomas (DGSAs).

SGSAs are recognised for their more aggressive biological behaviour in contrast to DGSAs, which are generally smaller, less invasive, and show a positive response to first-line somatostatin analogues. They frequently have a higher proliferative index, are larger at presentation, and show expansion of the suprasellar or cavernous sinuses. Their characteristic histology includes sparse secretory granules and fibrous structures that are cytokeratin-positive. In terms of immunohistochemistry, SGSAs are often negative for other anterior pituitary hormones but positive for PIT-1 and growth hormone. They are less responsive to standard treatment with octreotide, likely because they exhibit differential somatostatin receptor expression, primarily SSTR5 over SSTR2.

Differentiating between SGSA and DGSA is uncommon, but it has significant clinical implications since it affects prognosis, treatment plans, and long-term follow-up procedures. Headaches, vision field impairments, and the possibility of hypopituitarism are among the major mass effects of macroadenomas that frequently result from delayed diagnosis. Although, SGSAs are linked to increased recurrence rates, necessitating careful, ongoing multidisciplinary therapy that includes oncology, neurosurgery, endocrinology, and pathology specialists.

In this report, we describe the case of a 52-year-old man with a sellar–suprasellar pituitary macroadenoma, sparsely granulated somatotroph adenoma histology, and characteristic acromegaly symptoms. By reviewing the pertinent literature and presenting this case, we aim to highlight the diagnostic challenges, pathological characteristics, and therapeutic implications of SGSAs. Acromegaly arises from sustained overproduction of GH, typically caused by a pituitary somatotroph adenoma. The disorder progresses slowly, often remaining undiagnosed for years until the development of coarse facial features, acral hypertrophy, or symptoms related to local tumor expansion. Pituitary macroadenomas may compress the optic chiasm, resulting in visual field deficits, and can impair pituitary function through mass effect.

Among GH-producing adenomas, the sparsely granulated subtype is recognized for its relatively rapid growth, invasiveness, and reduced responsiveness to medical therapy. We describe a case of such a tumor presenting with characteristic acromegalic changes and early visual field involvement, managed surgically via an endoscopic transsphenoidal approach.

Case report

A 52-year-old man presented with a two-year history of progressive enlargement of both hands and feet, accompanied by facial broadening and mandibular prominence. Over the preceding two months, he had developed intermittent headaches and gradually progressive blurring of vision. There was no history of trauma, fever, or systemic illness.

Clinical examination

The patient was well built and well nourished. Vital parameters were within normal limits (BP 130/80 mm Hg, HR 54/min, SpO_2 96% on room air). Facial examination revealed coarse features with frontal bossing, thickened lips and nose, prognathism, and macroglossia. Both hands and feet were enlarged with widened soft tissues (***Fig. 1***). There was no pallor, lymphadenopathy, or peripheral edema.

Neurological examination showed the patient to be alert and oriented with normal higher mental functions. Cranial nerve assessment revealed mild bitemporal hemianopia on perimetry. Pupils were equal and reactive to light; the remaining cranial nerves were intact, and motor strength was normal in all limbs. Systemic examination was otherwise unremarkable.

Investigations

1. Routine hematological and biochemical investigations were within reference limits.

2. Hormonal evaluation:

- Growth Hormone: 50 ng/mL (markedly elevated)
- Insulin like Growth Factor 1 (IGF-1): 650.5 ng/mL
- ACTH, Cortisol, TSH, T3/T4, prolactin, LH, FSH, and testosterone: within normal limits.

3. Magnetic Resonance Imaging:

MRI of the sellar region demonstrated a T1-hypointense, T2-hyperintense, contrast-enhancing mass involving the sella turcica with suprasellar extension compressing the optic chiasm and the cavernous sinus (***Fig. 2***). Imaging findings were consistent with a pituitary macroadenoma abutting over the carotid artery with the cavernous sinus. According to the modified Knosp classification the lesion was graded as 3 A.

Surgical management

The patient underwent endoscopic trans-nasal trans-sphenoidal resection of the tumor (***Fig. 3***). Intraoperatively, the mass appeared soft, greyish-pink, and moderately vascular. Gross total excision was achieved without complications. Postoperative recovery was uneventful, with gradual improvement in headache and visual symptoms.

Postoperative investigations

1. Routine hematological and biochemical investigations were within normal limits.

2. Hormonal evaluation:

- Growth Hormone: 32.5 ng/mL (markedly elevated)
- Insulin like Growth Factor-1 (IGF-1)– 1: 550ng/mL
- Cortisol – 4.4 µg/dL
- TSH, T3/T4, prolactin, LH, FSH, and testosterone: within normal limits.

Postoperative imaging

Postoperative day 4 CT Brain Plain: postoperative sellar hematoma and pneumocephalus with postoperative changes in the sellar region in brain parenchyma (***Fig. 4***).

Follow-up investigations (4 months postoperatively)

1. Routine hematological and biochemical investigations were within normal limits.

2. Hormonal evaluation:

- Growth Hormone: 26.80 ng/mL (markedly elevated)
- Insulin like Growth Factor – 1 (IGF-1): 400 ng/mL
- Cortisol – 5.26 µg/dL
- TSH, T3/T4, prolactin, LH, FSH, and testosterone: within normal limits.

Fig. 1. Acromegalic features of the patient

Note. Photographs were obtained with the patient's informed consent.

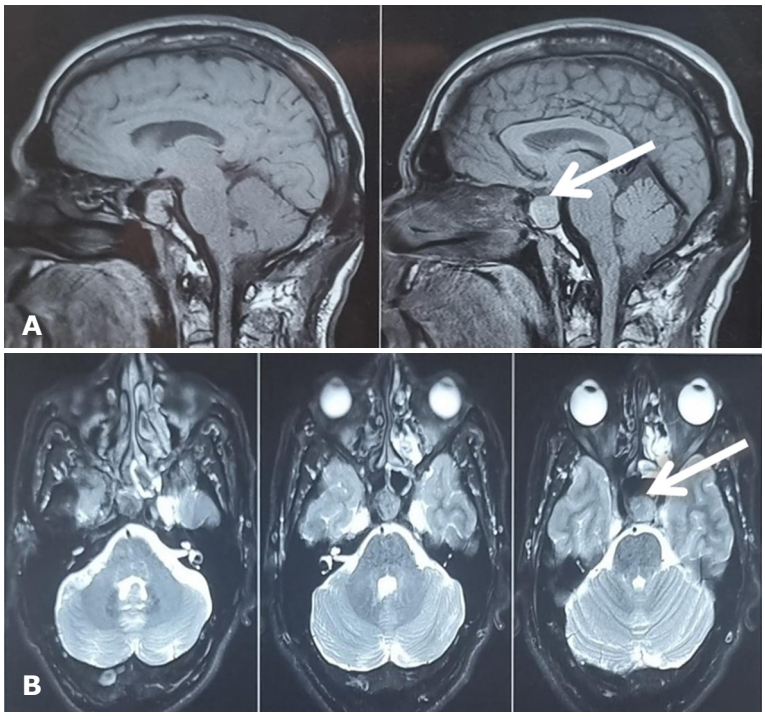

Fig. 2. Contrast enhancing suprasellar lesion suggestive of pituitary macroadenoma: sagittal (A) and axial (B) projections

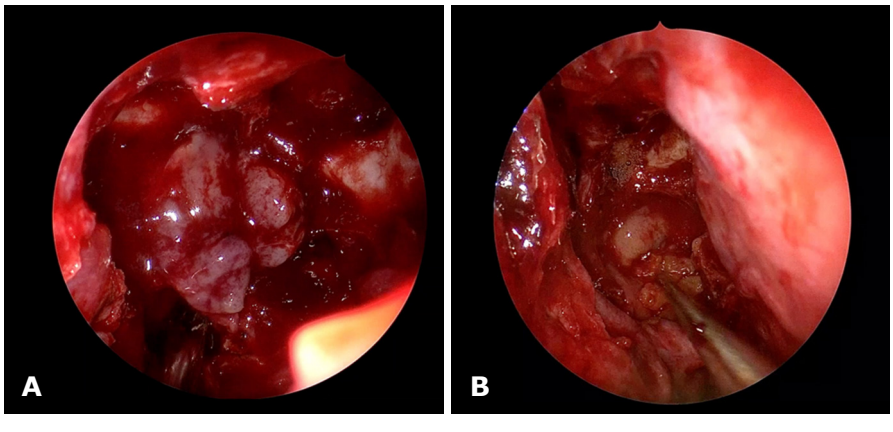

Fig. 3. Intraoperative images. A – Intraoperative pituitary tumor resection, B – Sellar Region after pituitary tumor resection reconstructed with Haddad Flap and supportive tissue with topical haemostatic agents

The patient remained clinically stable from the first postoperative day onward and follow – up imaging was subsequently performed.

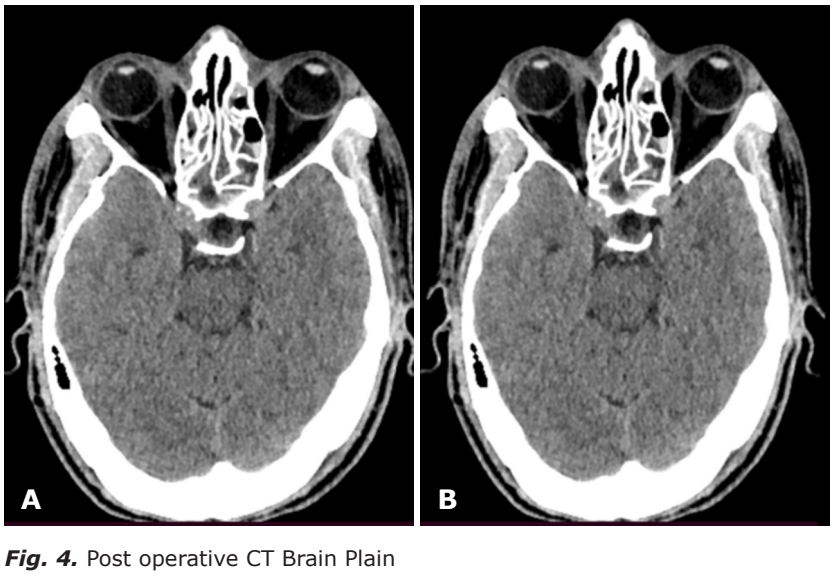

Fig. 4. Post operative CT Brain Plain

Magnetic Resonance Imaging (4 months postoperatively)

MRI of the sellar region demonstrated a T1-hypointense, T2-hyperintense, contrast-enhancing mass of 6mm. Imaging findings were consistent with residual pituitary macroadenoma (***Fig. 5***).

Histopathology and immunohistochemistry

Histopathological evaluation reported by NIMHANS, Bangalore. Microscopic examination revealed a pituitary adenoma composed of uniform cells arranged in sheets, nodules, and organoid nests. The tumor cells exhibited round-to-oval nuclei with stippled chromatin and moderate eosinophilic cytoplasm. Numerous paranuclear eosinophilic inclusions (fibrous bodies), characteristic of the sparsely granulated somatotroph subtype were noted. Mitotic figures were rare, and foci of vascular congestion and hemorrhage were present (***Fig. 6***).

Immunohistochemical profile
- Cytokeratin (CK): highlights many fibrous bodies

Transcription factor
- PIT-1: positive
- T-PIT and SF-1: negative

Pituitary hormones
- GH: positive
- PRL, ACTH, TSH, LH, FSH: negative

Ki-67 MIB-1 labelling index 3-4%

Final Diagnosis: Sparsely granulated somatotroph adenoma (GH-secreting pituitary macroadenoma)

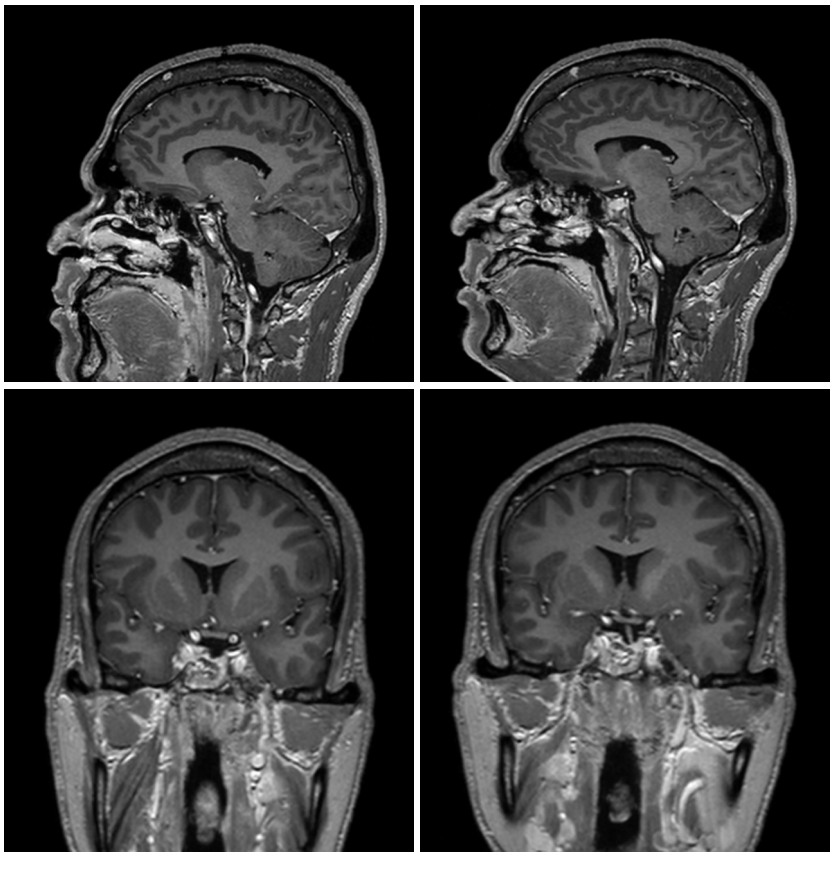

Fig. 5. Postoperative MRI brain with contrast: sagittal (A) and frontal (B) projections

GH – IHC Positive

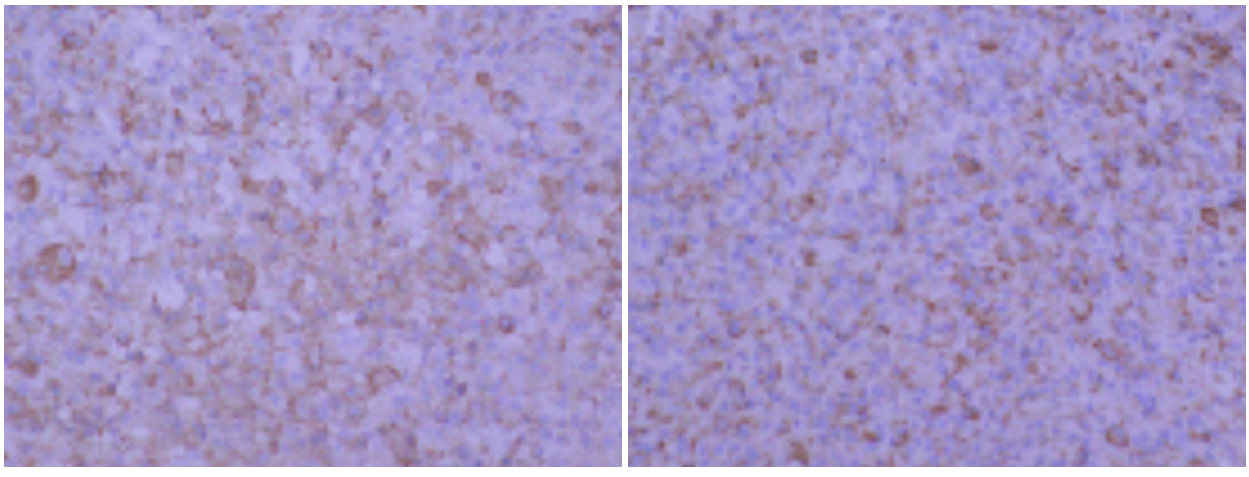

Pit1 – IHC x 100 Positive

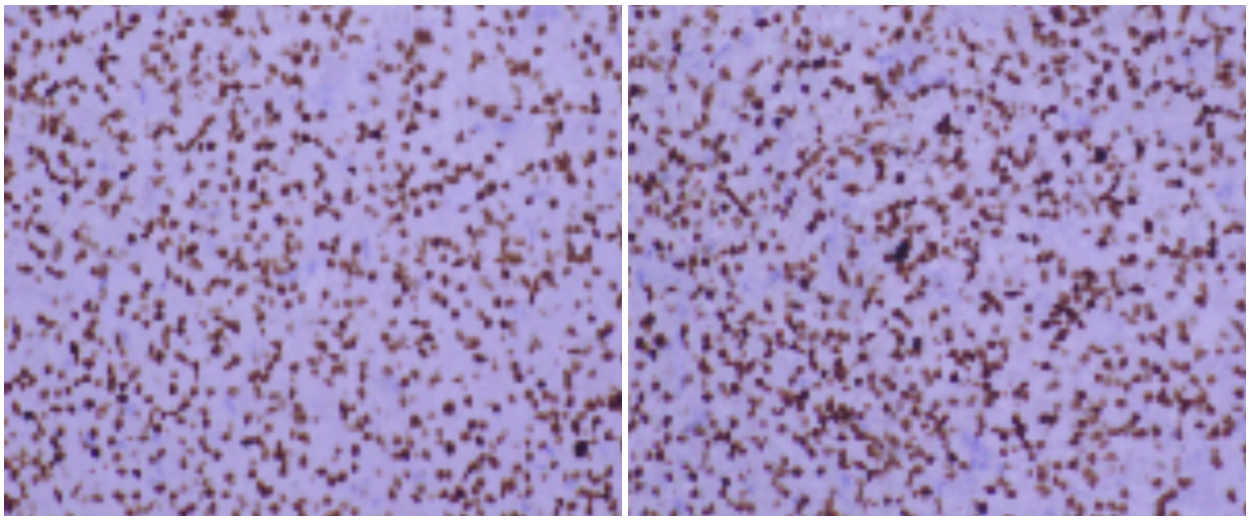

H & E x 200

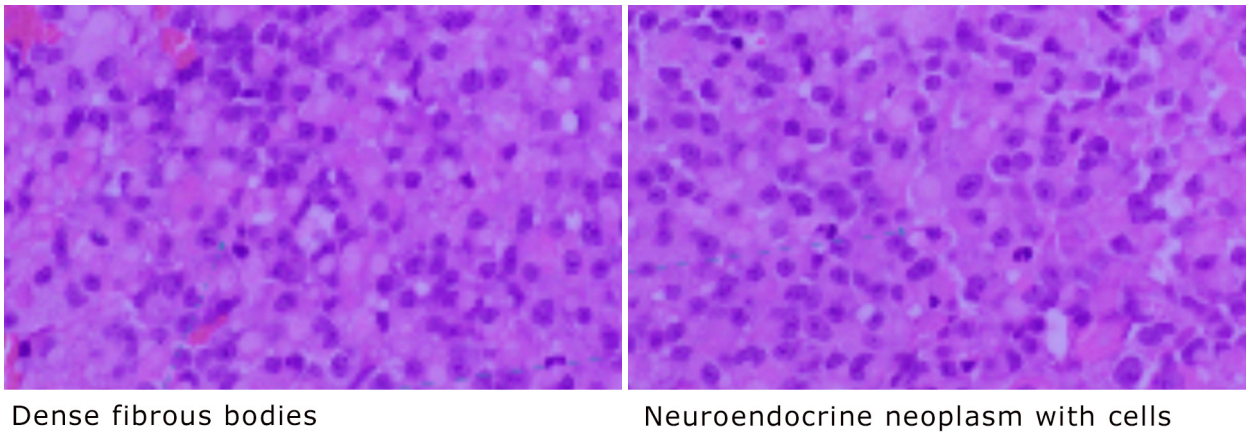

Dense fibrous bodies

Neuroendocrine neoplasm with cells arranged in sheets and vague nodules and sinusoidal pattern

Fig. 6. Histopathological and immunohistochemical findings

Discussion

Pituitary adenomas account for approximately 10–15% of all intracranial tumors; among these, GH-secreting adenomas represent 6–14% of cases. Based on their granulation patterns, somatotroph adenomas—the second most frequent pituitary neuroendocrine tumors [1, 2]—can be divided into two subtypes:

1. Sparsely granulated somatotroph adenomas (SGSAs) and

2. Densely granulated somatotroph adenomas (DGSAs).

Prevalence: A small percentage of all somatotroph tumours are sparsely granulated somatotroph adenomas, which are regarded as a more invasive and high-risk subtype [3-5].

Histopathology: Histologically, SGSAs are defined by chromophobic, poorly cohesive cells that are grouped in sheets or nests. They also often include paranuclear fibrous structures and light eosinophilic cytoplasm. On the other hand, DGSAs typically exhibit diffuse GH immunostaining and acidophilic cytoplasm [3, 6, 7].

In contrast to DGSAs, SGSAs exhibit lower rates of *GNAS* mutations and are PIT-1 positive immunohistochemically [8-10].

Sparsely granulated tumors are characterized by increased proliferative and invasive capacity, typically reflected in a higher Ki-67 (MIB-1) labelling index [9, 11-14].

PIT-1 positivity is a defining feature, whereas T-PIT and SF-1 are negative, aligning with somatotroph cell lineage.

The rare and distinct subtype of growth hormone (GH)-secreting pituitary adenomas known as sparsely granulated somatotroph adenomas (SGSAs) is distinguished by histological, and IHC markers. These tumours frequently pose diagnostic and therapeutic challenges because they are more aggressive, respond poorly to standard treatment, and recur more frequently than densely granulated somatotroph adenomas. [15-17].

Clinically, the present case is consistent with the typical acromegalic characteristics of SGSAs, including gradual acral enlargement, facial deformity, and related symptoms such as headaches and visual field abnormalities, especially bitemporal hemianopia caused by chiasmal compression. The pituitary aetiology was further reinforced by the absence of other systemic disorders and the lack of diurnal change in headache. Our patient's increased GH level (GH = 50 ng/mL) matched the clinical severity. Hypopituitarism, which is sometimes seen in large macroadenomas, or a plurihormonal adenoma were ruled out by the normal levels of other pituitary hormones.

Histopathologically, sparse secretory granules and paranuclear fibrous bodies distinguish SGSAs from densely granulated somatotroph adenomas. In the present case, cytokeratin (CK) immunostaining highlighted the fibrous bodies. By showing positive expression of GH and PIT-1 transcription factors and negative expression of other anterior pituitary hormones and transcription factors (TPIT, SF-1) [18-20], immunohistochemical staining was able to identify SGSAs. A stronger proliferative potential is indicated by a raised Ki-67 (MIB-1) labelling index of 3–4%, which is associated with a higher likelihood of aggressive behaviour and recurrence [21, 22].

From a therapeutic perspective, the main treatment for SGSAs is surgical resection using the transsphenoidal technique, which aims for gross complete excision while maintaining endocrine and neurological function. Surgery alone, however, is frequently insufficient due to the aggressive nature of these adenomas and the prevalence of partial resections. Owing to lesser somatostatin receptor subtype 2 (SSTR2) expression compared with densely granulated versions, adjuvant therapies such as radiation and medical therapy with somatostatin analogues show varied efficacy in SGSAs and result in lower response rates. Temozolomide is one of the novel medicines and chemotherapeutics that have shown promise in aggressive and resistant cases. Therefore, to maximise results and create customised treatment regimens, multidisciplinary strategy comprising endocrinologists, neurosurgeons, radiation oncologists, pathologists, and molecular geneticists is crucial [23-27].

Regular hormonal, clinical, and radiological follow-up is necessary because of the observed high recurrence rates, particularly in tumours with higher Ki-67 indices and inadequate resection. Timely intervention improves the prognosis when recurrence or residual disease is identified early [28, 29].

Research by Petersenn *et al*. has shown that SGSAs occur more frequently in patients under 40 years of age. Our male patient is the minority group within an already uncommon tumour subtype, despite the literature suggesting a slight female prevalence in SGSAs. SGSAs may paradoxically exhibit worse biochemical reactions to medical therapy than DGSAs, despite the fact that they frequently present with elevated GH levels because of their bigger size at diagnosis. SGSAs are less susceptible to traditional somatostatin analogues owing to their distinct somatostatin receptor expression patterns, characterized by a more frequent expression of SSTR5 than SSTR2 [30].

The mainstay of treatment for pituitary macroadenomas remains surgical excision via transsphenoidal approach. However, due to their invasive nature, SGSAs require multimodal management, including repeat surgery, radiotherapy, and advanced medical therapy with newer somatostatin analogues or temozolomide in refractory cases [8, 9, 31, 32]. Long-term monitoring is mandatory because of the high risk of recurrence, particularly in tumors with elevated Ki-67 index [11, 12].

Importance of Multidisciplinary Management

The rarity and aggressiveness of SGSAs demand an individualized, multidisciplinary approach encompassing endocrinology, neurosurgery, pathology, radiation oncology, and molecular genetics for optimal long-term outcomes [8, 9, 33].

Conclusion

In conclusion, we report a rare case of a sparsely granulated somatotroph pituitary macroadenoma presenting with progressive acral enlargement and visual field impairment. Prompt recognition of acromegaly and timely surgical intervention are critical to prevent

irreversible visual loss and systemic complications. Histopathological characterization is essential for predicting tumor behavior and guiding postoperative management.

SGSAs represent an uncommon and clinically challenging subset of growth-hormone secreting pituitary adenomas, with unique pathological and clinical features. Comprehensive multimodal management and careful long-term follow-up are essential to optimise patient outcomes and minimise morbidity.

Disclosure

Conflict of interest

The authors declare no conflict of interest.

Informed consent

Informed consent was obtained from the patient.

References

1. Vuong HG, Dunn IF. Clinical and prognostic significance of granulation patterns in somatotroph adenomas/tumors of the pituitary: a meta-analysis. Pituitary. 2023 Dec ;26(6):653-659. doi: 10.1007/s11102-023-01353-0
2. Larkin S, Ansorge O. Pathology And Pathogenesis Of Pituitary Adenomas And Other Sellar Lesions. 2017 Feb 15. In: Feingold KR, Adler RA, Ahmed SF, Anawalt B, Blackman MR, Chrousos G, Corpas E, de Herder WW, Dhatariya K, Dungan K, Hamilton E, Hofland J, Jan de Beur S, Kalra S, Kaltsas G, Kapoor N, Kim M, Koch C, Kopp P, Korbonits M, Kovacs CS, Kuohung W, Laferrère B, Levy M, McGee EA, McLachlan R, Muzumdar R, Purnell J, Rey R, Sahay R, Shah AS, Sperling MA, Stratakis CA, Trence DL, Wilson DP, editors. Endotext [Internet]. South Dartmouth (MA): MDText.com, Inc.; 2000–.
3. Cuevas-Ramos D, Fleseriu M. Pasireotide: a novel treatment for patients with acromegaly. Drug Des Devel Ther. 2016 Jan 11;10:227-39. doi: 10.2147/DDDT.S77999
4. Asa SL, Ezzat S. The cytogenesis and pathogenesis of pituitary adenomas. Endocr Rev. 1998 Dec;19(6):798-827. doi: 10.1210/edrv.19.6.0350
5. Roelfsema F, van den Berg G. Diagnosis, treatment and clinical perspectives of acromegaly. Expert Rev Endocrinol Metab. 2015 Nov;10(6):619-644. doi: 10.1586/17446651.2015.1096770
6. Gliga MC, Tătăranu LG, Popescu M, Chinezu L, Paşcanu MI. Immunohistochemical evaluation of biomarkers with predictive role in acromegaly: a literature review. Rom J Morphol Embryol. 2023 Jan-Mar;64(1):25-33. doi: 10.47162/RJME.64.1.03
7. Akirov A, Asa SL, Amer L, Shimon I, Ezzat S. The Clinicopathological Spectrum of Acromegaly. J Clin Med. 2019 Nov 13;8(11):1962. doi: 10.3390/jcm8111962
8. Jallad RS, Bronstein MD. Acromegaly in the elderly patient. Arch Endocrinol Metab. 2019 Nov-Dec;63(6):638-645. doi: 10.20945/2359-3997000000194
9. Mayr B, Buslei R, Theodoropoulou M, Stalla GK, Buchfelder M, Schöfl C. Molecular and functional properties of densely and sparsely granulated GH-producing pituitary adenomas. Eur J Endocrinol. 2013 Sep 12;169(4):391-400. doi: 10.1530/EJE-13-0134
10. Swanson AA, Erickson D, Donegan DM, Jenkins SM, Van Gompel JJ, Atkinson JLD, Erickson BJ, Giannini C. Clinical, biological, radiological, and pathological comparison of sparsely and densely granulated somatotroph adenomas: a single center experience from a cohort of 131 patients with acromegaly. Pituitary. 2021 Apr;24(2):192-206. doi: 10.1007/s11102-020-01096-2
11. Trouillas J, Roy P, Sturm N, Dantony E, Cortet-Rudelli C, Viennet G, Bonneville JF, Assaker R, Auger C, Brue T, Cornelius A, Dufour H, Jouanneau E, François P, Galland F, Mougel F, Chapuis F, Villeneuve L, Maurage CA, Figarella-Branger D, Raverot G; members of HYPOPRONOS; Barlier A, Bernier M, Bonnet F, Borson-Chazot F, Brassier G, Caulet-Maugendre S, Chabre O, Chanson P, Cottier JF, Delemer B, Delgrange E, Di Tommaso L, Eimer S, Gaillard S, Jan M, Girard JJ, Lapras V, Loiseau H, Passagia JG, Patey M, Penfornis A, Poirier JY, Perrin G, Tabarin A. A new prognostic clinicopathological classification of pituitary adenomas: a multicentric case-control study of 410 patients with 8 years post-operative follow-up. Acta Neuropathol. 2013 Jul;126(1):123-35. doi: 10.1007/s00401-013-1084-y
12. Bhayana S, Booth GL, Asa SL, Kovacs K, Ezzat S. The implication of somatotroph adenoma phenotype to somatostatin analog responsiveness in acromegaly. J Clin Endocrinol Metab. 2005 Nov;90(11):6290-5. doi: 10.1210/jc.2005-0998
13. Rass L, Rahvar AH, Matschke J, Saeger W, Renné T, Aberle J, Flitsch J, Rotermund R. Differences in somatostatin receptor subtype expression in patients with acromegaly: new directions for targeted therapy? Hormones (Athens). 2022 Mar;21(1):79-89. doi: 10.1007/s42000-021-00327-w
14. Paek KI, Kim SH, Song SH, Choi SW, Koh HS, Youm JY, Kim Y. Clinical significance of Ki-67 labeling index in pituitary macroadenoma. J Korean Med Sci. 2005 Jun;20(3):489-94. doi: 10.3346/jkms.2005.20.3.489
15. Asa SL, Ezzat S. The pathogenesis of pituitary tumors. Annu Rev Pathol. 2009;4:97-126. doi: 10.1146/annurev.pathol.4.110807.092259
16. Chiloiro S, Giampietro A, Migliore R, Palumbo C, Giambò P, Costanza F, Mattogno PP, Calandrelli R, Tartaglione T, Lauretti L, Rigante M, Gessi M, Gaudino S, De Marinis L, Bianchi A, Doglietto F, Pontecorvi A. The clinicopathological PANOMEN-3 classification predicts pituitary adenoma prognosis: a real-world retrospective single center study of a surgically treated cohort. Pituitary. 2025 Sep 7;28(5):97. doi: 10.1007/s11102-025-01562-9
17. Melmed S. Acromegaly pathogenesis and treatment. J Clin Invest. 2009 Nov;119(11):3189-202. doi: 10.1172/JCI39375
18. Lloyd RV. Molecular pathology of pituitary adenomas. J Neurooncol. 2001 Sep;54(2):111-9. doi: 10.1023/a:1012940929072
19. Kontogeorgos G. Classification and pathology of pituitary tumors. Endocrine. 2005 Oct;28(1):27-35. doi: 10.1385/ENDO:28:1:027
20. Asa SL, Mete O. Cytokeratin profiles in pituitary neuroendocrine tumors. Hum Pathol. 2021 Jan;107:87-95. doi: 10.1016/j.humpath.2020.10.004
21. Fusco A, Zatelli MC, Bianchi A, Cimino V, Tilaro L, Veltri F, Angelini F, Lauriola L, Vellone V, Doglietto F, Ambrosio MR, Maira G, Giustina A, degli Uberti EC, Pontecorvi A, De Marinis L. Prognostic significance of the Ki-67 labeling index in growth hormone-secreting pituitary adenomas. J Clin Endocrinol Metab. 2008 Jul;93(7):2746-50. doi: 10.1210/jc.2008-0126
22. Mastronardi L, Guiducci A, Puzzilli F. Lack of correlation between Ki-67 labelling index and tumor size of anterior pituitary adenomas. BMC Cancer. 2001;1:12. doi: 10.1186/1471-2407-1-12
23. Khan DZ, Hanrahan JG, Baldeweg SE, Dorward NL, Stoyanov D, Marcus HJ. Current and Future Advances in Surgical Therapy for Pituitary Adenoma. Endocr Rev. 2023 Sep 15;44(5):947-959. doi: 10.1210/endrev/bnad014
24. Darwish H, El-Hadi U, Haddad G, Najjar M. Management of Pituitary Adenomas: Mononostril Endoscopic Transsphenoidal Surgery. Basic Clin Neurosci. 2018 Mar-Apr;9(2):121-128. doi: 10.29252/nirp.bcn.9.2.121
25. Nista F, Corica G, Castelletti L, Khorrami K, Campana C, Cocchiara F, Zoppoli G, Prior A, Rossi DC, Zona G, Ferone D, Gatto F. Clinical and Radiological Predictors of Biochemical Response to First-Line Treatment With Somatostatin Receptor Ligands in Acromegaly: A Real-Life Perspective. Front Endocrinol (Lausanne). 2021 May 7;12:677919. doi: 10.3389/fendo.2021.677919
26. Ionovici N, Carsote M, Terzea DC, Predescu AM, Rauten AM, Popescu M. Somatostatin receptors in normal and acromegalic somatotroph cells: the U-turn of the clinician to immunohistochemistry report - a review. Rom J Morphol Embryol. 2020 Apr-Jun;61(2):353-359. doi: 10.47162/RJME.61.2.05
27. McCormack A. Temozolomide in aggressive pituitary tumours and pituitary carcinomas. Best Pract Res Clin Endocrinol Metab. 2022 Dec;36(6):101713. doi: 10.1016/j.beem.2022.101713

28. Bianchi A, Chiloiro S, Giampietro A, Gaudino S, Calandrelli R, Mazzarella C, Caldarella C, Rigante M, Gessi M, Lauretti L, De Marinis L, Olivi A, Pontecorvi A, Doglietto F. Multidisciplinary management of difficult/aggressive growth-hormone pituitary neuro-endocrine tumors. Front Endocrinol (Lausanne). 2023 May 3;14:1123267. doi: 10.3389/fendo.2023.1123267
29. Guo X, Zhang R, Zhang D, Wang Z, Gao L, Yao Y, Deng K, Bao X, Feng M, Xu Z, Yang Y, Lian W, Wang R, Ma W, Xing B. Determinants of immediate and long-term remission after initial transsphenoidal surgery for acromegaly and outcome patterns during follow-up: a longitudinal study on 659 patients. J Neurosurg. 2022 Jan 14;137(3):618-628. doi: 10.3171/2021.11.JNS212137
30. Brzana J, Yedinak CG, Gultekin SH, Delashaw JB, Fleseriu M. Growth hormone granulation pattern and somatostatin receptor subtype 2A correlate with postoperative somatostatin receptor ligand response in acromegaly: a large single center experience. Pituitary. 2013 Dec;16(4):490-8. doi: 10.1007/s11102-012-0445-1
31. Asa SL, Mete O, Perry A, Osamura RY. Overview of the 2022 WHO Classification of Pituitary Tumors. Endocr Pathol. 2022 Mar;33(1):6-26. doi: 10.1007/s12022-022-09703-7
32. Mercado M, Melgar V, Salame L, Cuenca D. Clinically non-functioning pituitary adenomas: Pathogenic, diagnostic and therapeutic aspects. Endocrinol Diabetes Nutr. 2017 Aug-Sep;64(7):384-395. English, Spanish. doi: 10.1016/j.endinu.2017.05.009
33. Mete O, Alshaikh OM, Cintosun A, Ezzat S, Asa SL. Synchronous Multiple Pituitary Neuroendocrine Tumors of Different Cell Lineages. Endocr Pathol. 2018 Dec;29(4):332-338. doi: 10.1007/s12022-018-9545-4

Case report

Ukrainian Neurosurgical Journal. 2026;32(2):105-111
doi: 10.25305/unj.344728

Single-Stage Salvage for Recurrent Carpal Tunnel Syndrome and Delayed Guyon's Canal Syndrome Following Open Release: A Case Report

Nhat D. H. Nguyen [1,2], Huy A. Pham [3], Phi D. Nguyen [4]

[1] Center of Orthopedic and Plastic Surgery, Hue Central Hospital, Hue city, Vietnam
[2] Biomedical Engineering Department, National Cheng Kung University, Tainan, Taiwan
[3] Division of Surgery, Hue University of Medicine and Pharmacy, Hue city, Vietnam
[4] Department of Orthopaedic - Burn - Plastic Surgery, City Children's Hospital, Tan Kien Ward, Binh Chanh District, Ho Chi Minh city, Vietnam

Received: 28 November 2025
Accepted: 26 January 2026

Address for correspondence*:*
Nhat D. H. Nguyen, Center of Orthopedic and Plastic Surgery, Hue Central Hospital, 16 Le Loi street, Hue city, 490000, Vietnam, email: nguyendanghuynhat@gmail.com

Introduction: Recurrent carpal tunnel syndrome (CTS) is commonly attributed to incomplete decompression or perineural scarring. However, delayed-onset ulnar nerve compression at Guyon's canal after carpal tunnel release (CTR) is extremely rare and presents diagnostic and therapeutic challenges.

Case report: We report the case of a 50-year-old man who developed dual neuropathies, recurrent median nerve compression, and new-onset ulnar nerve entrapment, approximately one year after open CTR. He presented with diffuse hand paresthesia, weakness, ulnar digit clawing, and impaired thumb opposition. Electrodiagnostic studies revealed severe axonal damage in both the median and ulnar nerves. Surgical intervention was performed via a single palmar incision, including dual nerve decompression, epineurolysis, hypothenar fat pad grafting, and opponensplasty using the extensor indicis proprius (EIP) tendon. At one-year follow-up, the patient demonstrated full sensory recovery, regained thumb opposition, improved grip and pinch strength, and no recurrence of symptoms.

Conclusion: This case highlights the importance of comprehensive clinical and electrodiagnostic reassessment in patients with recurrent or evolving symptoms after CTR. A single-stage, integrated surgical approach may constitute a viable management option in carefully selected patients with complex dual nerve entrapments and is presented as an illustrative example for comparable challenging clinical situations.

Keywords: *carpal tunnel syndrome; case report; Guyon's canal; median nerve; ulnar nerve*

Introduction

As the leading compression neuropathy, carpal tunnel syndrome (CTS) stems from pressure on the median nerve at the wrist, producing symptoms such as paresthesia, sensory loss, and hand weakness. While the etiology is often idiopathic, the condition is frequently linked to repetitive wrist use [1, 2]. Carpal tunnel release (CTR) remains the standard treatment, with open surgery considered the gold standard. Although endoscopic methods may allow for faster recovery, they carry higher technical demands and potential risks. Recurrence affects 3–25% of cases, often attributable to incomplete release, perineural scarring, or underlying conditions such as cervical radiculopathy or diabetic neuropathy. Persistent or recurrent cases may require revision surgery or opponensplasty to restore function [3, 4].

Ulnar neuropathy at Guyon's canal is a distinct nerve compression of the wrist. It is less common than CTS but can cause significant motor, sensory, or mixed deficits depending on the specific site of compression. Etiologies typically include ganglions, vascular abnormalities, trauma, osteoarthritis, and congenital anomalies. Notably, the development of ulnar nerve complications after CTR is rare and has historically been associated with endoscopic techniques rather than open surgery [5, 6].

This case presents a rare combination of recurrent CTS and delayed-onset ulnar nerve compression at Guyon's canal following an open CTR. While recurrent CTS is frequently documented in relation to incomplete release or fibrosis, secondary ulnar neuropathy remains uncommon and underreported. This dual entrapment highlights the necessity for meticulous evaluation and extended follow-up in patients presenting with persistent or evolving symptoms after carpal tunnel release.

Case report

A 50-year-old right-handed man developed worsening right-hand weakness, numbness, and ulnar-sided clawing one year after open CTR for median nerve compression. Initially, thenar atrophy was present, but ulnar nerve function remained intact. Postoperatively, median nerve symptoms improved except for weak thumb opposition. After 12 months, new paresthesia involving all digits and increasing weakness, particularly in the ulnar nerve distribution, suggested a secondary neuropathy. Physical examination revealed persistent thenar and hypothenar wasting, as well as claw deformity of the ring and little fingers. Vascular assessment using the Allen test was normal, indicating unobstructed ulnar inflow and adequate collateral circulation. Sensory evaluation demonstrated impaired two-point discrimination (>6 mm), while provocative testing yielded positive Phalen's tests and Tinel–Hoffmann signs over both the carpal tunnel and Guyon's canal, reproducing the patient's

paresthesia. Further motor assessment confirmed ulnar nerve dysfunction, evidenced by a positive Froment's sign and weakness in the ulnar-innervated intrinsic muscles (***Fig. 1***). Additionally, pre-existing chronic rigidity and distal phalangeal shortening resulting from a previous injury were noted in the proximal and distal interphalangeal joints of the little finger, unrelated to the current nerve pathology. Electrodiagnostic studies demonstrated absent sensory nerve action potentials (SNAPs) for the median nerve and prolonged distal motor latency (>6.5 ms). Similarly, ulnar nerve conduction studies revealed reduced motor conduction velocity across the wrist segment and denervation potentials in the abductor digiti minimi, confirming severe axonal damage in both the median and ulnar nerves. Plain radiographs of the wrist were obtained to rule out bony abnormalities or carpal instability, although findings were unremarkable. Musculoskeletal ultrasound or MRI was not performed given the high concordance between the clinical presentation and electrodiagnostic findings. Systemic causes, such as amyloidosis, were considered unlikely given the localized, mechanical pattern. Cervical pathology was excluded based on the absence of neck or radicular symptoms, normal cervical examination and imaging, and electrophysiological findings confirming localization of the neuropathies to the wrist without proximal involvement. The patient had no history of diabetes mellitus, rheumatoid arthritis, gout, or recent wrist trauma. Prior to considering revision surgery, a trial of conservative management was attempted, including night splinting and oral non-steroidal anti-inflammatory drugs (NSAIDs) for six weeks, but these measures failed to alleviate symptoms.

A single extended palmar incision allowed simultaneous exploration of the carpal tunnel and Guyon's canal. Intraoperative exploration revealed that the distal one-third of the transverse carpal ligament (TCL) remained intact, creating a persistent constriction band. The median nerve was found compressed specifically at this distal margin, confirming an incomplete primary release (***Fig. 2***). The intact median nerve, encased in scar tissue, was released along with the ulnar neurovascular bundle; both structures underwent epineurolysis. Opponensplasty was performed using the extensor indicis proprius (EIP) tendon, which was transferred subcutaneously around the ulnar aspect of the wrist, routed volar to the pisiform bone, to the abductor pollicis brevis (APB) insertion (***Fig. 3***). A protective layer was created over the median nerve using a hypothenar fat pad flap. Postoperatively, the hand was splinted for three weeks, followed by targeted rehabilitation.

At follow-up, the patient showed progressive functional recovery. At one month post-operatively, sensory symptoms had resolved, finger movement had returned, and therapy for thumb opposition began, despite mild discomfort near the pisiform from EIP transfer. By six months, intrinsic strength, grip, and pinch had significantly improved, with effective thumb opposition and only mild residual clawing (***Video https://theunj.org/article/view/344728/347100***). Electromyography (EMG) showed restored ulnar motor and sensory function, although APB compound muscle action potentials (CMAPs) were still absent. At one year, the patient achieved fine motor control, improved two-point discrimination (<5 mm), and reduced clawing (***Fig. 4***). EMG confirmed reinnervation of both nerves, including partial recovery of APB CMAPs. Disabilities of the Arm, Shoulder and Hand (DASH) scores reflected this progress, improving from 65.8 preoperatively to 38.3 at six months and 10.8 at one year (***Suppl. 1–3***).

Fig. 1. Preoperative clinical appearance of the right hand showing pronounced thenar atrophy, mild clawing of the fourth and fifth digits, and impaired opposition, including a view demonstrating the specific inability to perform active palmar abduction due to complete abductor pollicis brevis paralysis

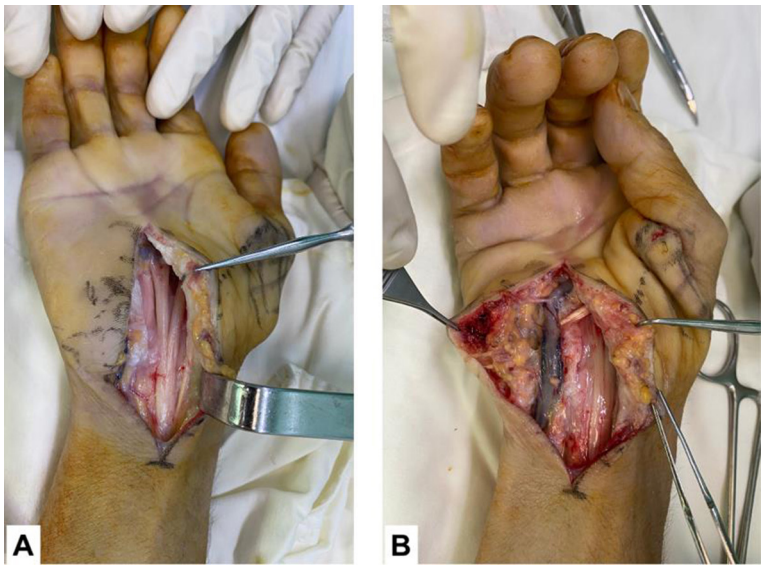

Fig. 2. Preoperative surgical plan and intraoperative findings illustrating combined decompression of the carpal tunnel and Guyon's canal through a single palmar incision: (A) An intact median nerve was confirmed after completing the distal ligament release; (B) Complete decompression of both median and ulnar nerves with preparation of a hypothenar-based adipose flap for protective coverage. *Note:* The ulnar vessels appear dilated due to venous congestion and tourniquet effect; however, arterial patency was confirmed intraoperatively

Fig. 3. The Extensor Indicis Proprius (EIP) tendon was transferred subcutaneously around the ulnar aspect of the wrist, passing volar to the pisiform bone, to the abductor pollicis brevis (APB) insertion. Additionally, a hypothenar-based adipose flap was prepared to provide soft tissue coverage over the decompressed median nerve

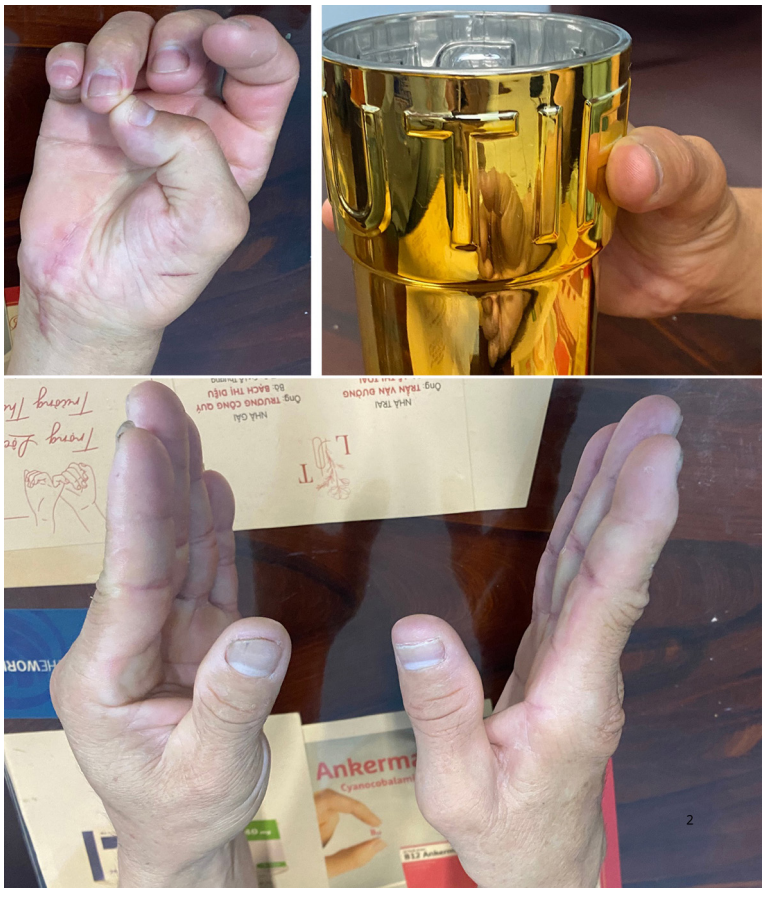

Fig. 4. One-year postoperative follow-up demonstrating functional recovery of the intrinsic hand musculature. The patient exhibits restored cylindrical grasp and stable key pinch. Effective thumb-to-index finger opposition is achieved, accompanied by enhanced palmar abduction and pronation

Supplementary 1 (https://theunj.org/article/view/344728/347088). The patient's preoperative DASH score was 65.8, indicating substantial functional impairment. This high score reflected significant difficulty in performing daily tasks, including tool use, gripping, lifting, and fine motor activities.

Supplementary 2 (https://theunj.org/article/view/344728/347089). At the 6-month follow-up, the patient's DASH score had improved to 38.3, reflecting moderate functional recovery and a meaningful reduction in disability during daily activities.

Supplementary 3 (https://theunj.org/article/view/344728/347090). By 12 months postoperatively, the patient's DASH score had decreased to 10.8, consistent with minimal disability and near-complete restoration of hand function.

Discussion

Persistent symptoms after CTR are most often due to incomplete ligament transection, whereas true recurrence involves the return of symptoms after initial relief. Common causes include technical errors, scarring, prolonged immobilization, or insufficient rehabilitation [2,5]. Although systemic conditions like amyloidosis can contribute, particularly in bilateral or atypical cases, our patient had no systemic signs, and the unilateral, anatomically consistent presentation pointed to mechanical compression [7]. Given the low clinical suspicion, tissue biopsy was deferred, with extended follow-up planned to monitor for any future systemic indicators.

To minimize perineural scarring after revision surgery, soft tissue interposition methods, such as fascial, muscle, and fat pad flaps, are commonly used [2,8,9]. In the present case, a hypothenar fat pad graft was chosen, as it permits straightforward harvest through the same surgical incision and provides a well-vascularized protective layer for coverage of the neurolysed median nerve. Importantly, the choice of this flap was guided by surgeon familiarity, anatomical feasibility in this patient, and the specific pattern and extent of scarring within the distal carpal tunnel. Although sensory symptoms resolved after the initial CTR, persistent thumb opposition loss due to thenar atrophy required EIP tendon transfer, as the deficit severely affected the patient's daily and occupational function. Biomechanically, the EIP tendon provided an optimal line of pull and adequate excursion with minimal donor-site morbidity. While the transfer necessitated routing through the ulnar scar, meticulous release ensured unimpeded gliding. Furthermore, because the

thumb metacarpophalangeal (MCP) joint exhibited no hyperextension instability, we opted for a direct insertion into the APB tendon, avoiding the additional complexity of the dorsal weaving to the extensor pollicis longus (EPL) [10].

A systematic review reported that CTS can alter the structure of Guyon's canal and impair ulnar nerve conduction, with 79% of studies showing a link between median nerve severity and ulnar dysfunction [11]. While standard CTR typically decreases pressure in Guyon's canal by relaxing the canal floor fibers, the opposite occurred in this patient. We hypothesize that the incomplete release of the distal transverse carpal ligament created a localized pressure point. Furthermore, postoperative scarring from the initial surgery likely tethered the ulnar neurovascular bundle, preventing its normal excursion and leading to secondary traction neuropathy (***Fig. 5***). This underscores that, while 'pillar pain' is common, progressive ulnar paresthesia suggests a mechanical etiology requiring re-exploration. This rare coexistence highlights the importance of clinical vigilance and repeat electrodiagnostic testing when symptoms persist or evolve after CTR.

A single-stage surgical approach was used to simultaneously decompress the carpal tunnel and Guyon's canal through one incision, minimizing tissue disruption and the risk of additional scarring. A hypothenar fat pad graft was placed over the median nerve to reduce perineural fibrosis, and thumb opposition was restored with an EIP tendon transfer. This integrated strategy led to complete sensory and motor recovery at 12 months, with no recurrence. Postoperative rehabilitation was crucial to recovery, emphasizing a structured program that included controlled motion, range-of-motion exercises, grip and pinch strengthening, opposition training, and sensory re-education.

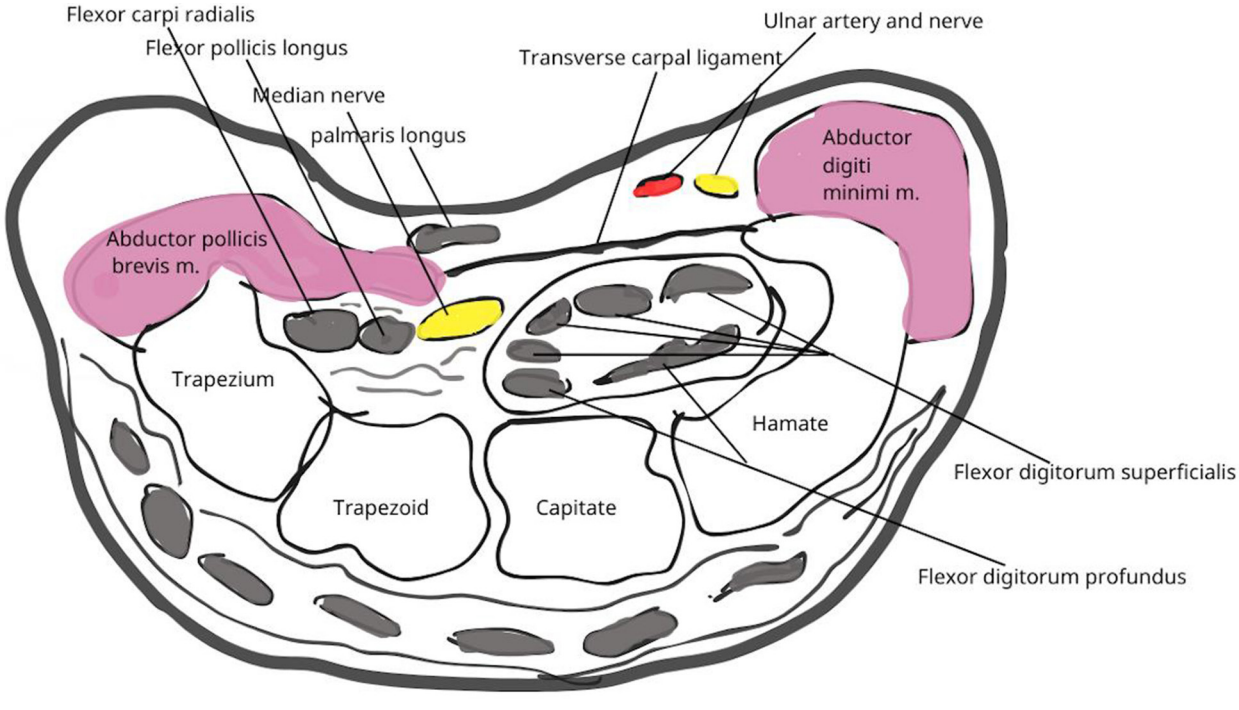

Fig. 5. This schematic illustrates the "Tethering Effect" arising from the shared boundary of the TCL between the carpal tunnel and Guyon's canal. It depicts how an incomplete distal TCL release creates a pressure point, while postoperative fibrosis extends into Guyon's canal to adhere to the ulnar neurovascular bundle

Graphical abstract

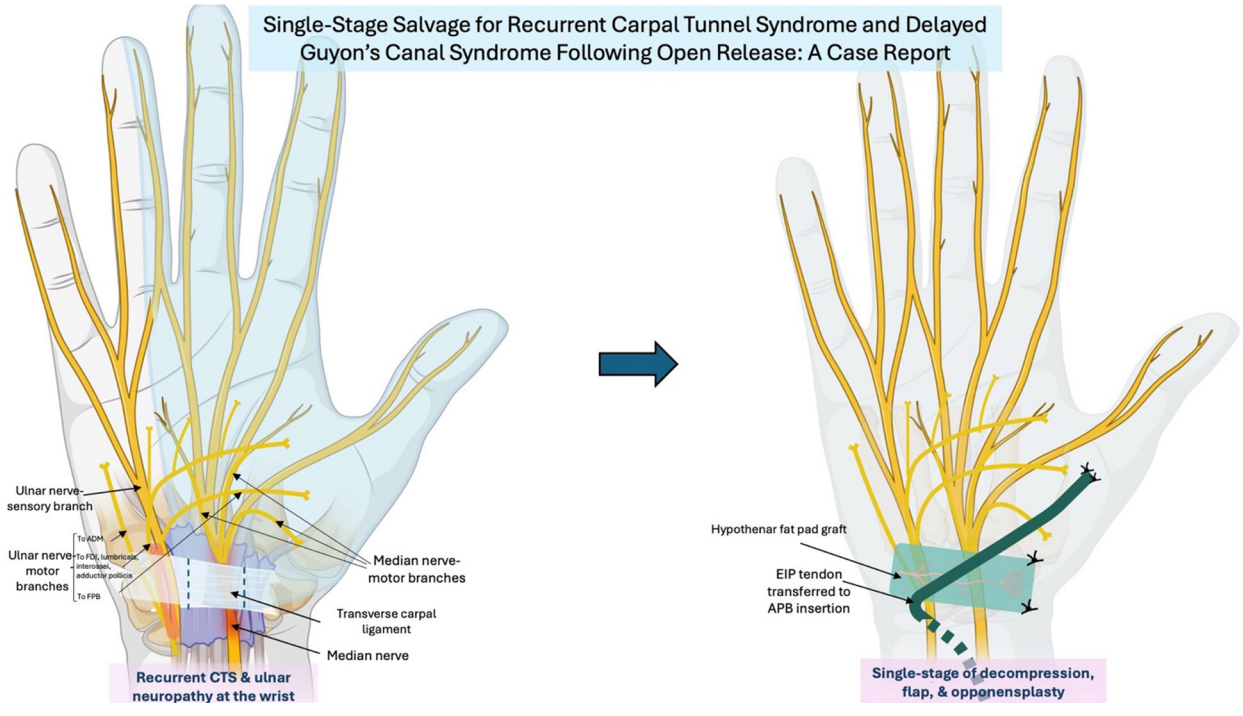

Summary diagram illustrating the coexistence of recurrent CTS and ulnar nerve entrapment at Guyon's canal. The schematic demonstrates the integrated surgical strategy, single-incision dual decompression, hypothenar fat pad grafting, and opponensplasty, used to achieve successful functional recovery in this patient.

Conclusion

This case highlights the rare coexistence of recurrent CTS and ulnar nerve entrapment at Guyon's canal. It emphasizes the importance of thorough clinical and electrophysiological evaluation in atypical presentations following CTR. The successful outcome using single-incision dual decompression, fat pad grafting, and opponensplasty supports this integrated approach as an effective strategy for managing complex compressive neuropathies.

Acknowledgement

The authors would like to thank their colleagues for their support and contributions during the preparation of this report. Special appreciation is extended to the patient for consenting to share his case and outcome.

Portions of the text were generated or edited with the assistance of ChatGPT (OpenAI, San Francisco, CA, USA). All statements were reviewed and verified by the authors.

Disclosure

Ethical approval

Ethical approval for this study was obtained from the Institutional Review Board of Hue Central Hospital (No. 263/QD-BVH). The study protocol adhered to the ethical standards outlined in the 1964 Declaration of Helsinki and its later amendments. All procedures performed in this study involving human participants were in accordance with these standards.

Statement of informed consent

Written informed consent was obtained from the patient to be included in the study. The use of individual information, disease statement, and images was accepted by the patient.

Declaration of conflicting interests

The author(s) declared no potential conflicts of interest concerning this article's research, authorship, or publication. There are no beneficial conflicts with any medical device company related to research and publication.

Funding

The author(s) received no financial support for the research, authorship, or publication of this article.

Authors' contributions:

NDHN conceived and designed the study, collected and organized data, performed formal analysis, and wrote the initial and final drafts of the article. HAP contributed to investigation, visualization, and critical review of the manuscript. PDN provided supervision and oversight. All authors have critically reviewed and approved the final draft and are responsible for the manuscript's content, integrity and originality. .

Use of artificial intelligence (AI)-assisted technology for manuscript preparation

The authors confirm that they have used AI-assisted technology to assist in the writing and editing of the manuscript.

References

1. Chammas M. Carpal tunnel syndrome. Chir Main. 2014 Apr;33(2):75-94. doi: 10.1016/j.main.2013.11.010
2. Krześniak NE, Noszczyk BH. Autologous Fat Transfer in Secondary Carpal Tunnel Release. Plast Reconstr Surg Glob Open. 2015 Jun 5;3(5):e401. doi: 10.1097/GOX.0000000000000374

3. Lattré T, Brammer S, Parmentier S, Van Holder C. Hypothenar fat pad flap surgery for end stage and recurrent carpal tunnel syndrome. Hand Surg Rehabil. 2016 Oct;35(5):348-354. doi: 10.1016/j.hansur.2016.08.003
4. Hirakawa A, Komura S, Nohara M, Masuda T, Matsushita Y, Akiyama H. Opponensplasty by the Palmaris Longus Tendon to the Rerouted Extensor Pollicis Brevis Transfer With Endoscopic Carpal Tunnel Release in Severe Carpal Tunnel Syndrome. J Hand Surg Am. 2021 Nov;46(11):1033.e1-1033.e7. doi: 10.1016/j.jhsa.2021.04.007
5. Ozdemir O, Calisaneller T, Gulsen S, Caner H. Ulnar nerve entrapment in Guyon's canal due to recurrent carpal tunnel syndrome: case report. Turk Neurosurg. 2011;21(3):435-7. doi: 10.5137/1019-5149.JTN.2959-10.1
6. Rengachary SS, Arjunan K. Compression of the ulnar nerve in Guyon's Canal by a soft tissue giant cell tumor. Neurosurgery. 1981 Mar;8(3):400-5. doi: 10.1227/00006123-198103000-00014
7. Gertz MA, Dispenzieri A. Systemic Amyloidosis Recognition, Prognosis, and Therapy: A Systematic Review. JAMA. 2020 Jul 7;324(1):79-89. doi: 10.1001/jama.2020.5493
8. Jones NF, Ahn HC, Eo S. Revision surgery for persistent and recurrent carpal tunnel syndrome and for failed carpal tunnel release. Plast Reconstr Surg. 2012 Mar;129(3):683-692. doi: 10.1097/PRS.0b013e3182402c37
9. Craft RO, Duncan SF, Smith AA. Management of recurrent carpal tunnel syndrome with microneurolysis and the hypothenar fat pad flap. Hand (N Y). 2007 Sep;2(3):85-9. doi: 10.1007/s11552-007-9025-7
10. Lemonas P, Laing T, Ghorbanian S, Malahias M, Ragoowansi R. Extensor indicis proprius opponensplasty - the burkhalter revisited. J Hand Microsurg. 2012 Dec;4(2):47-9. doi: 10.1007/s12593-012-0066-y
11. Ginanneschi F, Mondelli M, Cioncoloni D, Rossi A. Impact of carpal tunnel syndrome on ulnar nerve at wrist: Systematic review. J Electromyogr Kinesiol. 2018 Jun;40:32-38. doi: 10.1016/j.jelekin.2018.03.004

Case report

Ukrainian Neurosurgical Journal. 2026;32(2):112-118
doi: 10.25305/unj.349396

A clinical dilemma for treatment choice of extramedullary spinal plasmacytoma in patients with multiple myeloma: chemotherapy or surgery? A double-case clinical report

Tetiana V. Lymanets [1,2], Ganna S. Maslova [1], Yelizaveta O. Stadnik [1], Iuliia O. Gusachenko [2], Oleksandr L. Havlovskyi [3]

[1] Internal Medicine №1 Department, Poltava State Medical University, Poltava, Ukraine
[2] Hematology Department, Communal Enterprice "Poltava Regional Clinical Hospital n.a. M.V. Sklifosovsky Poltava Regional Council", Poltava, Ukraine
[3] Neurosurgery Department, Communal Enterprice "Poltava Regional Clinical Hospital n.a. M.V. Sklifosovsky Poltava Regional Council", Poltava, Ukraine

Received: 05 January 2026
Accepted: 09 February 2026

Address for correspondence: *Tetiana V. Lymanets, Internal Medicine №1 Department, Poltava State Medical University, 23, Shevchenko Str., Poltava, 36011, Ukraine, email: t.lymanets@pdmu.edu.ua*

Two presented case reports that highlight extramedullary spinal cord plasmacytomas in patients with diagnosed multiple myeloma are intended to change the paradigm of understanding the indication of surgical intervention. In the first case, the condition manifested as a relapse of *kappa* light chain multiple myeloma, whereas in the second case, it emerged as a primary manifestation of the same disease. Both patients received a combination chemotherapy of bortezomib, lenalidomide, and dexamethasone, which proved to be highly effective, eliminating the need for surgical intervention.

Keywords: *multiple myeloma; spinal cord plasmacytoma; soft tissue extramedullary disease; chemotherapy*

Introduction

Multiple myeloma (MM) is a malignant plasma cell disorder characterized by bone marrow infiltration and the production of monoclonal proteins. MM accounts for approximately 1% of all malignant neoplasms and about 15% of all hematologic malignancies [1, 2]. Clinically, it commonly manifests with anemia, hypercalcemia, renal dysfunction, osteolytic bone destruction, and immunodeficiency predisposing to recurrent infections [2–4]. In some patients, plasma cells acquire the ability to proliferate outside the bone marrow, leading to the development of extramedullary plasmacytomas (EMP). Spinal involvement may result in compression of the spinal cord or nerve roots, causing pain and neurological deficits [5]. Patients experiencing relapsed MM after several chemotherapy (CT) treatment lines face limited specific options with low chances for complete remission. The relapse also raises the likelihood of secondary infiltration into organs and systems due to soft tissue tumors spread [6, 7]. However, EMP could be a primary presentation of MM, which requires thorough diagnostic evaluation. Management of such cases requires a multidisciplinary approach, combining systemic therapy, surgery and radiotherapy [5].

Two case reports of extramedullary spinal cord plasmacytomas are presented: the first manifesting as a relapse of *kappa* light chain MM, and the second as a primary presentation of the disease type. Both patients received combined CT with bortezomib, lenalidomide and dexamethasone, which showed high effectiveness without surgical intervention.

Case report 1. This clinical case presents the results of patient's management with relapsed MM, which clinically manifested by spinal cord compression on the background vertebral plasmacytoma development at the level of Th5-Th7 [6].

The patient was a 49-year-old female diagnosed with stage III A (Durie-Salmon) *kappa* light-chain MM featuring extensive bone lesions including skull abnormalities and wedge-shaped vertebrae deformities at levels C6 and Th3-9 along with acute spinal cord compression leading to ischemic myeloneuropathy and sensory syndromes.

In August 2020 she was admitted to the Hematology Department of CE "Poltava Regional Clinical Hospital named after M.V. Sklifosovsky PRC" presenting with significant sensory loss in her lower limbs accompanied by paresthesia and gait disturbances as well as loss of bladder control. The above symptoms had developed gradually over two weeks.

According to anamnesis, the patient was diagnosed with MM in September 2012 following a myelogram indicating that plasma cells constituted

approximately 44%. Over time she received three lines of chemotherapy: VAD (vincristine-doxorubicin-dexamethasone) in 2012, achieving partial response; TCD (thalidomide-cyclophosphamide-dexamethasone) in 2015 followed by another TCD regimen in 2018 with thalidomide maintenance therapy until December 2019.

The progression of MM was noted in August 2020. Clinically, MM relapse was associated with worsening neurological symptoms and pelvic dysfunction. No back pain was noticed. Serum analysis showed free *kappa* light chains elevated at 344 mg/L (normal value up to 19.4 mg/L). MRI scan revealed an intradural extramedullary plasmacytoma compressing the spinal cord between Th5-Th7 (***Fig. 1***). Spinal stability was assessed according to Spine Instability Neoplastic Score (SINS) as potentially unstable (totally 11 points). The neurosurgeon recommended surgical intervention with spinal cord decompression in case of no response to systemic chemotherapy after treatment initiation.

To treat this third relapse, the patient commenced her fourth-line chemotherapy using VRD regimen (bortezomib 1.3 mg/m^2 1, 4, 8, 11 days, lenalidomide 25 mg per day 1-14 days, dexamethasone 20 mg/day 1, 2, 4, 5, 8, 9, 11, 12 days). This resulted in significant clinical improvement, post-treatment restoring sensation in lower extremities along with pelvic control functions after three cycles, which allowed to avoid surgical intervention in this case.

By April 2021, after completing eight cycles under VRD regimen a very good partial response was achieved per International Myeloma Working Group (IMWG) criteria, showing free *kappa* light chains reduced to 33.8 mg/L – a decrease by 90%. Subsequent MRI indicated substantial reduction in size regarding extramedullary neoplasm located around Th6, alongside changes consistent with previous spinal injury caused by plasmacytoma compression (***Fig. 2***). After completing the VRD in April 2021, the patient was followed by lenalidomide maintenance for two years.

Case report 2. This report presents a case of primary diagnosed MM with a plasmacytoma of the lumbar spine treated with VRD chemotherapy regimen as a first-line therapy and monitored by magnetic resonance imaging (MRI).

Fig. 1. MRI images of the first presented patient in August 2020 at the time of third relapse

Fig. 2. MRI control images of the first presented patient in April 2021 after 8 cycles of VRD chemotherapy

In February 2025, a 69-year-old male patient presented with progressive lumbar pain without preceding trauma which intensified with movement and changes in body position, radiated to both lower limbs. The pain was continuous, significantly limiting mobility and showed minimal response to treatment with nonsteroidal anti-inflammatory drugs. MRI of the lumbosacral spine (***Fig. 3***) performed on February 13, 2025, revealed spinal canal stenosis at the L3–L4 level, secondary lytic lesions involving Th11, Th12, and L3, pathological fractures of Th12 and L3 and deformities of the L1 and L4 vertebral bodies. A pathological MRI signal alteration was observed in the dorsal portion of the L3 vertebral body, appearing hypointense on T1-weighted images, hyperintense on T2 TIRM sequences and isointense on standard T2-weighted sequences. The lesion occupied approximately half of the vertebral body and extended to the vertebral arch, both left articular processes, the inferior right articular process, and the spinous process. Signs of central spinal canal stenosis at the L3–L4 segment were also present.

The patient received symptomatic pain relief therapy with minimal response. On June 2, 2025, the patient was evaluated by a neurosurgeon, who suspected spinal plasmacytoma and recommended a consultation with hematologist. Sternal bone marrow aspiration performed on June 3, 2025, demonstrated bone marrow infiltration by plasma cell lineage elements (plasmacytes – 35.5%, proplasmacytes – 4.5%, plasmablasts – 1.0%). Serum protein electrophoresis and immunofixation performed on June 10, 2025, revealed no monoclonal paraproteins, whereas urine electrophoresis detected Bence–Jones protein of the *kappa* type (0.216 g/L in the gamma zone). The β_2-microglobulin level was elevated to 3.65 mg/L.

Skeletal radiography performed on June 10, 2025, demonstrated multiple poorly demarcated lytic foci in the skull (1–3 mm in diameter), bilateral humeral bone lesions (up to 0.5 cm, predominantly on the right), and bilateral femoral bone lesions (up to 0.8 cm, predominantly on the right).

Based on the clinical, radiological and laboratory findings, the diagnosis of *kappa* light-chain MM, stage II according to the International Staging System (ISS), was established.

The patient was admitted to the Hematology Department of CE "Poltava Regional Clinical Hospital named after M.V. Sklifosovsky PRC". In June 2025, first-line chemotherapy according to the VRD regimen along with zoledronic acid was initiated. The neurosurgeon assessed spinal stability by the SINS score with 12 points as potentially unstable and the decision for surgical intervention was recommended to be postponed after completing the first course of VRD treatment. In July 2025, clinical improvement was achieved and pain was significantly released. Upon repeated neurosurgical consultation, the SINS score showed 10 points the decision was made to avoid spinal surgery and continue chemotherapy.

After six cycles of chemotherapy, the serum and urine M-spikes were no longer detectable: the complete response was achieved according to the criteria of the International Myeloma Working Group (IMWG). Follow-up MRI (***Fig. 4***), performed on December 27, 2025, revealed a visible reduction of the lesion at the L3 vertebral level and improvement of spinal canal stenosis, classified as Lee grade 3 at the L3–L4 segment. Clinically, the patient reported pain reduction, improved mobility and gradual recovery of daily activity tolerance. Considering the clinical improvement of symptoms and the visual reduction on MRI, continuation of chemotherapy according to the VRD regimen was recommended up to eight cycles followed by maintenance therapy with lenalidomide.

Fig. 3. *MRI images of the second patient obtained in February 2025 at the time of initial clinical picture developed*

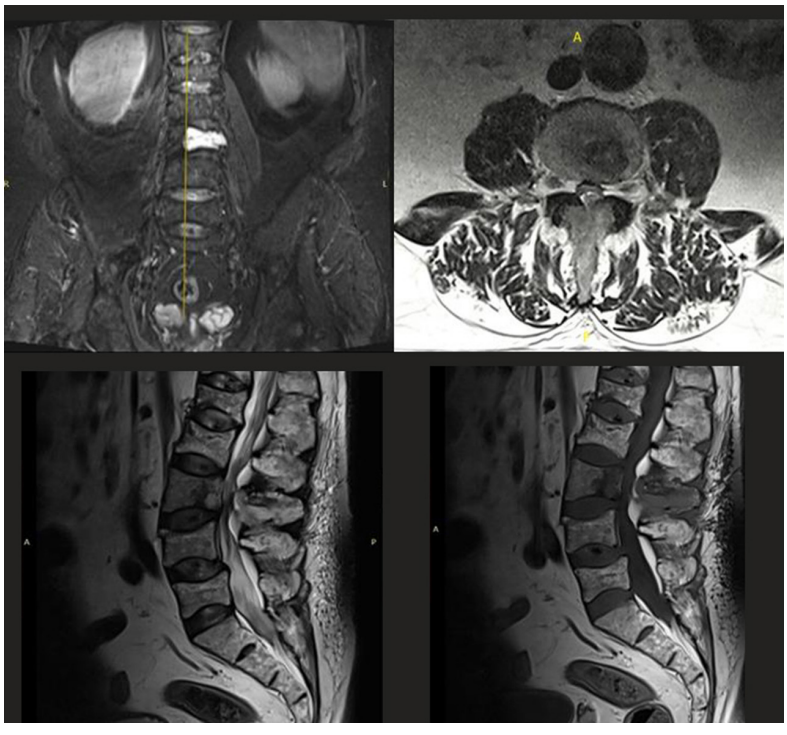

Fig. 4. MRI control images of the second patient obtained in December 2025 after 6 VRD cycles of chemotherapy

Discussion

MM is a malignancy of plasma cells characterized by bone marrow infiltration and the production of monoclonal proteins, and sometimes it manifests with neurological symptoms due to spinal cord compression by extramedullary plasmacytoma growth. According to the recommendations of a European Expert Panel, all patients with suspected solitary plasmacytoma should undergo bone marrow aspiration and biopsy to evaluate plasma cell morphology and the extent of marrow infiltration. Given the diagnostic and prognostic significance, the degree of clonal plasma cell infiltration should be assessed by flow cytometry, *kappa/lambda* light chain labeling on bone marrow aspirates or immunohistochemistry on biopsy samples and by the presence of numerous cytogenetic aberrations of the tumor cells [8, 9].

Soft-tissue involvement in MM has been recognized since the earliest descriptions of the disease. Historical autopsy reports demonstrated extra-skeletal infiltration in approximately 70% of patients with MM [1]. Soft-tissue plasmacytomas indicate a more aggressive phenotype of MM, reflecting the capacity of malignant plasma cell clones to proliferate and survive outside the bone marrow microenvironment. Extramedullary involvement in MM correlates with low responsiveness to therapy, rapid disease progression, and markedly reduced overall survival [10-14]. Data on the incidence of EMP remain limited. According to published studies, EMP is detected in approximately 7–17% of MM patients at diagnosis and in 6–20% during the disease course with variability largely depending on study design and diagnostic methods [11, 13]. Soft-tissue plasmacytomas may arise through three principal mechanisms: direct extension from skeletal lesions following cortical bone disruption; hematogenous dissemination resulting in infiltration of distant organs or soft tissues without bone involvement; in rare instances, development secondary to invasive diagnostic or therapeutic procedures [12]. The definition of EMP in MM has varied among studies. Some reports classify EMP only in cases of organ or tissue infiltration through hematogenous dissemination, but others classify soft-tissue developing from bones through direct growth from skeletal tumors [1, 11, 13]. According to Laura Rosiñol *et al.*, two distinct patterns of soft-tissue involvement in MM can be identified: EMP or extra-osseous type, characterized by lesions confined to soft tissues without direct bone contact and paraskeletal plasmacytomas, defined as soft-tissue masses that originate from bone lesions [1].

Due to the lack of consistent classification between EMP and para-skeletal plasmacytomas in published studies, accurate statistics on their respective incidence and outcomes remain uncertain. Available data on the incidence of plasmacytomas in MM are based primarily on observational studies. The frequency of EMP at the time of diagnosis has been reported to range from 1.7% to 4.5%, whereas paraskeletal plasmacytomas are observed in approximately 7% to 34.4% of patients [1].

The small number of reported cases and the absence of controlled studies limit the ability to assess the true efficacy of current treatments for soft-tissue involvement in MM, and therefore no standardized therapeutic approach can be recommended [1, 13]. The National Inpatient Sample data suggest that treating spinal involvement in MM should include a multimodal strategy with chemotherapy, bisphosphonates, radiation therapy, and surgery [5].

Alkylating agents, particularly high-dose melphalan, remain effective frontline therapy for patients with paraskeletal involvement, showing comparable response and survival rates to those without soft-tissue disease

[1, 14, 15]. Autologous stem cell transplantation (ASCT) provides similar outcomes in paraskeletal cases. Data on newer agents are limited: bortezomib appears more effective in para-skeletal than in EMP, while carfilzomib and immunomodulatory agents show reduced activity [1, 14]. Proteasome inhibitor-based regimens remain the most effective therapeutic option for patients with para-skeletal plasmacytomas. Combinations such as Dara-VMP (daratumumab, bortezomib, melphalan, prednisolone) or VRD are preferred, particularly in those not eligible for immediate ASCT [1, 14]. These data were proved by our two case reports, which showed high treatment effectiveness with VRD regimen.

In a retrospective analysis by Vittorio Montefusco *et al*., data from 2,332 newly diagnosed MM patients enrolled in eight FoNeSa Onlus and HOVON Foundation clinical trials were evaluated. Three of these trials included transplant-eligible and five transplant-ineligible patients. Treatment protocols varied among the studies. Three trials used an immunomodulatory agent (mostly lenalidomide), three included a proteasome inhibitor and four combined both types of therapy. Maintenance therapy was provided in six trials. Among all participants, 267 patients (11%) presented with soft-tissue plasmacytomas (243 paraskeletal, 12 extramedullary and 12 unclassified). Median progression-free survival was 26.1 months for patients with EMP and 25.2 months for those without plasmacytomas, while median overall survival reached 70.1 months and 79.9 months respectively [12, 16].

Currently, the International Myeloma Working Group provides no specific recommendations regarding the optimal frequency of plasmacytoma assessment. Clinical evaluation of palpable lesions should be performed at the beginning of each treatment cycle while PET/CT or MRI should be repeated approximately three months after therapy initiation to assess residual activity. If the disease persists, doctors should consider continuing the current treatment, adding local radiotherapy or switching to another systemic regimen, depending on how well the paraprotein levels and plasmacytoma have responded. If the reduction in plasmacytoma size is less than 50%, local radiotherapy and/or modification of systemic therapy should be considered. Continuation of the current therapeutic regimen is recommended when the lesion decreases by 50% or more [1].

There is no clear consensus on the use of radiotherapy in extramedullary myeloma, except for solitary plasmacytoma [15]. Prompt local radiotherapy is indicated in cases of spinal cord compression and should also be considered for patients with severe compressive pain, bulky plasmacytomas or residual localized disease following systemic treatment [1].

According to the Surgeon's Committee of the Chinese Myeloma Working Group of the International Myeloma Foundation, extramedullary plasmacytomas located in the limbs or spine should be managed surgically through intralesional, marginal or wide excision. Wide excision is recommended as the preferred approach, while marginal excision serves as an alternative when wide resection is not feasible. Radiotherapy should be administered after intralesional removal. The treatment plan should be developed together by a multidisciplinary team including surgeons, hematologists and radiation oncologists. Since surgery in MM is not aimed at achieving a radical cure, the focus is on relieving symptoms and improving the patient's quality of life. Surgical treatment primarily seeks to prevent or stabilize pathological fractures, decompress the spinal cord and nerve roots, reduce pain, restore mobility and maintain the structural stability of the spine and surrounding bone [17].

According to Jiajia Zhang *et al*., patients with MM and spinal canal invasion by extramedullary plasmacytoma were treated either with surgery plus chemotherapy or chemotherapy alone, mainly using bortezomib-based regimens. The study emphasized the importance of early detection of spinal involvement and showed that extramedullary disease responded well to novel agents. Surgical decompression was advised in cases of neurological compression to relieve symptoms and prevent further damage [18].

Martio *et al*. reported a case of a 75-year-old female with an epidural extramedullary plasmacytoma extending from T6 to L1. The patient underwent surgical decompression followed by systemic chemotherapy with bortezomib, cyclophosphamide and dexamethasone. This combined approach resulted in complete radiological remission with no residual or recurrent disease observed eight months postoperatively and sustained remission for more than fifteen months [19].

It is clear that every clinical case is unique and necessitates a cohesive and systematic evaluation before determining the most appropriate treatment strategy: chemotherapy, surgery, radiotherapy or its combinations. The comprehensive assessment for surgery indication was put forth by Fisher *et al*. [20] and Bilsky *et al*. [21], who have independently created practical assessment scales that facilitate the accurate and tailored evaluation of indications for surgical intervention in spinal tumor lesions.

Fisher *et al*. developed an evidence-based classification system for assessing spinal instability in patients with neoplastic disease of the spine. Their SINS incorporates six components: tumor location, mechanical pain, bone lesion quality, spinal alignment, vertebral body collapse, and posterolateral spinal element involvement. It helps to generate a comprehensive stability score ranging from 0 to 18. Scores stratify patients into stable (0-6 points), potentially unstable (7-12 points), or unstable (≥13 points) categories, thereby guiding neurosurgical consultation and management. The authors emphasized that spinal instability is one of multiple factors influencing treatment decisions, alongside neurological status, tumor histology, and patient-specific considerations. The study provides clinicians with a standardized framework to improve multidisciplinary communication and optimize care for patients with spinal neoplasia [20].

Bilsky *et al*. reported the development and validation of a six-point MRI-based grading system for epidural spinal cord compression (ESCC) in metastatic spinal disease, demonstrating that the scale provides good to excellent interrater and intrarater reliability, particularly when utilizing axial T2-weighted images. Their study emphasized the importance of distinguishing subtle degrees of thecal sac deformation and spinal cord abutment to inform surgical decision-making and stereotactic radiosurgery planning. The authors

concluded that this refined ESCC grading scale facilitates consistent classification of spinal cord compression, thereby enhancing communication across surgical and radiation oncology disciplines and offering a standardized framework applicable to multi-institutional clinical trials and treatment outcome assessments [21].

Bobinski *et al*. defined a significant correlation between higher SINS values and more advanced grades of ESCC in patients surgically treated for spinal metastases. These findings suggest that elevated SINS scores may serve as a reliable indicator of increased risk for the development of ESCC, reflecting the progressive biomechanical compromise of vertebral integrity due to metastatic disease. The study supports the clinical value of SINS as a tool for assessing tumor-associated spinal instability and the risk of ESCC [22].

Consequently, in the line with the presented double-case report findings, surgical intervention in extramedullary spinal plasmacytoma should be reserved for instances when high SINS scores (≥13 points) indicate mechanical instability and/or elevated ESCC grades reflect severe or progressive spinal cord compression refractory to systemic chemotherapy. It is strongly advised to evaluate these two scales when making decisions regarding the treatment strategy for patients with extramedullary spinal plasmacytomas.

Conclusion

Thus, summarizing the results of numerous studies, surgical treatment of extramedullary spinal plasmacytoma in patients with multiple myeloma should not be considered mandatory, and is indicated exclusively in cases of emergency spinal cord decompression after ineffective chemotherapy with novel agents, or for the purpose when solitary plasmacytoma is suspected in the absence of bone marrow infiltration by plasma cells.

Early diagnosis of extramedullary spinal plasmacytoma in multiple myeloma is crucial for preventing irreversible neurological complications and improving long-term outcomes without surgical intervention. The management of such cases should be based on a comprehensive, multidisciplinary approach that combine systemic chemotherapy, radiological assessment and, when indicated, surgical or radiation therapy. Collaboration among hematologists, radiologists and neurosurgeons is essential for optimizing treatment strategy.

Disclosure

Conflict of interest

The authors declare no conflict of interest.

Informed consent

Informed consent was obtained from both patients.

References

1. Rosiñol L, Beksac M, Zamagni E, Van de Donk NWCJ, Anderson KC, Badros A, Caers J, Cavo M, Dimopoulos MA, Dispenzieri A, Einsele H, Engelhardt M, Fernández de Larrea C, Gahrton G, Gay F, Hájek R, Hungria V, Jurczyszyn A, Kröger N, Kyle RA, Leal da Costa F, Leleu X, Lentzsch S, Mateos MV, Merlini G, Mohty M, Moreau P, Rasche L, Reece D, Sezer O, Sonneveld P, Usmani SZ, Vanderkerken K, Vesole DH, Waage A, Zweegman S, Richardson PG, Bladé J. Expert review on soft-tissue plasmacytomas in multiple myeloma: definition, disease assessment and treatment considerations. Br J Haematol. 2021 Aug;194(3):496-507. doi: 10.1111/bjh.17338
2. Rajkumar SV. Multiple myeloma: 2024 update on diagnosis, risk-stratification, and management. Am J Hematol. 2024 Sep;99(9):1802-1824. doi: 10.1002/ajh.27422
3. Gundesen MT, Schjesvold F, Lund T. Treatment of myeloma bone disease: When, how often, and for how long? J Bone Oncol. 2025 Apr 1;52:100680. doi: 10.1016/j.jbo.2025.100680
4. Rafae A, van Rhee F, Al Hadidi S. Perspectives on the Treatment of Multiple Myeloma. Oncologist. 2024 Mar 4;29(3):200-212. doi: 10.1093/oncolo/oyad306
5. Zehri AH, Calafiore RL, Peterson KA, Kittel CA, Osei JA, Wilson JL, et al. Surgical management of spinal multiple myeloma: insights from the National Inpatient Sample database. J Spine Surg. 2024 Sep 23;10(3):428-437. doi: 10.21037/jss-24-54
6. Skrypnyk IM, Maslova GS, Gusachenko IO, Lymanets TV. VRd Regimen for Treatment of Vertebral Plasmacytoma with Spinal Cord Compression. In: Poster abstract book of 7th Kaunas International Hematology Oncology Colloquium; 2022 May 26; Kaunas, Lithuania. Kaunas; 2022. p. 13. doi: 10.13140/RG.2.2.29202.63688.
7. Ostrovskyi VL, Skrypnyk IM, Maslova . GS, Shaposhnyk OA. FEATURES OF L-ARGININE-CITRULLINE CYCLE FUNCTIONING IN PATIENTS WITH MULTIPLE MYELOMA WITH CONCOMITANT CORONARY HEART DISEASE. Exp Oncol. 2025 Jul 11;47(1):76-82. doi: 10.15407/exp-oncology.2025.01.076
8. Caers J, Paiva B, Zamagni E, Leleu X, Bladé J, Kristinsson SY, Touzeau C, Abildgaard N, Terpos E, Heusschen R, Ocio E, Delforge M, Sezer O, Beksac M, Ludwig H, Merlini G, Moreau P, Zweegman S, Engelhardt M, Rosiñol L. Diagnosis, treatment, and response assessment in solitary plasmacytoma: updated recommendations from a European Expert Panel. J Hematol Oncol. 2018 Jan 16;11(1):10. doi: 10.1186/s13045-017-0549-1
9. Tsuber V, Kadamov Y, Brautigam L, Berglund UW, Helleday T. Mutations in Cancer Cause Gain of Cysteine, Histidine, and Tryptophan at the Expense of a Net Loss of Arginine on the Proteome Level. Biomolecules. 2017 Jul 3;7(3):49. doi: 10.3390/biom7030049
10. Steinhardt MJ, Schaefers C, Leypoldt LB, Blau IW, Harzer M, Zhou X, Riedhammer C, Kamili A, Kosch R, Topp LS, Molwitz I, Gross-Fengels NO, Melzer YF, Artzenroth J, Al-Bazaz M, Alsdorf W, Topp MS, Duell J, Mersi J, Waldschmidt J, Bokemeyer C, Einsele H, Kortüm KM, Weisel K, Rasche L. Activity of CAR-T cells and bispecific antibodies in multiple myeloma with extramedullary involvement. Blood Cancer J. 2025 Jul 30;15(1):126. doi: 10.1038/s41408-025-01330-9
11. Jiménez-Segura R, Rosiñol L, Cibeira MT, Fernández de Larrea C, Tovar N, Rodríguez-Lobato LG, Bladé E, Moreno DF, Oliver-Caldés A, Bladé J. Paraskeletal and extramedullary plasmacytomas in multiple myeloma at diagnosis and at first relapse: 50-years of experience from an academic institution. Blood Cancer J. 2022 Sep 16;12(9):135. doi: 10.1038/s41408-022-00730-5
12. Bladé J, Beksac M, Caers J, Jurczyszyn A, von Lilienfeld-Toal M, Moreau P, Rasche L, Rosiñol L, Usmani SZ, Zamagni E, Richardson P. Extramedullary disease in multiple myeloma: a systematic literature review. Blood Cancer J. 2022 Mar 21;12(3):45. doi: 10.1038/s41408-022-00643-3
13. Li Y, Sun Z, Qu X. Advances in the treatment of extramedullary disease in multiple myeloma. Transl Oncol. 2022 Aug;22:101465. doi: 10.1016/j.tranon.2022.101465
14. Bhutani M, Foureau DM, Atrash S, Voorhees PM, Usmani SZ. Extramedullary multiple myeloma. Leukemia. 2020 Jan;34(1):1-20. doi: 10.1038/s41375-019-0660-0
15. Bansal R, Rakshit S, Kumar S. Extramedullary disease in multiple myeloma. Blood Cancer J. 2021 Sep 29;11(9):161. doi: 10.1038/s41408-021-00527-y
16. Montefusco V, Gay F, Spada S, De Paoli L, Di Raimondo F, Ribolla R, Musolino C, Patriarca F, Musto P, Galieni P, Ballanti S, Nozzoli C, Cascavilla N, Ben-Yehuda D, Nagler A, Hajek R, Offidani M, Liberati AM, Sonneveld P, Cavo M, Corradini P, Boccadoro M. Outcome of paraosseous extramedullary disease in newly diagnosed multiple myeloma patients treated with new drugs. Haematologica. 2020 Jan;105(1):193-200. doi: 10.3324/haematol.2019.219139

17. Surgeon's Committee of the Chinese Myeloma Working Group of the International Myeloma Foundation. Consensus on Surgical Management of Myeloma Bone Disease. Orthop Surg. 2016 Aug;8(3):263-9. doi: 10.1111/os.12267
18. Zhang J, Zhong Y. Clinical analysis of 36 multiple myeloma patients with extramedullary plasmacytoma invasion of the spinal canal. Hematol Oncol. 2015 Jun;33(2):75-9. doi: 10.1002/hon.2126
19. Martio AE, Miotto GJ, Filho PMM, Chaves WS, Karam OR. Epidural Extramedullary Plasmacytoma Successfully Treated with Surgical Excision and Bortezomib, Cyclophosphamide and Dexamethasone. Curr Health Sci J. 2023 Apr-Jun;49(2):288-292. doi: 10.12865/CHSJ.49.02.288
20. Fisher CG, DiPaola CP, Ryken TC, Bilsky MH, Shaffrey CI, Berven SH, Harrop JS, Fehlings MG, Boriani S, Chou D, Schmidt MH, Polly DW, Biagini R, Burch S, Dekutoski MB, Ganju A, Gerszten PC, Gokaslan ZL, Groff MW, Liebsch NJ, Mendel E, Okuno SH, Patel S, Rhines LD, Rose PS, Sciubba DM, Sundaresan N, Tomita K, Varga PP, Vialle LR, Vrionis FD, Yamada Y, Fourney DR. A novel classification system for spinal instability in neoplastic disease: an evidence-based approach and expert consensus from the Spine Oncology Study Group. Spine (Phila Pa 1976). 2010 Oct 15;35(22): E1221-9. doi: 10.1097/BRS.0b013e3181e16ae2
21. Bilsky MH, Laufer I, Fourney DR, Groff M, Schmidt MH, Varga PP, Vrionis FD, Yamada Y, Gerszten PC, Kuklo TR. Reliability analysis of the epidural spinal cord compression scale. J Neurosurg Spine. 2010 Sep;13(3):324-8. doi: 10.3171/2010.3.SPINE09459
22. Bobinski L, Axelsson J, Melhus J, Åkerstedt J, Wänman J. The Spinal Instability Neoplastic Score correlates with epidural spinal cord compression -a retrospective cohort of 256 surgically treated patients with spinal metastases. BMC Musculoskelet Disord. 2024 Aug 15;25(1):644. doi: 10.1186/s12891-024-07756-9

Case report

Ukrainian Neurosurgical Journal. 2026;32(2):119-125
doi: 10.25305/unj.349403

Osteochondroma of inferior articular process in lumbar spine causing spinal stenosis: a case report

Tuan Anh Phan [1], An Hoang Dai [1], Minh Hoang Nguyen [1], Khang Trien Truong [2], Phi Duong Nguyen [3], Thi Cao [2]

[1] Hospital for Traumatology and Orthopedics, Ho Chi Minh City, Vietnam
[2] Department of Orthopedics and Rehabilitation, University of Medicine and Pharmacy at Ho Chi Minh City, Ho Chi Minh City, Vietnam
[3] Department of Orthopaedic-Burn-Plastic Surgery, City Children's Hospital, Ho Chi Minh City, Vietnam

Received: 05 January 2026
Accepted: 03 March 2026

Address for correspondence:
Thi Cao, Department of Orthopedics and Rehabilitation, School of Medicine, University of Medicine and Pharmacy at Ho Chi Minh City, 217 Hong Bang street, Ward Cho Lon, 70000, Ho Chi Minh City, Vietnam, e-mail: caothibacsi@ump.edu.vn

Osteochondroma is the most common benign bone tumor; however, spinal involvement is uncommon and may result in significant neurological compromise when neural structures are compressed. Osteochondroma arising from the lumbar facet joint is particularly rare and can clinically mimic degenerative spinal disorders. We report the case of a 47-year-old woman who presented with chronic low back pain and progressive right lower limb radiculopathy. Computed tomography demonstrated a 21 × 18 × 16 mm osseous lesion arising from the right inferior articular process of L3, showing clear cortical and medullary continuity with the parent vertebra. Magnetic resonance imaging revealed L3–L4 spinal canal stenosis with compression of the cauda equina, and the cartilage cap measured approximately 3 mm on T2-weighted imaging. The patient underwent posterior decompression with en bloc excision of the lesion. Segmental stability was preserved after facetectomy, and instrumentation was not required. Histopathological examination confirmed the diagnosis of osteochondroma. At the 12-month follow-up, the patient remained asymptomatic, with no radiological evidence of recurrence or instability. This case highlights the importance of comprehensive imaging evaluation, careful assessment of postoperative spinal stability, and complete excision including the cartilage cap to prevent recurrence.

Keywords: *osteochondroma; inferior articular process; spinal stenosis; spinal exostosis; bone tumor*

Introduction

Osteochondromas are common benign bone tumors composed of cortical and medullary bone with a hyaline cartilage cap; however, spinal involvement is rare, accounting for only about 1%–4% of all osteochondromas [1, 2]. In a comprehensive review of spinal osteochondromas, Yakkanti *et al.* identified 132 solitary cases and 17 cases associated with multiple hereditary exostoses, with most lesions arising from the posterior column and frequently presenting with neurological symptoms requiring surgical excision [1]. The cervical spine is the most involved region, followed by thoracic and lumbar segments [3]. Although lumbar spinal osteochondromas have been reported, cases arising specifically from the inferior articular process (IAP) are very rare, and only a small number of individual case reports have detailed similar presentations at these levels [3, 4].

Moreover, many previously published cases have described either chronic symptom duration over months to years or incidental findings, whereas relatively few reports provide detailed criteria for postoperative spinal stability assessment without instrumentation. For example, Woo *et al.* reported a solitary lumbar osteochondroma arising from the L3 IAP presenting with sciatica; surgical excision led to symptom resolution, although objective dynamic stability evaluation was not discussed [2]. Similarly, Shigekiyo *et al.* presented lumbar osteochondroma cases originating from the articular process in elderly patients with radiculopathy, highlighting the diagnostic challenge due to mimicry of degenerative spinal disorders [4].

This report describes a rare case of lumbar osteochondroma arising from the right L3 inferior articular process in a 47-year-old female presenting with acute radicular pain and neurogenic claudication after minor trauma. This case is noteworthy because – unlike many previous reports – it demonstrates a rapid clinical course, precise imaging characterization, and surgical decompression with en bloc excision that preserved segmental stability without instrumentation, as confirmed by dynamic radiographs. These findings expand current knowledge on clinical presentation and optimal management strategies for this uncommon entity.

Case Presentation

A 47-year-old female presented with a 1-month history of progressive low back pain and right-sided radicular pain accompanied by paresthesia, which developed after a minor slip and fall injury. Notably, the clinical course was relatively rapid. The patient reported neurogenic claudication occurring after walking approximately 100 meters. There were no bowel or

bladder disturbances. Conservative management with nonsteroidal anti-inflammatory drugs (NSAIDs) and muscle relaxants for three weeks failed to provide symptom relief.

There was no personal or family history of bone tumors or multiple hereditary exostoses. Neurological examination demonstrated decreased muscle strength (Medical Research Council grade 4/5) in the right L4 and L5 myotomes, accompanied by reduced sensation in the corresponding dermatomal distributions. Deep tendon reflexes were preserved. The detailed preoperative neurological findings are summarized in ***Table 1***.

Plain radiographs of the lumbar spine demonstrated a focal osseous mass at the right L3–L4 facet joint (***Fig. 1***). Computed tomography revealed a well-defined exophytic lesion measuring 21 × 18 × 16 mm arising from the right inferior articular process (IAP) of L3, with clear cortical and medullary continuity with the parent vertebra, consistent with osteochondroma (***Fig. 2A, 2B***). Magnetic resonance imaging (MRI) showed significant spinal canal stenosis at the L3–L4 level with compression of the cauda equina (***Fig. 2C, 2D***). The cartilage cap thickness measured approximately 3 mm on T2-weighted imaging, without irregularity or features suggestive of malignant transformation.

Given the presence of progressive motor weakness, radiculopathy and neurogenic claudication secondary to canal compromise, surgical decompression was indicated. Under general anesthesia, the patient was positioned prone. Intraoperative fluoroscopy with needle markers was used to confirm accurate localization of the L3–L4 level (***Fig. 3A***). The surgical level was identified and marked on the skin surface (***Fig. 3B***). A 3-cm midline posterior incision was subsequently made. Unilateral exposure of the right L3 lamina and L3–L4 facet complex was achieved. Unilateral muscle exposure was performed on the right side, followed by deep exposure using diathermy to the L3 lamina and L3/L4 facet.

Approximately one quarter of the right L3 lamina and the entire inferior articular process (IAP) were resected en bloc using an osteotome (***Fig. 4A***). The lesion originated from the right inferior articular process and projected medially into the spinal canal, as illustrated schematically in ***Fig. 4B***. The right L3 IAP was sent for histopathological examination, while the right ligamentum flavum remained intact. Particular attention was paid to preserving the superior articular process of L4 and maintaining more than 50% of the facet joint complex, as well as the posterior ligamentous structures, to minimize the risk of postoperative instability. Hemostasis was carefully achieved, after which the incision was closed in layers with placement of a drainage tube, and the wound was finally covered with sterile dressing. The total operative time was 50 minutes, with an estimated blood loss of 40 mL.

Histopathological examination confirmed the diagnosis of osteochondroma, demonstrating typical features including a fibrous perichondrium, lobules of hyaline cartilage forming the cartilage cap, and an underlying stalk of mature cancellous bone (***Fig. 4C***).

Postoperatively, the patient experienced immediate relief of back pain (VAS 2) and almost complete resolution of right-sided radicular pain (VAS 1), with no residual paresthesia. No postoperative complications were observed. Follow-up radiographs confirmed complete resection of the pathological lesion at the right L3 inferior articular process, with no evidence of residual tumor. Postoperative standing and dynamic flexion–extension radiographs were obtained to objectively assess segmental stability, with radiographic criteria for instability defined as sagittal translation >4.5 mm and angular motion >15° at the L3–L4 segment. The patient was able to sit and ambulate on postoperative day 1 and was discharged from the hospital on postoperative day 3.

At 3 months of follow-up, radicular symptoms had completely resolved. At 6 months, neurological examination was normal. At 12 months, the patient was able to walk 3 kilometers daily without pain or claudication. Follow-up CT demonstrated no evidence of tumor recurrence, and dynamic radiographs confirmed no instability (***Fig. 5***).

Table 1. Preoperative Neurological Examination Findings (MRC grade)

Level	Muscle Strength (Right)	Muscle Strength (Left)	Sensation (Right)	Sensation (Left)	Reflex (Right)	Reflex (Left)
L2	5/5	5/5	2/2	2/2	—	—
L3	5/5	5/5	2/2	2/2	—	—
L4	4/5	5/5	1/2	2/2	Normal	Normal
L5	4/5	5/5	1/2	2/2	—	—
S1	5/5	5/5	2/2	2/2	Normal	Normal

Notes. MRC = Medical Research Council muscle strength grading system (0–5 scale). Sensory function graded on a 0–2 scale (0 = absent, 1 = decreased, 2 = normal)

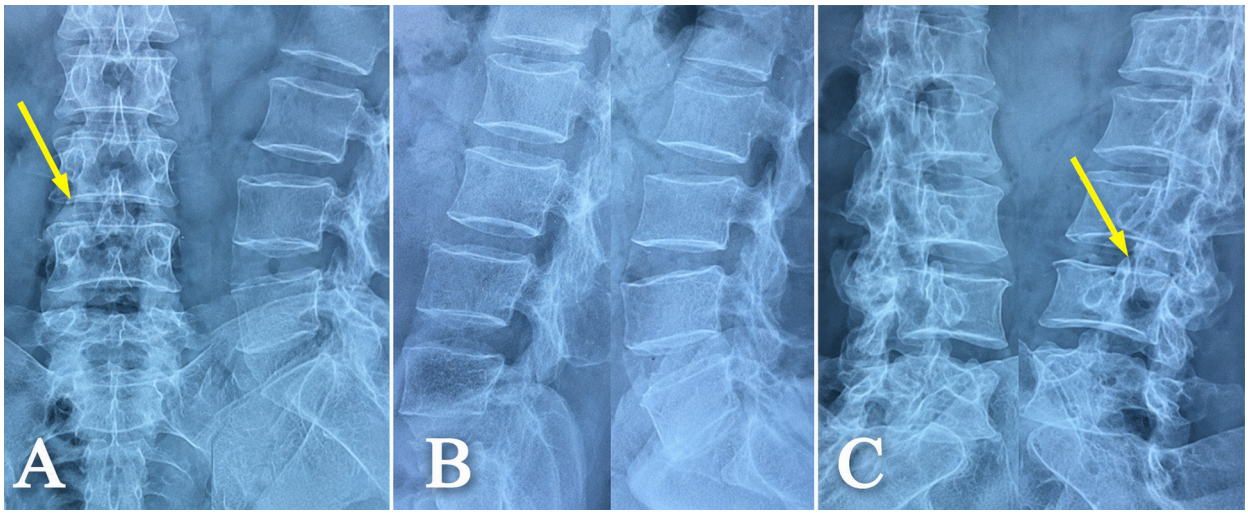

Fig.1. Preoperative lumbar spine radiographs. A - Anteroposterior view demonstrating a focal osseous prominence at the right L3–L4 facet region (arrow); B - Dynamic lateral views in flexion and extension; C - Right oblique view highlighting the exophytic bony lesion arising from the posterior elements (arrow)

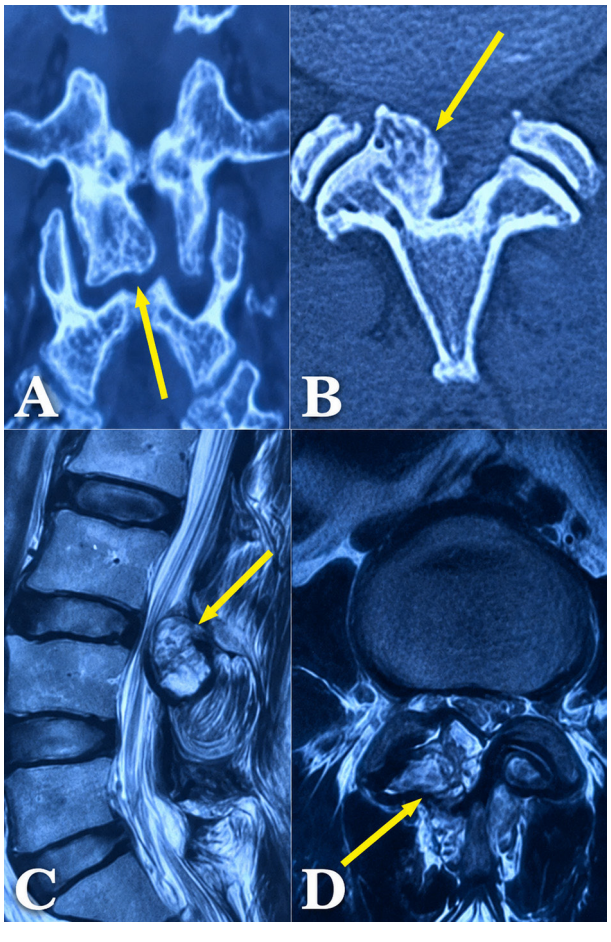

Fig. 2. Cross-sectional imaging of the lesion. A - Coronal CT reconstruction demonstrating an exophytic osseous lesion arising from the right inferior articular process of L3 (arrow), with cortical and medullary continuity with the parent vertebra; B - Axial CT image confirming the lesion projecting into the spinal canal (arrow); C - Sagittal T2-weighted MRI showing significant spinal canal stenosis at the L3–L4 level caused by the lesion (arrow); D - Axial T2-weighted MRI demonstrating compression of the cauda equina (arrow)

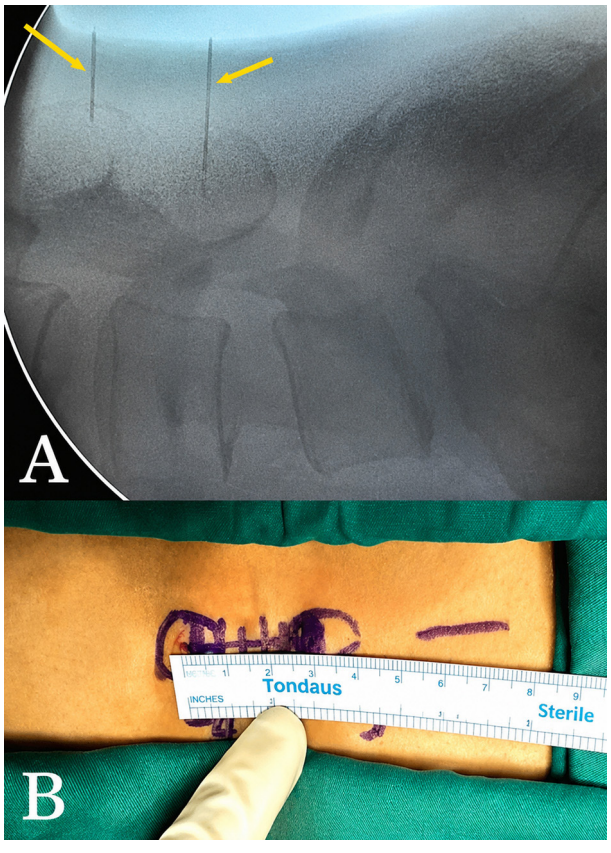

Fig. 3. Intraoperative localization of the surgical level. A - Lateral fluoroscopic (C-arm) image showing two needle markers (arrows) used to confirm the L3–L4 level prior to facetectomy; B - Skin marking and surface localization of the L3–L4 level before incision

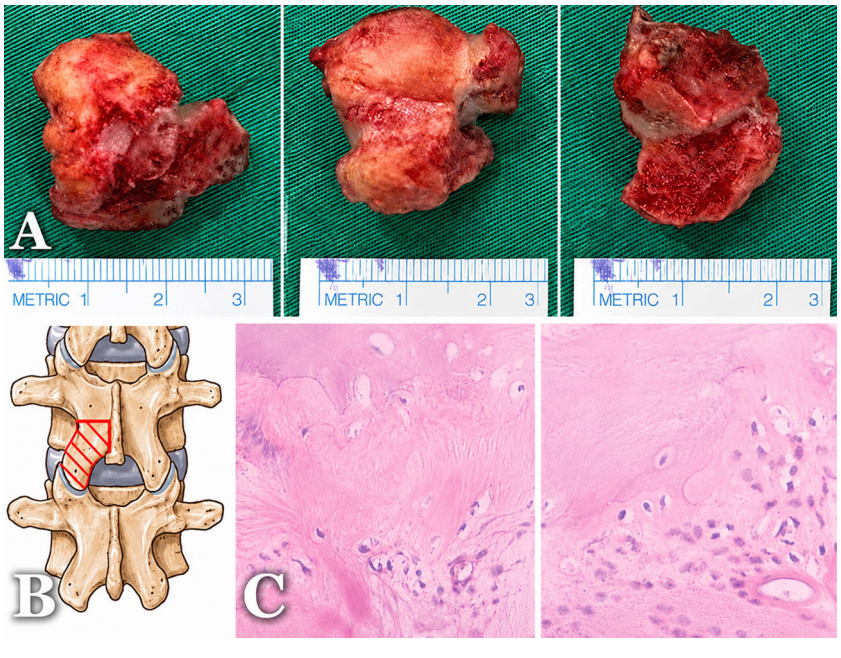

Fig. 4. Gross specimen, schematic illustration, and histopathological findings. A - En bloc resected osseous mass with measurement scale, demonstrating the lobulated morphology of the lesion; B - Schematic illustration showing the tumor arising from the right inferior articular process of L3 and projecting into the spinal canal; C - Histopathological examination confirming osteochondroma, characterized by a hyaline cartilage cap overlying mature cancellous bone.

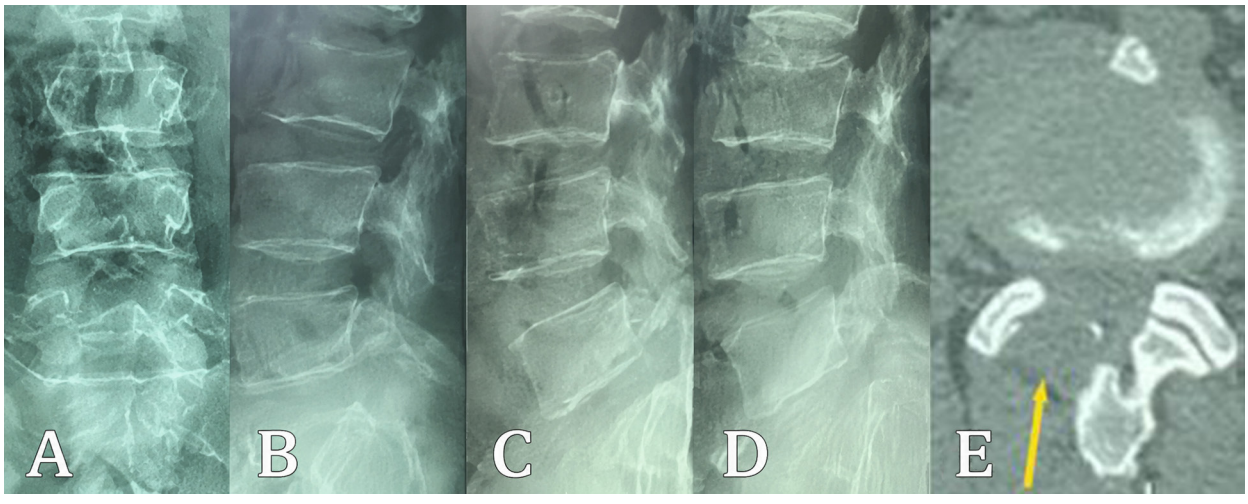

Fig. 5. One-year postoperative follow-up imaging. A-D - Standing anteroposterior, lateral, and dynamic flexion–extension radiographs demonstrating preserved alignment and no evidence of segmental instability at the L3–L4 level; E - Axial CT image at the previous tumor site showing complete resection without residual or recurrent lesion

Discussion

Osteochondromas are benign osseocartilaginous tumors arising from aberrant enchondral ossification of the growth plate and are defined radiologically by continuity of both cortical and medullary bone with the parent skeleton [5, 6]. They are generally considered as hamartomatous proliferations, with growth typically ceasing at skeletal maturity, and may occur either as solitary lesions or as part of multiple hereditary exostoses (MHE), an autosomal dominant condition associated with mutations in the EXT1/EXT2 tumor suppressor genes [7]. Patients with MHE often develop multiple lesions and carry a higher risk of malignant transformation compared with solitary osteochondromas [7].

Although osteochondromas are the most common benign bone tumors, spinal involvement remains uncommon, reported in fewer than 5% of cases [8]. The cervical spine—particularly the upper cervical levels—is most frequently affected, whereas lumbar lesions are distinctly rare [3, 4]. Large literature syntheses have confirmed this distribution and demonstrated a predominance of lesions arising from the posterior elements. For instance, Yakkanti *et al*. (2018) [1] reviewed solitary spinal osteochondromas and highlighted both the posterior element predilection and neurologic presentations requiring surgery. Similarly, Lin *et al*. (2022) updated the literature on spinal osteochondroma and emphasized the predominance of cervical involvement and posterior column origin. Within the lumbar spine, osteochondromas arising from the facet or articular processes are particularly rare but clinically important because of their proximity to the spinal canal and neural foramina [3]. Case reports and small series have described symptomatic lumbar articular process lesions presenting with radicular symptoms [2], underscoring that this entity may mimic degenerative lumbar pathology and therefore be overlooked.

Neurological compromise from spinal osteochondroma is itself uncommon, affecting a small minority of patients, and typically manifests as radiculopathy and/or progressive myelopathy depending on level and direction of growth. Acute neurological deterioration is rarely described but may occur when the lesion rapidly encroaches on the spinal canal or foramen, or when superimposed factors exacerbate stenosis. In the present case, the clinical course was notable for relatively rapid symptom progression after minor trauma, with radicular pain, paresthesia, and neurogenic claudication caused by cauda equina compression at L3–L4. This presentation broadens the recognized clinical spectrum of lumbar articular process osteochondroma and reinforces that even benign, slow-growing lesions can become symptomatic over a short interval when canal compromise reaches a critical threshold.

Imaging plays a pivotal role in establishing diagnosis and guiding surgical planning. Plain radiographs may reveal a bony outgrowth but can be limited by overlapping spinal structures. CT remains the most reliable modality for confirming the pathognomonic cortical and medullary continuity and delineating the extent of osseous involvement [5]. MRI provides complementary information regarding neural compression and characterization of the cartilage cap, which is essential for assessing malignant transformation risk [5]. In adults, a cartilage cap thickness greater than 1–2 cm and/or irregular signal characteristics should raise suspicion for secondary chondrosarcoma [5,8]. In our patient, the cartilage cap measured approximately 3 mm without suspicious features, supporting a benign lesion and correlating with the low reported malignant transformation risk for solitary osteochondromas [5, 7].

Management is determined by symptoms and imaging findings. Asymptomatic lesions can be observed with periodic clinical and radiologic follow-up [7]. However, progressive pain or neurological compromise constitutes a clear indication for surgical decompression and tumor removal [7]. The primary surgical objective is complete excision, including the cartilage cap, because residual cartilaginous tissue is a recognized risk factor for recurrence [7, 8]. Contemporary posterior

decompression techniques allow safe resection of posterior element tumors with acceptable morbidity even in anatomically constrained regions [7]. In the present case, posterior decompression with en bloc excision of the L3 inferior articular process achieved immediate symptom relief, and histopathology confirmed the diagnosis of osteochondroma.

A key technical consideration in lumbar facet or articular process osteochondroma is the balance between adequate decompression and preservation of segmental stability. Facetectomy—especially when extensive—may predispose to postoperative instability. Finite-element biomechanical data indicate that segmental motion increases with graded facetectomy, becoming more pronounced when facet resection exceeds approximately 45%, and worsening further with larger resections, thereby increasing the risk of iatrogenic instability [9]. Therefore, we deliberately preserved the superior articular process of L4, maintained more than half of the facet joint complex, and protected the posterior ligamentous structures. Importantly, these intraoperative stability-preserving measures were complemented by objective postoperative assessment using standing and dynamic flexion–extension radiographs, applying explicit instability thresholds (translation >4.5 mm; angular motion >15°). As no pathological translation or excessive angular motion was detected, instrumented fixation was not indicated. Although instrumented fusion is often considered following the resection of posterior spinal elements to prevent iatrogenic instability, we deliberately opted against instrumentation in this case based on several biomechanical and clinical rationales. First, the osteochondroma was an exophytic, surface-growing lesion without destructive infiltration of the load-bearing spinal columns. The en bloc resection functioned as hemifacetectomy, allowing us to preserve the pars interarticularis, the L4 superior articular process, spinous process, interspinous ligament, supraspinous ligament, and the contralateral facet joint. Biomechanical studies indicate that preserving more than 50% of the facet complex, along with an intact anterior column and posterior ligamentous complex, is generally sufficient to maintain segmental stability. Second, avoiding a rigid fusion at the L3-L4 level preserves the patient's natural lumbar kinematics and significantly mitigates the long-term risk of adjacent segment disease (ASD). For a localized, benign pathology, performing an instrumented fusion would represent an unnecessary overtreatment associated with increased surgical morbidity, blood loss, and muscle stripping. The patient was thoroughly counseled on this motion-preserving strategy, with a mutual agreement to perform strict radiographic monitoring for any delayed instability. The objective dynamic radiographs obtained at the one-year follow-up validated this approach, demonstrating complete absence of pathological translation or angular motion.

Prognosis after timely decompression is generally excellent, particularly when surgery is performed before irreversible neural injury [7]. Most patients experience significant symptom relief and functional recovery, and recurrence is uncommon following complete excision [2, 10]. Nevertheless, careful long-term surveillance is warranted because recurrence has been reported in cases of incomplete cartilage cap removal [8]. In our patient, 12-month clinical and radiologic follow-up demonstrated durable symptom resolution, no evidence of tumor recurrence on CT, and preserved segmental stability on dynamic radiographs.

In summary, although lumbar osteochondroma is rare, lesions arising from the articular process can cause clinically significant canal compromise and neurogenic claudication. Lumbar osteochondroma should be considered in patients presenting with atypical radiculopathy or claudication when imaging reveals a focal exophytic osseous lesion. Combined CT and MRI are essential for accurate diagnosis and cartilage cap evaluation. In selected cases, limited facetectomy with preservation of stabilizing structures, supported by objective dynamic radiographic assessment, may allow safe omission of instrumentation while maintaining postoperative stability.

Disclosure

Ethics approval and consent to participate

This study was conducted in accordance with the principles of the Declaration of Helsinki. Ethical approval was waived as this was a single case report without identifiable patient information, in accordance with institutional policy.

Consent for publication

Written informed consent was obtained from the patient for publication of this case report and accompanying images. A copy of the written consent is available for review by the Editor-in-Chief of this journal upon reasonable request.

Availability of data and materials

All data generated or analyzed during this study are included in this published article. No additional datasets were generated.

Competing interests

The authors declare that they have no competing interests.

Funding

The authors received no financial support for the research, authorship, and/or publication of this article.

Acknowledgments

The authors are grateful to the medical staff of the Hospital for Traumatology and Orthopedics, Ho Chi Minh City, for their assistance in patient management.

References

1. Yakkanti R, Onyekwelu I, Carreon LY, Dimar JR 2nd. Solitary Osteochondroma of the Spine-A Case Series: Review of Solitary Osteochondroma With Myelopathic Symptoms. Global Spine J. 2018 Jun;8(4):323-339. doi: 10.1177/2192568217701096
2. Woo HJ, Cho DC, Bae KJ, Sung JK. Solitary lumbar spinal osteochondroma presenting with sciatic pain: a case report. Kor J Spine. 2010;7(3):173–176. https://www.e-neurospine.org/journal/view.php?number=356
3. Lin GX, Wu HJ, Chen CM, Rui G, Hu BS. Osteochondroma Arising From the Inferior Articular Process of the Lumbar Spine in a Geriatric Patient: A Case Report and Literature Review. Geriatr Orthop Surg Rehabil. 2022 Jan 25;13:21514593211073028. doi: 10.1177/21514593211073028
4. Shigekiyo S, Nishisho T, Takata Y, Toki S, Sugiura K, Ishihama Y, Manabe H, Tezuka F, Yamashita K, Sakai T, Maeda T, Sairyo K. Intracanalicular Osteochondroma in the Lumbar Spine. NMC Case Rep J. 2019 Dec 18;7(1):11-15. doi: 10.2176/nmccrj.cr.2019-0031

5. Murphey MD, Choi JJ, Kransdorf MJ, Flemming DJ, Gannon FH. Imaging of osteochondroma: variants and complications with radiologic-pathologic correlation. Radiographics. 2000 Sep-Oct;20(5):1407-34. doi: 10.1148/radiographics.20.5.g00se171407
6. Tepelenis K, Papathanakos G, Kitsouli A, Troupis T, Barbouti A, Vlachos K, Kanavaros P, Kitsoulis P. Osteochondromas: An Updated Review of Epidemiology, Pathogenesis, Clinical Presentation, Radiological Features and Treatment Options. In Vivo. 2021 Mar-Apr;35(2):681-691. doi: 10.21873/invivo.12308
7. Bottner F, Rodl R, Kordish I, Winklemann W, Gosheger G, Lindner N. Surgical treatment of symptomatic osteochondroma. A three- to eight-year follow-up study. J Bone Joint Surg Br. 2003 Nov;85(8):1161-5. doi: 10.1302/0301-620x.85b8.14059
8. Agarwal S, Majety SK, Agarwal R, Veluru C, Earni SC, Anumolu A. Atypical presentation of L3 vertebral body osteochondroma mimicking cauda equina syndrome: a case report. Ann Med Surg (Lond). 2025 Aug 15;87(10):6785-6790. doi: 10.1097/MS9.0000000000003734
9. Ahuja S, Moideen AN, Dudhniwala AG, Karatsis E, Papadakis L, Varitis E. Lumbar stability following graded unilateral and bilateral facetectomy: A finite element model study. Clin Biomech (Bristol). 2020 May;75:105011. doi: 10.1016/j.clinbiomech.2020.105011

Case report

Ukrainian Neurosurgical Journal. 2026;32(2):126-130
doi: 10.25305/unj.353968

A Case of late post-traumatic paradoxical nasal cerebrospinal fluid leak: a multidisciplinary approach to diagnosis and treatment

Oksana Y. Skobska [1], Oleksandr S. Hotin [2], Andriy O. Diadechko [2], Daryna V. Draganchuk [1]

[1] Group of Otoneurology, Romodanov Neurosurgery Institute, Kyiv, Ukraine
[2] Department of trauma brain injury, its consequences, and CSF disorders, Romodanov Neurosurgery Institute, Kyiv, Ukraine

Received: 09 March 2026
Accepted: 03 April 2026

Address for correspondence:
Oksana Y. Skobska, Group of Otoneurology, Romodanov Neurosurgery Institute, 32 Platona Maiborody st., Kyiv, 04050, Ukraine, e-mail: skobska@i.ua

Nasal cerebrospinal fluid (CSF) leakage occurs in 12–30% of patients with skull base fractures, whereas its late paradoxical form is observed in only 2% of traumatic brain injury (TBI) cases and represents an extremely rare and insufficiently studied phenomenon.

A retrospective analysis of this clinical case was performed, illustrating the complexity of differential diagnosis and emphasizing the priority of clinical reasoning in the management of complex patients with TBI.

Ten years after sustaining severe TBI with a fracture of the petrous part of the right temporal bone, the patient developed paradoxical nasal CSF leakage that had not been verified at the outpatient stage. Following comprehensive evaluation at the Romodanov Neurosurgery Institute of the National Academy of Medical Sciences of Ukraine, the patient underwent surgical treatment, which resulted in complete resolution of the CSF leak. The patient was discharged in satisfactory condition without signs of recurrence.

The presented case demonstrates an exceptionally rare combination in adults (0.05–1.0%) of meningoencephalocele and a porencephalic cyst associated with a growing skull base fracture, which led to the development of late post-traumatic paradoxical nasal CSF leakage. In the absence of access to β2-transferrin testing, the key diagnostic marker was identified as the combination of nasal CSF leakage with a specific audiometric pattern (mixed hearing loss with an intact tympanic membrane), which required mandatory verification using combined neuroimaging modalities (computed tomography and magnetic resonance imaging). A surgical strategy focused on watertight duraplasty proved effective, ensuring cessation of CSF leakage and partial regression of the conductive component of hearing loss despite the high recurrence risk reported in the literature.

Conclusions: Timely diagnosis of late post-traumatic paradoxical nasal CSF leakage is critically important for preventing intracranial complications; however, it remains a challenging task in patients with a history of TBI. The presented clinical case highlights the necessity of a multidisciplinary approach for accurate verification of the pathology and selection of effective treatment strategies in the remote post-traumatic period.

Keywords: *paradoxical rhinorrhea; post-traumatic nasal cerebrospinal fluid leak; multidisciplinary approach; CSF fistula; pure-tone audiometry; hearing loss; diagnostic markers*

Introduction

Nasal cerebrospinal fluid (CSF) leakage is a rare but clinically significant complication of traumatic brain injury (TBI). In cases of basilar skull fractures, the incidence of post-traumatic CSF leakage increases to 12–30%. Several reviews have reported that nasal CSF leakage develops in approximately 2% of patients with TBI. These data underscore the need for careful assessment and monitoring of patients with suspected skull base fractures [1].

Late post-traumatic CSF leakage, manifesting months or years after injury, is considered a rare complication. In most cases, post-traumatic CSF leakage occurs within the first 48 h or during the first 3 months after trauma. Clinical reports describing the development of CSF leakage later than 3 months after injury have been presented only in isolated publications [1].

Late paradoxical nasal CSF leakage is an uncommon phenomenon described predominantly in the form of isolated case reports and small case series. No large systematic studies providing data on its incidence have been conducted. General epidemiological data on cranial CSF leaks indicate considerable variability depending on etiology and the type of skull fracture [2].

Paradoxical nasal CSF leakage represents a clinical condition in which a defect in the middle ear or mastoid process results in communication between the CSF spaces and the nasal cavity through the Eustachian

tube or pathological fistulas, clinically manifesting as unilateral clear nasal discharge [3].

The presented clinical observation of late post-traumatic paradoxical nasal CSF leakage is of methodological interest, illustrating the complexity of differential diagnosis and emphasizing the priority of clinical reasoning. A detailed retroprospective analysis of the patient's medical records was performed with comparison of clinical and instrumental findings.

Clinical Case

Patient R., born in 1984.

Medical history. Ten years earlier (26 May 2015), the patient sustained severe TBI as a result of a road traffic accident. Multislice computed tomography (MSCT) of the brain performed in Bila Tserkva on 26 May 2015 revealed cerebral contusions with lesions in both frontal lobes and the right temporal lobe, as well as traumatic subarachnoid hemorrhage. A longitudinal fracture of the petrous part of the right temporal bone and linear fractures of the temporal and occipital squamae were identified. No surgical intervention was performed. There were no documented signs of CSF leakage during the acute period.

History of present illness. Approximately 2 months before admission, the patient noticed discharge of clear fluid from the right nasal cavity. Otolaryngologists at the local healthcare facility did not confirm the diagnosis of nasal CSF leakage. The patient was referred by a neurologist to the Romodanov Neurosurgery Institute of the National Academy of Medical Sciences of Ukraine (Kyiv).

Complaints at admission. Periodic headache and leakage of clear fluid from the right nasal passage.

Otolaryngological consultation. Objective findings (preoperative examination dated 25 November 2025): anterior rhinoscopy demonstrated deviation of the nasal septum to the left, causing obstruction of the left common nasal meatus and relative widening of the right nasal cavity. The mucosa of the inferior and middle nasal turbinates was hypertrophic, pale pink with areas of cyanotic discoloration. Nasal breathing was moderately impaired. Transparent watery rhinorrhea from the right nasal cavity was observed, with increased intensity during forward bending (positional test) and coughing. The unilateral nature of the discharge raised suspicion of CSF leakage and warranted further diagnostic evaluation. Assessment of olfactory function revealed right-sided hyposmia of mixed origin, whereas olfaction on the left side remained intact.

Given the lack of routine availability of β2-transferrin testing in Ukraine, verification of cerebrospinal fluid in the nasal secretion was performed using a qualitative glucose test. The study was conducted with strict adherence to the biomaterial collection protocol. Measures were taken to prevent contamination with blood or purulent content. A positive glucose test result from the right nasal secretion supported the diagnosis of right-sided late post-traumatic paradoxical nasal CSF leakage.

Otoscopy: on the left side, the tympanic membrane was intact and transparent, without signs of inflammation; anatomical landmarks were clearly visualized, and mobility was preserved. On the right side, the tympanic membrane was thickened and opaque, with reduced excursion (mobility) during pneumatic testing. Signs of serous effusion behind the membrane were visualized. The clinical findings were verified as Eustachian tube dysfunction with impaired ventilatory function. The results of pure-tone threshold audiometry are presented in ***Fig. 2*.**

Oropharyngoscopy: the palatine tonsils were hypertrophic, exhibiting pronounced cryptic architecture and isolated fibrinopurulent deposits; palpation revealed moderate tissue density. The mucosa of the posterior pharyngeal wall and soft palate showed no signs of active inflammation. Regional cervical lymph nodes were not enlarged. The clinical picture was verified as chronic tonsillitis in remission.

No signs of involvement of the caudal group of cranial nerves (dysarthria, dysphagia, or dysphonia) were detected. The functions of the oculomotor group, trigeminal nerve, and facial nerve were preserved, without pathological changes. Gustatory sensitivity was intact. No spontaneous nystagmus was observed. Mild static ataxia (slight unsteadiness) was noted in the Romberg position.

Conclusion. Suspected right-sided late post-traumatic paradoxical nasal CSF rhinorrhea; right-sided chronic mixed hearing loss; right-sided hyposmia of mixed etiology**.**

Ophthalmological examination (25 Nov 2025). Visual acuity: OD = 1.0, OS = 1.0. Visual fields were unchanged. The optic discs were pale pink with well-defined margins; the retinal arteries were narrowed and tortuous. Hypertensive retinal angiopathy was diagnosed.

Internal medicine examination (25 Nov 2025). Grade II, stage III arterial hypertension with a risk of developing heart failure grade 0–I. Grade II obesity.

MSCT of the brain (07 Nov 2025). A non-united fracture of the calvarial bones and skull base on the right was identified, with fragment diastasis of up to 9 mm, extending to the petrous part of the right temporal bone with fragment diastasis of up to 4 mm and communication between the middle ear structures (canals) and an intracranial focus of encephalomalacia in the right temporal lobe, which communicated with the posterior horn of the right lateral ventricle. The right middle ear cavity and mastoid air cells were filled with fluid-colloid content. Foci of encephalomalacia measuring 52 × 34 mm were detected in both frontal lobes and the right temporal lobe. Periventricularly and diffusely within the cerebral white matter, foci of leukoaraiosis and enlarged perivascular spaces of the basal ganglia were observed bilaterally. The cortical sulci of the cerebral hemispheres and cerebellum were clearly visualized. The ventricular system was asymmetric and dilated. The convexital cerebrospinal fluid spaces, insular and basal cisterns were irregularly enlarged, and the sulci were deepened. Midline structures were not displaced (***Fig. 1***).

An elective surgical procedure was performed on 26 November, 2025.

The patient was positioned in the left lateral decubitus position. A lumbar drain was inserted. Following skin preparation with antiseptic solutions, a horseshoe-shaped incision of the soft tissues was made in the right temporo-occipital region. A free bone flap was created from a single burr hole using an electric trephine.

The dura mater was tense, and cerebral pulsation was absent. The dura mater was opened in an arcuate fashion. Access to the posterior surface of the petrous part of the temporal bone was achieved. During the approach, a porencephalic cyst communicating with the temporal horn of the right lateral ventricle was opened. Revision of the temporal bone revealed an old fracture line extending into the petrous part of the temporal bone, with formation of CSF fistula in the region of the posterior surface of the petrous temporal bone. Diastasis of the bony edges extending into the petrous temporal bone was identified. The porencephalic CSF cyst was adjacent to the bony defect of the petrous temporal bone wall, with formation of a meningoencephalocele measuring 0.5 × 2.0 cm extending into the petrous cavity. The bony defect was reconstructed using a temporalis muscle graft, Surgispon® sponge, and TachoComb® collagen sponge fixed with butyl cyanoacrylate glue. Satisfactory cerebral pulsation was noted. Interrupted sutures were placed on the dura mater. The dural defect was repaired using a TachoComb® sponge. The bone flap was repositioned and secured with bone sutures. Layered closure of the soft tissues was performed. An aseptic dressing was applied.

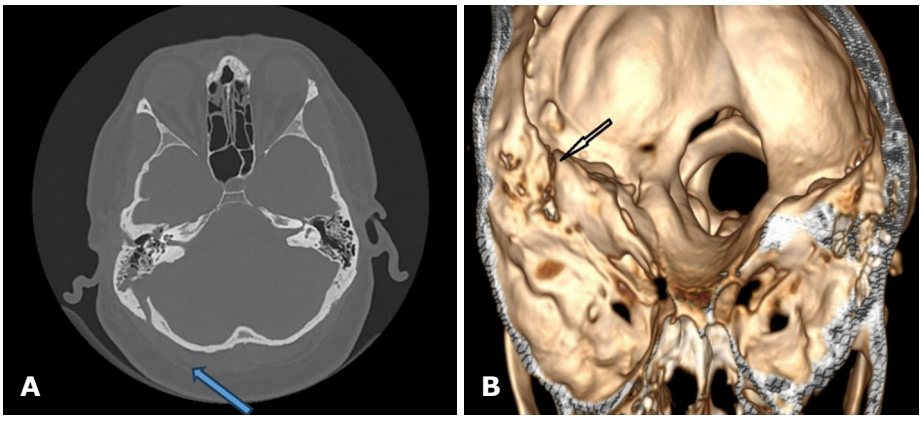

Fig. 1. MSCT of the patient's temporal bones: A — axial projection in the bone window; B — 3D reconstruction. Arrows indicate the fracture line of the petrous part of the right temporal bone with marked fragment diastasis

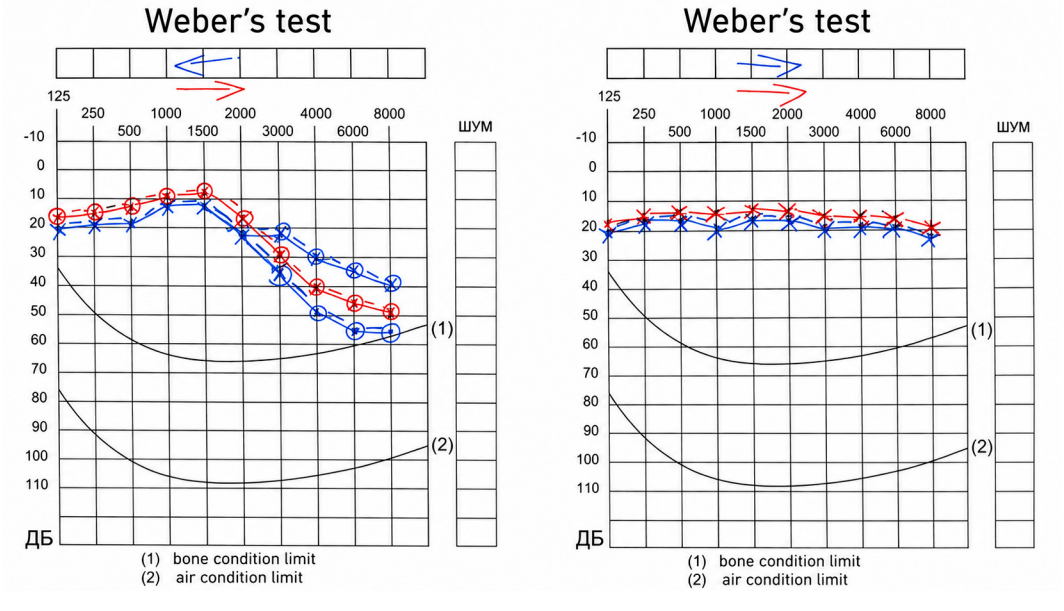

Fig. 2. Dynamics of pure-tone threshold audiometry for air and bone conduction (0.25–8.0 kHz): blue line — preoperative assessment (25 Nov 2025); red line — postoperative follow-up (09 Dec 2025). Left ear: preservation of hearing thresholds within 0–20 dB for both air and bone conduction at frequencies of 250–8000 Hz before and after surgery. Right ear: preoperatively, mixed hearing loss with predominance of conductive and high-frequency sensorineural components was observed. Air conduction thresholds remained within normal limits (≤20 dB) at frequencies up to 2000 Hz, with gradual elevation of thresholds to 60 dB at frequencies up to 8000 Hz. The air–bone gap within the 3000–8000 Hz range was 15–25 dB (mean 16–20 dB). Postoperatively, positive dynamics were observed due to a reduction in the conductive component (decrease in the air–bone gap) while the sensorineural deficit persisted

Given the presence of a porencephalic cyst and associated meningoencephalocele, the risk of recurrent CSF leakage was considered moderately high. To prevent CSF hypertension and ensure watertight closure of the defect, an external lumbar drain was maintained postoperatively for 7 days. Concurrent dehydration therapy was administered. Following drain removal, no clinical signs of nasal CSF leakage were observed. No CSF leakage was detected.

Otolaryngology consultation (09 Dec 2025): positive clinical dynamics were noted. Audiometric findings demonstrated improvement in hearing function of the conductive type (***Fig. 2***). The glucose provocation test using the Valsalva maneuver was negative, indicating the absence of CSF leakage after surgical intervention.

The patient was discharged in satisfactory condition with marked positive clinical dynamics, including the absence of nasal CSF leakage, regression of the cephalgic syndrome, and objective restoration of auditory function. A course of acetazolamide was recommended for correction of CSF dynamics, along with adherence to a protective regimen avoiding physical exertion and continued follow-up by specialists.

Discussion

The presented clinical case demonstrates a complex pathogenetic relationship between traumatic injury to the skull base structures and the development of delayed post-traumatic paradoxical CSF leakage. Analysis of this case revealed insufficient diagnostic vigilance regarding nasal CSF leakage at the outpatient stage of otorhinolaryngological care. Despite pronounced rhinorrhea, specific diagnostic evaluation and differential diagnosis aimed at excluding a CSF fistula were not performed in a timely manner. This highlights the need to improve awareness among primary- and secondary-care physicians regarding the management algorithms for patients with suspected CSF leakage, particularly in cases of atypical rhinosinusitis.

A key diagnostic indicator in this case was the combination of characteristic rhinorrhea with a specific audiometric pattern, namely mixed hearing loss on the affected side. This finding suggested the presence of cerebrospinal fluid within the middle ear cavity despite an intact tympanic membrane. The conductive defect caused by impaired sound transmission in the middle ear was combined with a sensorineural component. Such an audiometric configuration is typical of chronic otitis media, otosclerosis, or post-traumatic changes involving both peripheral and conductive structures of the auditory analyzer. The air conduction curve demonstrated a descending configuration. The audiogram pattern served as an indirect sign of the presence of CSF within the tympanic cavity. The observed postoperative dynamics corresponded to partial restoration of middle ear functional status following surgical intervention while preserving the sensorineural deficit. Postoperative monitoring confirmed the effectiveness of the selected surgical strategy, which resulted in cessation of CSF leakage and partial regression of the conductive component of hearing loss.

A limitation of this clinical observation is the absence of laboratory verification using β2-transferrin testing, which is considered the reference standard for confirming the presence of cerebrospinal fluid in nasal secretions. In Ukraine, this test has not been implemented in the routine practice of specialized neurosurgical centers, possibly because of the requirement for expensive equipment, the need for methodological validation, and logistical and organizational challenges. Consequently, alternative diagnostic approaches were employed. It should be noted that qualitative glucose testing is characterized by low specificity and a risk of false-positive results in cases of contamination of the sample with blood or purulent discharge. Therefore, the diagnostic concept was based on a systematic approach involving comprehensive analysis of clinical and instrumental otoneurological examination findings, neuroimaging data, and dynamic patient monitoring.

The pathogenesis of CSF leakage in this case was associated with the combination of several critical factors. First, the patient had a growing skull fracture, a rare pathology in the adult population. According to the literature, the incidence of this condition ranges from 0.05 to 1.0% among skull fracture cases, with the majority of observations (approximately 90%) occurring in children younger than 3 years of age. Detection of this pathology in an adult patient is considered exceptional and requires heightened clinical vigilance [4]. The second critical factor was the presence of a porencephalic cyst communicating with the inferior horn of the right lateral ventricle. This resulted in herniation of brain tissue and formation of a meningoencephalocele through the fracture diastasis of the petrous temporal bone (***Fig. 3***).

In the available scientific literature, the combination of a growing skull fracture with concurrent formation of a meningocele or meningoencephalocele has been described only in isolated clinical case reports, confirming the rarity of this pathology. In particular, G.W. Britz *et al*. (1998) reported a rare case of CSF leakage in an adult patient in whom a parietal bone defect was associated with the formation of a meningocele, thereby confirming the possibility of development of this pathology in adulthood [5, 6]. This substantially limits the possibility of extrapolating the available data to formulate universal conclusions regarding pathogenetic mechanisms and optimal treatment strategies in adult patients.

From a clinical perspective, such a combination of pathological changes is fundamentally important because the presence of a meningo(encephalo)cele modifies the surgical strategy. In particular, there is a need not only for reconstruction of the bony defect but also for reliable watertight repair of the dura mater, which is critical for the prevention of recurrent CSF leakage and ascending intracranial infectious complications [7].

For diagnostic verification, combined neuroimaging is recommended: computed tomography for precise assessment of bony destruction and magnetic resonance imaging for verification of dural defects, objective evaluation of the extent of prolapse, and assessment of parenchymal status. According to the literature, magnetic resonance imaging enables differentiation between prolapse patterns (isolated herniation of brain tissue, leptomeningeal cyst, or combined variants), which is critically important for preoperative planning.

When a meningo(encephalo)cele is confirmed, the primary surgical objective is watertight duraplasty. In adult patients, the choice of material for cranioplasty

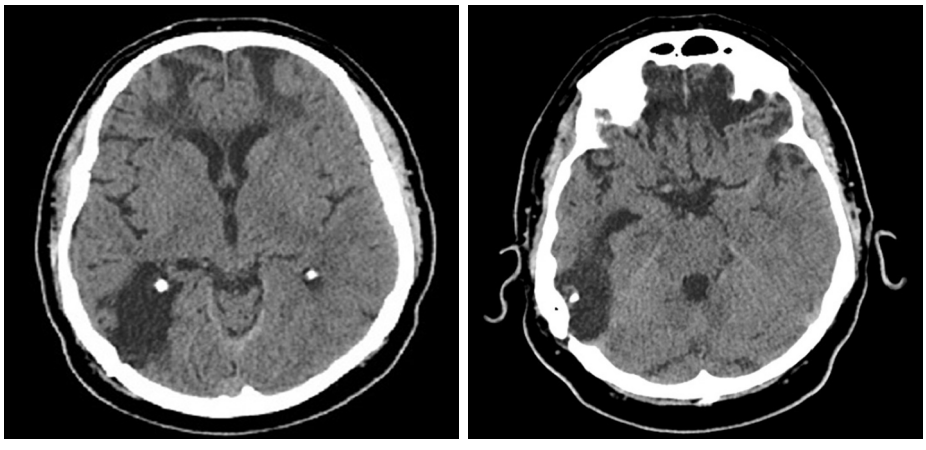

Fig. 3. MSCT of the brain. Porencephalic cyst of the temporal region

should be based on assessment of the risk of resorption, cosmetic requirements, and the presence of associated factors (history of infection, need for revision surgery).

Analysis of the literature data indicates a high incidence of postoperative infectious complications and recurrent CSF leakage.

Conclusions

The diagnosis of delayed post-traumatic paradoxical nasal CSF leakage remains a challenging issue in clinical practice. Delayed verification of this pathology may lead to severe intracranial complications, including fatal outcomes.

The presented clinical case highlights the necessity of considering paradoxical nasal CSF leakage in the differential diagnosis of rhinorrhea of unclear etiology in patients with a history of traumatic brain injury, even many years after the trauma. Confirmation of the diagnosis and selection of the optimal treatment strategy require coordinated collaboration among the otolaryngologist, radiologist, and neurosurgeon. Treatment efficacy directly depends on a multidisciplinary approach and timely diagnosis.

Disclosure

Conflict of interest

The authors declare no conflict of interest.

Informed consent

Written informed consent was obtained from the patient.

References

1. Sharifi G, Mousavinejad SA, Bahrami-Motlagh H, Eftekharian A, Samadian M, Ebrahimzadeh K, Rezaei O. Delay Posttraumatic Paradoxical Cerebrospinal Fluid Leak with Recurrent Meningitis. Asian J Neurosurg. 2019 Jul-Sep;14(3):964-966. doi: 10.4103/ajns.AJNS_95_18
2. Mughal Z, Martinez-Devesa P, Boukas A, Jeyaretna S, Qureishi A. Contemporary Management of Cerebrospinal Fluid Rhinorrhoea: A Review of the Literature. J Clin Med. 2025 Feb 4;14(3):995. doi: 10.3390/jcm14030995
3. Mohanraj L, Chinnusamy R. Diagnosis and Management of Paradoxical Cerebrospinal Rhinorrhea in Mondini's Dysplasia. Indian J Otolaryngol Head Neck Surg. 2024 Oct;76(5):4851-4854. doi: 10.1007/s12070-024-04903-5
4. Yan XH, Qiu K, Gao Y, Ren J, Cheng D, Pang W, Song Y, Yang W, Yu R, Zhao Y. Growing Skull Fracture of Temporal Bone in Adults: A Case Report and Literature Review. Ear Nose Throat J. 2020 Dec;99(10):654-657. doi: 10.1177/0145561320914774
5. Britz GW, Kim DK, Mayberg MR. Traumatic leptomeningeal cyst in an adult: a case report and review of the literature. Surg Neurol. 1998 Nov;50(5):465-9. doi: 10.1016/s0090-3019(97)00233-4
6. Zhao Q, Ying J, Chen Y, Chen F, Zhang T, Jing J. Clinical and imaging characteristics of growing skull fractures in children. Sci Rep. 2024 Mar 7;14(1):5673. doi: 10.1038/s41598-024-56445-z
7. Etter MM, Vernik T, Licci M, Guzman R, Soleman J, Greuter L. Surgical management of growing skull fractures: How I do it. Acta Neurochir (Wien). 2025 Aug 29;167(1):233. doi: 10.1007/s00701-025-06646-w